Polyamide 6 fibre recycling by twin-screw melt extrusion of mixed thermoplastic polymers

Siti Zaharah Binti Kunchi Mon

Submitted in accordance with the requirements for the degree of
Doctor of Philosophy

The University of Leeds
School of Design

November, 2019

The candidate confirms that the work submitted is his/her own, except where work which has formed part of jointly-authored publications has been included. The contribution of the candidate and the other authors to this work has been explicitly indicated below. The candidate confirms that appropriate credit has been given within the thesis where reference has been made to the work of others.

Chapter 4

Kunchimon, S.Z., Tausif, M., Goswami, P. and Cheung, V., 2019. Polyamide 6 and thermoplastic polyurethane recycled hybrid Fibres via twin-screw melt extrusion. *J. Polym. Res.* **26**. 162-175. https://doi.org/10.1007/s10965-019-1827-0

Chapters 6 and 7

Kunchimon, S.Z., Tausif, M., Goswami, P. and Cheung, V., 2019. From hybrid fibres to microfibres; the characteristic of polyamide 6/polypropylene blend via one-step twin-screw melt extrusion. *Polym. Eng. Sci*. https://doi.org/10.1002/pen.25327

The author of this thesis performed the experiment and analytical works and prepared the paper draft and co-authors provided suggestions to finalise the submission.

This copy has been supplied on the understanding that it is copyright material and that no quotation from the thesis may be published without proper acknowledgement.

© 2019 The University of Leeds and Siti Zaharah Binti Kunchi Mon

Acknowledgements

I would like to express my sincere gratitude to both of my awesome supervisors, Dr Vien Cheung and Dr Muhammad Tausif for the advice, time and guidance to introduce me to the world of research. Without them, my PhD journey will not be this beautiful. Not to forget, thanks to Prof Dr Parikshit Goswami, who is my first supervisor during my early years of study. His motivation, enthusiasm and criticism are incredible and keep inspired me through these years.

Deeply grateful and thanks to staff and fellow researchers at the School of Design who assist and guide me to conduct lab works; Dr Tim Smith, Dr Tom O'Haire, Dr Andrew Hebden, Mr. Jianguo Qu and Dr Matthew Clark for the TGA experiment. Thanks go to also Mr. Michael Brookes who produced the microscopy images presented in this work. Many thanks to Prof Tom Cassidy who is willing to spare his busy time to teach me to use twisting machine and Dr Jane Scott for inviting me to join her knitting class. I also want to thanks Mr. Algy Kazlauciunas from School of Chemistry for the microscopy images of PA6 and PET blend and Ms. Lesley Neve from School of Earth and Environment for the XRD experiments.

I met many beautiful souls who cherish my days in the PhD room whom directly or indirectly motivate me to complete this thesis; Najua, Soojin, Jihye, Gyeonghwa, Mia, Tian, Nani, Nicole, Bintan, Xenia, Ana, Zi, Pendo, Zohreh and many more. Thank you for sharing your hope, dreams, laughter and smile whenever I need it.

This PhD will not be possible without financial support from my employer, Universiti Tun Hussein Onn Malaysia and Malaysia Ministry of Education which I appreciated and acknowledged.

Lastly, for my family, my husband and my lovely kids, Aqil and Aqilah, who always stand by my side and keen to live abroad with me, your endless love and supports mean so much to me. For my late father whom I lost during my final year of PhD, you will always be in my heart.

Abstract

Textile wastes consist of multi-component materials are hardly recycled due to challenge to sort and separate the waste into a single component. Textile products dominantly produced from a non-renewable source that can be recycled several times before the end of life. Mixed-waste can be recycled together without sorting by thermo-mechanical process to produce hybrid fibres. The aim of this study was to investigate the potential on upcycling polyamide 6 (PA6) polymer mixed with secondary polymers via one-step twin-screw melt extrusion. Three secondary polymers were chosen in this study; thermoplastic polyurethane (TPU) which has interaction with PA6, and two polymers which do not have interaction with PA6; polyethylene terephthalate (PET) and polypropylene (PP). Different blending composition was prepared between PA6 and secondary polymers before being extruded into hybrid fibres through melt extrusion. The secondary polymers were then removed from the hybrid fibres to investigate the properties of the leftover of PA6 component. The fibres were characterised using attenuate total reflectance Fourier Transform Infrared Spectroscopy (ATR-FTIR) and microscopy techniques, the mechanical and thermal properties were investigated via tensile strength and differential scanning calorimetry (DSC) and thermogravimetric analysis (TGA). The results showed that the blending of PA6 with interacting polymer TPU creates novel fibres morphology with multi-connected porous fibres. The mean diameter of PA6:TPU hybrid fibres when the PA6 content at 50% and 80% are 136 and 126 μm, respectively. Thermal and chemical results demonstrated strong interaction happen between PA6 and TPU. Meanwhile, the co-extrusion of PA6 with non-interacting polymer PP and PET formed PA6 micro and nanofibres in the blend, respectively. In PA6:PP blend, the SEM images show the PA6 microfibres with mean diameters of 0.76 μm and 1.13 μm developed in the hybrid fibres with PA6 content 50% and 60%, respectively. The phase inversion between PA6 and PP happened at the composition of 65% of PA6 showing the development of PA6 microfibres in a unique fibre morphology. In PA6:PET blend, PA6 nanofibres with mean diameter of 532 nm to 1026 nm were obtained. The diameter of PA6 nanofibres increase when PA6 content increase in the blend. Later, single jersey knitted fabric was produced from PA6:PP 60:40 blend composition and was treated later to remove the PP component. The treatment process exposed the development of PA6 microfibres fabric which has excellent behaviour in wicking and improved in ball burst strength compared to the untreated fabric. The success of upcycling PA6 fibres with value added properties through single-step melt extrusion can be applied to other mixed polymer waste.

Table of Contents

Acknowledgements ..... **ii**

Abstract ..... **iii**

Table of Contents ..... **iv**

List of Tables ..... **viii**

List of Figures ..... **ix**

Chapter 1 Introduction **1**

1.1 Overview 1

1.2 Research aim and objectives 3

Chapter 2 Literature Review **5**

2.1 Textile waste 5

2.2 Textile recycling 6

2.2.1 Mechanical recycling 7

2.2.2 Chemical recycling 7

2.3 Polyamide 8

2.3.1 Polyamide 6 waste 9

2.3.2 Recycled polyamide 6 fibres 10

2.3.2.1 Mechanical Properties 10

2.3.2.2 Chemical Properties 11

2.3.2.3 Thermal Properties 12

2.4 Textile fibres 13

2.4.1 Single component fibres 13

2.4.2 Bicomponent fibres 15

2.5 Polymer blend in textile fibre 21

2.5.1 Factors affect the properties of blend fibre 22

2.5.2 Interacting blend of PA6:TPU 24

2.5.3 Non-Interacting blend of PA6:PP and PA6:PET 26

2.5.3.1 Morphology of the blend 27

2.5.3.2 Thermal properties 30

2.5.3.3 Mechanical properties 30

2.6 Melt spinning 31

2.7 Conclusions 33

Chapter 3 Methodology **34**

3.1 Materials 34

3.2 Fibre extrusion 35

3.2.1 Drying of polymer pellets 36
3.2.2 Melt extrusion.....36
3.3 Fibre treatment 37
3.4 Microscopy.....38
3.4.1 Light microscopy 39
3.4.2 Scanning electron microscopy (SEM).....41
3.5 Capillary rheometry.....42
3.6 Thermal properties.....43
3.6.1 Differential scanning calorimetry.....44
3.6.2 Termogravinometric analysis 46
3.7 Fourier Transform Infrared Spectroscopy 48
3.8 Tensile properties 48
3.9 Roller Drawing 49
3.10 Winding.....51
3.11 Knitted fabric production 52
3.12 Fabric testing 53
3.12.1 Sample preparation.....53
3.12.2 Fabric specification 53
3.12.3 Fabric structure 55
3.12.4 Bending length 55
3.12.5 Vertical wicking test.....55
3.12.6 Ball burst strength 57
Chapter 4 Production of partially miscible hybrid fibres of polyamide 6 and thermoplastic polyurethane polymer 58
4.1 Introduction 58
4.2 Part 1: PA6:TPU-D 59
4.2.1 Viscosity and fibre production 59
4.2.2 Morphology of the as-spun fibres.....60
4.2.3 Polymer extraction 64
4.2.4 Fibre and pore diameters.....69
4.2.5 Thermal properties.....73
4.2.6 X-ray diffraction.....79
4.2.7 Chemical properties 81
4.2.8 Tensile properties 84
4.3 Part 2: PA6:TPU-A.....87
4.3.1 Morphology of the fibre 88

4.3.2 Thermal properties 88
4.3.3 Chemical properties 91
4.3.4 Tensile properties 94
4.4 Conclusions 95
Chapter 5 Manufacturing of hybrid fibre from polyamide 6 and polyethylene terephthalate 96
5.1 Introduction 96
5.2 Viscosity and fibre production 97
5.3 Polymer extraction 98
5.4 Fibre morphology 99
5.5 Fibre diameters 103
5.6 Thermal properties 105
5.7 Tensile properties 106
5.8 Conclusions 111
Chapter 6 The effect of non-interacting blend between polyamide 6 and polypropylene polymer 112
6.1 Introduction 112
6.2 Viscosity of the polymers 112
6.3 Fibre morphology 113
6.4 Fibres diameters 117
6.5 Thermal properties 121
6.6 Chemical properties 130
6.7 Tensile properties 132
6.8 Conclusions 140
Chapter 7 Properties of upcycled polyamide 6 fabrics 141
7.1 Introduction 141
7.2 Production of PP-40 hybrid fibre 141
7.3 Production of PP-40 knitted fabric 142
7.4 Fabric 143
7.5 Physical properties 144
7.6 Fabric Strength 146
7.7 Wicking properties 148
7.8 Bending length 149
7.9 Conclusions 150
Chapter 8 Conclusions and Future work 151
8.1 Conclusions 151

8.2 Contributions 153
8.3 Suggestions for future work 154
List of References 156
Appendix A 168
Appendix B 169

List of Tables

Table 2.1 Porous fibres and fibre diameter. 18

Table 3.1 Types of polymer. 34

Table 3.2 Blend composition of the fibre. 35

Table 3.3 The temperature setting, screw speed and take-up speed of melt extruder (refer to Table 3.2 for blend composition). 37

Table 3.4 Solvents and extraction method of secondary polymer. 38

Table 3.5 Draw ratio of the feed roller and draw roller 50

Table 4.1 Shear rate and viscosity of the PA6:TPU-D hybrid fibre.....60

Table 4.2 Processing parameter of TPU-D 20. 63

Table 4.3 Mass loss of PA6:TPU-D hybrid fibres after being treated in DMSO and formic acid for 3 and 24h. 65

Table 4.4: Thermal properties of as-spun fibres sample. 75

Table 4.5 TGA results for PA6:TPU-D hybrid fibres before and after DMSO treatment. 76

Table 4.6 ATR-FTIR wavenumber for PA6, TPU-D and hybrid fibres. 82

Table 4.7: Carbonyl phase absorbance intensity of the TPU-D and hybrid fibres 83

Table 5.1 Shear rate and viscosity of PA6 and PET polymer.....97

Table 5.2 Fibres mass loss in formic acid and NaOH treatment. 99

Table 5.3 The morphology of fibres based on Jordhamo model. 103

Table 5.4 DSC results on PA6:PET hybrid fibres. 108

Table 6.1 Mass loss of PP component after treated with toluene. 115

Table 6.2 Viscosity ratio of PA6 and PP and expected morphology for the hybrid fibres. 117

Table 6.3 Percentage of fibres diameter reduction after drawing. 120

Table 6.4: Results of DSC test on as-spun PA6:PP hybrid fibres (untreated).....126

Table 6.5: Results of DSC test on as-spun PA6:PP hybrid fibres (treated).....126

Table 6.6 Thermal degradation of as-spun PA6:PP hybrid fibres (untreated and treated). 128

Table 6.7 Tex of the as-spun and drawn PA6:PP fibres.....140

List of Figures

Figure 2.1 Ring opening polymerisation of PA6 (Richards, 2005).....9

Figure 2.2 Interaction of water molecules with PA6 polymer (Reimschuessel, 1998). 9

Figure 2.3 Stress strain diagram of PA6 filaments at different draw ratio (Reimschuessel, 1998).....11

Figure 2.4 Principle of synthetic fibres production (Imura et al., 2014). 14

Figure 2.5 Shapes of spinneret holes and as-spun fibre cross-sections (NPTEL, 2013). 15

Figure 2.6 The cross sectional view of 4DG™ fibre (Fiber Innovation Technology, 2015).....15

Figure 2.7 Different mechanism used to produce various types of bicomponent fibre a) core/sheath, b) side by side, c) pie wedge and d)island in the sea (NPTEL, 2013).....17

Figure 2.8 Types of bicomponent fibres a) side-by-side, b) core-sheath, c) pie-wedge, d) island-in-the-sea (Ayad et al., 2016).....17

Figure 2.9 Cross sectional view of the high surface area filament (Pourdeyhimi and Chappas, 2012).....20

Figure 2.10 Schematic diagram of two immiscible polymer blend fibre with different composition of polymer A and polymer B: *left*- polymer A as a major component, *middle*- co-continuous phase when the composition of two polymers almost in the same amount, *right*- polymer A as a minor component.....22

Figure 2.11 Size of disperse phase based on polymer viscosity.....23

Figure 2.12 Size of disperse phase based on dispersed phase content.....23

Figure 2.13 Size of disperse phase based on shear rate.....24

Figure 2.14 Basic chemistry of thermoplastic polyurethane (Huntsman, 2010). 25

Figure 2.15 Schematic diagram of polymer melt extrusion. 32

Figure 2.16 Different types of rotating screw (top view); a) single screw, b) twin screw. 32

Figure 2.17 The movement of high viscosity polymer in an extruder. 33

Figure 3.1: Preparation of fibres for cross-section view under LM: 1- prepare the perforated plate, 2- insert needle threader through one of the holes, 3-insert a bundle of fibres into the wire loop of the needle threader, 4- pull the wire loop and the fibres through the hole, 5- cut the fibres at both sides of the plate, 6- the cut fibres (show by arrow) ready to be viewed under LM. 39

Figure 3.2 Examples of fibre cross-section images captured by LM: a) PA6 fibres and b) TPU-D 50 untreated fibres.....39

Figure 3.3 Illustration of bulk and true cross-section area.....40

Figure 3.4 Step of measuring PA6:TPU-D hybrid fibre cross-section area in ImageJ software. 41

Figure 3.5 Example of images of a) TPU-D 50 and b) PP-60 treated fibres viewed under light microscope (*left*) and scanning electron microscope (*right*). 42

Figure 3.6 Capillary Rheometer.....42

Figure 3.7 DSC diagram.....44

Figure 3.8 Basic DSC curve diagram. 45

Figure 3.9 DSC heating curve of PA6 and PP hybrid fibres. 46

Figure 3.10 TGA diagram. 47

Figure 3.11 Example of TGA curve. 47

Figure 3.12 ATR-FTIR diagram. 48

Figure 3.13 Tenacity against elongation curve. 49

Figure 3.14 Filament drawframe.....50

Figure 3.15 Filament drawing mechanism.....51

Figure 3.16 PP-40 yarn carrier; *left*- spool and *right*-cone.....51

Figure 3.17 Twisting machine.....52

Figure 3.18 Double-bed flat knitting machine (10-gauge). 52

Figure 3.19 Template for sample size on top of the treated fabric. 53

Figure 3.20 Course and wale of knitted fabric. 54

Figure 3.21 Hanging pear loop illustration. 55

Figure 3.22 Vertical wicking test using wicking solution. 56

Figure 3.23 Vertical wicking test using water. 57

Figure 3.24 Ball burst tooling clamp (left) and ball probe (right). 57

Figure 4.1 Viscosity of PA6 and TPU-D at 230°C. 59

Figure 4.2 SEM images of PA6:TPU-D hybrid fibres and single component fibres in cross-section view (left) and longitudinal view (right).....61

Figure 4.3 Micrograph of TPU-D fibres produced at different processing temperature (range 200°C~230°C) pores appear in the fibres produced at 220°C were shown in dotted circles. 62

Figure 4.4 SEM mages of TPU-D 20 fibres produced at different screw speed in cross-sectional view (top) and fibre longitudinal view (bottom). 64

Figure 4.5 SEM images of TPU-D 20 produced at different winder take-up speed in cross-sectional view (top) and fibre longitudinal view (bottom).....64

Figure 4.6 Micrograph of TPU-D 20 (upper) and TPU-D 50 (lower) before (left) and after treatment with DMSO for 3h (middle) and 24 h (right). 66

Figure 4.7 SEM images of PA6:TPU-D hybrid fibres after 24 h treatment in DMSO in cross-sectional view (upper) and longitudinal view (lower). 67

Figure 4.8 SEM images of TPU-D 50 after treated with formic acid for 3 and 24 h in cross-sectional view (upper) and longitudinal view (bottom). 68

Figure 4.9: Fibre morphology of TPU-D 50 before and after treatment in formic acid. 69

Figure 4.10 Micrograph of PA6, TPU-D, TPU-D 20 and TPU-D 50 fibre cross-section. 69

Figure 4.11 Fibre cross-section and pore area of the single component and hybrid fibres (bulk and true area). (*n*=30) 70

Figure 4.12 Fibre diameter of the PA6:TPU-D hybrid fibres and single component fibres. 71

Figure 4.13 Frequencies of the pore size developed in TPU-20 and TPU-50 fibres from 30 specimen for each. (n_{PA6-50}=1046, n_{PA6-80}=1170) 72

Figure 4.14 Porous fibres using freezing spinning method. (Cui et al., 2018).....73

Figure 4.15 DSC curve of the fibres in a) heating and b) cooling cycle.....74

Figure 4.16 DSC curve of hybrid fibres before and after treatment with DMSO in a) heating and b) cooling cycle. 77

Figure 4.17 TG (top) and DTG (bottom) curve of hybrid fibres before and after treatment. 78

Figure 4.18 XRD results of (top)-single component fibres and hybrid fibres, (middle)-TPU-D 20 and (bottom)-TPU-D 50 hybrid fibres untreated and treated with DMSO. 80

Figure 4.19 The FTIR spectra of PA6:TPU-D hybrid fibres and single component fibres (normalised at 2866 cm^{-1}). 81

Figure 4.20 Carbonyl region of the FTIR spectra for TPU-D and hybrid fibres (normalised at 2866 cm^{-1}).....83

Figure 4.21 FTIR spectra of PA6 crystal form (α and γ-crystal) in the fibres.....84

Figure 4.22 Mechanical properties of PA6, TPU-D and hybrid fibres. (*n*=10) 85

Figure 4.23 Tenacity vs elongation curve of PA6, TPU-D and hybrid fibres. 86

Figure 4.24 Mechanical properties of the TPU-D fibres produced at different processing temperature (200 and 230 °C). 87

Figure 4.25 DSC curve of the PA6 and TPU-A 20 hybrid fibres untreated and treated. 89

Figure 4.26 SEM images of TPU-A 20 hybrid fibres: (left) untreated and (right) treated in DMSO.....90

Figure 4.27 ATR-FTIR spectra of the PA6, TPU-A and TPU-A 20 untreated and treated. 91

Figure 4.28 Carbonyl group spectra of: (top) PA6, TPU-A, TPU-A 2- untreated and TPU-A 20 treated and (bottom) larger image for the PA6, TPU-A 20 untreated and TPU-A 20 treated. 93

Figure 4.29 Tenacity and elongation of the PA6, TPU-A and TPU-A 20 untreated and treated fibres. 94

Figure 4.30 Tenacity vs elongation representative curve of PA6, TPU-A and TPU-A 20 untreated and treated fibres. 95

Figure 5.1 Viscosity of PA6 and PET at 270 °C. 97

Figure 5.2 Cross section view of the PA6:PET hybrid fibres (taken using Leica Microscope). 100

Figure 5.3 SEM images on PET-50 and PET-60 hybrid fibres before treatment. 101

Figure 5.4 Morphology of PA6:PET hybrid fibres. 102

Figure 5.5 SEM images of PA6:PET hybrid fibres after PET etched in NaOH. 102

Figure 5.6 PA6:PET hybrid fibres diameter. 104

Figure 5.7 Diameter of PA6 fibrils. 104

Figure 5.8 DSC curve of PA6 and PET single component fibre (cooling and second heating cycle). 105

Figure 5.9 DSC second heating curves of PA6:PET hybrid fibres (untreated and treated). 107

Figure 5.10 DSC cooling curves of PA6:PET hybrid fibres (untreated and treated). 107

Figure 5.11 Mechanical properties of PA6:PET hybrid fibres; tenacity (top), elongation (middle) and Young modulus (bottom). 109

Figure 5.12 Tenacity vs elongation at break of PA6:PET hybrid fibres. 110

Figure 6.1 Shear viscosity of PA6 and PP pellets at 230 °C. 113

Figure 6.2 SEM images of PA6:PP hybrid fibres before and after treated (cross-section and longitudinal view). 114

Figure 6.3 Illustration of PA6:PP hybrid fibre structure in different weight compositions. 115

Figure 6.4 SEM image of PP-50 showing phase separation between PA6 fibril and PP matrix. 116

Figure 6.5 Diameter of as-spun and drawn PA6:PP hybrid fibres (untreated). 118

Figure 6.6 Diameter of as-spun and drawn PA6 microfibres (treated). 118

Figure 6.7 Microscopy images of as-spun PA6:PP hybrid fibre. 119

Figure 6.8 Microfibres diameter distribution of PA6 microfibres (as-spun and drawn fibres). (*n*=50) 121

Figure 6.9 DSC curves on second heating cycle of PA6:PP hybrid fibres (as-spun and treated fibre). 123

Figure 6.10 DSC curves on cooling cycle of PA6:PP hybrid fibres (as-spun and treated fibre). 125

Figure 6.11 Thermal degradation of as-spun PA6:PP hybrid hybrid fibres. 127

Figure 6.12 Derivative weight curve of as-spun PA6:PP hybrid fibres. 127

Figure 6.13 Illustration of PP-35 fibre morphology. 128

Figure 6.14 Thermal degradation of PA6:PP hybrid fibres (untreated and treated). 129

Figure 6.15 Derivative weight curve of PA6:PP hybrid fibres (untreated and treated). 129

Figure 6.16 FTIR spectra of PA6:PP as-spun hybrid fibres and single component fibres untreated and after treated in toluene. (Normalised at 1634 cm^{-1})..... 131

Figure 6.17 Tenacity of as-spun and drawn PA6:PP hybrid fibres (untreated and treated). 133

Figure 6.18 Tenacity-elongation curve of as-spun PA6:PP hybrid fibres(untreated and treated). 135

Figure 6.19 Tenacity-elongation curve of drawn PA6:PP hybrid fibres (untreated and treated). 136

Figure 6.20 Elongation at break for as-spun and drawn PA6:PP hybrid fibres (untreated and treated). 138

Figure 6.21 Initial Young's modulus of as-spun and drawn PA6:PP hybrid fibres (treated and untreated). 139

Figure 7.1 Paper spool (left) and cone (right). 142

Figure 7.2 PP-40 circular plain jersey knitted fabric before treatment. 143

Figure 7.3 PP-40 circular plain jersey knitted fabric after treated with toluene..... 143

Figure 7.4 The structure of PP-40 knitted fabric untreated (a, b & c) and treated (a', b' & c') viewed under light microscope (a,b, a' & b') and SEM (c & c'). 144

Figure 7.5 Mass and thickness of untreated and treated PP-40 fabric..... 145

Figure 7.6 Courses, wales and stitch density of untreated and treated PP-40 fabric. 146

Figure 7.7 Ball burst strength of the PP-40 untreated and treated fabrics. 147

Figure 7.8 Example of PP-40 treated fabrics after ball burst strength test. 147

Figure 7.9 The representative curve of force vs extension of PP-40 untreated and treated fabrics. 148

Figure 7.10 Vertical wicking results of PP-40 treated fabrics. 149

Figure 7.11 Bending length of PP-40 fabrics. 149

Chapter 1
Introduction

1.1 Overview

Textile waste has been an issue around the world with 92 million tonnes waste recorded in 2015 (Global Fashion Agenda and The Boston Consulting Group, 2017). With the increasing demand on textiles, the amount of waste generated is expected to increase up to 148 million tonnes by 2030. At the moment, only 25% of the waste is recovered via reuse and recycling route where most of it either incinerated for energy recovery or send off to landfill (Ellen MacArthur Foundation, 2017). Over two-third of textile raw materials are produced from plastic sources, hence incineration or landfill disposal has negative impacts on the environment.

Reuse and recycling can be the preferred option for textile waste. By reusing the product, the life of the product can be extended and the landfill can be avoided. However, recycling is needed for the products that are no longer useable. Four types of recycling approaches can be applied to textile waste; fabric recycling, fibre recycling, polymer recycling and monomer recycling (Ellen MacArthur Foundation, 2017; Sandin and Peters, 2018). The most widely adopted recycling approach in the industry are fabric and fibre recycling. Meanwhile for polymer and monomer recycling, the fibre production is limited to single component polymers such as polyethylene terephthalate (PET) or known as polyester fibres, Polyamide 6 (PA6), and cellulose-based fibres (Palme et al., 2017).

Even though the efforts to recycle the textile wastes into textile fibres have been in place, the conversion of textile waste into materials for clothing is extremely low (<1%) (Ellen MacArthur Foundation, 2017). The nature of textiles products that usually consists of more than one material, either by using blended yarns (e.g. polyester/cotton yarns), bicomponent fibres (core-sheath, pie-wedge, island in the sea types, etc.) or fabric coated with polymer, limits the recycling process. The mix-material products result in complex waste where component polymers cannot be practically separated by commercially relevant technologies. The sorting and separation of mix-materials waste into single component polymers is challenging and results in unsuitability of a large proportion of waste for recycling. There is a paucity of technologies and facilities to sort and separate the mixed waste materials also limits the potential of recycling multi-component products (Östlund et al., 2015).

As most of the textile products are made from plastic sources, thermo-mechanical processing can be used to recycle mixed-waste product. The mixed-waste can be directly blended, melted and re-extruded to produce blended fibres. The mixing of two different polymers is called binary blending and three different polymers is ternary blending. In polymer blends, selection of polymers, blend composition, the viscosity of the polymers and processing conditions affect the morphology and subsequently the properties of the blended fibres. In textile industry, common polymers used to produce synthetic fibres are polyethylene terephthalate (PET) (51%), polypropylene (PP) (~5%) and polyamide (PA) (5.4%) (Textile Exchange, 2018).

The possibility of mixed-waste textile product containing these polymers are high. For examples, polyamide and polyester were commercially produced as bicomponent fibres (Radici Group, n.d.). In carpet industry, polyamide was used as a face fibres and polypropylene as a bottom layer or backing fabric. Marine products such as inflatable raft and life jacket use polyamide as a base fabric and coated with polyester or thermoplastic polyurethane to make it durability against water (Erez, 2018). Complex materials exist in textiles result to the mixed-waste materials once entered the recycling centre. Even for textiles made from a single component, when collected as a waste, can also be mixed with varieties of other textile sources.

Among common synthetic polymers used for textile fibres, polyamide is considered as an expensive polymer (USD2.32-2.42/kg) compared to PET (USD1.22-1.23/kg) (YNFX, 2020).Over 4.55 million tonnes of polyamide was produced in 2014 (Wesołowski and Płachta, 2016). Two types of polyamide frequently use as textile fibres are PA6 and PA6,6 with PA6 dominates the usage in apparel industry (86%) compared with PA6,6 (14%) (Wesołowski and Płachta, 2016).

PA6 or also known as nylon 6 is widely used in many applications such as apparel, carpet, parachute fabrics, tire cord, ropes and tents (Wesołowski and Płachta, 2016). Increasing demand of polyamide products contribute to the abundance of polyamide waste too. For example, carpet which contains approximately 24% of PA6 fibres, is thrown to landfill every year. Fibre grade PA6 is a high value thermoplastic polymer that has a low rate of degradation in landfill. Therefore, to avoid landfill, another option for PA6 waste is by recycling the PA6 containing products. Several studies have shown that reprocessing PA6 fibres into several cycles can be done successfully. However, the repetitive process of melting PA6 fibres may slightly decrease the mechanical properties and stability of the polymer (Tuna and Benkreira, 2017).

Polyamide and other thermoplastic textiles polymers can be processed several times. Recycling the mixed-waste containing different thermoplastic polymers without separation process can be done by thermo-mechanical recycling. Two polymers can be melted and extruded into new hybrid fibres. Blending of PA6 with other materials such as acrylonitrile–butadiene–styrene (Aparna et al., 2017) (ABS) cellulose acetate butyrate (CAB) (Zhang et al., 2015) and chitosan (Dotto et al., 2017) into hybrid fibres were studied previously.

Blending of two different polymers can create interacting and non-interacting behaviour of the polymer blend. Amide group of PA6 and urethane group of TPU create interaction through hydrogen bonding. Non-interacting behaviour was found on the blending of PA6:PET and PA6:PP due to low chemical interaction (Hajiraissi et al., 2017). To improve the interaction on PA6:PET and PA:PP, compatibiliser was used (Aparna et al., 2017). However, the non-interacting behaviour of these polymers can benefit in the production of microfibres or nanofibres.

A study on the interacting and non-interacting behaviour of possible polymers found in textile waste was crucial. There is a paucity of reported work on the blending of polyamide with TPU as hybrid fibres when prior research focused on composite (Cai et al., 2019), injection moulding (Xu et al., 2019) and compressed moulding (Rashmi et al., 2017). Blending of PA6:PET and PA6:PA6 was studied before however focusing on addition of compatibiliser for improving of interfacial connection and the optimisation of the blend focus on PET and PP in the blend (Aslan et al., 1995; Liao et al., 2015; Aparna et al., 2017; Hajiraissi et al., 2017). With the increasing of textile waste collected and lack of technologies to separate the waste, added with high price of PA6, a study on the PA6 blending with other polymers into fibres is needed.

1.2 Research aim and objectives

The aim of this research is to investigate the effect of blending of PA6 polymer with interacting and non-interacting polymer commonly used in textile fibres production. Subsequently, the developed fibres will be processed into fabric form to evaluate their performance for apparel applications. The objectives of this research are to:

i. produce interacting hybrid fibres consisting of PA6 as main polymer blending with thermoplastic polyurethane (TPU) as secondary polymer.
ii. produce non-interacting hybrid fibres consisting of PA6 as main polymer blending with polyethylene terephthalate (PET) and polypropylene (PP) as secondary polymers.

iii. Investigate the properties of the interacting and non-interacting hybrid fibres that blended in different weight composition by:
    a. removal of secondary polymer.
    b. assess the morphology of the hybrid fibres before and after removal of secondary polymer under.
    c. characterise the properties of the fibres concerning thermal, chemical and mechanical and fibre diameter.

iv. produce fabrics made of hybrid fibres and investigate the properties of the fabrics before and after removal of secondary polymer.

Chapter 2
Literature Review

Textile waste has been considered as an environmental issue. The scenario of textile waste management and current methods on recycling textile waste are presented in this chapter. Previous studies on recycling Polyamide 6 and its properties were reported. Different types of textile fibres; single and bicomponent fibres, were also discussed, including the method to produce fibres. Finally, the blending of two polymers in producing textile fibres, with melt spinning approach that is suitable for thermo-mechanical recycling of the polymer blend, will be discussed.

2.1 Textile waste

Textile waste has been an issue all around the world. It is reported that over 92 million tonnes of textile waste generated globally in 2015 and the numbers are expected to increase up to 148 million tonnes by 2030 due to growing global population (Global Fashion Agenda and The Boston Consulting Group, 2017). In UK alone, 921,000 tonnes of textile waste collected in 2017 which end up in landfill (WRAP, 2019).

Textile waste can be divided into two categories: pre-consumer waste and post-consumer waste. Pre-consumer waste refers to by-product materials generated by textile industries such as surplus fabrics, yarns and fibres, whereas post-consumer waste is contributed by the owners of textiles including clothing and textile household such as bed linen, curtains, towels and floor covering (Echeverria et al., 2019).

Textile waste can be either reused, recycled, incinerated or sent off to landfill. Almost 55% of textile waste collected in UK was sent to landfill and only 36% was recovered through reuse and recycling process (WRAP, 2019). Most of the waste was reused domestically through second hand or charity shop or exported to developing countries. Only small proportion of the waste was recycled, currently into down-cycle application such as wiper, insulation materials and padding mattress while less than 1% of the waste was recycled back into textile fibre (Ellen MacArthur Foundation, 2017).

The route of the textile waste can be improved, to conserve the resources. The unwanted clothes, mostly exported to third-world country where there are no proper recycling and collecting facilities, will end up wasting the valuable materials into landfill. Moreover, in 2015, East African Community announced to ban an importation of used clothing that will affect the utilisation of the collected textile waste in the future (SMART Secondary Materials and Recycled Textiles, n.d.).

Over two-third of textile raw materials derived from petroleum resources have high compostable times in landfill, compost and aquatic environments. The risk of harmful gas emission to the atmosphere such as methane (CH_4) and carbon dioxide (CO_2) is also a significant concern (UNEP, 2002). Department for Environment Food & Rural Affairs (DEFRA, 2013) estimated that 3 tonnes of CO_2 can be saved with reusing or recycling of 1 ton of general waste. Sending off the waste into landfill or incinerating bring harmfulness to the environment and contribute directly to the global climate change. The more optimum option for handling the waste is either reuse until the end of product life or recycling.

2.2 Textile recycling

Textile recycling industries were developed with a target to reduce both pre-consumer and post-consumer wastes and conserve resources while minimising the amount of waste going to landfill (Echeverria et al., 2019). Moreover, most of the textile products are recyclable and have a potential to replace virgin materials. The UK government has also been promoting recycling as more and more waste has been directed towards landfills. Approximately GBP 82 million were spent on disposing the textile waste in landfill (Ellen MacArthur Foundation, 2017). Serious actions have been taken to emphasise recycling such as increasing the landfill tax. It was expected that by 2030, municipal waste including textile waste sent to landfill will reduced to 10% (Bukhari et al., 2018).

Several organisations are involved in recycling textile waste such as Waste & Resources Action program (WRAP), Department for Environment, Food & Rural Affairs (DEFRA) and Carpet Recycling United Kingdom (CRUK). WRAP has launched several plans to promote the usage of textile waste such as European Clothing Action Plan, Sustainable Clothing Action Plan (SCAP) and Love Your Clothes campaign to raise awareness of the value of clothing. CRUK focuses on carpet recycling and acts as a centre and connector for companies and organisations involved in carpet recycling. The target is to decrease the number of carpet waste that goes to landfill and develop close loop recycling of carpets.

London based company Worn Again have a collaboration with several companies to develop FIBERSORT technology with the aim to produce an automated sorting technology that can sort a variety of post-consumer textile waste (Worn Again, 2016). These show that the effort has been made by the private sector to emphasise on the recycling industry. However, these examples limit the recycling effort only onto a single component polymer. Textiles waste consists of mix-materials that encounter

difficulties to be sorted and separated were send off to other easier route either landfilled or incinerated (Robert, 2016).

Textile recycling can be divided into fabric recycling, yarn and fibre recycling and polymer/monomer recycling which can be accomplished by either through mechanical, thermal, chemical processing or combination of these processing (Ellen MacArthur Foundation, 2017; Sandin and Peters, 2018).

Fabric recycling makes use of fabrics from pre-consumer waste generated by garment industries (e.g. off-cut fabrics, rejected fabrics) or post-consumer waste contributed by the users of the textiles (e.g. unwanted clothes, old clothes) and converted into new clothes or products. Tonlè, is an example of a company that produced textile products from the pre-consumer waste and managed to save 10 tonnes of waste being send to landfill in 2014 (Explorer, 2019). For fibre and polymer recycling, the methods can be simplified as mechanical recycling and chemical recycling.

2.2.1 Mechanical recycling

Fibre recycling, also referred to mechanical recycling, mechanically shredding the fabric to reclaim fibres for subsequent conversion into yarns or nonwovens. Polyester and cotton fibres, which dominantly used in textile industry were mechanically shredded during recycling process. The reclaimed cotton fibres result to shorter and lower cotton fibre quality thus produced coarser yarn count. Therefore, cotton waste was recovered into down-cycling route such as insulation materials, blankets, wipes, etc (Sandin and Peters, 2018). Pure Waste Textiles Ltd. be able to produce new 100% recycled cotton t-shirt from shredded textile cotton waste (Pure Waste Textiles, n.d.). Apart from recycling into yarn, the recycled cotton and polyester fibres were also produced into nonwoven fabrics for household application (Sharma and Goel, 2017). Low quality fibres restrict the recycling process into fibres found suitable approaches as reinforced composites(Serra et al., 2019; Meng et al., 2019), pressed into compressed mould (Dissanayake et al., 2018), sound absorption panel (Santhanam et al., 2019) or reinforced in brick or mortar (Orasutthikul et al., 2017; Kimm et al., 2018).

2.2.2 Chemical recycling

Other method for textile waste recycling is chemical recycling, either by polymer recycling or monomer recycling. Polymer recycling can be achieved by treating the fibres chemically/mechanically while keeping the polymer or oligomer intact.

Monomer recycling is a process where the polymers/oligomers are broken down to the monomer level. Textile waste consists of synthetic fibres made from thermoplastic polymers which can be chemically recycle to produce new fibres with identical properties to the virgin raw materials. ECONYL Regeneration yarn for example, was produced by recycling textile waste and fishing nets (Moorhouse and Newcombe, 2018). Some examples of regenerated fibres produced through chemical recycling were MIPAN Regen fibres, which are made by recycling PA6 post-consumer waste, REPREVE® PA6,6 fibres made of 100% recycled polyamide fabric (UNIFI, 2008) and CYCLEAD™ fabrics which are made by recycled PA6 fibres (Toray, 2007). The separation of polyester from cotton/polyester blend for example, involved chemical process such as hydrolysis and dissolving in solvent (Ling et al., 2019).

2.3 Polyamide

Polyamides are linear macromolecules containing amide (-CONH-) linkage. Two popular variances in the textile and plastic industries are PA6 and PA6,6. Other popular polyamides available commercially are polyamide 11, 12, 46 and 69. PA6 widely used in the apparel industry (86%) compared to PA6,6 (14%) (Wesołowski and Płachta, 2016). In this study, the research will concentrate on the polymer derived from PA6 which is mainly used for clothing.

PA6 or polycaprolactam is made by ring opening polymerisation of caprolactam monomer. The ring opening of ε-caprolactam monomer occurs when the monomer is heated at 250-280°C at atmosphere pressure for 12-24 hrs as shown in Figure 2.1 (Richards, 2005) and the complete process of ring opening can be seen in Appendix A. The polymerisation could be initiated by water, acid or very strong base such as sodium hydride (NaH), but water is the favoured option in the industry (Richards, 2005). The amide bonds (-CONH-) developed lactam provide hydrogen bonding between chains hence contribute to the excellent properties of PA6 such as stiffness and toughness (John and Furukawa, 2012). The H-bonds also make the PA6 categorised under hygroscopic material as water molecules can form H-bonds with the amide groups as shown in Figure 2.2 (Reimschuessel, 1998).

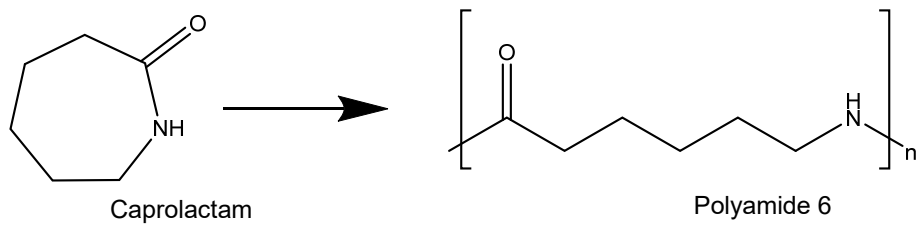

Figure 2.1 Ring opening polymerisation of PA6 (Richards, 2005).

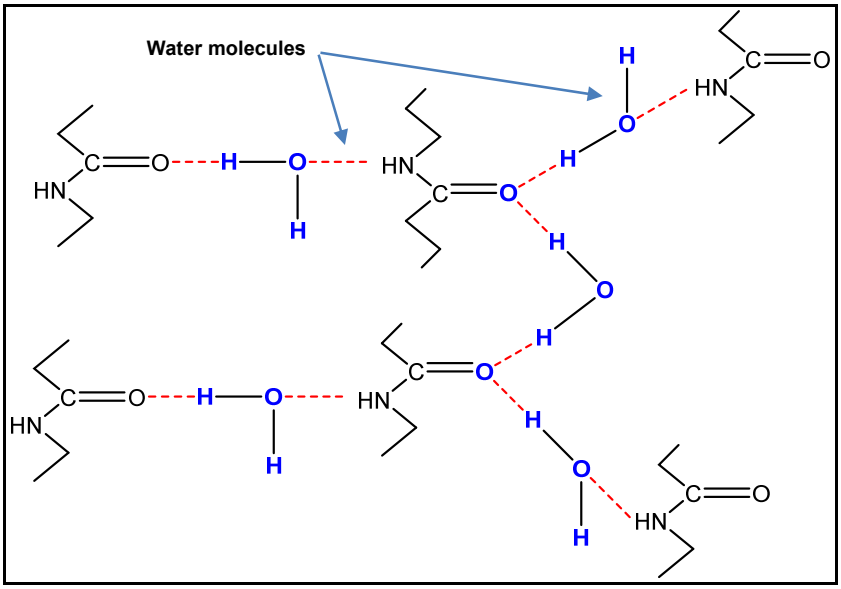

Figure 2.2 Interaction of water molecules with PA6 polymer (Reimschuessel, 1998).

The important parameter of polyamide is the molecular weight or molecular mass. Molecular weight influences the melt viscosity of the polymer namely; higher molecular weight contributed to higher melt viscosity. The melt viscosity of the polymer influences the movement of the polymer chains, namely higher melt viscosity tends to reduce the polymer chain movement (Grümer and Hopmann, 2018).

2.3.1 Polyamide 6 waste

Polyamide is a significant textile fibre with 5.7 million tonnes produced annually comprising 5.4% of the synthetic fibre market and was ranked second among all the textile fibres (Textile Exchange, 2018). The application of polyamide in textile industries is apparel, carpet and industrial filament such as tire cord and ropes (Wesołowski and Płachta, 2016).

From these applications, carpet waste can be collected easily and the amount is significant. The volume of carpet waste for disposal rose by 400,000 tonnes every year in the UK alone (Hilton et al., 2019). Carpet is classified as textiles and is extensively used in buildings and automobile as well as in aircrafts. The surface of carpet acts as a feet insulator from cold floor, sound proof and also adds to the décor of a room. 698 million m^2 of new carpets were produced in the United Kingdom in 2016 to replace the old carpets(Hilton et al., 2019). The huge quantity of fibres consumed to produce carpets lead to an enormous volume of waste, which dominant by nylon fibre (50-70%) (Mohammadhosseini et al., 2018).

2.3.2 Recycled polyamide 6 fibres

Early work on the extrusion of polyamide waste into filaments was conducted by Esfahani (1983) which reported that re-extrusion of PA6 and PA6,6 waste polymers up to 5 cycles is possible. A study conducted by Meyabadi et al. (2010) also showed that PA6 waste can be recycled into filaments. The blending of recycled PA6 with virgin PA6 showed an improvement in the tensile and thermal properties of recycled PA6. Other than the above, to the best of authors' knowledge, there is no published work on the recycling of polyamide waste into PA6 filaments or fibres. Other studies on this domain focused on the reprocessing of polyamide waste via injection moulding up to 16 cycles (Su et al., 2007; Crespo et al., 2013; Grümer and Hopmann, 2018). These studies proved that recycling the polyamide waste into multiple processing cycles are achievable. Besides, polyamide waste polymers were recycled into reinforced composites (Pan et al., 2016; Hasan et al., 2018), cement mortar and concrete reinforcement (Orasutthikul et al., 2017).

2.3.2.1 Mechanical Properties

The common tensile properties for filaments or fibres are tenacity, initial modulus, breaking elongation and work of rupture. Polyamide's relative mass, the extrusion speed, draw ratio, and heat treatment influence the tensile properties of the fibres.

Early study conducted by Esfahani (1983) on the recycling PA6 fibres found that the tenacity of PA6 fibre decreases slightly with the increasing number of cycles with 48.7 $cNtex^{-1}$ ($5.5gd^{-1}$) and 43.7 $cNtex^{-1}$ (4.94 gd^{-1}) reported for the first and fifth cycle respectively. The other tensile properties (the work of rupture, Young's modulus and breaking elongation) also show a similar trend to that of tenacity. Similarly, the study done by Meyabadi et al. (2010) also suggest that the tensile strength and modulus of recycled PA6 fibres are slightly lower than the virgin PA6 fibres. The loss of the

molecular weight during spinning process might influence the tensile strength for recycled PA6 fibres. In contrast, it was reported that the tensile strength of recycled PA6 slightly increases with increasing number of cycles when processed via injection moulding (Lozano-González et al., 2000; Su et al., 2007). However, opposite results were reported for elongation where almost 70% reduction occurred; this might be due to degradation of the PA6 polymer after 10 processing cycles which results in the reduced molecular weight of the polymer (Lozano-González et al., 2000; Crespo et al., 2013).

The tensile strength of PA6 filaments also depends on the draw ratio (D/R) during the spinning process. The ratio between 1 and 2.5 gives plasticity and ductile properties to the material, while D/R ratios higher than 2.5 turn the PA6 into brittle material (Reimschuessel, 1998) as shown in Figure 2.3. It was mentioned that higher draw ratios give higher tenacity and initial modulus but decrease the elongation and work of rupture of the fibres (Rahbar and Mrm, 2011). The increasing value of tenacity and modulus is because of the increase in orientation and crystallisation of the filaments during the drawing process (Ali, 2019).

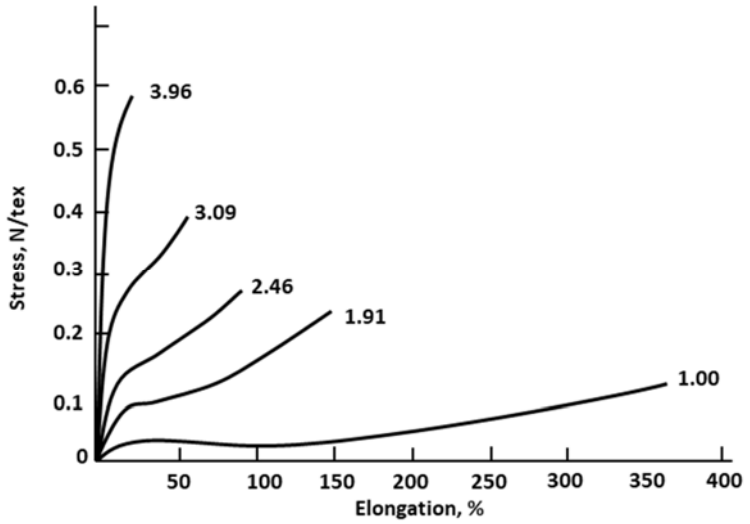

Figure 2.3 Stress strain diagram of PA6 filaments at different draw ratio (Reimschuessel, 1998).

2.3.2.2 Chemical Properties

There are several factors could affect the chemical properties of polyamide: exposure to heat, oxidation, exposure to certain alkalis, acids and solvents that can lead to degradation of polyamides (Reimschuessel, 1998; Richards, 2005). In the production of PA6 fibres, the drying process of PA6 chips before extrusion and the spinning

process itself exposes the polymer to heat and oxygen; this exposure can cause deterioration of the PA6 polymer. Reprocessing PA6 waste multiple times expose the polymer to more heat and oxygen thus effecting their chemical properties. Several studies reported that the molecular weight and the melt viscosity of PA6 decreases with each processing cycle (Su et al., 2007; Meyabadi et al., 2010; Crespo et al., 2013); this is because of the molecular chain scission (Su et al., 2007; Crespo et al., 2013). The presence of moisture in the PA6 polymer gives plasticiser properties and also causes a reduction in the viscosity (Crespo et al., 2013). The loss of molecular weight, reduction in viscosity and molecular chain scission suggest that the chemical properties of recycled PA6 change after every reprocessing cycle and lead to the degradation of the polymer.

2.3.2.3 Thermal Properties

Studying thermal properties of PA6 polymer is necessary to identify suitable condition for fibre and fabric production and to find the relationship between structure and crystallinity of the fibre (Ali, 2019). The melting temperature (T_m) and glass transition temperature (T_g) are of significant importance.

Glass transition temperature (T_g) is the starting point of transition from glass to rubbery phase whilst the melting temperature (T_m) is where the polymer changes from a solid phase to a liquid phase entirely. For PA6, the T_g *and* T_m usually happened in the range of 40-55 °C and 215-220 °C, respectively. After recycling, the melting temperature remains constant after one cycle while the glass transition temperature decreases 13% compared to virgin PA6 (Meyabadi et al., 2010). A study by Su et al. (2007) reported that the melting temperature slightly decreases after 16th reprocessing cycle. Not much work has been published on the melting temperature of recycled PA6.

PA6 is a semi crystalline polymer which consists of amorphous and crystalline regions. PA6 comprises of α and γ crystals which makes it different from PA6,6 which only has α crystal form. After the recycling process, the crystallinity of PA6 increases due to three factors: the presence of impurities which increases the nucleation, memory effects of thermal and mechanical stress histories and lower chain length during recycling process that increases the polymer chain mobility (Crespo et al., 2013). The as-extruded PA6 contains a mixture of amorphous and crystalline regions with poor order and orientation. In the drawing process the molecules orientate themselves parallel or almost parallel to the fibre axis (Ali, 2019).

There are several methods that can be used to study the thermal properties of the PA6 such as differential scanning calorimetry (DSC), thermomechanical analysis (TMA) and dynamic mechanical analysis (DMA).

2.4 Textile fibres

Textile fibres are the key element in producing various types of textile products. The fibres can be categorised into natural or synthetic fibres. Natural fibres such as cotton, wool and silk come from nature resources either plant or animal based, where the fibre properties are varying depend on nature given. Synthetic fibres such as polyamide and polyester which commonly produced from fossil fuel, are man-made fibres with the fibre properties can be controlled during fibre production. The synthetic fibres can be produced either as a single component or bicomponent fibres. The shape of the fibres is generally round in shape but non-circular cross section fibres were also produced for certain application.

2.4.1 Single component fibres

Synthetic fibres generally produced by extruding a polymer liquid through a spinneret to form continuous long fibres called filaments. The spinneret can consist of single hole or up to several hundred tiny holes. The size of the spinneret influences the shape and diameter of the extruded fibres. Fibres with diameter less than 1 denier (approximately ~10 μm) is called microfibres. Fibres that is less than 1000nm is called nanofibres with <100nm is called true nanofibres and other diameter is called fibres. The fibres can be produced using melt spinning for thermoplastic polymer such as polyester and polyamide, or wet spinning, dry spinning and electrospinning for non-thermoplastic polymer such as rayon, modacrylic and spandex. Figure 2.4 shows the principle of producing synthetic fibres.

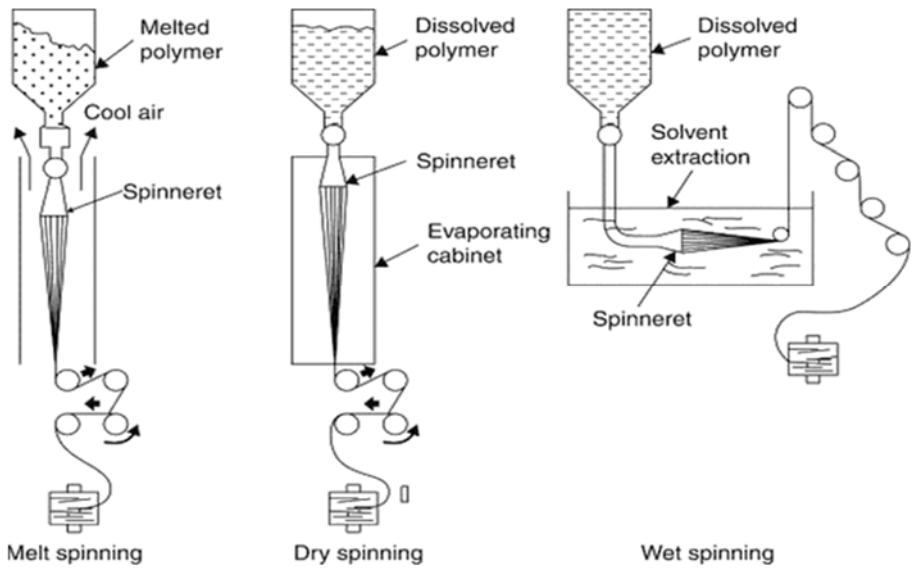

Figure 2.4 Principle of synthetic fibres production (Imura et al., 2014).

The properties of filaments or fibres can be modified by changing the cross sectional shape of the filaments or the fibres. The typical cross section of the synthetic filaments are circular, however, non-circular cross section (NCCS) fibres can give definite novel properties to the fibres.

Some examples of NCCS of filaments are shown in Figure 2.5. The contour shape of NCCS filaments could increase the bulk of the resultant fabric, trap soil and dust, give lustre effect, improve moisture transportation and can act as heat and sound insulator. Most of the NCCS filaments were produced by changing the spinneret orifice shape to the required NCCS filament shape. However, the final shape of the filaments does not always correspond to the spinneret orifice shape; this is due to extrudate swell that occurs when a viscoelastic polymer (melt or solution) emerges from the spinneret (Yousefi et al., 2018).

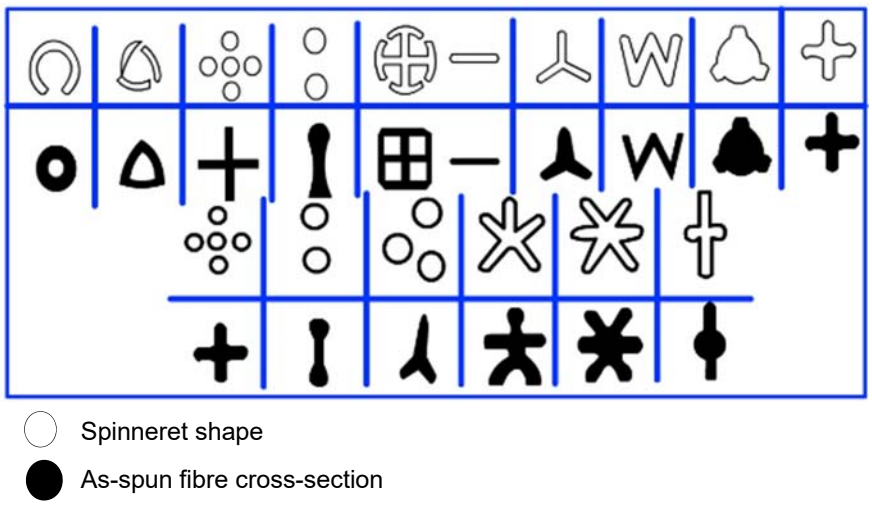

Figure 2.5 Shapes of spinneret holes and as-spun fibre cross-sections (NPTEL, 2013).

The NCCS filaments have larger surface area in comparison to round or nearly round filaments as the additional contours of the filaments create extra surface for a given mass. The Eastman Chemical Company has developed and commercialised their 4DG™ fibre which has eight deep grooves and several arms that are useful for thermal insulation, filtration, and moisture transportation (Fiber Innovation Technology, 2015) as shown in Figure 2.6. The fibre was produced by using a unique spinneret design and limiting the capacity for the exudate to swell and contract to a circular geometry. There are however several disadvantages of this fibre (Pourdeyhimi and Chappas, 2012). The 4DG™ fibre cannot be spun less than 50 to 60 µm, therefore this limits the end application of the fibre. Additionally, the arms of the fibre often break and sometimes interlock with each other during spinning process resulting in low surface to volume ratio (Pourdeyhimi and Chappas, 2012).

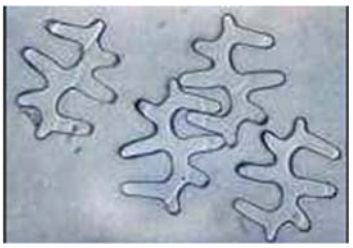

Figure 2.6 The cross sectional view of 4DG™ fibre (Fiber Innovation Technology, 2015).

2.4.2 Bicomponent fibres

Bicomponent technology has been used widely to increase the performance of synthetic polymer. Two different polymers were melted separately to create

bicomponent fibres (see Figure 2.7). Several type of bicomponent fibre shapes are available such as side-by-side, core-sheath, island-in-the-sea and pie-wedge as shown in Figure 2.8 (Ayad et al., 2016). The side-by-side shape used to create crimp in the fibre, with one of the polymer shrinks more than the other when exposed to heat. The core-sheath types can be used in thermally bonded nonwoven fabrics; the outer component has low melting temperature and act as adhesive when subjected to appropriate heat. The pie-wedge and island-in-the-sea fibre types use two incompatible polymers which can be split after extrusion using mechanical, thermal or chemical method and produced fine fibres or microfibres (Ayad, et al., 2016). Core-sheath types fibre produced single hollow fibres while multiporous fibres can be found in natural fibres such as sisal, kenaf, jute, abaca, tampico, curaua and coir with pore diameter in the range of 3 to 8 μm (details in Table 2.1)

Bicomponent fibres are also produced using melt spinning method with additional mechanisms such as by using 2 or 3 different extruders to produced core/sheath bicomponent fibres (Ayad et al., 2016) or changing the shape of spinneret holes for noncircular cross section fibres (Bunge et al., 2018). Examples of spinneret shapes are shown in Figure 2.5.

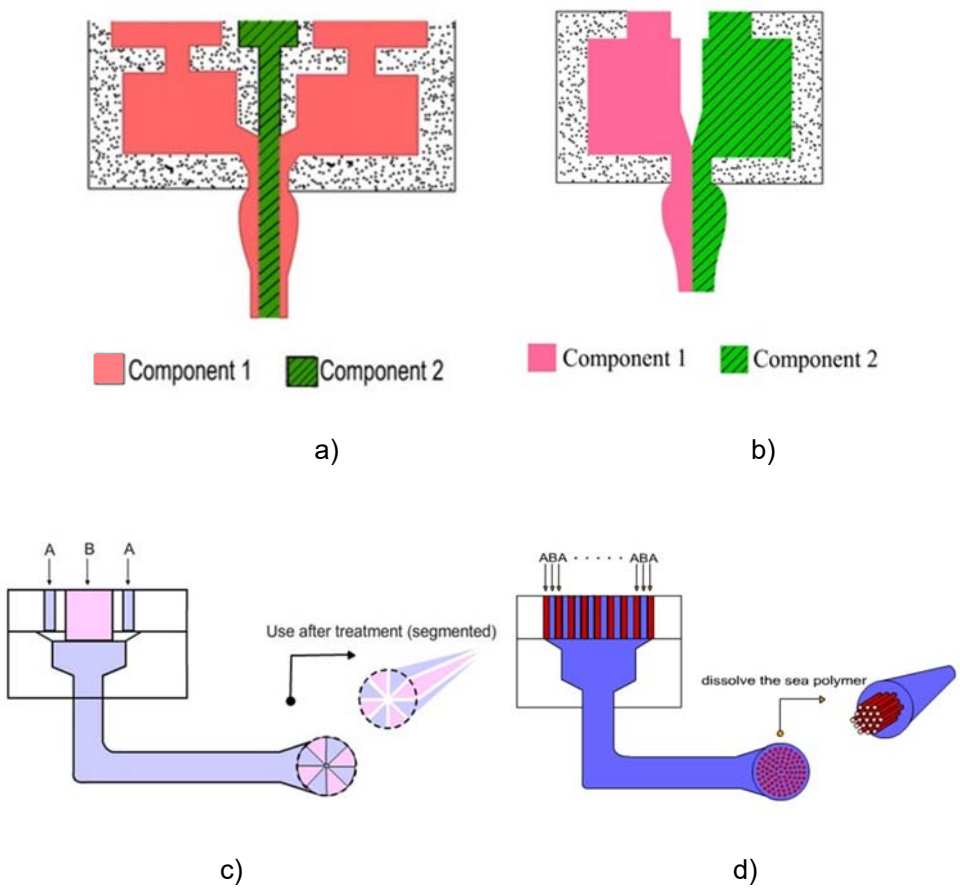

Figure 2.7 Different mechanism used to produce various types of bicomponent fibre a) core/sheath, b) side by side, c) pie wedge and d)island in the sea (NPTEL, 2013).

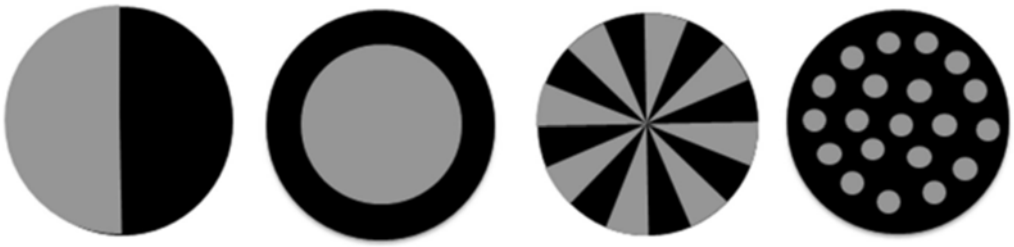

Figure 2.8 Types of bicomponent fibres a) side-by-side, b) core-sheath, c) pie-wedge, d) island-in-the-sea (Ayad et al., 2016).

Table 2.1 Porous fibres and fibre diameter.

Fibre	Cross-section view	Fibre diameter (μm)	Pore/lumen diameter	Application	Tensile strength (MPa)	Reference
Sisal	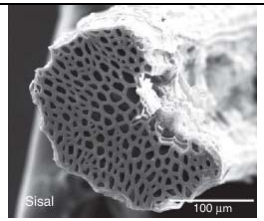	15-30	8	Ropes, strings, bag fabrics, plaiting, mat, fishnet	484±135	(Alves Fidelis et al., 2013)
Kenaf	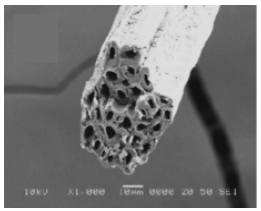	13-20	3-7	Paper, rope, wound dressing fabric		(Kim et al., 2011)
Jute	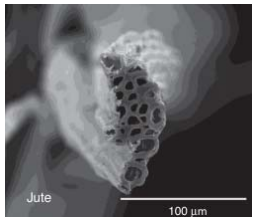	15-35	6.7	Sack, packaging, conveyor belt, upholstery, decorative fabrics	249±89	(Kicińska-Jakubowska et al., 2012; Alves Fidelis et al., 2013)

Abaca	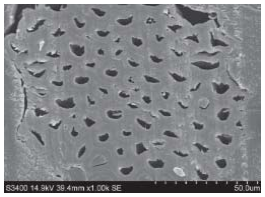	10-30		Plaiting, thicj fabric, fishnet, sail, ship rope, paper, construction board		(Kicińska-Jakubowska et al., 2012)
Tampico	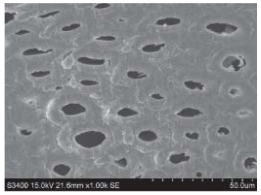	20-30		Ropes and cords, brooms and brushes, filing for mattresses		(Kicińska-Jakubowska et al., 2012)
Curaua	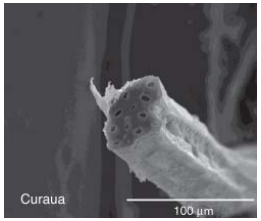	26-64	4.0	Dashbords, ropes, threads, net	543±260	(Alves Fidelis et al., 2013)
Coir	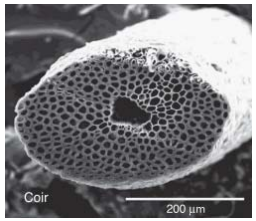	10-16		Brushes, mattresses, bags, ropes, automotive industry	90±35	(Alves Fidelis et al., 2013)

The *Monvelle* produced by Monsanto (now known as Solutia) is an example of commercial side-by side bicomponent fibre using PA6 and polyurethane (Saunders et al., 1975). This fibre were used in hosiery products develops crimp when the fibres immersed in hot water. Another example of commercial PA6 bicomponent fibre is *Sideria* produced by Kanebo; this is a core-sheath bicomponent fibre with PA6 and polyurethane (Kanebo, 2007). This fibre is also used in hosiery products. Other than that, bicomponent fibres PA6/PP core/sheath (Bosak, 2005; Dasdemir et al., 2012; Ayad et al., 2016) and PA6/polyethylene (PE) (Hufenus et al., 2013) were also studied.

Pourdeyhimi and Chappas (2012) patented an innovation for producing a high surface area fibre by using a bicomponent technique which has an internal (middle region) and an external sheath as shown in Figure 2.9. The internal sheath is made of thermoplastic polymer while the external sheath is manufactured from a dissolvable polymer. It was claimed that 1 to 3 denier fibres could be produced using this invention. The bicomponent fibres were produced using co-extruding or extruding two polymers from the same spinneret. The external sheath dissolves after extrusion and leaves the internal region with high surface area. The challenging part of producing this bicomponent fibre is the selection of suitable polymers for the internal and external part as well as the viscosity of both polymers. As mentioned before, the viscosity of the polymer plays an important role in the production of bicomponent fibres. The polymer viscosity influences the cross sectional shape of the fibres and the low viscosity polymers tend to encapsulate high viscosity polymers. Besides, exudate swell might affect the cross sectional shape of the middle region.

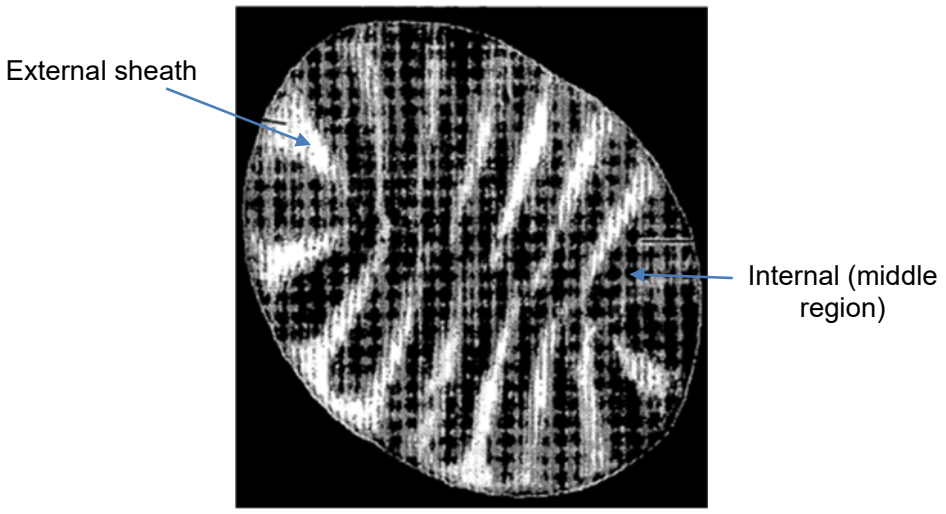

Figure 2.9 Cross sectional view of the high surface area filament (Pourdeyhimi and Chappas, 2012).

Suitable solvent could be used to dissolve unwanted polymers to produce microfibres or NCCS fibres. Producing NCCS fibres from Island-in-the-sea bicomponent fibres is one of such example and this process of producing NCCS fibres were patented by Pourdeyhimi and Chappas (2012). One component of the island-in-the-sea bicomponent fibre was dissolved in a suitable solvent where the selection of solvent depends on the polarity and the chemical nature of the polymer (Suvari et al., 2019).

Appropriate selection of polymers used in the production of bicomponent fibres is necessary to ensure the compatibility of the bicomponent fibres; this will affect the mechanical properties and interfacial morphology of the filaments. For side-by-side and core-sheath types, the interfacial adhesion between polymer surfaces determines the strength and compatibility of the bicomponent fibres (Ayad et al., 2016). The interface adhesion is influenced by the polymer's crystallisation temperature (Arvidson et al., 2012). Therefore the selection of location (core and sheath) depends on the cooling rate of the polymer. A study by Ayad et al. (2016) shows that poor adhesion occurs when PP acts as a core and PA6 as a sheath. PP which has lower crystallisation temperature than PA6 tends to shrink during cooling process thus create a gap between PP and PA6 interfacial surface. Excellent adhesion happens when the same PA6 is used as core and the PP as sheath material. Meanwhile, for pie wedge and island-in-the-sea types, incompatibility between polymers are desirable for the easier splitting process after extrusion (Wang et al., 2017a).

Polymer melt viscosity influences the cross sectional shape of the bicomponent fibres where low viscosity polymers tend to encapsulate higher viscosity polymers (Ayad, et al., 2016). The ratio of viscosity between the polymers influences the encapsulation; high ratio produces strong encapsulation, while low ratio provides weak encapsulation.

2.5 Polymer blend in textile fibre

Blending of two or more polymers are economically viable with the aim to improve the properties of the mixture, mainly in injection and compression mould industry. Polymers with different properties, when blended, produced immiscible or partially immiscible blend.

In the blending of two immiscible polymers, phase separation between polymers usually happens. Blend composition and viscosity of the polymers influence the morphology of the fibres. A major portion in the blend will act as a matrix and encapsulate minor portion as shown in Figure 2.10. Because of the phase separation,

the minor component will disperse in the major component in the form of droplet, sphere or fibril, regarding the processing condition and material behaviour. In melt spinning, there is a possibility to get a fibril form in the blend with the help of elongation forces through winding or drawing process.

When the composition of the blend is almost the same, co-continuous phase of blend can be achieved due to phase transition of the polymer. In this phase, both polymers neither act as a matrix nor a disperse otherwise interconnected to the same group and form a random morphology (Figure 2.10 *middle*). Co-continuous phase region may exhibit improvement in tensile strength and impact behaviour (Pötschke and Paul, 2003).

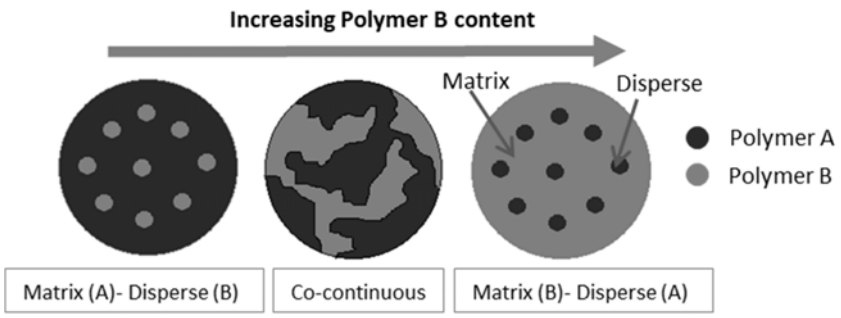

Figure 2.10 Schematic diagram of two immiscible polymer blend fibre with different composition of polymer A and polymer B: *left*- polymer A as a major component, *middle*- co-continuous phase when the composition of two polymers almost in the same amount, *right*- polymer A as a minor component.

2.5.1 Factors affect the properties of blend fibre

Morphology of the polymer blend is affected by the type of polymer, the viscosity ratio, blend ratio and shear rate during processing.

Viscosity of the polymer is crucial factor in polymer blend. A minor component of the blend can develop a fine and uniform disperse phase if it has viscosity lower than matrix phase. Otherwise, coarser disperse phase might develop if the minor component has higher viscosity than the matrix phase (Favis, 2000). Illustration of the effect of polymer viscosity is shown in Figure 2.11. Other than that, the viscosity ratio between the polymers also influences the size of the droplet/fibrils. If the viscosity of the disperse phase increases, the viscosity ratio increases thus increases the average diameter of the droplet but reduces the number of droplets formed.

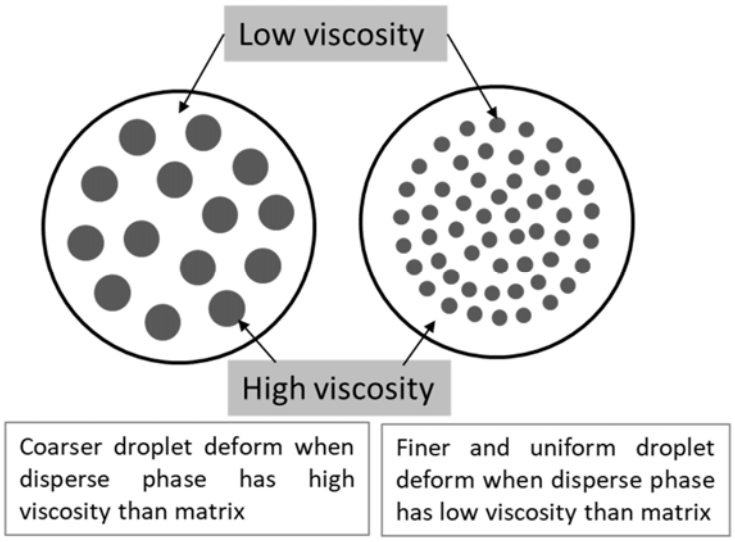

Figure 2.11 Size of disperse phase based on polymer viscosity.

Ratio of the polymers in the blend influences the size of the droplet in the disperse phase. When the fraction of the minor polymer increases in the blend, the droplet size will increase due to coalescence of the droplet (Figure 2.12) (Tavanaie et al., 2013; Zhang et al., 2015).

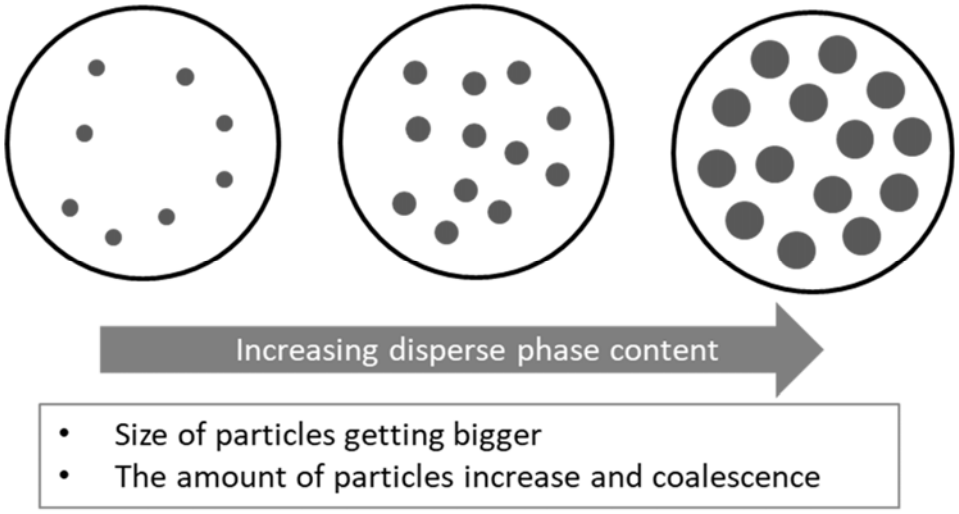

Figure 2.12 Size of disperse phase based on dispersed phase content.

Polymer blend can accomplish by melting both polymers in melt extruder. In melt extrusion, the rotating screw in the barrel produces shear stress that influences the size of the droplet particle as illustrate in Figure 2.13. Increasing the shear rate result in the decrease of the droplet size and increase number of particles (Lu et al., 2017). The shear stress also can influence the shape of the dispersed phase.

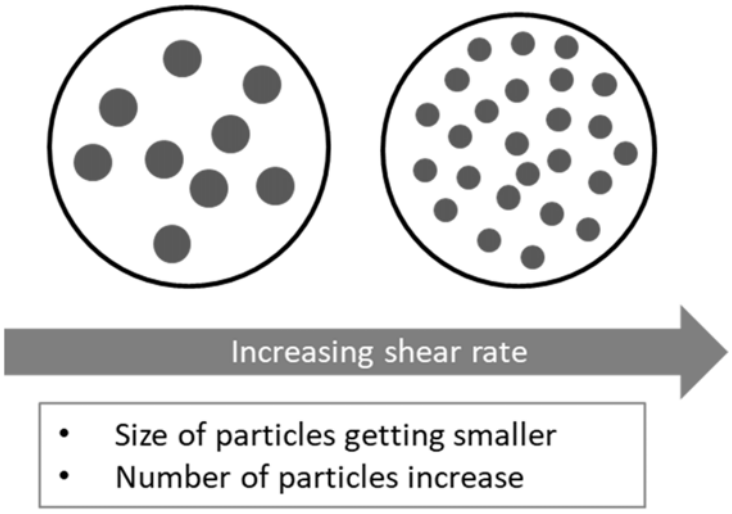

Figure 2.13 Size of disperse phase based on shear rate.

2.5.2 Interacting blend of PA6:TPU

Excellent properties of TPU in elongation, strength, elasticity and breathability increase its application in textile industry. Used as coating on constructed textile and nonwoven fabric, the TPU coated fabric can be found in medical, pharmaceutical, sportswear and filtration applications (Akovali, 2012). The TPU coated polyamide fabrics were used as marine products including buoyancy control product, inflatable raft and life vest jacket (Erez, 2018). The usage in marine application for example inflatable raft, found short lifespan of the product when puncture or broke down. Both TPU and PA6 are highly expensive polymers. Recycling textile waste can extend the life of the polymer and reduce the usage of virgin polymer to produce new product.

TPU was first developed in 1937 and has favourable properties such as high elongation and high strength, high elasticity, excellent resistance to oil, grease, abrasion, solvents and chemicals (Huntsman, 2010). The example of TPU elastomer is spandex, also known as Lycra and other brand names such as *Elaspan, Acepora, Creora* and *ESPA*. TPU elastomer consists of the hard and soft segments as shown in Figure 2.14 (Hiltz, 1998; Huntsman, 2010). The hard segment is constructed from a chain extender and diisocyanate, while the soft segment is a suitable diol (Huntsman, 2010). Variety of TPU can be produced by changing the ratio of hard to soft segment. The soft segment gives flexibility and elastomeric properties while hard segment gives toughness to the TPU elastomer.

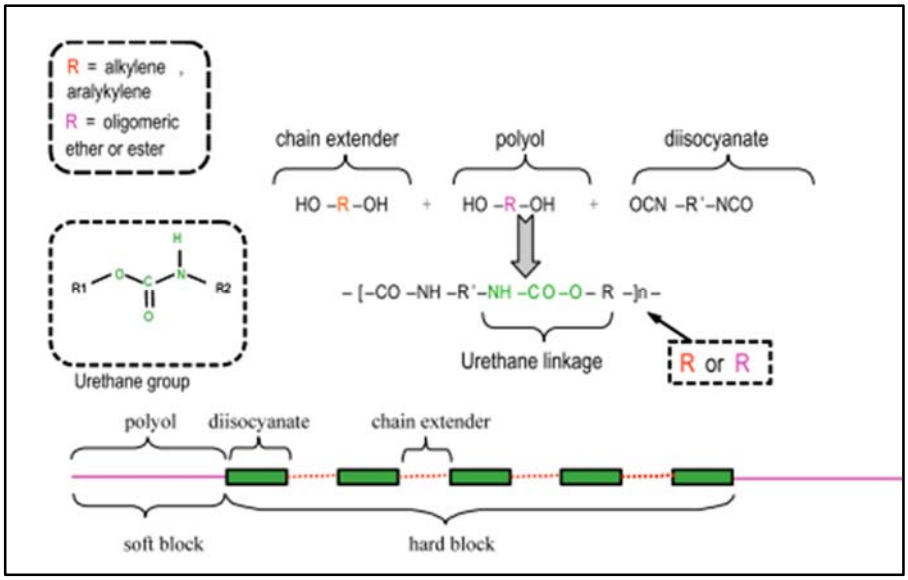

Figure 2.14 Basic chemistry of thermoplastic polyurethane (Huntsman, 2010).

The blending of TPU in PA6 improves the toughness, abrasion resistance, resistance to hydrolysis, and hardness without brittleness properties of PA6 (Zo et al., 2014). The combination of TPU with PA6 is immiscible but compatible due to an intermolecular hydrogen bond between the polyamide and the TPU (Genovese and Shanks, 2001; Zo et al., 2014). The interconnection between PA6 and TPU polymer contributes to the improvement of mechanical and thermal properties of PA6 (Zo et al., 2014). Haponiuk (1995) in his study also mentioned that the compatibility of PA6 and TPU blending depends on the chemical structure and concentration of TPU soft segments. The flexible ether group can increase the toughness of the PA6 due to the elastic properties of TPU (Genovese and Shanks, 2001). Furthermore, the melting temperature of PA6:TPU is lower than pure PA6 and the decrease in the melting temperature is proportional to the increase in TPU weight in the blend (Haponiuk and Balas, 1995). Most of the studies relating to the blending of PA6 and TPU are in composite science (Zo et al., 2014) or in injection moulding work (Haponiuk and Balas, 1995). There is limited work that focus on the production of PA6:TPU filaments or fibres.

A study conducted by John and Furukawa (2012) has shown that PA6 filaments coated with TPU have increased the tensile strength and the breaking elongation of the filaments. In his study, monofilament PA6 was cleaned in a water bath for 15 min and dried at room temperature before being dip-coated with TPU solution for 3 min. The thickness of the coating film was 20 μm. The coated filaments were dried at 100°C for 24 h to ensure fully annealing process. The urethane-amide interaction contributed to the improvement of the mechanical properties of the filaments and

approximately 10 μm interface region was formed between PA6 and TPU by this method.

Several studies have successfully blended TPU with polylactic acid (PLA) (Jašo et al., 2015) and polypropylene (PP) (Jašo et al., 2013) to produce PLA and PP microfibres respectively. In the study conducted by Jašo et al. (2015), TPU and PLA polymers were blended in a mixer for 15 min at 190°C and then pelletised. The blended pellets were dried for 5 h in vacuum at 80°C before being extruded through 1 mm die and hot drawn later. The TPU was then dissolved using dimethylformamide (DMF) to get PLA microfibres. The diameter of TPU/PLA filaments were in the range of 325 to 345 μm after hot drawing and the diameter of PLA microfibres were in the range of 200-800 nm. Almost the same method was used for producing PP microfibres (Jašo et al., 2013). The diameter of TPU:PP filaments produced were approximately 400 μm, and the diameter of PP microfibres were 200-800 nm. Several studies show the potential of blending PA6 with TPU as it increases the mechanical properties of the polymer blend. However, there is not much work that focus on the mixing of PA6 and TPU using a conventional melt spinning method.

2.5.3 Non-Interacting blend of PA6:PP and PA6:PET

Besides PA6, polypropylene (PP) and polyethylene terephthalate (PET) or known as polyester fibres are among important textiles fibres that widely produced. The possibility to find a mixture of PA6:PP and PA6:PET in textile products are also high. For example, in carpet industry, the face fibre of the carpet is commonly made by polyamide fibres and the carpet backing was made by PP. Due to high volume of carpet waste collected every year (Sotayo et al., 2015), the potential of PA6 and PP blending can be occurred during recycling/recovery process. Moreover, PA6 and PP have wide application in textile industry. Dyeing properties of PP was improved with the presence of PA6. By adding PP in PA6 the toughness and impact strength of PA6 can be improved and cost and water absorption property of PA6 can be reduced (Aparna et al., 2017).

Combination of PA6 and PET is incompatible however was found benefits in the production of bicomponent fibres such as island-in-the-sea, pie wedge and side-by-side (Radici Group, n.d.). Non-interacting behaviour of both polymers makes it easily split during separation or extraction process (Wang et al., 2017a). Hence, significant amount of mix-material products consist of both polymers combination; PA6:PET and PA6:PP in the recycling centre are expected.

2.5.3.1 Morphology of the blend

The morphology of the non-interacting polymers depends on the processing condition of the blend. Compression and injection moulding produce droplet-matrix morphology (Liao et al., 2015) while melt extrusion developed fibril-matrix morphology with the presence of elongation force after the molten polymer exit the spinneret via winding or drawing process. Ternary blend of PA6:PP and compatibiliser shows “island-in-the-sea” effect in the blend fibres (Hajiraissi et al., 2017).

When PA6 content in the blend was less than 50%, the PA6 dispersed in the fibre and PP became a matrix phase (Liao et al., 2015; Hajiraissi et al., 2017). The number of droplet/fibrils in the blend increases if the PA6 content increases and the structure became coarser (Afshari et al., 2001; Liao et al., 2015; Potente et al., 2000). The phase inversion between polymers can be seen when the ratio of blend was almost similar and produces co-continuous phase of the PA6:PP blend (Afshari et al., 2001; Liao et al., 2015). If there was more than 60% of PA6 in the blend, the PA6 became a matrix and encapsulated the PP (Liang et al., 1983; Takahashi et al., 1996a).

In polymer blend, the phase continuity can be predicted using rheological model introduced by Jordhamo et al., (1986). The Jordhamo model was developed to predict the phase continuity of the blends, based on the polymer volume fraction at low shear rate mixing. Based on Jordhamo model (Eq. 2.1), the position of the polymer in the blend not only depends on blend composition but also the viscosity of the polymer. At lower shear rate, the phase position of the polymer can be determined by calculating the viscosity and the weight fraction of the polymer, represent by η_x and ϕ_x, respectively with number 1 and 2 represent polymer 1 and polymer 2. The prediction is based on the Jordhamo value where polymer 1 became a matrix if the value obtained is less than 1, it will dispersed in the blend if the value is more than 1 and the phase inversion happened when the value is close to 1.

However, the rules of polymer flows should be taken into consideration where the polymer with low viscosity but having major weight fraction in the blend will become a matrix in the blend. Therefore, Jordhamo model is suitable to find phase inversion in between polymer blends. For example, Afshari et al., (2001) predict that the phase inversion of PP/PA6/compatibiliser blend occurred at 45/50/5 blend composition, calculated using Jordhamo model. Morishita et al. (2017) found that PPS at 21% weight dispersed in 78% PA6 by referring to the rules of polymer proportion. Liu et al. (2018) also used Jordhamo model to predict the co-continuous phase of the biodegradable polymer, poly(L-lactide) (PLLA) and core-shell rubber (CSR) blend.

$$\frac{\eta_1}{\eta_2}\frac{\phi_2}{\phi_1} = 1 \qquad \text{Eq. 2.1}$$

Where,

η_1	=	Viscosity of polymer 1
η_2	=	Viscosity of polymer 2
ϕ_1	=	Weight fraction of polymer 1
ϕ_2	=	Weight fraction of polymer 2

In Jordhamo study, mechanical blend of polystyrene (PS) and polybutadiene (PB) with different blend compositions were produced. The morphology of the PS/PB blend were found follows the model equation introduced. Since then, many researchers had used this model to predict the phase flow of the polymer blend (Favis and Chalifoux, 1988; Vinckier et al., 1996; Afshari et al., 2001; Li and Shimizu, 2004; Morishita et al., 2017; Liu et al., 2018; Pustak et al., 2018). This model is not reliable for high shear rate mixing and cannot predict the shape and size of the dispersed phase. However, Jordhamo model can be used as an initial step to predict the polymer blend morphology (Dobrovszky and Ronkay, 2017).

In polymer blend, viscosity ratio of the polymers influences the size of the disperse phase. The viscosity of both polymers can be used to get the viscosity ratio in the blend, calculated using Eq. 2.2. The viscosity ratio will influence the diameter of the droplet developed in the blend, the lower the viscosity ratio, the finer the droplet will be obtained. The estimated viscosity of the polymer during extrusion can be measured by considering the shear rate of the polymers during the processing, calculated using Eq. 2.3 (Martin, 2013).

$$Viscosity\ ratio, k = \frac{viscosity\ dispersed, \eta_d}{viscosity\ matrix, \eta_m} \qquad \text{Eq. 2.2}$$

$$Shear\ rate = \frac{\pi \times D \times n}{h \times 60} \qquad \text{Eq. 2.3}$$

Where,

D	=	screw outside diameter (mm)
n	=	Screw speed (rpm)
h	=	Overflight gap between the tip of the screw and the inner wall of the barrel (mm)

Takahashi et al., (1996a) in their study found that finer PP fibrils produced when the viscosity ratio is below 1 and coarser fibrils were obtained for viscosity ratio is above 1.

Most of previous studies added compatibiliser in the blend of non-interacting polymer. The compatibiliser act as medium to enhance the interaction between both polymers interfacial surfaces. Improvement in the interfacial surfaces will result in better dispersion and produce finer droplet/fibrils in the blend. Without compatibiliser, finer droplet/fibrils are hardly formed. PP fibrils diameter in the range of 0.5-5 μm were produced without compatibiliser (Hajiraissi et al., 2017)(Liang et al., 1983; Hajiraissi et al., 2017) and the diameter reduced to 0.2-1.0 μm with the presence of compatibiliser (Afshari et al., 2001; Takahashi et al., 1996a).

Screw speed in extruder relates to the flow shear rate that influences the dispersed phase distribution in the matrix; higher screw speed reflects to higher shear rate thus decrease the size of droplet/fibril (Afshari et al., 2001). However, other study reports that the particle size is not necessary decrease when screw speed increases, causing the viscoelastic behaviour of the polymer that can contribute to the particle size as well (Barangi et al., 2008).

Using high temperature during spinning leads to lower viscosity of the polymers thus the polymers flow easily and encourage coalescence (Potente et al., 2000). Golfazani et al. found that processing PA6/PP at 250°C produce coarser fibril than at 190°C (Golfazani et al., 2012). However, Hajiraissi et al. found that fibrillar shape occurred when the blend was processed above the melting temperature of matrix phase and lower than melting point of dispersed phase (Hajiraissi et al., 2017).

2.5.3.2 Thermal properties

Thermal properties of the polymer relate to the morphology of the polymers. PA6, PP and PET are semi-crystalline polymers which have liquid (amorphous) and solid (crystal) state while TPU is an amorphous polymer. Semi-crystalline polymers, when heated, require certain amount of energy to melt the crystal state into molten state and will be visible in a DSC curve as an exothermic peak. During cooling cycle, the crystal will solidify and release energy and shown in DSC curve as an endothermic peak. Since PA6:PP and PA6:PET are non-interacting polymer, the blending will developed individual melting and crystallisation peaks, each represents the specific polymer when observed in the DSC (Wang et al., 2017b).

Even though the blending of PA6:PP and PA6:PET is a non-interacting blend, the solidification cycle of the blend can affect the crystallinity of polymers. Jafari & Gupta (1998) found that PA6 (disperse) which solidify earlier than PP (matrix) was not interrupted by the molten PP during cooling cycle. However, when PP started to solidify, the crystallisation of PP was affected by the solidified PA6 and decreased the crystallinity of the PP. This is called as a nucleation effect.

The crystallinity of the PA6, PP and PET can be measured separately based on the melting enthalpy for each peak, shown in Eq. 2.4, Eq. 2.5 and Eq. 2.6 (Afshari et al., 2005) The percentage crystallinity of the PA6, PP and PET can be calculated with the reference value of melting enthalpy which are 230.1 J g^{-1} (Sichina, 2000), 209.2 J g^{-1} (Khanna, 1990) and 140 J g^{-1} (Fakirov and Evstatiev, 1993), respectively.

$$PA6\ crystallinity, X_{PA6} = \frac{\Delta H_{f,PA6}}{\Delta H^0{}_{f,PA6}} \times \frac{1}{w_{PA6}} \times 100\% \qquad \text{Eq. 2.4}$$

$$PP\ crystallinity, X_{PP} = \frac{\Delta H_{f,PP}}{\Delta H^0{}_{f,PP}} \times \frac{1}{w_{PP}} \times 100\% \qquad \text{Eq. 2.5}$$

$$PET\ crystallinity, X_{PET} = \frac{\Delta H_{f,PET}}{\Delta H^0{}_{f,PET}} \times \frac{1}{w_{PET}} \times 100\% \qquad \text{Eq. 2.6}$$

2.5.3.3 Mechanical properties

The strength of the non-interacting polymer blend is either increased or decreased than single polymer depending on the composition of the polymer in the blend. By

increasing PA6 content from 5 to 15% in the blend of PA6:PP, the strength was increased and then slightly decreased when 20% of PA6 added (Asiaban & Moradian, 2012; Jaziri et al., 2008; Takahashi et al.,, 1996b). For PA6:PET, the optimum strength was found when PA6 content was in the range of 70-80% in the blend (Papero et al., 1967; Varma and Dhar, 1988). Increasing PET content decreased the fibre strength. The reduction in strength is due to the microvoids or micropores at the interface of PP and PA6 which lead to decrease in the tenacity of the fibre (Afshari et al., 2005).

The compatibilisers are commonly used to increase the strength of the blend. The presence of compatibiliser improved the interfacial adhesion of both polymer and reduced gaps at the interface of both polymers thus improved the strength of the fibres (Yoon et al., 1997; Lin et al., 2014).

2.6 Melt spinning

Majority of synthetic fibres including P6, PP, PET and TPU used in textile application are thermoplastic polymer which can be melted several times. Thermo-mechanical recycling approach can be used for mix-wasted materials containing of different thermoplastic polymers and extruded into new hybrid fibres.

Melt spinning or melt extrusion is the process where melted polymers are being extruded through small holes and spun into filaments. The melt spinning is an economically viable process and does not have to use any solvent in the process (Aranishi and Nishio, 2017). In melt extrusion, the polymer chips are melted and passed through the spinneret containing small holes, typically 100-400 μm in diameter (Richards, 2005). The shape of the spinneret hole normally is circular producing circular cross sectional fibres. Noncircular cross sectional shape can also be created by changing the shape of the spinneret holes. Noncircular cross section filaments give special effects to the filament properties such as lustre, opacity, air permeability, insulation, and resistance to soiling (Liu et al., 2014). Details of noncircular cross sectional shape is mention in section 2.4.1 (Single component fibres).

Filaments that come out from the spinneret hole undergo quenching process before being winded up onto a package. The process speed is normally around 1000 m min^{-1} (Richards, 2005) however this could be as high as 6000 m min^{-1} (Reimschuessel, 1998). All aliphatic polyamides that melt below 280-290°C are produced by melt extrusion (Reimschuessel, 1998). A schematic diagram of melt spinning is shown in Figure 2.15.

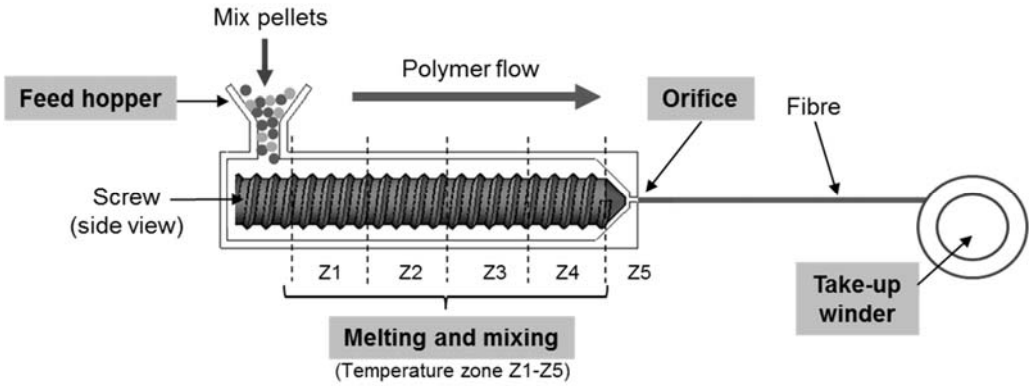

Figure 2.15 Schematic diagram of polymer melt extrusion.

When the polymer enters the hot extruder it melts and the rotating screw conveys the molten polymer to the spinneret hole. Two types of the rotating screw are used, single and twin rotating screw type (Figure 2.16). A single screw is used to convey the polymer through the spinneret, processing at low shear rate and not suitable for mixing two different polymers. Single screw normally used to produce single component fibres. The twin screw extruder is a good mixing device and can blend two or more materials uniformly. In this study, twin screw melt spinning machine was used to produce hybrid fibres from blending of several polymers.

a) b)

Figure 2.16 Different types of rotating screw (top view); a) single screw, b) twin screw.

The structure and properties of the fibres depend on the spinning condition during production as well as the rheological properties of the polymer. Spinning conditions including temperature along the extruder, melting temperature, feed rate, screw speed, type of screw, screw geometry, diameter and shape of spinneret hole and take-up speed give effect to the properties of the filaments.

Increasing take up speed enhances the tenacity and modulus, but will reduce the breaking elongation (Afshari et al., 2005). This is due to an increased molecular chain orientation imparting axial strength and stiffness but compromising on the extension.

The rheology of the melted polymer influences the relative movement of the polymer in the extruder. The high viscosity polymers tend to move slower than the low viscosity polymers, preferring to cling to the outer wall of the extruder as shown in Figure 2.17 (Richards, 2005).

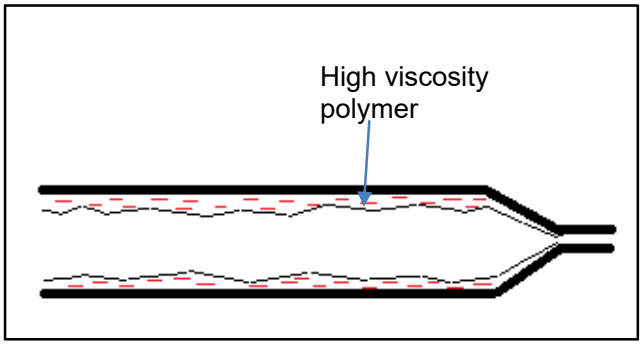

Figure 2.17 The movement of high viscosity polymer in an extruder.

2.7 Conclusions

In summary, textile wastes have become global issues and recycling is the best method to avoid send the waste going to landfill. Majority of textile wastes are thermoplastic polymer, made from non-renewable resources that can be recycled several times. However, mix-materials consist in the textile products limit the recycling process due to lack of facilities and technologies. Due to complex components in one product, thermo-mechanical approach using melt spinning is most applicable to recycle two or more polymers components. PA6 classified as an expensive textile fibre was the main focus for this study. The blending of PA6 with other textile polymers, grouped into interacting (PA6:TPU) and non-interacting blend (PA6:PP and PA6:PET), extruded as hybrid fibres using melt spinning will be studied thoroughly in the next chapters.

Chapter 3
Methodology

This chapter describes the materials and methods to produce hybrid fibres along with methods to obtain upcycled PA6 fibres. The testing on fibres characterisation was also explained. The fibres were characterised based on thermal properties: differential scanning calorimetry (DSC) and thermogravimetric analysis (TGA), rheology properties (capillary rheometry), chemical properties (ATR-FTIR) and mechanical properties (tensile strength, breaking elongation and Young modulus). The method to produce PP-40 (refer to Table 3.2) knitted fabrics was explained along with the treatment conducted to obtain treated fabric. Several fabric testing conducted to study the fabric properties are also included in this chapter.

3.1 Materials

Five extrusion grade polymers were used in this work: polyamide 6 (PA6) as a main polymer and four other polymers as secondary polymer, two different grade of thermoplastic polyurethane (TPU), thermoplastic polyether-polyurethane SP9305A (TPU-A) and thermoplastic polyether-polyurethane 1278D (TPU-D), polyethylene terephthalate (PET) and polypropylene (PP). Details of the polymers are given in Table 3.1.

Table 3.1 Types of polymer.

Polymer	Type	Company	Country	Melting temperature (°C)
Polyamide 6	*Radilon S 35F 100NT*	Radici Group, Gandino,	Italy	223
Thermoplastic polyurethane 1278D	*Elastollan®1278 D 11U000*	BASF Polyurethanes GmbH, Lemförde,	Germany	189
Thermoplastic polyurethane SP9305A	*Elastollan® SP 9305 A*	BASF Polyurethanes GmbH, Lemförde,	Germany	140
Polyethylene terephthalate	N/A	ICI	Pakistan	251
Polypropylene	*Capilene® T 89 E*	Carmel Olefins Ltd	Israel	165

3.2 Fibre extrusion

Four different polymer blends were prepared to produce hybrid fibres: i) PA6 and TPU-D, ii) PA6 and TPU-A, iii) PA6 and PET and iv) PA6 and PP. The pellets were manually mixed based on the weight composition listed in Table 3.2. The weight composition for each blend is based on the trial production of the blend in the melt spinning. Each blends were identified with the secondary polymer and its weight composition used in the blend, for example 80% of PA6 blend with 20% PP was indicated as PP-20. Single component fibres were also produced from each polymer. PA6, PET and TPUs were dried prior extrusion while PP pellets were used as provided by the supplier.The dried and mixed pellets were directly used for melt extrusion.

Table 3.2 Blend composition of the fibre.

Blend	Fibre	PA6	PP	PET	TPU 1278D	TPU 9305A
	PA6	100	-	-	-	-
PA6:TPU-D	TPU-D 20	80	-	-	20	-
	TPU-D 50	50	-	-	50	-
	TPU-D	-	-	-	100	-
PA6:TPU-A	TPU-A 20	80	-	-	-	20
	TPU-A 50	50	-	-	-	50
	TPU-A	-	-	-	-	100
PA6:PET	PET-20	80	-	20	-	-
	PET-30	70	-	30	-	-
	PET-40	60		40		
	PET-50	50		50		
	PET-60	40		60		
	PET-70	30		70		
	PET-80	20	-	80	-	-
	PET	0		100		
PA6:PP	PP-20	80	20	-	-	-
	PP-35	75	35	-	-	-
	PP-40	60	40	-	-	-
	PP-50	50	50	-	-	-
	PP	-	100	-	-	-

3.2.1 Drying of polymer pellets

Polymers pellets PA6, PET and TPUs, were dried in the vacuum oven (Gallenkamp, 1000 mbar) and conventional oven to remove moisture content in the pellets. Preliminary drying process was done on the PA6 pellets, to find an appropriate drying time (Appendix B). The result shows that the drying time has no significant changes to PA6 properties if the drying temperature is kept below 140°C for 24 h. However, the duration of drying virgin PA6 pellets is recommended to be more than 3 h to remove moisture from the pellets. In this study, the pellets were dried at 100°C for at least 6 hours.

3.2.2 Melt extrusion

The melt extruder used in this study was a twin-screw extruder, *Rondol-Microlab* manufactured by Rondol Technology Ltd., France. Twin-screw extruder has better mixing function compared to single-screw extruder, which is the main reason it has been chosen in this study. A winder was used to collect the extruded fibres from the orifice exit and wound the fibres onto a bobbin. A schematic diagram of the twin screw melt extruder and winder assembly is illustrated in Figure 2.15. The system consists of a feed hopper, melting and mixing area, orifice and take-up winder. The feed hopper is an entrance for the polymer pellets to get into the melt extruder. It also controls the volume of the pellets that can be fed at one time. The polymer pellets then go through to the melting and mixing area which comprises of co-rotating twin screw (10 mm diameter, 200 mm length) and four heating zone (Z1 to Z4) that can be set up to 300 °C for each zone. Subsequently, the melted and mixed polymer was directed to the single orifice (2 mm diameter) die which is also equipped with heating zone (Z5). The extrudate from orifice outlet, called fibres, were collected by take-up cross-winder which was positioned approximately 1 m from the outlet. The same process was repeated for other polymer blends. The fibres were produced at variable temperature profile, screw speed and take-up winder speed as shown in Table 3.3.

Table 3.3 The temperature setting, screw speed and take-up speed of melt extruder (refer to Table 3.2 for blend composition).

Fibre	Temp Zone 1 (°C)	Temp Zone 2 (°C)	Temp Zone 3 (°C)	Temp Zone 4 (°C)	Temp Die Zone (°C)	Screw speed (RPM)	Take up speed (m min^{-1})
PA6, TPU-D 20, TPU-D 50, TPU-D	170	180	210	220	230	40, 60, 80	24.5
PA6, TPU-A 20, TPU-A 50, TPU-A	165	180	200	210	220	60	20
PA6, PET-20, PET-30, PET-40, PET-50, PET-60, PET-70, PET-80, PET	230	250	260	260	260	60	24.5
PA6, PP-20, PP-35, PP-40, PP-50, PP	170	185	230	230	230	60	24.5

3.3 Fibre treatment

After the production of the hybrid fibres, the process of removing the secondary polymer (TPU-D, TPU-A, PET and PP) from hybrid fibres was conducted to investigate the potential of producing upcycled PA6 fibres. To achieve this objective, the hybrid fibres were fully immersed in specific solvents and method of extraction as presented in Table 3.4. After each extraction, fibres were collected and rinsed with water to precipitate PA6. The as-spun hybrid fibres will be called untreated fibres and the hybrid fibres after removing the secondary polymers will be called the treated fibres.

Table 3.4 Solvents and extraction method of secondary polymer.

Hybrid fibres	Solvent	Duration (h)	Temperature (°C)	Apparatus set up
PA6:TPU-DTPU-D	Dimethyl sulfoxide (DMSO)	3, 24	Room temperature	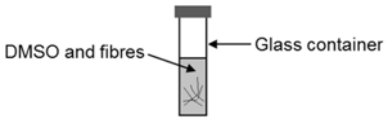
PA6:TPU-A	Dimethyl sulfoxide (DMSO)	3	Oil bath 90 °C	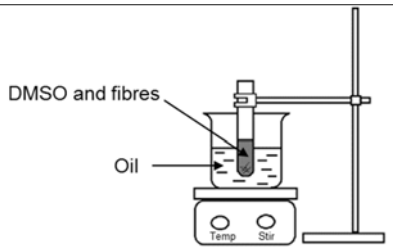
PA6:PET	Sodium hydroxide	3	Boiling water 100 °C	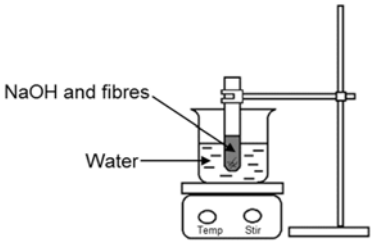
PA6:PP	Toluene	3	100	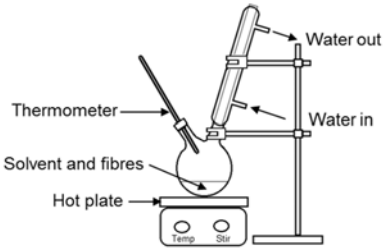

3.4 Microscopy

The changes in the fibres morphology before and after treatment were examined by microscopy. Two microscopy techniques were used in this study; light microscopy and scanning electron microscopy (SEM).

3.4.1 Light microscopy

Light microscope (LM) is able to view fibre structure that is not visible to naked eyes with the help of visible light and magnifying lenses. Under LM, details of the fibre structure can be produced at better resolution either in single or a bulk of the fibres.

Before viewed under the LM, fibres were prepared following the AATCC Test Method 202159 as shown in Figure 3.1. The cross-section of fibres were observed under a Leica M205C light microscope. The examples of fibre's cross-section viewed under LM are shown in Figure 3.2. The images from LM are used to measure the cross-section area of the fibres. A minimum of 30 fibre images of each sample were analysed using ImageJ software to get mean value of fibre cross-sectional area.

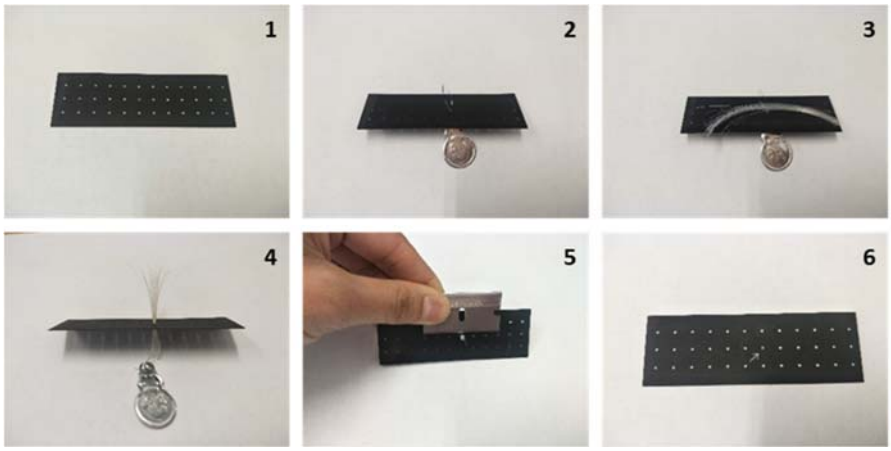

Figure 3.1: Preparation of fibres for cross-section view under LM: 1- prepare the perforated plate, 2- insert needle threader through one of the holes, 3-insert a bundle of fibres into the wire loop of the needle threader, 4- pull the wire loop and the fibres through the hole, 5- cut the fibres at both sides of the plate, 6- the cut fibres (show by arrow) ready to be viewed under LM.

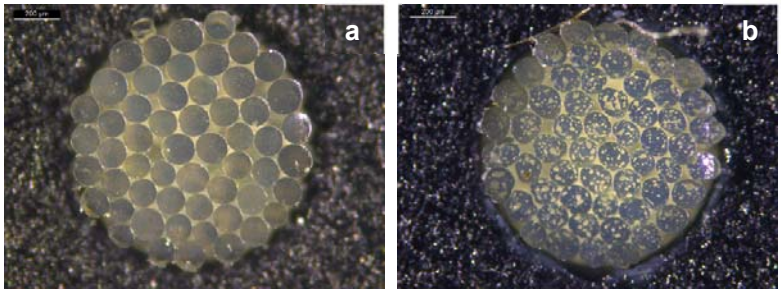

Figure 3.2 Examples of fibre cross-section images captured by LM: a) PA6 fibres and b) TPU-D 50 untreated fibres.

Most of the fibres produced through melt extrusion with the circular die shape will produced circular and round shape fibres as shown in Figure 3.2 (a). The diameter

of fibres was calculated by using Eq. 3.1 with *d* is a fibre diameter and *A* is the cross-section of fibre area. The diameter of the non-circular shape hybrid fibres (PA6:TPU-D shown in Figure 3.2 (B)) was calculated by using Eq. 3.1 (Tran et al., 2016) assuming the 'circular equivalent diameter' (CED) of the fibres obtained from the fibre cross-section area (bulk)(illustrated in Figure 3.3).

$$d_{CED} = \sqrt{\frac{4A}{\pi}} \qquad \text{Eq. 3.1}$$

$$True\ cross\ sectional\ area = Bulk\ area - total\ area\ of\ pores \qquad \text{Eq. 3.2}$$

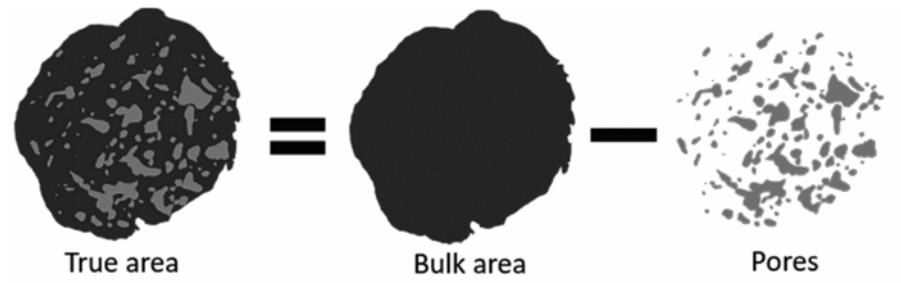

Figure 3.3 Illustration of bulk and true cross-section area.

To get the true cross-sectional area of PA6:TPU-D hybrid fibres, the bulk and total pores area in the fibres were measured using ImageJ software. First, the image taken using LM was opened in the ImageJ software. Then, the scale was set based on the scale provided in the image (*Analyze* > *Set Scale*). Using a pencil tool, fibre area was sketch as shown in Figure 3.4 (1). Next, the image was duplicate and new image box will appear as shown Figure 3.4 (2) (*Image* > *Duplicate*). To measure the fibre bulk cross-section area, the Analyze and Measure were chosen (*Analyze* > *Measure*). To measure the pores area, the image colour should be adjusted by click (*Image* > *Adjust* > *Threshold* > *Apply*). The image will change colour as shown in Figure 3.4 (3). To determine the pores area, click (*Analyze* > *Analyze particles* > *OK*). Copy and paste the particle size measurement in Microsoft Excel to get the total pore area. The true cross-sectional area of the fibres was measured using Eq. 3.2. At least thirty images of each fibres were analysed to get the mean value of the total pores and bulk area of the fibres.

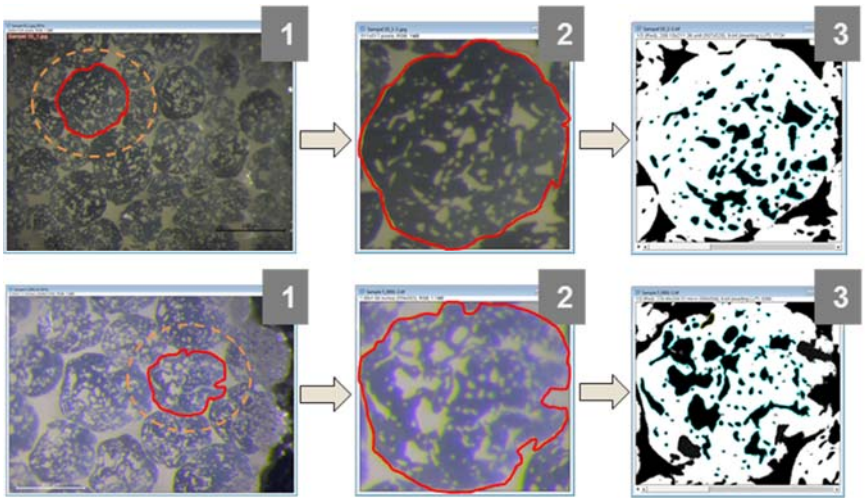

Figure 3.4 Step of measuring PA6:TPU-D hybrid fibre cross-section area in ImageJ software.

3.4.2 Scanning electron microscopy (SEM)

Some of the treated fibres obtained in this study having a structural change that is difficult to be observed clearly on LM as shown in Figure 3.5 (*left*), owing to wavelength of the light. SEM can be used to observe fine microstructural detail as electrons have much smaller wavelength compared to lightshown in Figure 3.5 (*right*). Therefore, SEM was used to investigate the structure of the fibre particularly the treated fibres. Hitachi S-2600N SEM fitted with a tungsten electron source and secondary electron detector was used to obtain the morphology of the cross-section and surface of the fibres. Fibres samples were placed on a 12 mm diameter pinned stub with conductive tape and were frozen in a standard freezer overnight at -20 °C. All samples were then gold coated in an Emitech K550X sputter coater at 25 mA for 4 mins to avoid the sample charging. The samples were placed in a specimen chamber and observed in a high vacuum at an acceleration voltage of 3 kV with working distance of 4 to10 mm. SEM images were also viewed using Jeol JSM-6610LV scanning electron microscopy (SEM) at 8 kV acceleration voltage with 1000x magnification. At least 3 micrographs were taken from each sample.

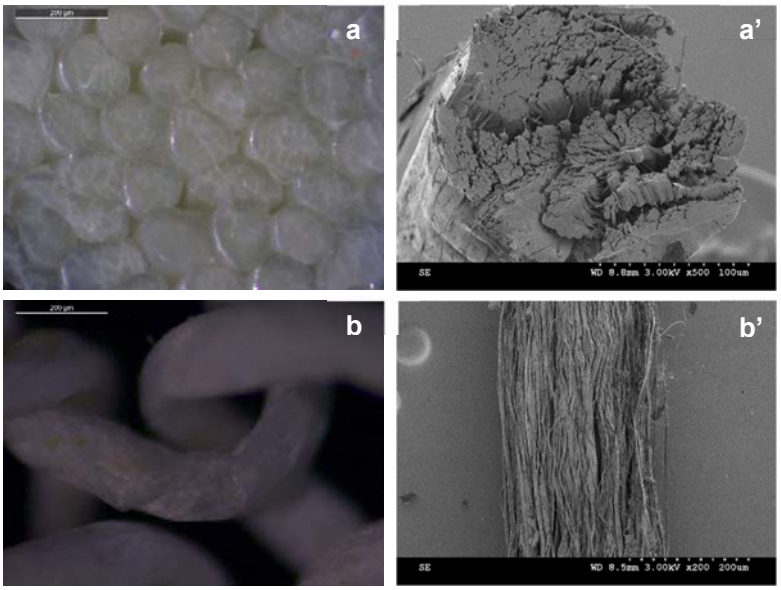

Figure 3.5 Example of images of a) TPU-D 50 and b) PP-60 treated fibres viewed under light microscope (*left*) and scanning electron microscope (*right*).

3.5 Capillary rheometry

The viscosity of the polymers is vital to the development of final hybrid fibre morphology. To understand the molten flow of the polymer during melt spinning, the viscosity of the polymer was determined using capillary rheometry.

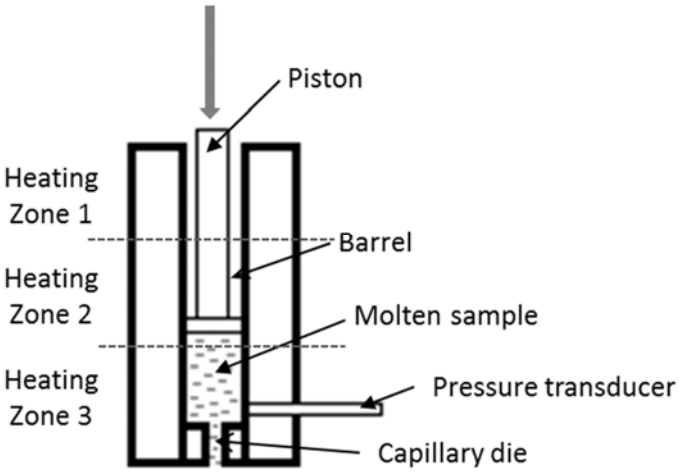

Figure 3.6 Capillary Rheometer.

The viscosity of the polymer was measured using a RH2000 capillary rheometer manufactured by Bohlin Instruments, UK. The equipment has 16 mm diameter barrel, equipped with three heating zones and 1 mm capillary die diameter as illustrated in

Figure 3.6. Approximately 30 g polymer pellets were filled in the barrel and heated at a designated temperature. The selected temperature was based on the temperature used in the melt extrusion process. For PA6, PP, TPU-A and TPU-D, the processing temperature at the melt extruder is 230 °C, and for PA6 and PET blend, the processing temperature is 260 °C. The temperature for all heating zone was held constant. The molten polymer was forced to extrude through the capillary die by altering the piston speed between 1-35 mm min^{-1} resulting in an apparent shear rate of 30 to 1050 s^{-1} with an interval of 150 s^{-1}. A pressure transducer located near to the die records the pressure when the polymer is in a steady state condition. The shear viscosity of the polymers can be calculated by Eq. 3.3. The shear stress and shear rate of the polymer are calculated by Eq. 3.4 and Eq. 3.5, respectively. The morphology of hybrid fibres can be predicted using Jordhamo model shown in Eq. 2.1

$$Viscosity, \eta = \frac{shear\ stress, \sigma_s}{shear\ strain, \gamma} \qquad \text{Eq. 3.3}$$

$$Shear\ stress, \sigma_s = \frac{Pr}{2l} \qquad \text{Eq. 3.4}$$

$$Shear\ rate, \gamma = \frac{4Q}{\pi r^3} \qquad \text{Eq. 3.5}$$

Where,

P	=	Pressure drop at the die (N m^{-2})
r	=	Capillary radius (m)
l	=	Capillary length (m)
Q	=	Volume flow rate (m^3 s^{-1})

3.6 Thermal properties

The study of thermal properties of the fibres is necessary to identify suitable condition for fibres and fabric production (Richards, 2005) and to find the relationship between the structure and crystallinity of the fibres (Khanna, 1990). Two methods: differential

scanning calorimetry (DSC) and thermogravinometric analysis (TGA) were used to study changes of the thermal properties of the untreated and treated hybrid fibres.

3.6.1 Differential scanning calorimetry

DSC has been widely used to identify the thermal behaviour of the polymers. In DSC, the sample is placed in a sample pans and heated together with empty reference pan as shown in Figure 3.7. Certain amount of energy is required to heat or cool the sample. The difference of the heat flow into a sample and a reference pan is measured as a function of temperature. Basic DSC curve is shown in Figure 3.8. However, the curve will vary according to the materials/sample properties and thermal history.

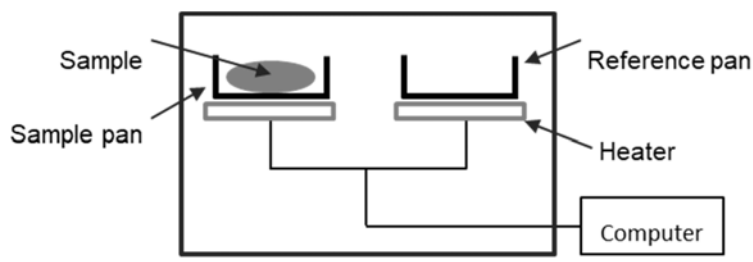

Figure 3.7 DSC diagram.

During the scanning process, three state changes of the sample can be observed: glass transition, melting and crystallisation state. The glass transition is the change of the sample from glassy to rubbery state, which normally happens when the polymer has an amorphous region, called as glass transition temperature. When the temperature increases, the crystalline region begins to melt (T_{onset}) and more energy required to melt the crystal structure. This melting transition produces endothermic peak or melting peak, called melting temperature (T_m) which indicates the heat flow in the sample. When cooled, the liquid crystal will solidify and the heat flow will release from the sample developed the exothermic peak or crystallisation peak, called crystallisation temperature (T_c). The area under the melting curve indicates the energy required to melt the crystal, called melting enthalpy (ΔH_m). The melting enthalpy can be used to estimate the percentage of the crystallinity of the sample calculated from Eq. 3.6 where ΔH_m is melting enthalpy and ΔH_m^0 is a reference value of melting enthalpy obtained from the perfect crystal of the same material.

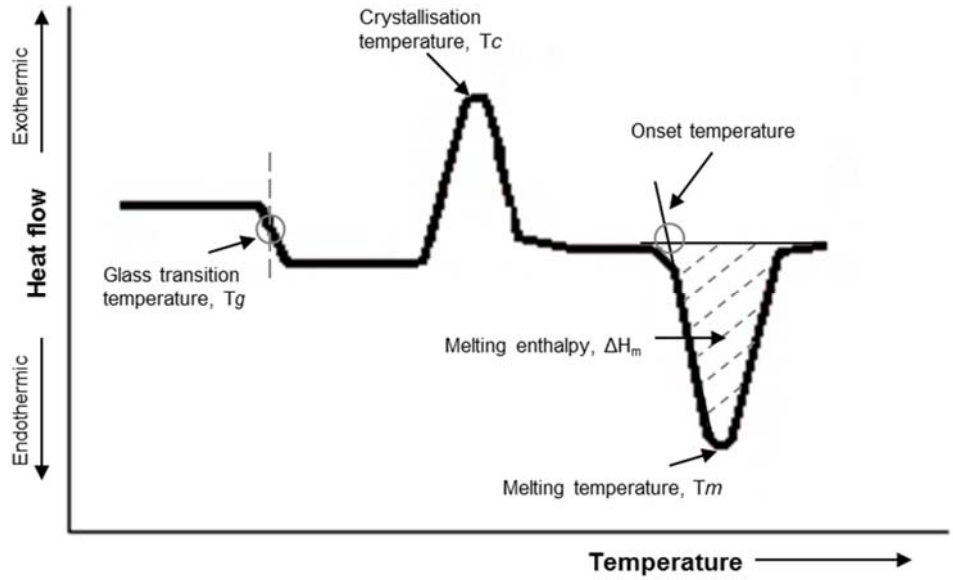

Figure 3.8 Basic DSC curve diagram.

$$\% \, Crystallinity = \frac{\Delta H_m}{\Delta H_m^0} \times 100 \qquad \text{Eq. 3.6}$$

DSC analysis was performed to study the effect of mixing two polymers on the thermal properties of the hybrid fibres. In polymer blend, the miscibility of the blend can be detected by observing the glass transition temperature or melting temperature of the component polymers in the DSC curve. If the polymer blend is compatible to each other, the melting peak of the blend will show only one peak and might be slightly different from their parent polymer. However, if the blend is incompatible, two melting peaks will be observed as shown in Figure 3.9. The percentage crystallinity of the blend polymer can be estimated with the addition of the weight composition of each blend, *w,* as shown by Eq. 2.4, Eq. 2.5 and Eq. 2.6. Crystallinity effects thermal, mechanical, optical and chemical properties of polymer. The amount of crystallinity in polymers generally ranges between 10-80%.

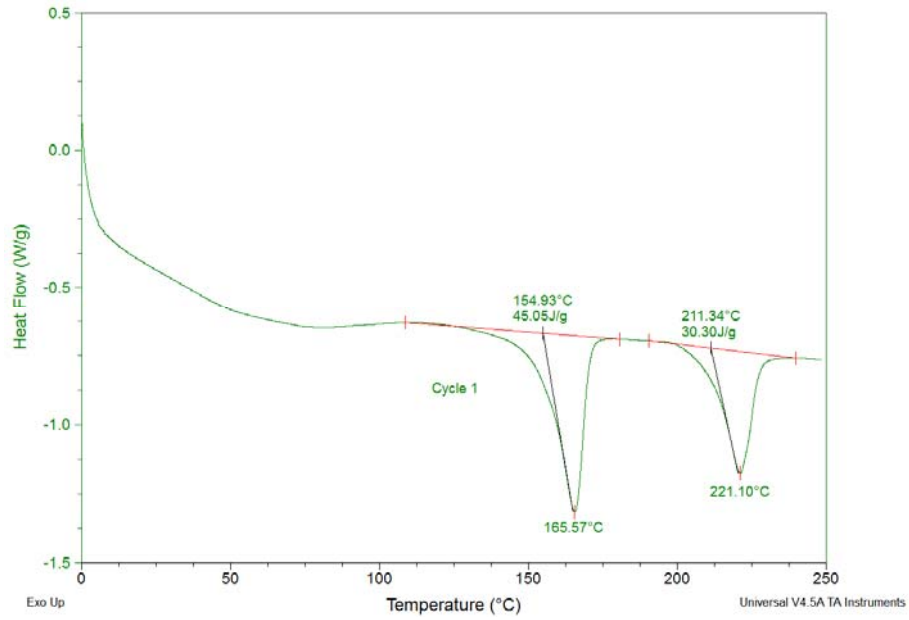

Figure 3.9 DSC heating curve of PA6 and PP hybrid fibres.

$$\%\ Crystallinity\ of\ polymer\ X \quad = \frac{\Delta H_{mx}}{\Delta H^0_{mx}\ \times\ w_x} \times 100 \qquad \text{Eq. 3.7}$$

Where,

ΔH_m	=	Melting enthalpy (J g^{-1})
ΔH^0_m	=	Reference value of melting enthalpy (J g^{-1})
w	=	Weight fraction in the blend
x	=	Respective polymer

A Q2000 DSC apparatus from TA instrument was used in this work. 5-7 mg undried fibres were cut and placed in an aluminium pan before heating-cooling-heating from 0-250 °C (for PA6:PET, the heating temperature is 0-280 °C) at 10 °C heating rate in a 25 mL min^{-1} nitrogen (N_2) controlled atmosphere.

3.6.2 Termogravinometric analysis

The thermogravinometry analysis (TGA) was used to study the thermal stability and degradation of the untreated and treated hybrid fibres. TGA measures the changes of the sample mass per unit time or temperature. The sample was placed in a aluminuim pan and heated in a controlled atmosphere as shown in Figure 3.10.

During heating, the sample under-goes mass changes by oxidation, decomposition and desorption which can be used to analyse the thermal stabilities and decomposition of the sample. Figure 3.11 shows an example of TGA curve for one step desomposition. The onset temperature and end temperature indicate the starting and end point of decomposition, respectively.

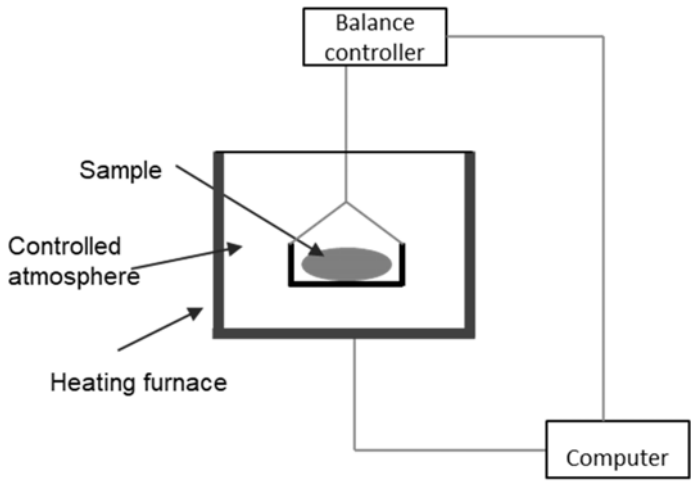

Figure 3.10 TGA diagram.

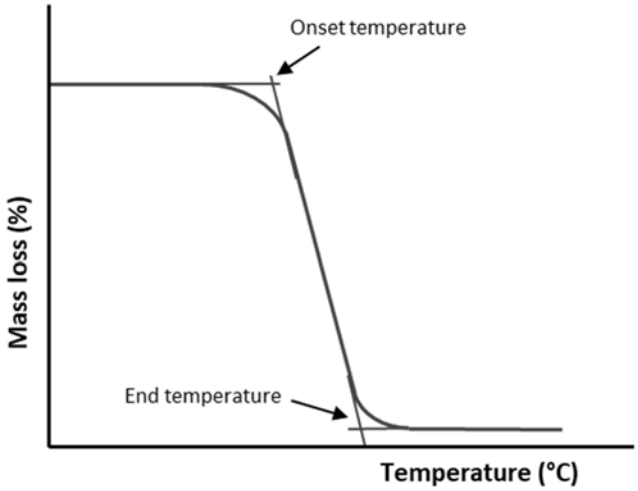

Figure 3.11 Example of TGA curve.

In this study, thermal decomposition of the fibres was carried out on a thermogravimetric analyzer (TGA)(TGA Q50). The temperature range was set from 25 °C to 600 °C under nitrogen atmosphere (25 mL min $^{-1}$) at the heating rate of 10 °C min^{-1}.

3.7 Fourier Transform Infrared Spectroscopy

Fourier Transform Infrared (FTIR) spectroscopy is a well-established technique to identify the component polymers in fibres. The FTIR equipped with Attenuated Total Reflectance (ATR) can be used to study possible changes in chemical structure on fibres surface before and after treatment. The sample is placed under the ATR crystal and the infrared beam passes through the sample (Figure 3.12). The infrared radiation is absorbed/transmitted by different molecules of the sample at a different wavelength which is then plotted as transmittance/absorbance intensity against the wavelength number.

A bundle of fibres was placed on the ATR-FTIR (Perkin Elmer Spectrum BX spectrophotometer) crystal. The wavelength was set from 600-4,000 cm^{-1} with 32 scans, 4 cm^{-1} and scanning interval was 2 cm^{-1}.

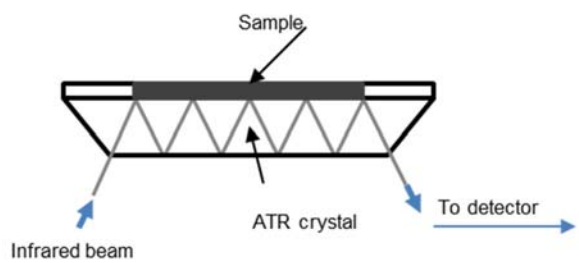

Figure 3.12 ATR-FTIR diagram.

3.8 Tensile properties

Tensile properties of fibres are important for fibre processing and the performance of textile products in use. Tensile properties are measurement of the strength, elongation, breaking point and initial modulus of fibres under uniaxial force applied along the fibre axis. The example of tenacity-elongation curve is shown in Figure 3.13. The fibre strength or tenacity is measured by dividing the force needed to break the fibres with the mass per unit length of the fibre as shown in Eq. 3.8. The strain or elongation of the fibres is usually present as a percentage can be calculated by Eq. 3.9. Breaking point indicates the position where the fibres snap. Initial modulus is the ratio of the tenacity and the elongation of the fibres within the elastic region of tenacity-elongation curve, Eq. 3.10.

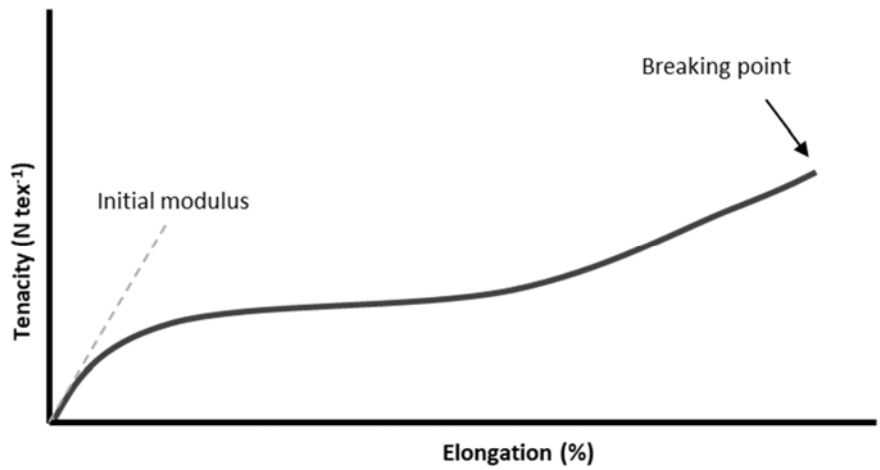

Figure 3.13 Tenacity against elongation curve.

$$Tenacity = \frac{Force\ (N)}{Mass/length\ (tex)} \quad \text{Eq. 3.8}$$

$$Elongation = \frac{Extension\ (mm)}{Initial\ length\ (mm)} \quad \text{Eq. 3.9}$$

$$Initial\ modulus = \frac{Tenacity\ (N\ tex^{-1})}{Elongation} \quad \text{Eq. 3.10}$$

The tensile properties of single fibres were measured using single column tensile strength tester (Instron 5540 and Titan) following BS EN 13895 (gauge length: 20-100 mm at 500-1000 mm min^{-1} cross-head speed). At least 10 specimens were tested for each fibre to calculate average value.

3.9 Roller Drawing

The PP-40 was melt extruded and drawn to produce knitted fabric. Drawing of fibres increases the strength of the fibres. The PP-40 fibres were cold drawn on a draw-frame machine (Figure 3.14).

Preliminary test was conducted to get draw ratio on different gear number by fixing the master drive at 40%, shown in Table 3.5. The PP-40 fibres were drawn at gear number 45 with the draw ratio of 2 The mechanism of the drawing process is illustrated in Figure 3.15.

Table 3.5 Draw ratio of the feed roller and draw roller

Gear no.	Feed roll A (s/rotation)	Draw roll B (s/rotation)	Draw ratio (A/B)
20	23.2	5.3	4.4
25	18.7	5.3	3.5
30	15.5	5.3	2.9
35	13.3	5.3	2.5
40	11.7	5.3	2.2
45	10.4	5.3	2
50	9.3	5.3	1.8
55	8.4	5.3	1.6
60	7.7	5.3	1.5
65	7.1	5.3	1.3
70	7.1	5.3	1.3

Figure 3.14 Filament drawframe.

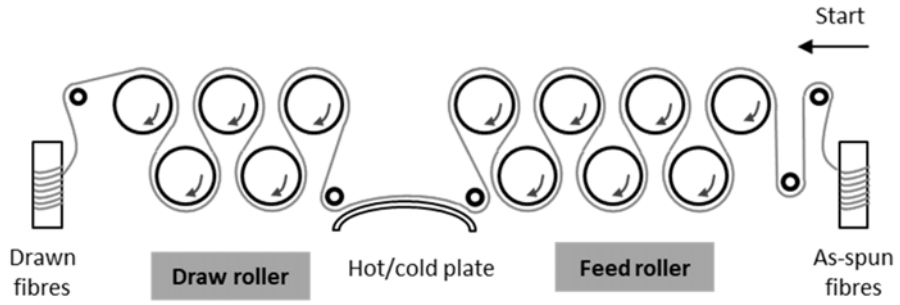

Figure 3.15 Filament drawing mechanism.

3.10 Winding

Drawn PP-40 was winded on a paper spool as shown in Figure 3.16 (*left*). There are some difficulties to produce the fabric directly from the spool. Therefore, the drawn PP-40 hybrid fibres were rewound onto a cone (Figure 3.16 (*right*)) that more suitable for fabric production. The fibres were rewound by twisting machine (DirectTwist-2B, Agteks Ltd., Turkey) as shown in Figure 3.17.

Figure 3.16 PP-40 yarn carrier; *left*- spool and *right*-cone.

Figure 3.17 Twisting machine.

3.11 Knitted fabric production

Single filament of PP-40 hybrid fibres was used to produce circular plain knitted fabric. The fabrics were produced on a 10-gauge double-bed flat knitting machine (hand-driven) as shown in Figure 3.18. The fabrics were treated to remove the PP component in boiling toluene for 3 h (Table 3.4). After treatment, the fabrics were washed using water and dried at room temperature for at least 24 h. The untreated and treated fabrics were conditioned at 20±2°C and a relative humidity of 65±5% for 24 h prior to performance testing.

Figure 3.18 Double-bed flat knitting machine (10-gauge).

3.12 Fabric testing

Several tests were conducted to study the effect of removing PP component from the fabrics on performance of the fabrics. Fabric structure (observed by light microscope and SEM), fabric specification, water absorption (vertical wicking test), drapability (bending length) and mechanical (ball burst strength test) properties of the fabrics were conducted.

3.12.1 Sample preparation

Prior to testing, samples for each testing were prepared and cut as shown in Figure 3.19. At least 3 samples for each test were prepared.

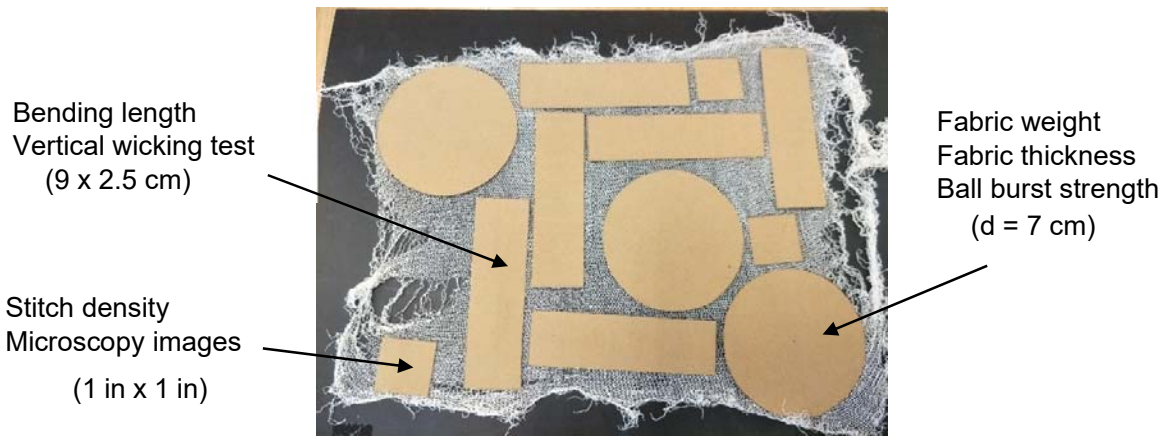

Figure 3.19 Template for sample size on top of the treated fabric.

3.12.2 Fabric specification

The physical properties of fabric such as fabric mass per area, thickness, number of courses and wales per inch and sticth density were measured.

a) Fabric mass per area

Mass per unit area of the fabrics was assessed using ASTM D3776-09 (2002) Option C – small swatch of fabric. The sample size was modified due to the limited fabric size obtained. Three samples with each having an area at least 38.5 cm^2 were prepared. The samples were weight on digital balance (Adventurer™ Ohaus) and recorded in gram (g). Fabric mass per unit area was calculated based on Eq. 3.11.

$$Mass\ per\ area\ (g/m^2) = \frac{mass\ of\ sample, (g)}{sample\ area\ (m^2)} \qquad \text{Eq. 3.11}$$

b) Fabric thickness

Fabric thickness were measured using BS EN ISO 5048-1996 on Shirley Thickness Gauge. Three samples of each fabric having an area at least 38.5 cm^2 were prepared. The sample was placed between the reference plate and circular presser-foot equipped with 50 g pressure load. The distance between the reference plate and the circular presser-foot was recorded after 5 s.

c) Courses per inch (CPI), wales per inch (WPI) and stitch density

CPI and WPI of the untreated and treated fabric were measured with magnifying glass. The sample size 1 x 1 in was prepared according to the course and wales wise of the fabric. Then the samples were placed under magnifying counting glass and the CPI and WPI were counted and recorded. The loop created horizontal to the fabric is called course.Wales is the loop produced by the same needle and are vertical to the fabric as shown in Figure 3.20. The stitch density of the fabric is measured by Eq. 3.12. Stitch density represents the looseness or tightness of the fabric; the higher the value, the denser the fabric.

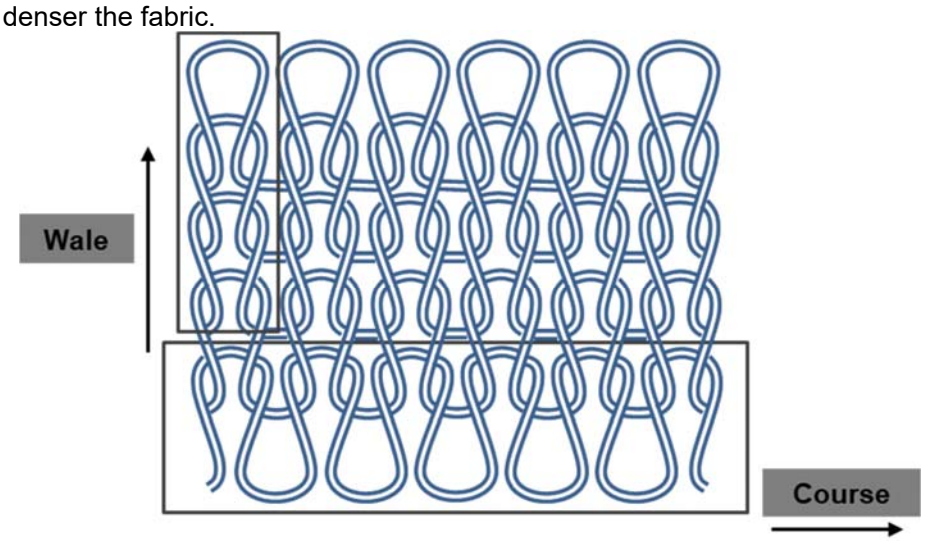

Figure 3.20 Course and wale of knitted fabric.

$$Stitch\ density = CPI\ x\ WPI \qquad \text{Eq. 3.12}$$

3.12.3 Fabric structure

The structure of the untreated and treated fabrics was view under light microscope (Leica M205C) and SEM. The procedure for this images is the same as procedure mentioned in section 3.4 (Microscopy).

3.12.4 Bending length

Bending length is related to the rigidity of the fabric, thus influences the drapability and the handle of the fabric. Common test to measure the fabric bending length is cantilever test where the length of the fabric deforms under its own weight was recorded. However, the PP-40 knitted fabrics produced in this study are stiff and tend to curl and twisted during cantilever test, therefore difficult to record the bending length. Other method suggested by (Peirce et al., 1930) is the hanging loop test which is done by clamping the two end of the fabrics and hung downward vertically to form loop shape. Three different loop shapes: ring, pear or heart shape can be used. The hanging pear loop test was chosen considering the limited fabric length obtained and method suitable for stiff fabric.

In this test, rectangular samples with 9 cm length (L) and 2.5 cm width were prepared. The end of the fabric strip was clamped and hung downward as shown in Figure 3.21. The vertical distance from the clamp to the bottom of the loop was recorded as the height of the loop, *h*. At least 3 samples were measured to get the average value of the loop height in course and wale directions.

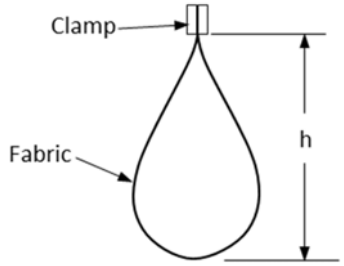

Figure 3.21 Hanging pear loop illustration.

3.12.5 Vertical wicking test

The ability of the fabric to transport liquid was conducted by measuring the vertical wicking behaviour in course and wale direction. At first, a wicking solution consists of distilled water, Azonine Scarlet 4BS red dye (0.15 g/l) and non-ionic detergent (0.12 g/l) was prepared. The samples were hung and with the bottom samples immersed in the solution as shown in Figure 3.22. The rise in height was recorded after 30 mins.

However, we found out that the water and dye were separated on samples during wicking testing. The separated components make it difficult to record the height of the solution. Second method was prepared by giving a colour to the samples before immersing them in a dye bath as shown in Figure 3.23.

Figure 3.22 Vertical wicking test using wicking solution.

Before the test, both untreated and treated fabrics were coloured/dyed into red colour using different method, based on the outer component of the fibres. The untreated fabric which has PP as an outside component and PA6 located inside of the fibres were dyed with red dispersed dye. The dyeing process was conducted in Roaches Pyrotec 200 lab dye machine for 3 h at 100 °C. The treated fabrics, which only hasve PA6 microfibres as a component were easily dyed by immersing in the dye solution (0.15g/l Azonine Scarlet dye dissolved in 1 litre distilled water) for 30 mins. The rectangular samples with 9 x 2.5 cm measurement were prepared for this test. The samples were hung vertically with their lower part dipped in the distilled water (Figure 3.23). The height of the water absorbed by the fabric was recorded for 5, 10, 15 and 30 minutes. Six samples for each fabric: three in course and wale direction, respectively, were used in this test.

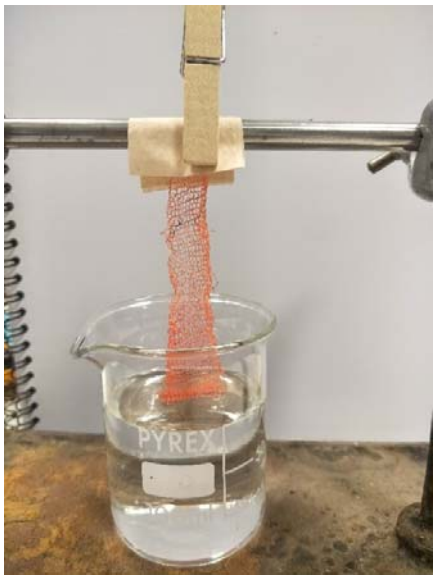

Figure 3.23 Vertical wicking test using water.

3.12.6 Ball burst strength

To evaluate the strength of the fabric, Titan ball burst strength test was used by using 25.4 mm ball probe and ball burst tooling clamp as shown in Figure 3.24. Three samples from each fabric were used to get the average value of the fabric strength in Newton (N). The fabrics were conditioned at 20±2°C and a relative humidity of 65±5% for at least 24 h before testing.

Figure 3.24 Ball burst tooling clamp (left) and ball probe (right).

Chapter 4
Production of partially miscible hybrid fibres of polyamide 6 and thermoplastic polyurethane polymer

4.1 Introduction

This chapter describes the production of hybrid fibres from polyamide 6 (PA6) polymer blended with thermoplastic polyurethane (TPU) polymer via a single step twin-screw melt spinning process. TPU is widely used as a coating on top of textile fabrics due to its excellent stretchability, mechanical properties, water proofing and breathability (Oertel and Brentin, 1992; Akovali, 2012). Inflatable raft, life vests and other marine products use TPU coating on top of the polyamide woven fabrics. As these applications are multi-polymer configurations, it poses challenges during recycling as no commercial methods are available for sorting and separation into component polymers. Previous studies have reported the blending of PA6 and TPU in injection moulding and compression moulding, but there is paucity of work on PA6 and TPU fibre blending. The blending of PA6 and TPU produces partially miscible polymer owing to hydrogen bonding between amide group in PA6 and urethane group in the TPU (John and Furukawa, 2009; Rashmi et al., 2013).

Variety of TPUs can be produced by changing the ratio of hard to the soft segments and also by changing the constituent chemistries. Commercially, a ‘D’ symbol used in the TPU series number (e.g., Elastollan®1278 D) denotes the rigid types of TPUs, meanwhile ‘A’ symbol (e.g., Elastollan®9305 A) denotes the flexible types of TPUs (Huntsman, 2010). Therefore, two types of TPU with different grade were chosen in this study; TPU 1278D (TPU-D) and TPU 9305A (TPU-A) denote the rigid and flexible type of TPU, respectively. To maximise the usage of PA6 in the blending, the PA6 composition was set higher than secondary polymer (TPU); 50% and 80%. The morphology, chemical, thermal and mechanical properties of the fibres were investigated and discussed in this chapter. The discussion was divided into Part 1 and Part 2, covering the blending of PA6:TPU-D and PA6:TPU-A, respectively.

4.2 Part 1: PA6:TPU-D

4.2.1 Viscosity and fibre production

The viscosity of polymers was measured to understand the rheology behaviour of the polymers during melt extrusion. The final morphology and the properties of the as-spun fibres are affected by the distribution of the polymers during melt extrusion process, which influenced by the apparent viscosity of the polymers. (He et al., 2014; Tang et al., 2003; Tavanaie et al., 2013).

For PA6 and TPU-D, the apparent viscosity was measured at 230 °C (Figure 4.1), corresponding to the highest processing temperature (die temperature) of the polymer during fibre extrusion. PA6 shows higher viscosity at 230 °C than TPU-D. The PA6 has melting temperature at 220 °C and therefore has high viscous at 230 °C while TPU-D which melts at 189 °C has lower viscosity at 230 °C. The viscosity of both polymers reduced when the shear rate increased showing the non-Newtonian fluid behaviour with shear thinning effects.

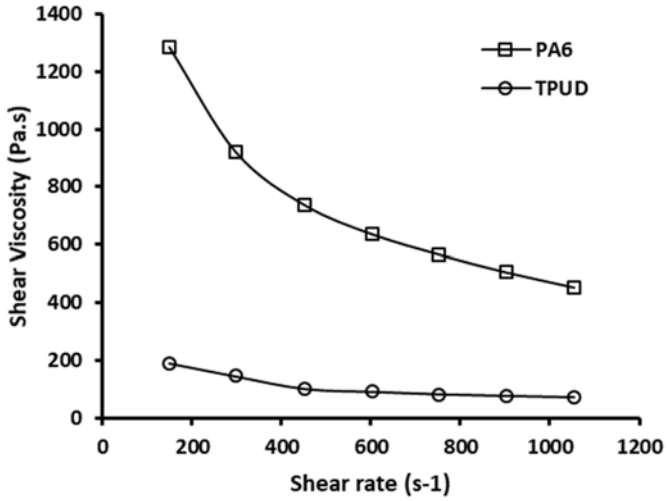

Figure 4.1 Viscosity of PA6 and TPU-D at 230°C.

In the production of PA6:TPU-D hybrid fibres, the screw speed used was set at 40, 60 and 80 rpm with the screw diameter of 10 mm and the overflight gap of 0.1 mm. The viscosity ratio and estimated shear rate for PA6:TPU-D hybrid fibres extruded at 230 °C are shown in Table 4.1, calculated using Eq. 2.2 and 2.3, respectively.

Table 4.1 Shear rate and viscosity of the PA6:TPU-D hybrid fibre.

Screw speed (rpm)	Shear rate (s^{-1})	PA6 Viscosity, η_{PA6} (Pa.s)	TPU-D Viscosity, η_{TPUD} (Pa.s)	Viscosity ratio (η_{TPUD}/η_{PA6})
40	209	1130	170	0.15
60	314	890	120	0.13
80	419	770	100	0.13

The viscosity ratios between PA6 and TPU-D for three cases show the value smaller than 1, thus better dispersion of TPU-D in the PA6 matrix should be expected (Kirchhoff, 2007). The increasing of the screw speed also expected to the decrement of the droplet size (Tavanaie et al., 2013). However, the final morphology of the PA6:TPU-D hybrid fibres appears different from the previous study as discussed in section 4.2.2 (Morphology of the as-spun fibres).

After the rheology testing, both single component fibres, PA6 and TPU-D, and PA6:TPU-D hybrid fibres were produced via melt spinning as mentioned in section 3.2.2 (Melt extrusion*)*. Two blend compositions of PA6:TPU-D were produced; 80:20 (TPU-D 20) and 50:50 (TPU-D 50) together with 100% PA6 (PA6) and 100% TPU-D (TPU-D) as reference fibres. The 20:80 (TPU-D 80) of PA6:TPU-D was not successfully produced at 230 °C processing temperature due to the very low viscosity of the TPU. In TPU-D 80, major component in the blend is TPU-D which has low viscosity at 230 °C. When the viscosity is too low, the polymer become delicate thus difficult to form into fibres. The TPU-D 20 and TPU-D 50 were also produced at higher processing temperature than 230 °C (240 °C & 260 °C), however the fibres were not successfully formed due to the low viscosity of TPU-D.

4.2.2 Morphology of the as-spun fibres

In polymer blend, phase separation between two partially or fully immiscible polymers was expected with the dispersed phase that was formed into droplet, sphere or fibril shape (Tavanaie et al., 2013) or produced into co-continuous morphology as shown in Figure 2.10. In this study, the blending of PA6 and TPU-D produced multi-porous fibres as shown in Figure 4.2. Furthermore, the phase separation between these two polymers also hardly be seen. In other studies, obvious phase separation can be seen between TPU and other polyamide group; PA6 (Chiu and

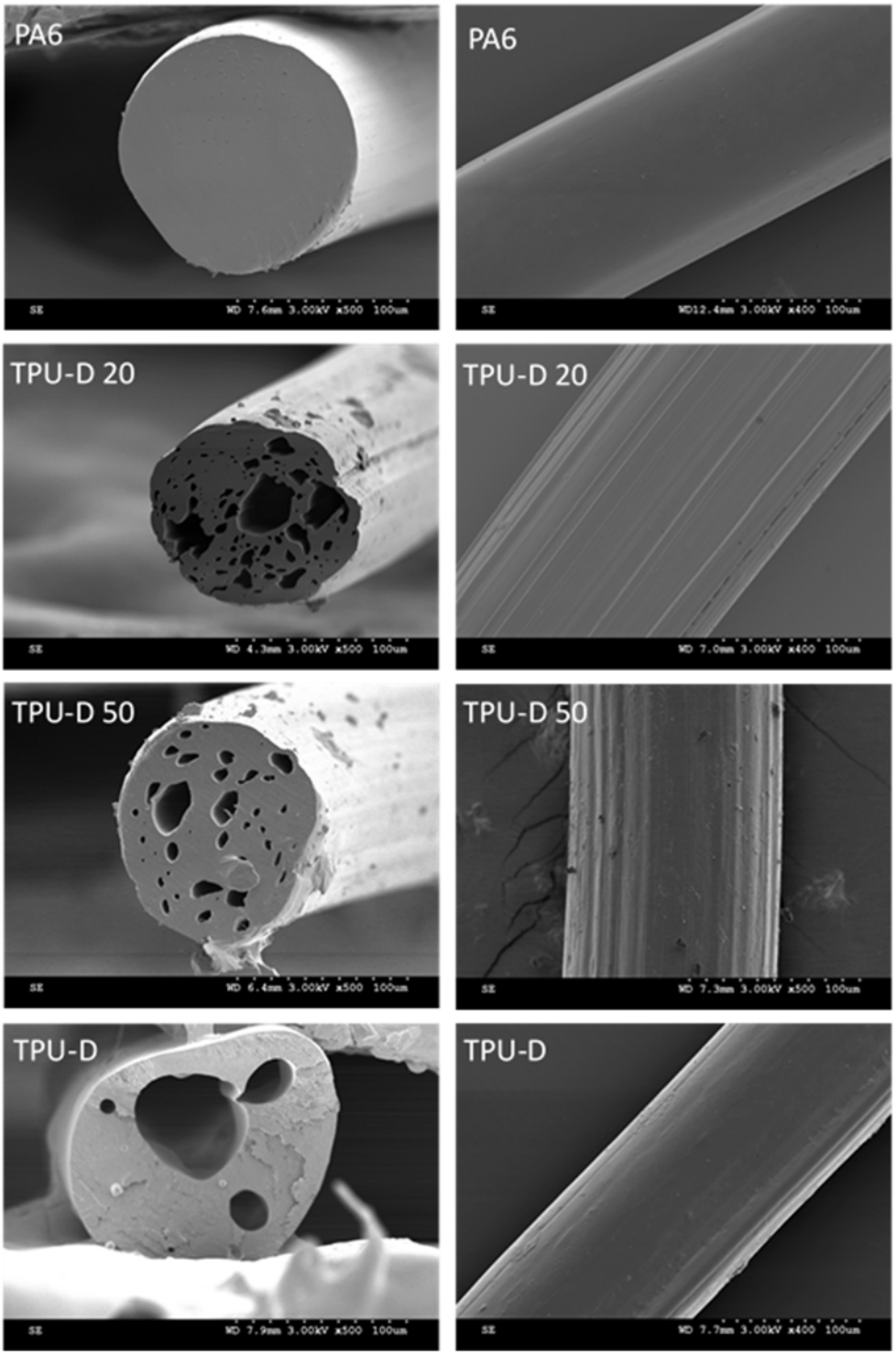

Figure 4.2 SEM images of PA6:TPU-D hybrid fibres and single component fibres in cross-section view (left) and longitudinal view (right).

Chuang, 2009), PA10 (Zhang et al., 2005), PA11 (Rashmi et al., 2017) and PA1212 (Li et al., 2008). As compared with the single component of PA6 and TPU-D fibres, dissimilar morphology was observed in the hybrid fibres. PA6 fibres, as expected, produced cylindrical fibre shape with smooth fibre surface, typical fibre shape for man-made fibre. The added 20% of TPU-D in the PA6 modified the fibre structure into multi-porous fibres with grooved fibre surface as seen in Figure 4.2 (TPU-D 20). The multi-porous fibres can also be viewed in the TPU-D 50 (Figure 4.2 (TPU-D 50)), with the fibre surface smoother than TPU-D 20. Meanwhile, the TPU-D single component fibres demonstrated the present of pores in the fibres when produced at 230 °C.

The existence of pores in the TPU-D fibres is unlikely to develop in standard TPU fibres. To clarify the present of pores, TPU-D fibres were produced at different processing temperatures starting from 200 °C to 230 °C with interval of 10 °C. The microscopy images in Figure 4.3 show that no pore was formed in the TPU-D fibres produced at 200 and 210 °C. The development of pores started to appear in the TPU-D fibres produced at 220 °C, shown in dotted circles, and significant pores clearly seen in the fibres produced at 230 °C.

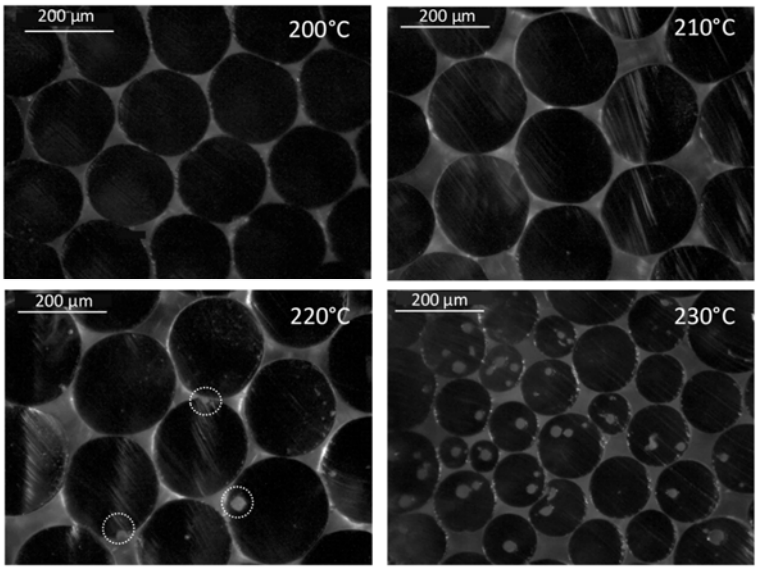

Figure 4.3 Micrograph of TPU-D fibres produced at different processing temperature (range 200°C~230°C) pores appear in the fibres produced at 220°C were shown in dotted circles.

Producing the TPU-D fibres at high temperature tends to degrade the TPU and causes release of carbon dioxide, oxidation and chain scission in the polymer (Lu

et al., 2003). The high processing temperature of TPU-D in this study (~45°C higher than melting temperature) causes the TPU-D to degrade hence produce gas bubbles and leaves pores in the TPU-D fibres. Therefore, the developed pores in TPU-D fibres produced at high processing temperature clarifies the existence of multi-pores in the PA6:TPU-D hybrid fibres. The presence of small pores was also found by Chiu and Chuang (2009) in the compressed mould of PA6:TPU (80:20) and Zo et al. (2014) in the PA6 and TPU blend composites, which were produced in the temperature range of 230 to 260°C.

To study the effect of shear rate and elongation force on the morphology of the hybrid fibres, the TPU-D 20 was produced at different screw speed and take-up winder speed as mentioned in Table 4.2. The SEM images in Figure 4.4 and Figure 4.5 show the presence of pores in all the fibres nevertheless the processing parameters of the melt extrusion. This proves that the pores developed in the hybrid fibres are not cause by the mechanical interaction between both polymers during melt extrusion which produced at higher shear rate. The surface of the TPU-D 20 fibres produced at different screw speed and take-up speed was also groovy, unlike the PA6 single component fibres which can benefit to higher fibre surface area.

Table 4.2 Processing parameter of TPU-D 20.

Screw speed (rpm)	Take-up winder speed (m min^{-1})
40	24.5
	40
60	24.5
	40
80	24.5
	40

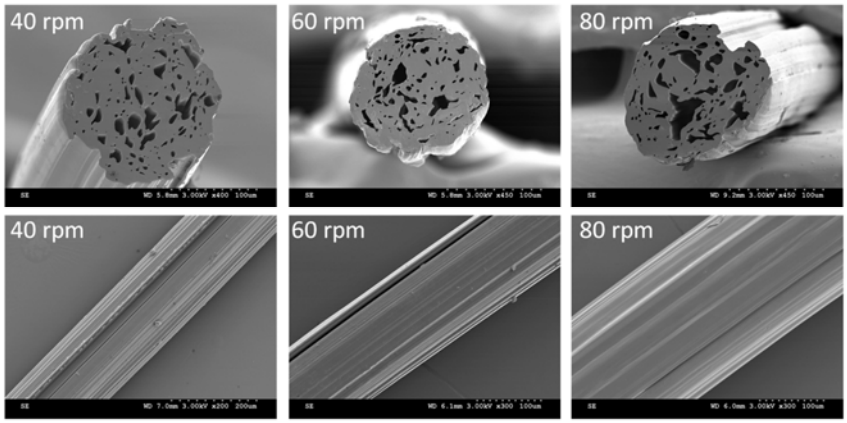

Figure 4.4 SEM mages of TPU-D 20 fibres produced at different screw speed in cross-sectional view (top) and fibre longitudinal view (bottom).

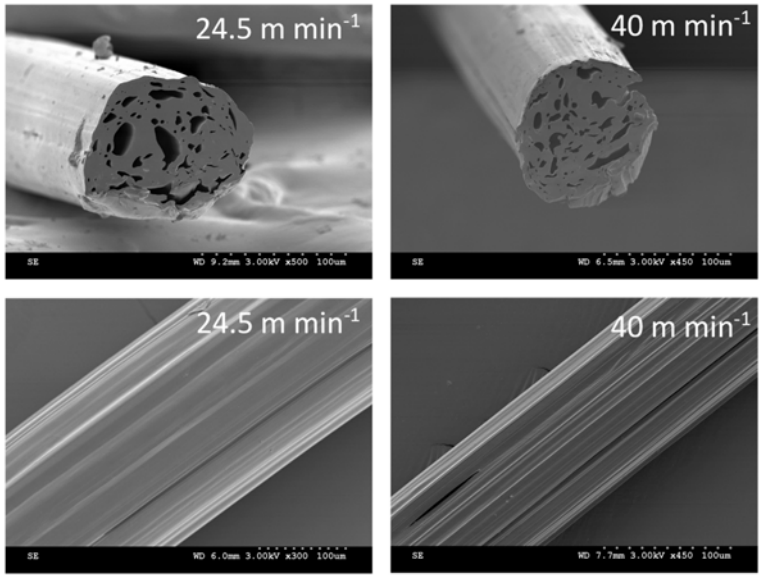

Figure 4.5 SEM images of TPU-D 20 produced at different winder take-up speed in cross-sectional view (top) and fibre longitudinal view (bottom).

4.2.3 Polymer extraction

After extrusion of the fibres, the single component and hybrid fibres (TPU-D 20 & TPU-D 50) were treated with dimethyl sulfoxide (DMSO) to remove the TPU-D component from the hybrid fibres. The extraction method was performed as mentioned in section 3.3 (Fibre treatment). The TPU-D was immersed in the DMSO for 3 h and 24 h and the mass before and after the treatment was recorded and the mass loss was calculated using Eq. 4.1.

$$Mass\ loss\ (\%) = \frac{mass\ before - \ mass\ after}{mass\ before} \times 100 \qquad \text{Eq. 4.1}$$

From the observation during the experiment, the TPU-D fibres were found completely dissolved after 15 mins in DMSO. The PA6 and hybrid fibres, however, remained in the fibre form after the chemical treatment. The percentage of the TPU-D component loss during the treatment in DMSO (refer to Table 4.3), indicates that it was not fully eliminated from the hybrid fibres. For TPU-D 20 hybrid fibres, approximately 6% of TPU-D left in the fibres. While in TPU-D 50, approximately 20% of TPU-D remains in the fibres after the treatment. Dissolving hybrid fibres in short and long period did not show notable difference in terms of mass loss.

Table 4.3 Mass loss of PA6:TPU-D hybrid fibres after being treated in DMSO and formic acid for 3 and 24h.

Fibre	Duration	TPU-D mass loss in DMSO (%)	PA6 mass loss in Formic acid (%)
PA6	3	0	100
TPU-D 20	3	14	Disintegrated
	24	15	Disintegrated
TPU-D 50	3	30	26
	24	30	27
TPU-D	3	100	-

Figure 4.6 shows the light microscopy images of hybrid fibres before and after treatment with DMSO to remove the TPU component. The morphology of TPU-D 20 appears to be not much affected by the DMSO treatment, either in 3 h or 24 h of treatment. However, TPU-D 50 treated for 3 h and 24h shows modifications in the fibre morphology. The pores existed in the TPU-D 50 before treatment (Figure 4.6 lower left) were no longer seen in most of the 3h and 24h treated fibres (Figure 4.6 lower middle and right). Some of the TPU-D 50 hybrid fibres treated for 3h were not affected by DMSO treatment (shown by dotted circle in Figure 4.6, lower middle). The fibres in the dotted circles still have pores as the fibres before treatment whereas in other fibres, no obvious pores can be seen. This might be cause by the shorter time (3h) exposed in the DMSO or DMSO has not reached to certain areas in the fibres.

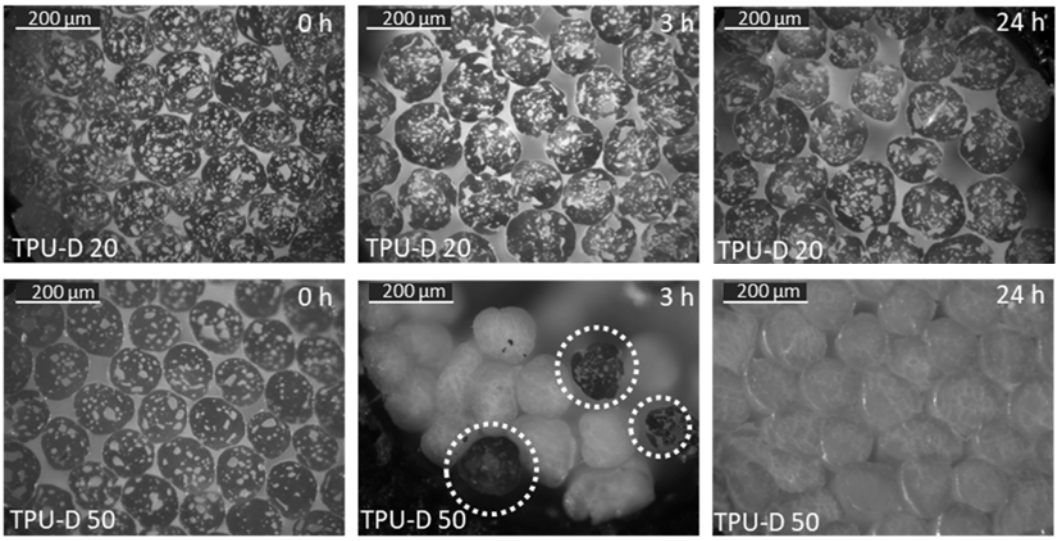

Figure 4.6 Micrograph of TPU-D 20 (upper) and TPU-D 50 (lower) before (left) and after treatment with DMSO for 3h (middle) and 24 h (right).

Significant difference can be seen between the TPU-D 50 for 3h and 24 h microscopy images where fibres were completely treated with DMSO for 24 h (Figure 4.6 lower right). The changes of the fibre morphology are related to the function of DMSO to extract the TPU-D component from the fibres. The DMSO has the ability to get inside the fibres through the pores and extracts the TPU-D component. However, the shape of the pores is also affected by the removal of TPU-D hence the fibre morphology changed. The residue of TPU-D in the fibre after treatment might attached to the PA6 or the TPU-D was trapped inside the fibres.

To get closer observation of the fibre morphology after treatment, high magnification SEM images of the hybrid fibres after 24 h treated with DMSO were obtained as shown in Figure 4.7. The morphology of the fibres after treatment shows dissimilarity to the as-spun fibres (shown in Figure 4.2). The transformation of the fibre cross-sectional structure can be seen with the changes of pore size where smaller pores were obtained in both of the treated fibres. However, the fibre surface was not affected by the DMSO treatment (Figure 4.7 lower). This shows that TPU-D is located inside the fibres while PA6 dominantly surrounded the fibres and encapsulated the TPU-D.

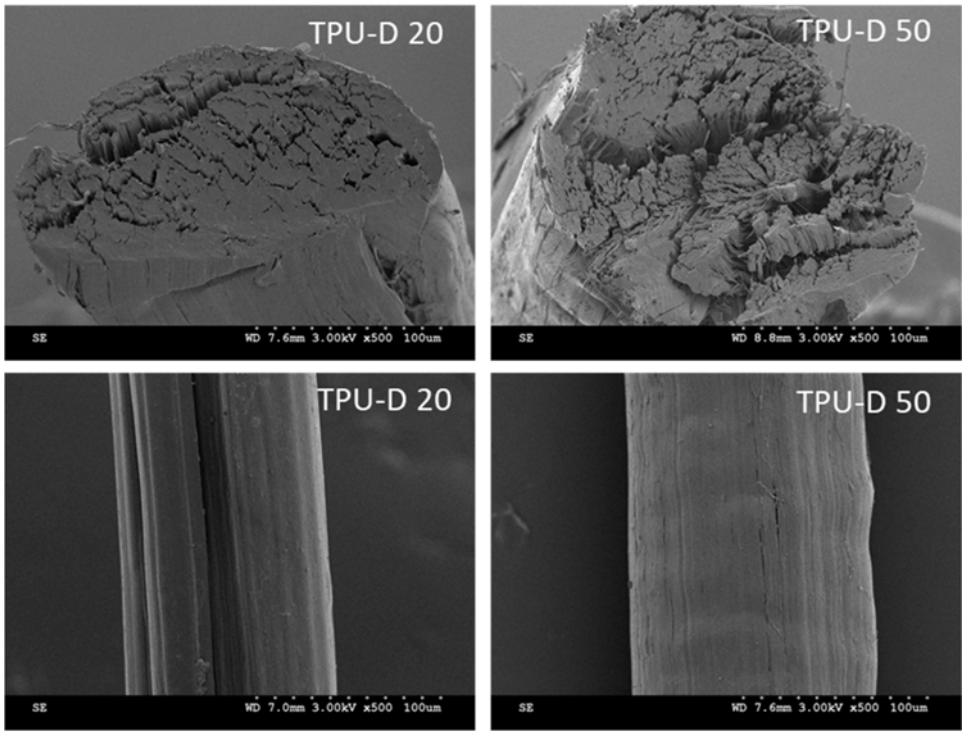

Figure 4.7 SEM images of PA6:TPU-D hybrid fibres after 24 h treatment in DMSO in cross-sectional view (upper) and longitudinal view (lower).

The PA6:TPU-D hybrid fibres and PA6 fibres were also treated in formic acid for 3 and 24 h at room temperature, to discover the morphology of the fibres when PA6 was detached from the hybrid fibres (Table 4.3 and Figure 4.8). During the treatment, single component PA6 fibres were completely dissolved after 3 hours soaked in formic acid. The TPU-D 20 was found disintegrated in both treatment's duration showing that the PA6 which has major composition (80%) in the blend, encapsulated the TPU-D, thus the fibres collapsed after the removal of the PA6.

In TPU-D 50 hybrid fibres, 27% of the PA6 loss was recorded, leaving ~23% remain in the fibres. The morphology of the TPU D-50 after removal of PA6 (Figure 4.8) was observed to be changed compared to the fibre before treatment (Figure 4.2). The unique cross-section of the TPU-D 50 was observed in Figure 4.8, with the fibre surface shown 'uneven-tree-trunk' effect. The fibres surface is definitely affected by the formic acid because of the PA6 is dominant at the fibre surfaces, based on the images shown in Figure 4.7. Longer exposure to the formic acid might affect the fibre surface where it becomes coarser when treated for 24 h. The pores in the fibres, even after 24 h treatment, can still be seen even the changes of the shape can be traced.

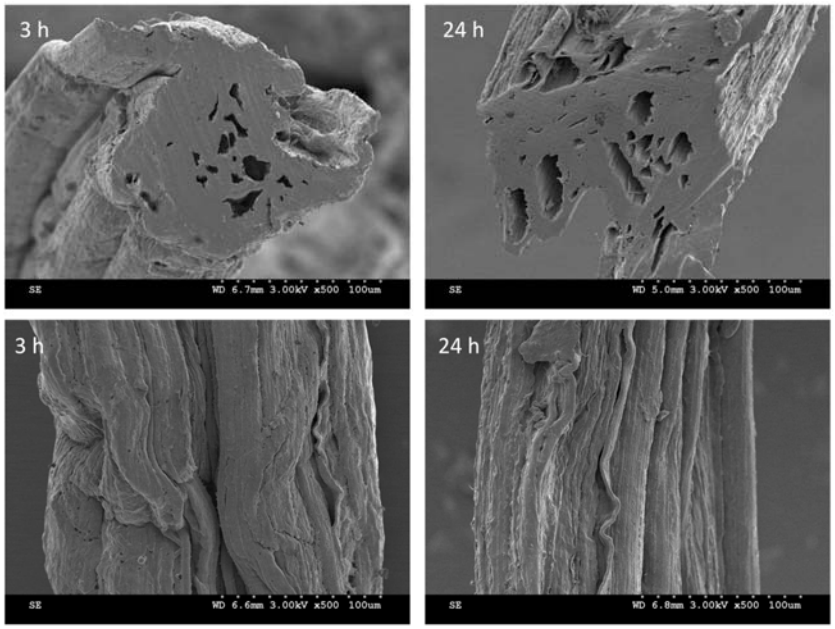

Figure 4.8 SEM images of TPU-D 50 after treated with formic acid for 3 and 24 h in cross-sectional view (upper) and longitudinal view (bottom).

The mass loss obtained in Table 4.3 indicates that both PA6 and TPU-D were not fully removed through both treatments. The high composition of the PA6 in the blend results the PA6 to encapsulate the TPU-D in TPU-D 20. Two possibilities can be assumed to have happened in the TPU-D 50, based on the mass loss of both component and the structural changes of the fibre morphology. First, the fibre morphology of the TPU-D 50 can be assumed as shown in Figure 4.9 where PA6 covered the fibre surface while unique shape of TPU-D was formed inside. When the fibres were soaked in the formic acid, PA6 at the fibre surface was dissolved and revealed the unique shape of TPU-D (Figure 4.9 right) that was not affected by formic acid, as also shown in Figure 4.8. Second, significant portion of the PA6 component might has trapped in the TPU-D component where formic acid cannot reach, based on the mass loss shown in Table 4.3. In other study related to TPU, the TPU dispersed in the PA6 matrix as sphere (Li et al., 2008; Rashmi et al., 2017) and sphericity (Zhang et al., 2005).

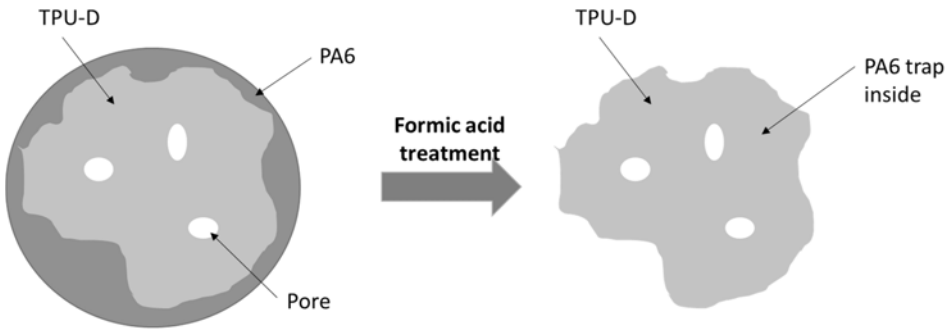

Figure 4.9: Fibre morphology of TPU-D 50 before and after treatment in formic acid.

4.2.4 Fibre and pore diameters

Linear density of the fibres obtained was 5.8, 17.0, 16.6 and 12.8 tex for PA6, TPU-D 20, TPU-D 50 and TPU-D, respectively. However, the structure of PA6:TPU-D hybrid fibres consists of multipores in the fibres, therefore fibre cross-sectional area (bulk and true, as mentioned in section 3.4.1) and the pores areas were measured. The light microscopy images (Figure 4.10) were used and the fibre areas were determined in ImageJ software.

Figure 4.11 presents the mean value for the cross-sectional area (bulk and true) and pore area of the as-spun fibres.

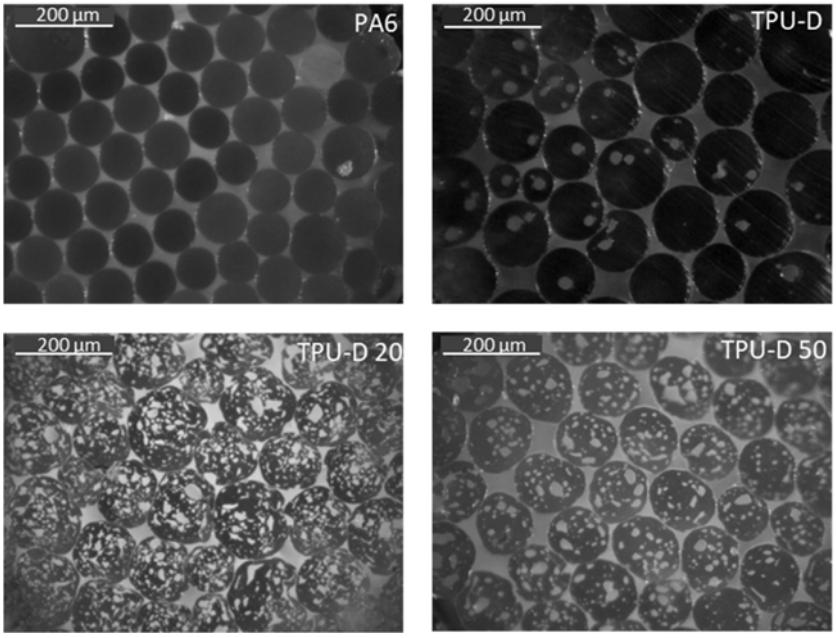

Figure 4.10 Micrograph of PA6, TPU-D, TPU-D 20 and TPU-D 50 fibre cross-section.

The cross-section of the hybrid fibres is categorised as non-circular, therefore the "circular equivalent diameter" (CED) was measured to represent the fibres diameter. The CED was calculated using Eq. 3.1, with d is fibre diameter and A is fibre cross-section area (bulk).

To obtain the fibre diameter, only cross-sectional area (bulk) of the fibres was considered. From Figure 4.11 and Figure 4.12, it can be concluded that the fibre diameter is corresponded with the fibre bulk area. Larger fibre area represents larger fibre diameter. The bulk area of the TPU-D 20 is greater than TPU-D 50 and both hybrid fibres bulk area was in between the PA6 and TPU-D. The result reflects the fibre diameter showing that the TPU-D 50 produces smaller fibre diameter than TPU-D 20 while PA6 has the finest fibre and the TPU-D has the largest fibre diameter. The fibre diameters for the as-spun PA6, TPU-D 20, TPU-D 50 and TPU-D were 114±1.2, 136±3.2, 126±1.5 and 151±6 μm, respectively. Based on Figure 4.10 (TPU-D) the diameter of TPU-D is irregular along the fibres.

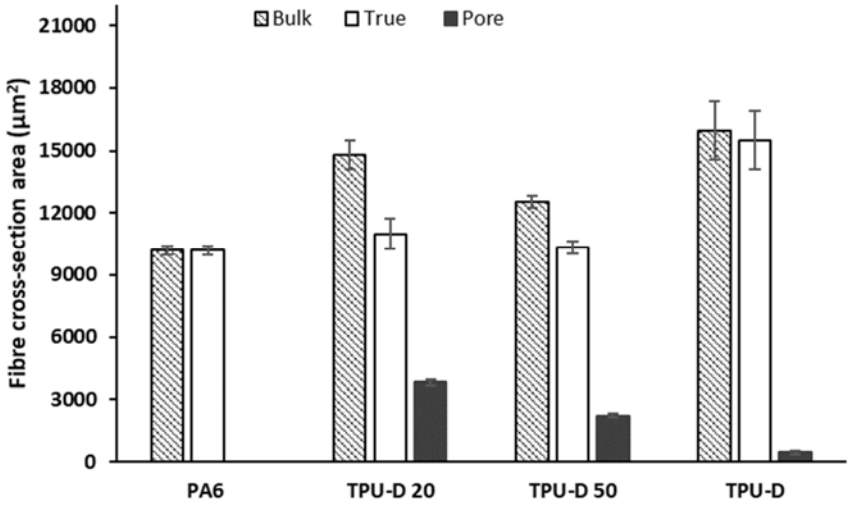

Figure 4.11 Fibre cross-section and pore area of the single component and hybrid fibres (bulk and true area). (*n*=30)

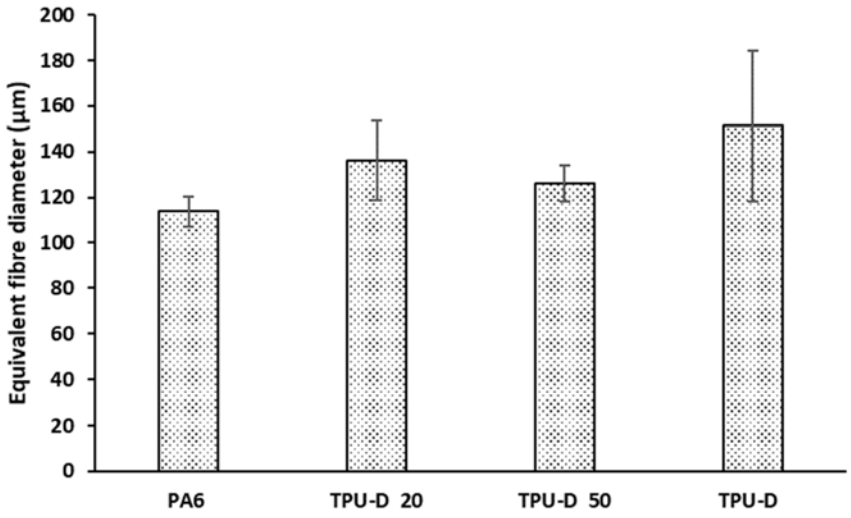

Figure 4.12 Fibre diameter of the PA6:TPU-D hybrid fibres and single component fibres.

Figure 4.11 also presents the cross-sectional area (true) and pores mean value of the hybrid fibres and TPU-D. The true area of the hybrid fibres, after eliminating the pores area, display similarity to the PA6 fibre area. This indicates that the pores developed in the hybrid fibres cause the cross section of the fibres expanded and influenced the bulk area and the final diameter of the hybrid fibres.

The diameter of pores developed in the hybrid fibres was calculated using Eq. 3.1 with d is a pore diameter and A is a pore cross-section area. The mean value of pore in TPU-D 20 and TPU-D 50 was 7.9±7.8 and 6.7±6.2 µm, respectively with the pores diameter distribution shown in Figure 4.13. Variable pore size dimension developed in both hybrid fibres with most of the pore diameters were below 20 µm. TPU-D 20 has maximum pore size of 58 µm and TPU-D 50 biggest pore size is 48 µm. Size and number of pores can give impact on the properties of the fibre with possible application such as sound absorption, insulation, moisture absorption, filtration and more.

The size of the PA6:TPU-D hybrid fibre produced in this study is almost similar with the fibre produced by Cui et al., (2018) (Figure 4.14). Cui produced porous fibres mimicking polar bear hair using “freeze spinning” technique and show excellent properties in thermal insulation. The fibres were produced from silk fibroin/chitosan solution by varied freezing temperature. The diameter of the fibres was 200 µm with the pore size in the range of 20-85 µm.

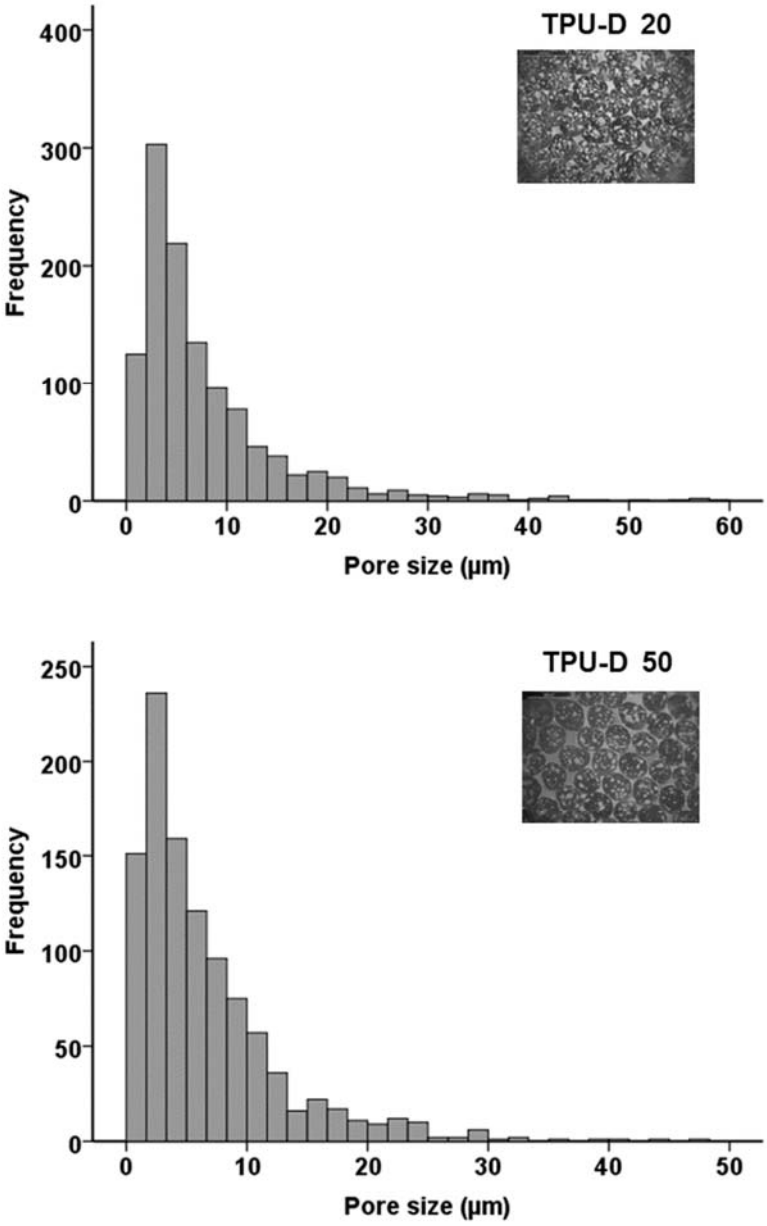

Figure 4.13 Frequencies of the pore size developed in TPU-20 and TPU-50 fibres from 30 specimen for each. ($n_{PA6\text{-}50}$=1046, $n_{PA6\text{-}80}$=1170)

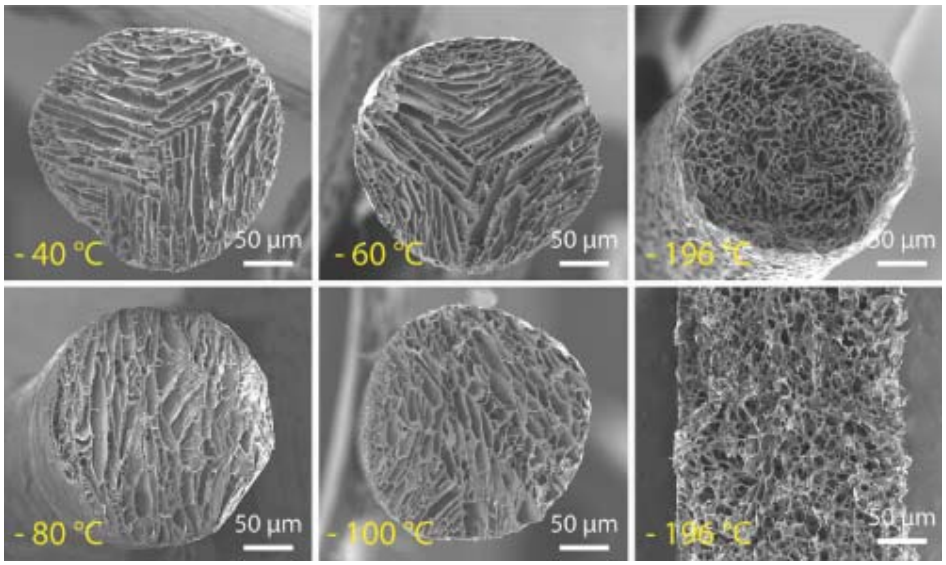

Figure 4.14 Porous fibres using freezing spinning method. (Cui et al., 2018)

4.2.5 Thermal properties

Two methods were used to study the thermal properties of the PA6:TPU-D hybrid fibre; differential scanning calorimetry (DSC) and thermogravinometry analysis (TGA).

The DSC curves of the PA6:TPU-D hybrid fibres with comparison to the pure polymers are presented in Figure 4.15 while Table 4.4 shows detail of the melting and crystallisation behaviour of the fibres. The melting behaviour of the fibres was determined from the second heating scan as the previous thermal history was removed during first heating scan.

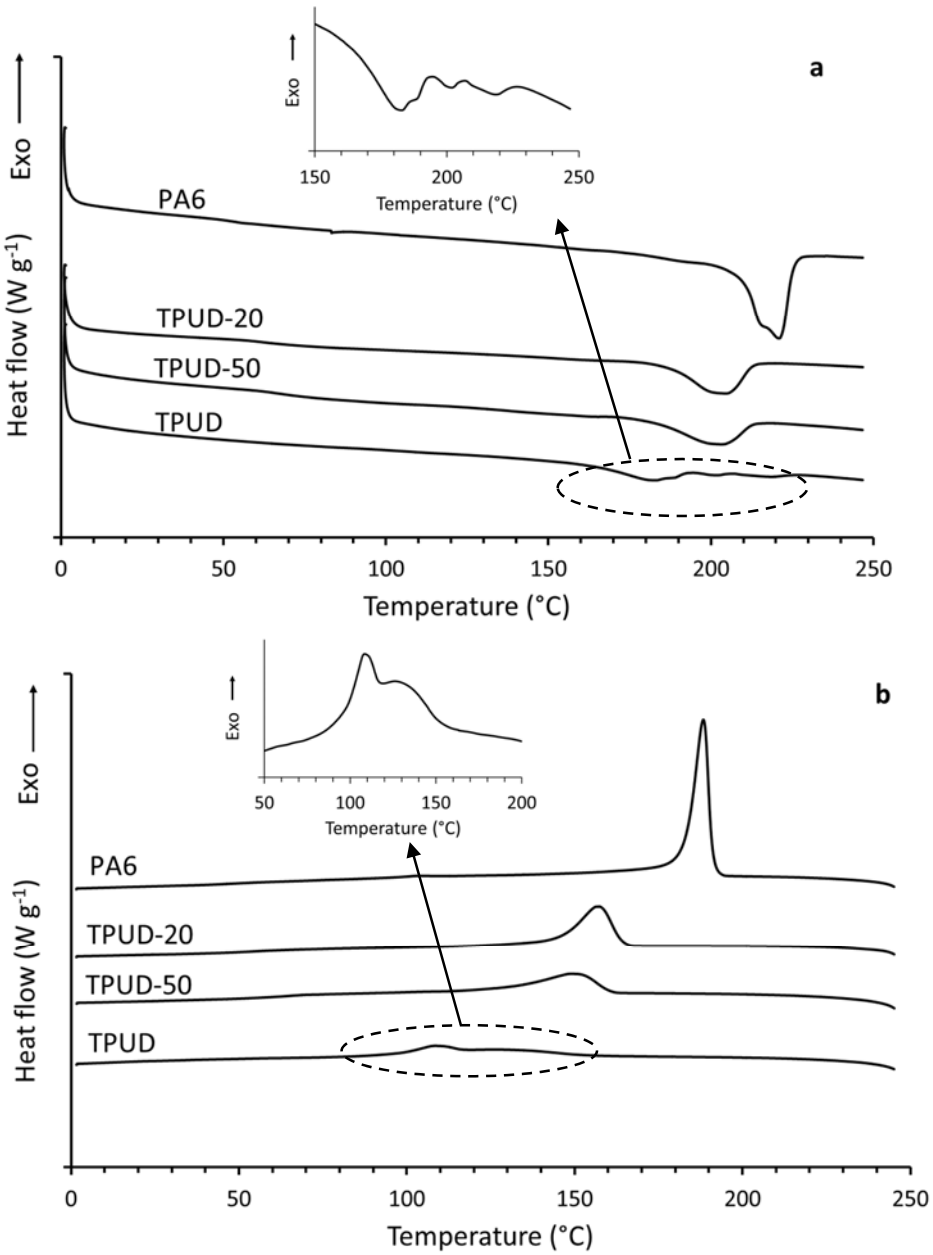

Figure 4.15 DSC curve of the fibres in a) heating and b) cooling cycle.

Both PA6:TPU-D hybrid fibres show single endothermic peak which melted at the same temperature, 204°C. In comparison to pure polymers, the melting peak of the hybrid fibres are lower than PA6 and higher than TPU-D. The maximum melting peak of PA6 shows at 221°C while TPU-D fibres completely melted at 182°C with small endothermic peaks appear at 202°C and 220°C. The single endothermic peak of the PA6:TPU-D hybrid fibres indicates the existence of extensive interaction between these two polymers. The melting point of the hybrid fibres can be possibly related to the hydrogen bonding developed in the blend (Genovese and Shanks, 2001; John and Furukawa, 2009; Zo et al., 2014). The interaction between amide

group of PA6 and urethane/urea group in TPU creates partial interaction between the polymers thus changes the thermal properties of the hybrid fibres.

In the PA6 melting curve, a shoulder peak appears at 215 °C, near to the maximum melting peak. Several possibilities can be attributed to the existence of the shoulder peak; the recrystallisation effects after the first heating cycle (Schick, 2009) or the development of two different crystal shape in the PA6 or same kind of crystal formation with different thickness (Millot et al., 2015). In PA6, two types of crystal form can be expected, α and γ-form, that melt at 222°C and 213°C, respectively (Stankowski et al., 2008). Meanwhile, in TPU-D melting curve, two small endothermic peaks are observed at 202°C and 220°C. TPU-D is an amorphous polymer and contains soft and hard segments where the small peaks are related to the disordering crystallinity of the hard segments (Frick and Rochman, 2004).

Table 4.4: Thermal properties of as-spun fibres sample.

Fibre	*Melting temperature* (°C)	Melting enthalpy (J g^{-1})	*PA6 Crystallinity (%)*	*Crystallisation temperature* (°C)
PA6	221	59.6	25.9	188
TPU-D 20	204	25.9	14.1	153
TPU-D 50	204	24.1	20.9	148
TPU-D	182	9.0	-	108

The reduction of PA6:TPU-D hybrid fibre melting temperature is also related to the crystallinity of PA6 in the fibres. From Table 4.4, the addition of 20% of TPU-D in the hybrid fibres was seen reduced the crystallinity of PA6 to 14%, calculated using Eq. 3.7. In the blend of 50:50 PA6:TPU-D, the decreasing of PA6 crystallinity were also observed however showing better crystallinity than TPU-D 20. The interaction between PA6 and TPU-D altered the PA6 crystallinity significantly in TPU-D 20 rather than in TPU-D 50. The blending of these two polymers might disorder the PA6 crystal form (Zhou et al., 2012) proven in the XRD result and chemical properties in section 4.2.6 and 4.2.7, respectively. The decrement of PA6 crystallinity in the hybrid fibres corresponds to the strength of the fibres as discussed in section 4.2.8 (Tensile properties).

The same trend was observed for crystallisation behaviour of hybrid fibres, which also located in between of PA6 and TPU-D fibres (Figure 4.15(b)). The crystallisation temperature of TPU-D 20 seems higher than TPU-D 50 by 5°C. Two

exothermic peaks of TPU-D shown at 108 and 128 °C corresponding to the soft segment of TPU-D (Rashmi et al., 2017). Thermal properties of the hybrid fibres after the treatment with DMSO were not markedly affected as shown in Figure 4.16. It shows that the residue of TPU-D still exists in the hybrid fibres and influenced the thermal properties of the fibres.

The thermal stability of the hybrid fibres was investigated by TGA and results are shown in Figure 4.17. The details of the TGA results are listed in Table 4.5. TPU-D fibres start to decompose at 298 °C, earlier than PA6 which starts to degrade at 419 °C. Thermal stability of the PA6:TPU-D hybrid fibres before and after treatment was found located in between of the parent polymers. The TPU-D 50 decomposed earlier than TPU-D 20 which attributed to the volume of the TPU-D component in the fibres. The increasing of the TPU-D content in the blend decreases the thermal stability of the hybrid fibres. The location of the TPU-D which was dispersed in the PA6 matrix also delayed the degradation of the TPU-D in the hybrid fibres, which degraded later than pure TPU-D fibres. The degradation of TPU-D and hybrid fibres were found in two steps which influenced by the incompatible blend between the hard and soft segments of TPU-D.

Thermal stability of the hybrid fibres after the DMSO treatment showed improvement for the T_{onset} compared to the untreated fibres. As showing before, the mixing of TPU-D and PA6 was partially miscible thus, after the treatment, TPU-D component still presence in the hybrid fibres. However, the amount of TPU-D in the fibres might decrease and the degradation of the hybrid fibres begin later than hybrid fibres before treatment. From Figure 4.17 (bottom), the curve for hybrid fibres after being treated shows one step degradation significantly similar with the PA6 degradation even though the temperature is slightly decreased.

Table 4.5 TGA results for PA6:TPU-D hybrid fibres before and after DMSO treatment.

Fibre	Untreated				DMSO treated			
	T_{onset} (°C)	T_{50} (°C)	T_{max} (°C)	Residue (%)	T_{onset} (°C)	T_{50} (°C)	T_{max} (°C)	Residue (%)
PA6	419	441	465	1.5	-	-	-	-
TPU-D 20	373	416	462	6.0	409	429	462	-6
TPU-D 50	345	390	456	2.7	375	406	444	-0.5
TPU-D	298	351	426	13.7	-	-	-	-

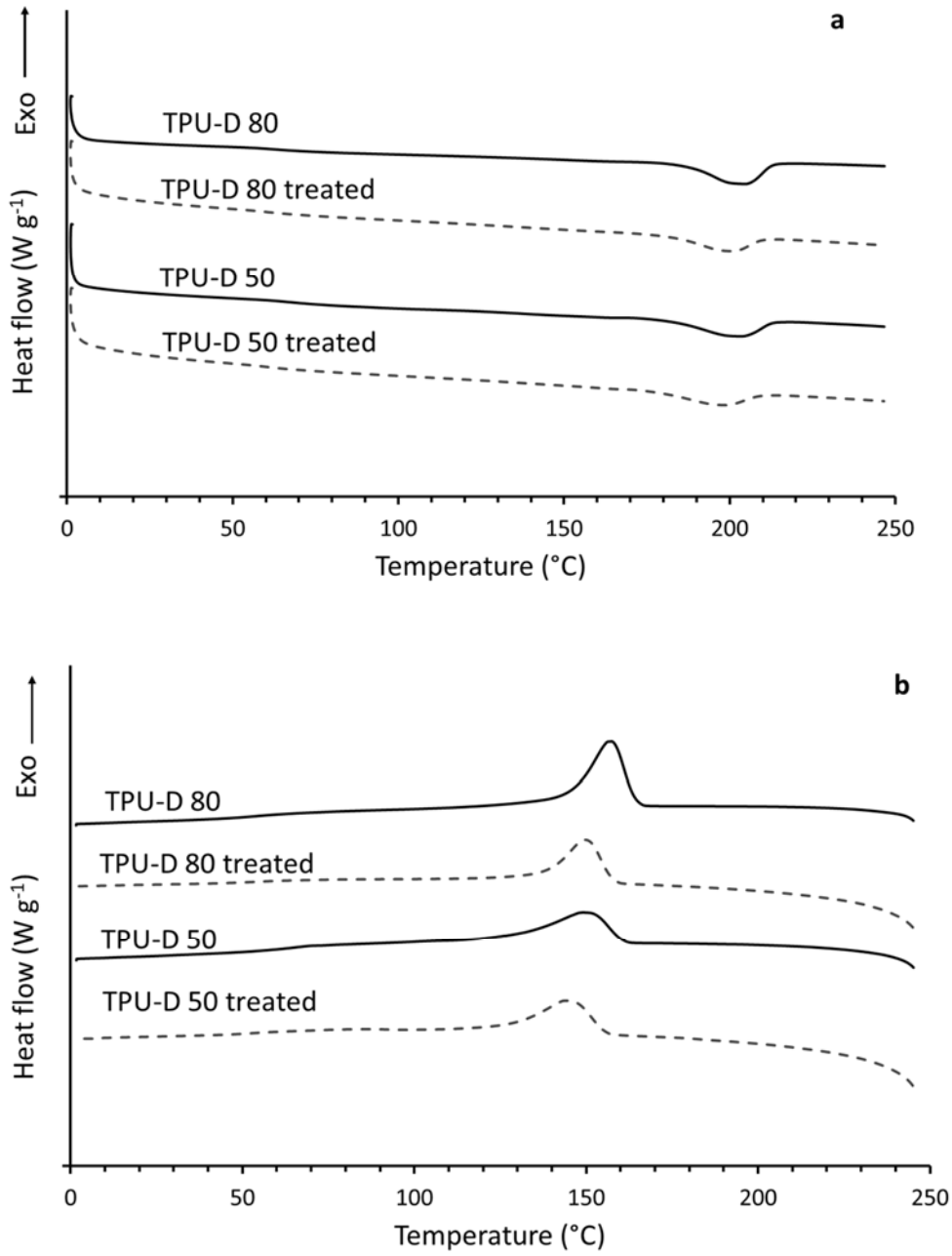

Figure 4.16 DSC curve of hybrid fibres before and after treatment with DMSO in a) heating and b) cooling cycle.

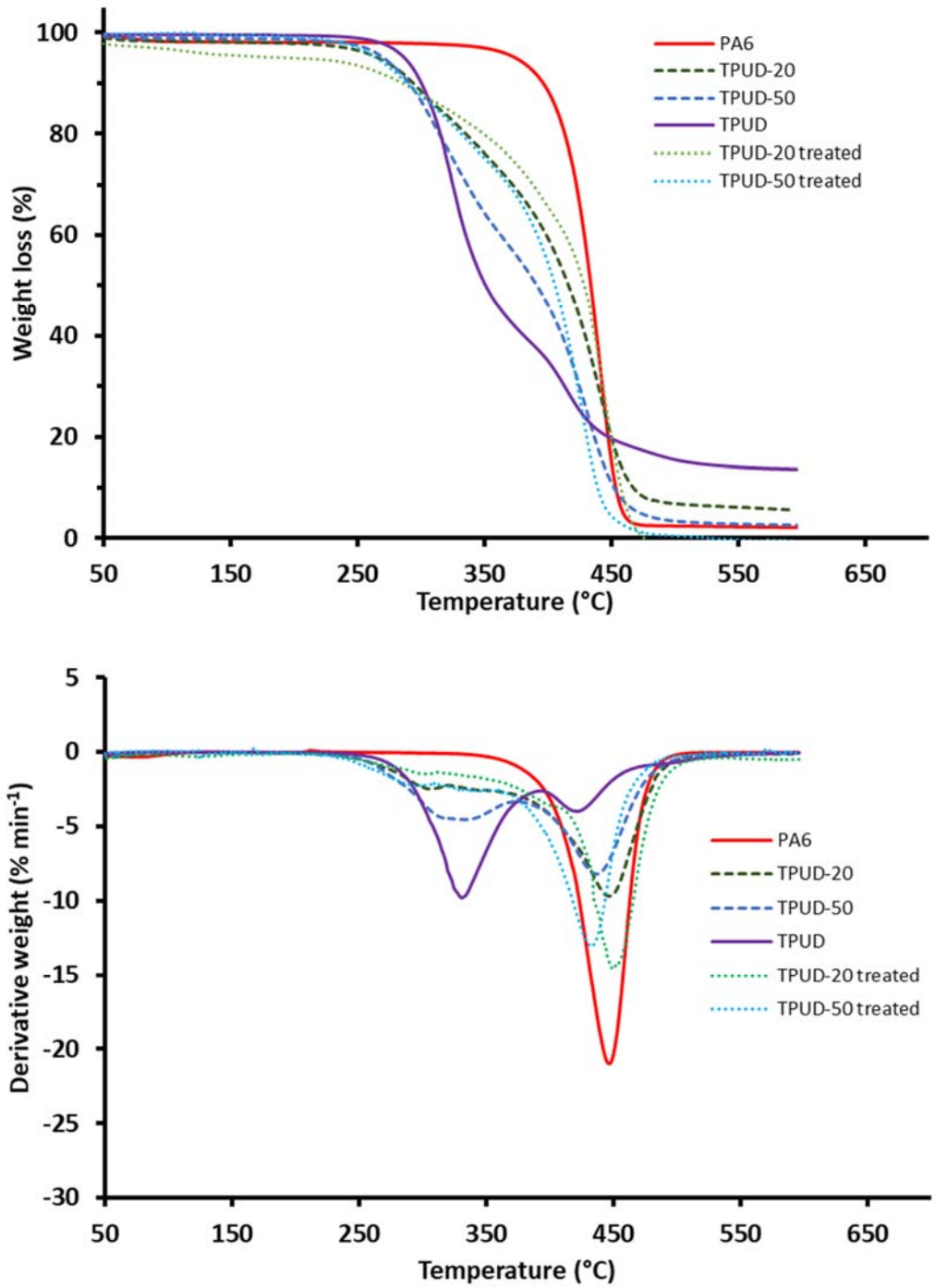

Figure 4.17 TG (top) and DTG (bottom) curve of hybrid fibres before and after treatment.

4.2.6 X-ray diffraction

The X-ray diffraction (XRD) results of the single component fibres and hybrid fibres are displayed in Figure 4.18 (top). PA6 fibres show a sharp peak at 21.3° that represent the PA6 γ-crystal structure. There are two types of PA6 crystal structures that normally observed: α-crystal (α_1= 20.1° and α_1= 22.6°/23.5°) and γ-crystal (21.3°). The moderate spinning process with take-up speed less than 9 km min^{-1} tends to produce γ-crystal in a PA6 fibres (S. Murase et al., 1997). The XRD pattern for TPU-D fibres shows that the fibres have amorphous nature with broad peak appears at 20.6°. The PA6 crystal structure distorted when 20% of TPU-D was added where a small proportion of α-crystal can be seen while γ-crystal still dominants in the TPU-D 20 hybrid fibres. Meanwhile in TPU-D 50 hybrid fibres, the α-crystal structures dominate the fibres with peaks appeared at 20.5° and 22.7° represent α_1 and α_2, respectively. Two new peaks at 14° and 17° appeared on the TPU-D 50 hybrid fibres which corresponded to the crystallinity of the hard segment of TPU-D component (Liu et al., 2017). The blending of PA6 and TPU-D does affect the crystal structure in the fibres especially in TPU-D 50. The various type of crystal developed in the TPU-D 50 improved the fibres strength which will be discussed in detail in section 4.2.8 (Tensile properties).

The XRD result of the fibres after the treatment in DMSO is shown in Figure 4.18 (middle and bottom). TPU-D 20 treated fibres show significant different with the untreated fibres. The removal of TPU-D has changed the PA6 crystal structure into α-crystal with two peaks appeared at 20.4° and 23.3° correspond to the α_1 and α_2 crystal, respectively. In TPU-D 50 hybrid fibres (treated), due to the removal of significant amount of TPU-D, the peak at 14° disappeared while peak 17° still appeared with low intensity. The peak observed at 17° indicates that the TPU-D hard segment crystal stills exist in the hybrid fibres and has not been removed during the treatment. The PA6 crystal in the TPU-D 50 treated however show the α_1-type crystal at 20.2° and γ-type crystal at 21.6°.

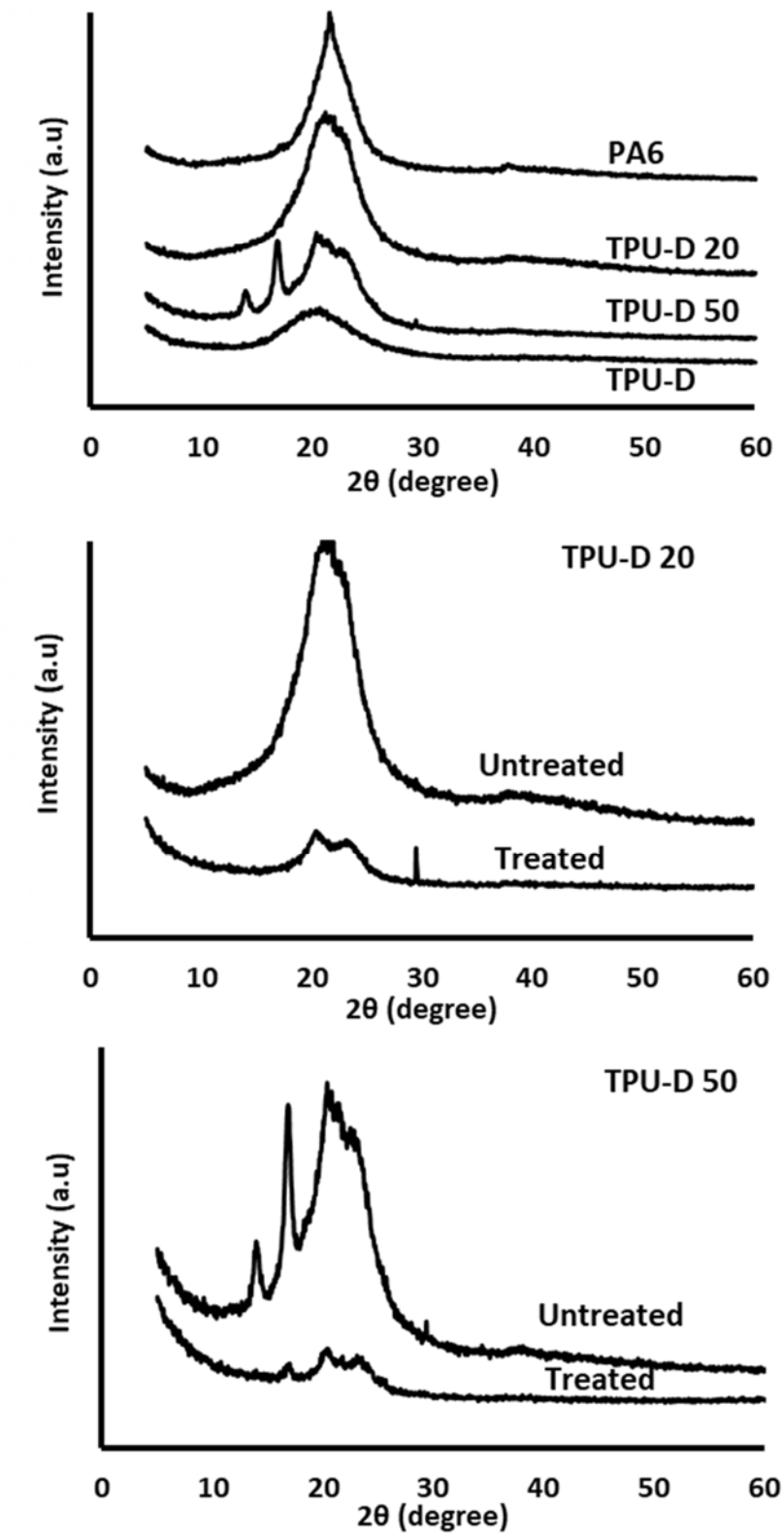

Figure 4.18 XRD results of (top)-single component fibres and hybrid fibres, (middle)-TPU-D 20 and (bottom)-TPU-D 50 hybrid fibres untreated and treated with DMSO.

4.2.7 Chemical properties

Figure 4.19 displays ATR-FTIR spectra of the single component fibres and hybrid fibres. The PA6 components; N-H (3291 cm^{-1}), C-H (2922 & 2864 cm^{-1}), amide I (1633 cm^{-1}) and amide II (1538 cm^{-1}) and TPU-D components; C=O (1698 cm^{-1}) and C-O-C (1218 & 1062 cm^{-1}) can be seen clearly in both hybrid fibres spectra. No new peak or missing peak was observed. The peaks of all main PA6 and TPU-D components were not significantly changed in the hybrid fibres except for TPU-D carbonyl component (C=O) as shown in Table 4.6.

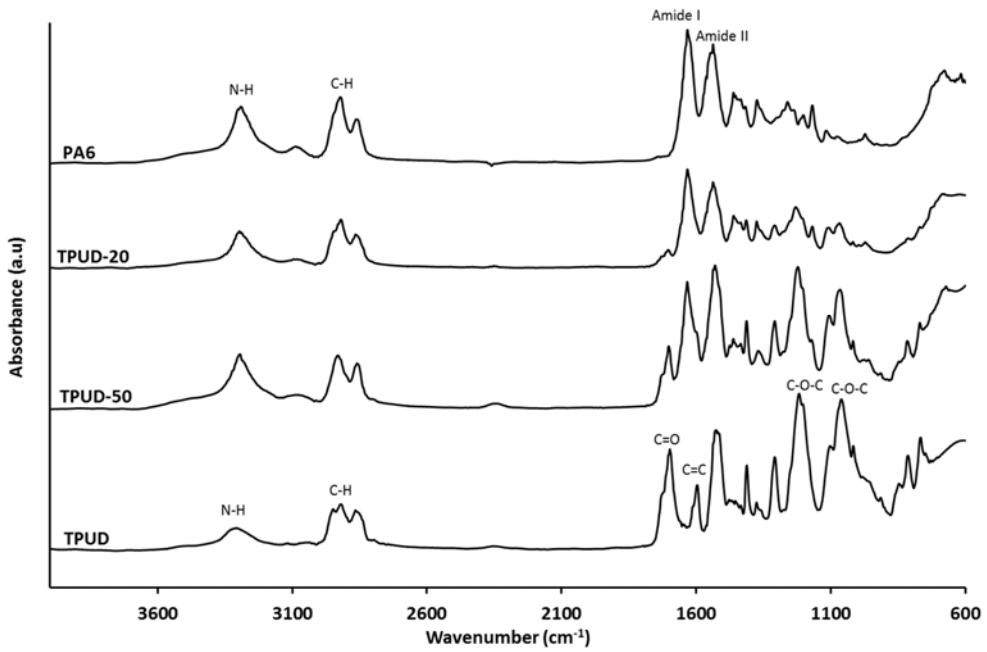

Figure 4.19 The FTIR spectra of PA6:TPU-D hybrid fibres and single component fibres (normalised at 2866 cm^{-1}).

The peaks of TPU-D carbonyl group (C=O, 1698 cm^{-1}) were found slightly shifted to 1705 cm^{-1} and 1703 cm^{-1} for TPU-D 20 and TPU-D 50, respectively. This TPU-D carbonyl region is associated with the crystalline region of urethane and urea groups (Todros et al., 2014) where the carbonyl peak 1698 cm^{-1} classified in urea groups. In this study, the free urea (keto group C=O) of TPU-D has changed to H-bonded urethane group (~1702 cm^{-1}) in both of the hybrid fibres, obviously in TPU-D 50, as shown in Figure 4.20. Amide group of PA6 and urea group of TPU-D interact with each other created hydrogen bonding thus shift the carbonyl peak in the hybrid fibres (John and Furukawa, 2009; Rashmi et al., 2017).

Table 4.6 ATR-FTIR wavenumber for PA6, TPU-D and hybrid fibres.

Wavenumber (cm^{-1})				
PA6	TPU-D 20	TPU-D 50	TPU-D	Assignments
-	-	-	3308	N-H and O-H
3291	3296	3295	-	N-H stretch
			2948	C-H stretching
2922	2919	2930	2921	C-H stretching
2863	2865	2859	2866	C-H stretch
-	1705	1703	1698	C=O stretch (free urea carbonyl)
1633	1633	1634	-	C=O stretch (amide I band)
-	-	-	1596	C=C stretching in benzene ring(Todros et al., 2014)
1538	1538	1524	1525	N-H (amide II band)
1462	1462	1462	-	CH2 scissoring
1375	1376	1370	1376	
-	1310	1309	1309	Aromatic C-N vibration
1261				
-	1230	1222	1218	C-O stretch urethane
1167	1167	-	-	CO-NH
1117	1107	1107		C-C stretching(John and Furukawa, 2012)
-	1068	1066	1061	Asymmetric C-O-C stretching in ether group
973	973	-	-	CO-NH
			814	C_H out of the plane aromatic ring
		770	767	CH2 rocking (polyether)

The effect of the blend on the carbonyl region of TPU-D was further analysed based on the absorbance intensity of the carbonyl group as shown in Figure 4.20 and Table 4.7. The hybrid fibres show lower absorbance intensity compared to TPU-D fibres which can be related to the amount of TPU-D content in the fibres. TPU-D 50 which has more TPU-D contents than TPU-D 20 shows high absorbance in all carbonyl phase. The carbonyl region relates to the TPU-D crystallisation region, thus reduced the amount of TPU-D, decreased the intensity. The intensity of the carbonyl group of the hybrid fibres after the treatment in DMSO was also shown in Figure 4.20. The

carbonyl peaks in both treated hybrid fibres decreased, obviously seen in TPU-D 50, showing that significant amount of TPU-D component was removed from the fibres.

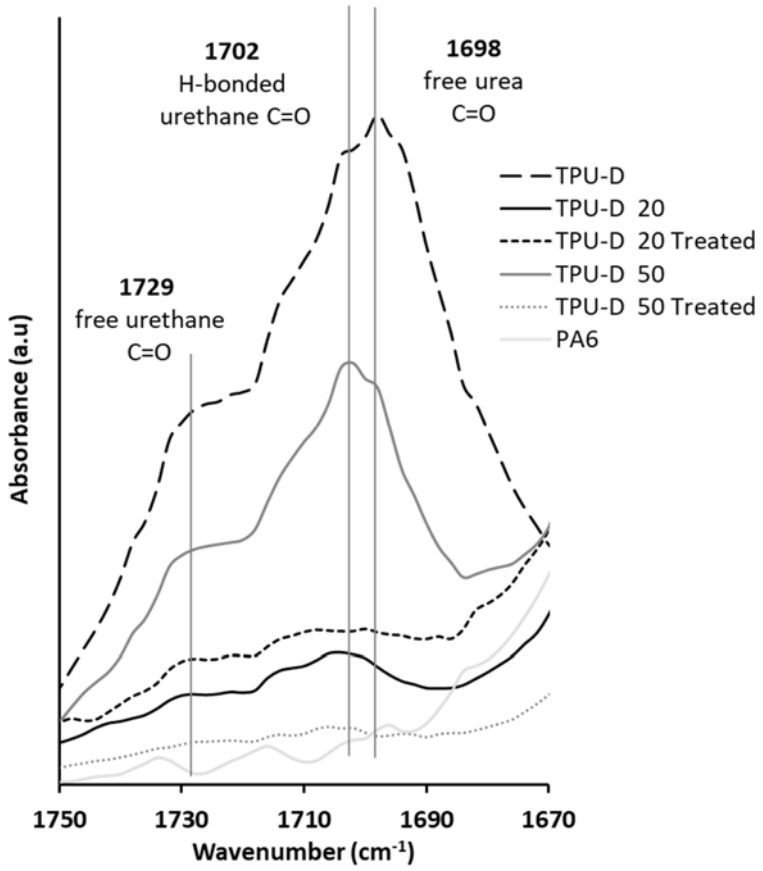

Figure 4.20 Carbonyl region of the FTIR spectra for TPU-D and hybrid fibres (normalised at 2866 cm^{-1}).

Table 4.7: Carbonyl phase absorbance intensity of the TPU-D and hybrid fibres

C=O phase	Wavenumber (cm^{-1})	Absorbance Intensity				
		TPU-D	TPU-D 50	TPU-D 20	TPU-D 50 Treated	TPU-D 20 Treated
Free urethane	1729	1.38	0.86	0.33	0.16	0.48
H-bonded urethane	1702	2.33	1.55	0.48	0.21	0.58
Free urea	1698	2.46	1.46	0.43	0.18	0.57

Several studies used ATR-FTIR result in the range of 850 to 1150 cm^{-1} to investigate the crystal type in the fibres (Figure 4.21). The PA6 spectra shows several peaks represent the γ-type crystal at 1630, 1169 and 973 cm^{-1} and α-type at 1202 cm^{-1}.

Both hybrid fibres show a γ-type crystal at 1630 cm^{-1}, in the untreated and treated fibres. In TPU-D 20, small peaks at 1169 and 973 were observed but not in the TPU-D 50. The TPU-D 50 spectra has more similarity to the TPU-D spectra than PA6. However, the removal of TPU-D from the TPU-D 20 shows no significant difference conversely with the TPU-D 50. The result is not corresponding well with the XRD result (discussed in section 4.2.6), therefore the ATR-FTIR might not give accurate information related to polymer crystallinity.

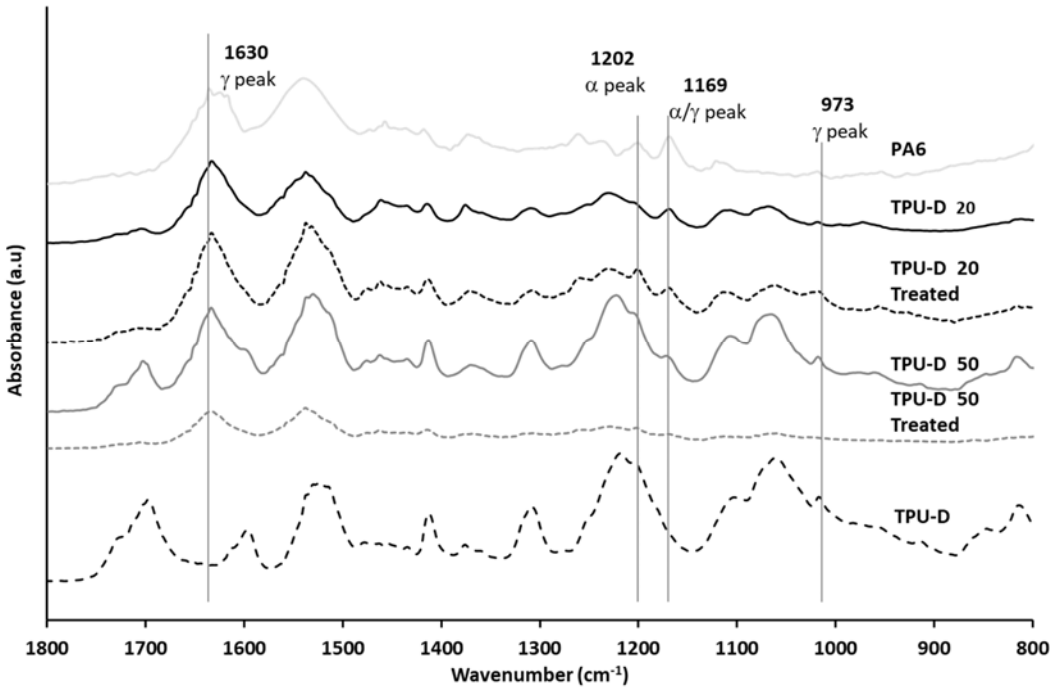

Figure 4.21 FTIR spectra of PA6 crystal form (α and γ-crystal) in the fibres.

4.2.8 Tensile properties

The mechanical properties of the hybrid fibres and single component fibres and the tenacity vs elongation curves are displayed in Figure 4.22 and Figure 4.23, respectively. The blending of PA6 and TPU-D as hybrid fibres shows lower strength than PA6 fibres but higher than TPU-D fibres. Several factors affecting the mechanical properties of the fibres are the fibre morphology, interfacial surface tension and crystallinity of the fibres (Tavanaie et al., 2013).

The morphology of both hybrid fibres (discussed in the morphology of the as-spun fibres, section 4.2.2) produced interconnected multiporous fibres with groove effect on the fibre surfaces. The TPU-D 20 that has more pores showed lesser strength than TPU-D 50. The pores introduced weak links in between the fibres content thus

reduce the mechanical performance of the hybrid fibres. A study by Chiu and Chuang (2009) showed that the mechanical properties of the PA6:TPU blend also reduced after the blend. Other study by John and Furukawa (2012) on the PA6 fibre coated with TPU film showed an improvement on the PA6 fibre strength which the TPU delayed the micro-crack formation on the fibre surface. However, in this study, the TPU-D was dispersed inside the hybrid fibres thus did not assist on the fibre strength.

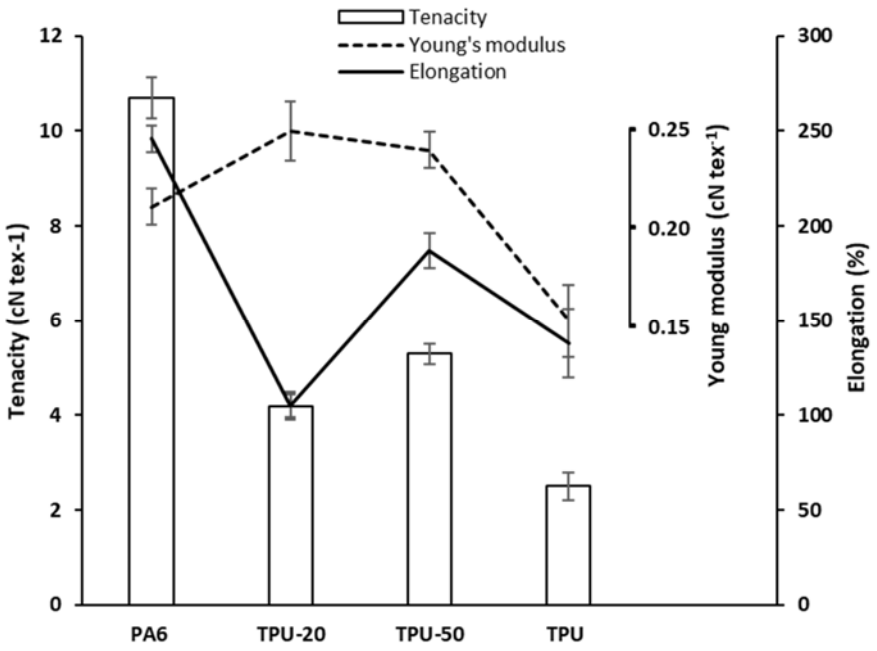

Figure 4.22 Mechanical properties of PA6, TPU-D and hybrid fibres. (*n*=10)

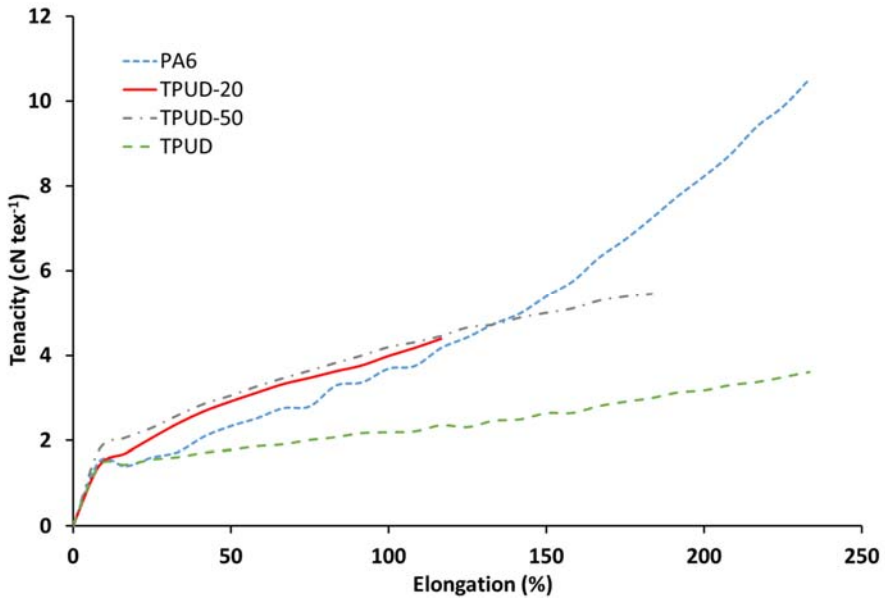

Figure 4.23 Tenacity vs elongation curve of PA6, TPU-D and hybrid fibres.

The blending of PA6 and TPU-D is partially miscible which is connected through chemical interaction of hydrogen bonding between amide group and urethane/urea group of TPU-D. The removal of TPU-D using DMSO treatment proved that the TPU-D and PA6 are partially miscible with small amount of TPU-D left in the fibres. The interaction between these two polymers is good however, significant number of pores developed in the hybrid fibres weaken the fibre structure and reduce the mechanical properties.

The crystallinity of the fibres as mentioned in thermal properties section can also be related to the strength of the hybrid fibres. In Table 4.4, it shows that the TPU-D 20 displays lower PA6 crystallinity than TPU-D 50. Furthermore, various type of crystal developed in the TPU-D 50 improved the fibres strength which was discussed in X-ray diffraction (section 4.2.6). The strength of the fibres depends on the amount of the crystallinity in the fibres, the higher the crystallinity in the fibres, the higher the strength of the fibres (Eltahir et al., 2016).

The TPU-D 50 has breaking elongation in between of PA6 and TPU-D while TPU-D 20 hybrid fibres exhibit the lowest breaking elongation compared to other fibres. The morphology of the hybrid fibres which has pores inside the fibre, restricts the elongation of the fibres. The breaking elongation also decreases in the hybrid fibre due to the hydrogen bonding developed in between the polymers that restrict the movement of the molecules (Todros et al., 2014). The Young's modulus of the hybrid

fibres show higher value, showing that the PA6:TPU-D hybrid fibre are stiffer than the single component fibres.

The strength of the TPU-D single component fibres produced at 200°C and 230°C (die temperature) is shown in Figure 4.24. The fibres produced at lower temperature exhibits better strength and elongation at break which increased 196% and 62%, respectively, than the fibres produced at higher temperature. Processing TPU-D at high temperature significantly degrades the fibres and affects the strength of TPU-D fibre. Therefore, the blending of PA6 and TPU-D at 230 °C affects the strength of the TPU-D and results to the reduction of the hybrid fibres strength.

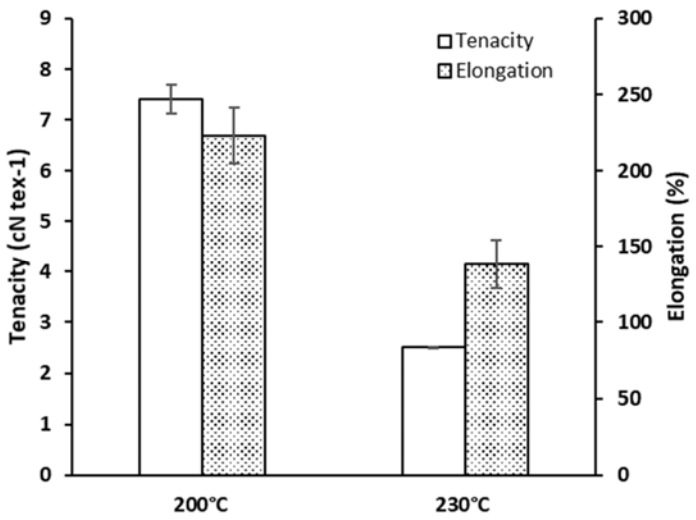

Figure 4.24 Mechanical properties of the TPU-D fibres produced at different processing temperature (200 and 230 °C).

4.3 Part 2: PA6:TPU-A

A study on the PA6 blend with TPU polymer was further investigated using TPU-A polymer. TPU-A polymer has higher soft segment composition than TPU-D polymer. The same method on fibre production was applied on this hybrid fibre. The hybrid fibres were also treated with DMSO to investigate the position of both polymers after melt extrusion. The study focuses on the morphology of the hybrid fibres. Only one blend composition was successfully produced for this blend; which used 80% of PA6 and 20% of TPU-A (TPU-A 20).

4.3.1 Morphology of the fibre

The morphology of the TPU-A 20 untreated and treated fibres is shown in Figure 4.26. The untreated TPU-A 20 produced fibres with circular cross-section with the fibre surface were not completely the same smooth as PA6 fibres (Figure 4.2). The untreated TPU-A 20 hybrid fibres also show the development of pores inside the fibres except the pores were not as significantly as the TPU-D 20 and TPU-D 50, as discussed previously in Part 1. The formation of TPU-A fibrils can also be seen from the SEM images shown in dotted circles in Figure 4.26 (left). The production of fibrils in the polymer blend might be due to the elongation forces applied during the winding process after the fibre extruded from die. In common practice, the fibrils or microfibres production is typically achieved by using bicomponent fibre technique (island-in-the-sea) which requires specific equipment.

The TPU-A 20 hybrid fibres that were treated in DMSO to remove the TPU-A component were viewed under SEM (Figure 4.26 (right)). After the treatment, the cross-sectional view of the fibres shows that the TPU-A polymer were oriented mostly at the centre of the hybrid fibres, encapsulated by the PA6 matrix. This has been proved by the treatment, where the fibres did not collapse after the treatment. The blending of PA6 and TPU was immiscible but compatible (due to the hydrogen bonding) therefore the separation between these two polymers is expected (Chiu and Chuang, 2009).

4.3.2 Thermal properties

The DSC curves of the TPU-A 20 hybrid fibre before and after treatment are shown in Figure 4.25. Since the TPU-A polymer used in this study was dominated by soft segment, the melting peak of the TPU-A was hardly seen in the DSC curve. The broad peaks appeared at 50-100 °C are related to the desorption of moisture. The melting enthalpy of PA6, TPU-A 20 untreated and treated is 56.2 J g^{-1}, 34.8 J g^{-1} and 38.0 J g^{-1}, respectively. Using Eq. 3.7, the percentage of PA6 crystallinity in the PA6, TPU-A 20 untreated and treated fibres is 30.5%, 18.9% and 20.6%, respectively. The PA6 crystal structure decrease after the blending with TPU-A, which is similar to the blending of PA6 with TPU-D polymer, discussed previously in Part 1. The PA6 crystallinity slightly increased after removal of TPU-A.

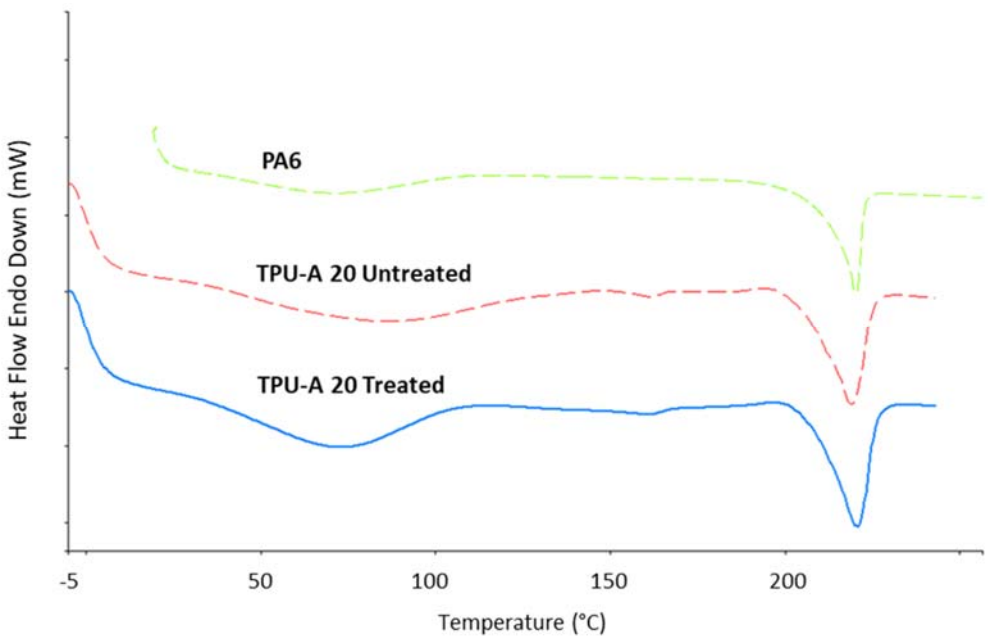

Figure 4.25 DSC curve of the PA6 and TPU-A 20 hybrid fibres untreated and treated.

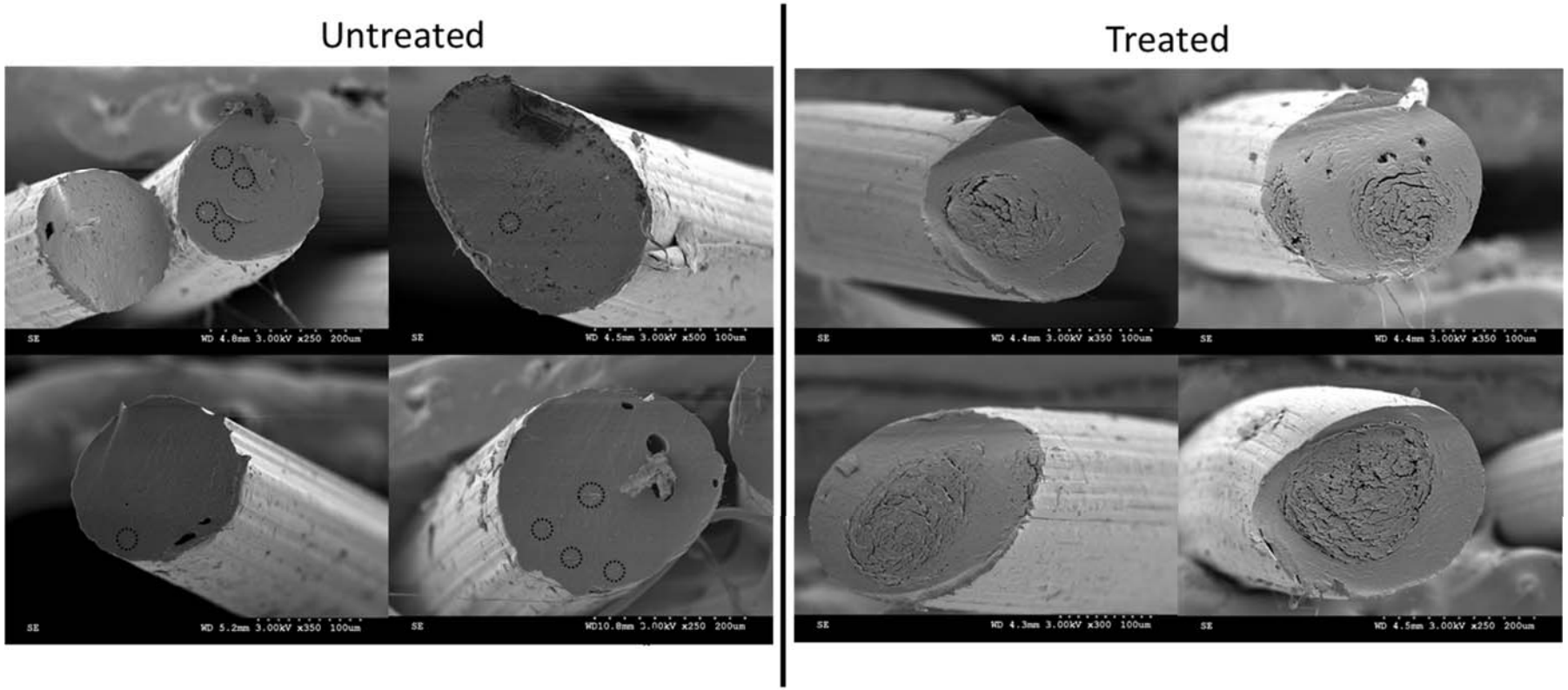

Figure 4.26 SEM images of TPU-A 20 hybrid fibres: (left) untreated and (right) treated in DMSO.

4.3.3 Chemical properties

Figure 4.27 displays ATR-FTIR spectra of the PA6, TPU-A and TPU-A 20 untreated and treated. The PA6 components: N-H (3294 cm^{-1}), C-H (2925 & 2861 cm^{-1}), amide I (1633 cm^{-1}) and amide II (1538 cm^{-1}) and TPU-A components: C=O (1732 cm^{-1} and 1686 cm^{-1}) can be seen in the TPU-A 20 untreated hybrid fibres. There is no new peak observed in the TPU-A 20 untreated hybrid fibres. The absorbance frequency of the carbonyl group of the hybrid fibres was lower than TPU-A fibres (shown in the grey circle in Figure 4.27) which relates to the amount of TPU-A in the blend. The absorbency becomes lower for TPU-A 20 treated indicates that a significant proportion of TPU-A was removed from the hybrid fibres as a result of the DMSO treatment.

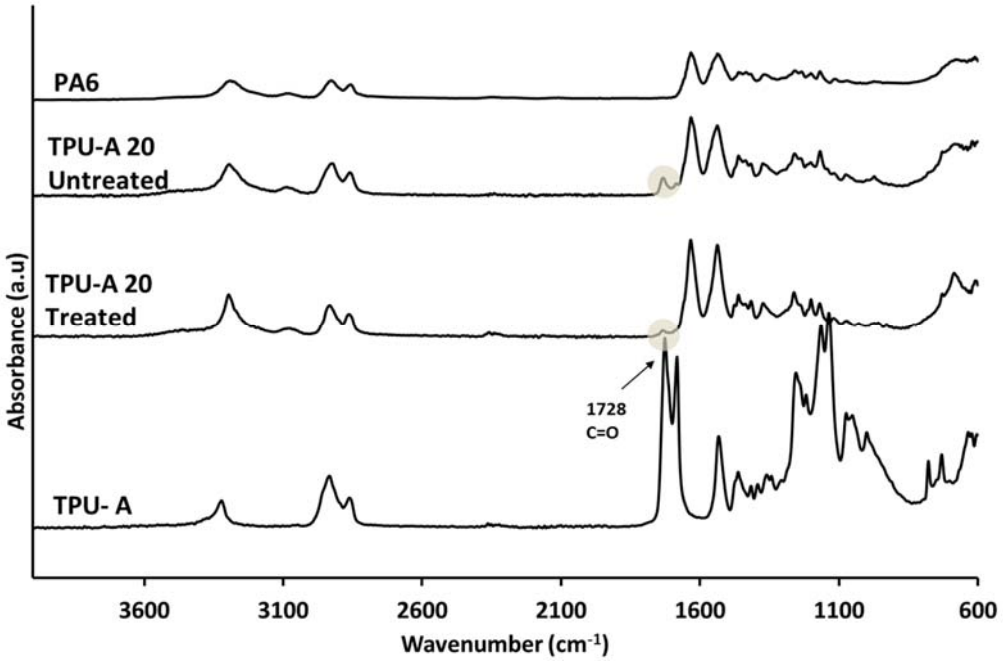

Figure 4.27 ATR-FTIR spectra of the PA6, TPU-A and TPU-A 20 untreated and treated.

Two peaks of carbonyl group (C=O) appeared on the TPU-A (1728 cm^{-1} and 1683 cm^{-1}) which are obviously different with TPU-D (Figure 4.19) that only has one carbonyl peak at 1698 cm^{-1}. There are three possible carbonyl regions reported that involved peaks around 1732 cm^{-1}, 1714 cm^{-1} and 1685 cm^{-1} (Rashmi et al., 2017). Peak around 1732 cm^{-1} did not involve in the hydrogen bonding, peak at 1714 cm^{-1} has poorly ordered intramolecular hydrogen bonding and good at mixing phase and peak at 1683 cm^{-1} develop strong hydrogen bond to amine group and can be effective in phase separation.

Clear ATR-FTIR spectra of the carbonyl group for the fibres is shown in Figure 4.28. The peak of TPU-A at 1728 cm^{-1} was slightly increased to 1732 cm^{-1} after the blending with PA6 and maintain at peak 1732 cm^{-1} after the treatment in DMSO. This shows that this region were not affected during DMSO treatment. The peak at 1683 cm^{-1} of TPU-A was shifted to 1686 cm^{-1} in TPU-A 20 untreated fibres and disappeared after the treatment in DMSO. This might indicate that the region might not have strong hydrogen bonding thus easily be removed with other TPU component during DMSO treatment.

Two different scenarios can be seen between TPU-A and TPU-D hybrid with PA6. The TPU-A has a carbonyl region at the 1685 cm^{-1} that are significant in phase separation between soft and hard segment. Meanwhile the TPU-D is dominated by 1703 cm^{-1} that is described as good at mixing phase (Rashmi et al., 2017). The good separation of the TPU-A has produced a clear separation between PA6 and TPU-A in the hybrid fibres thus the TPU-A fibrils can be obtained. The TPU-D which has great mixing phase mixed well with PA6 thus distributed in the PA6 matrix at the same time degraded and developed pores.

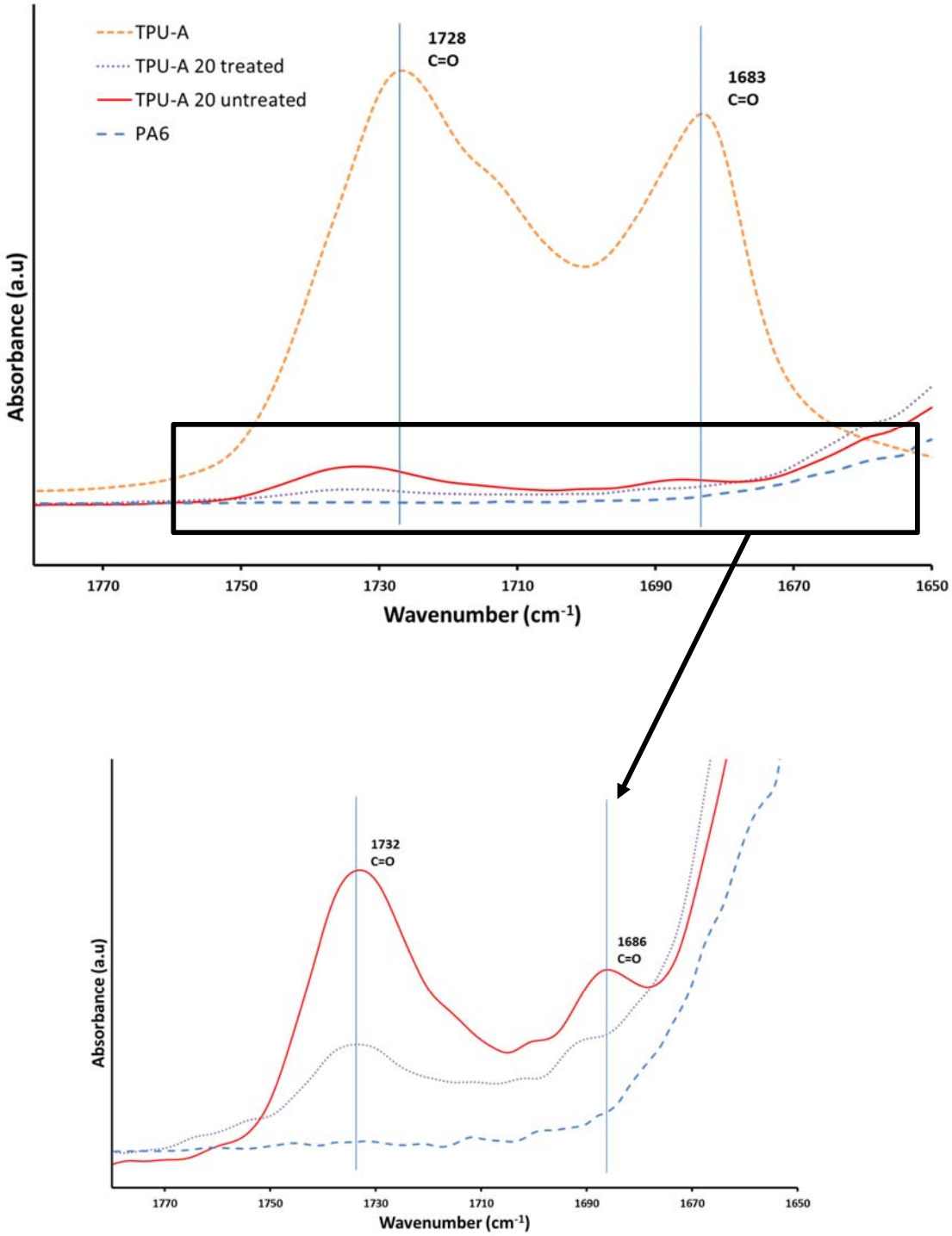

Figure 4.28 Carbonyl group spectra of: (top) PA6, TPU-A, TPU-A 2- untreated and TPU-A 20 treated and (bottom) larger image for the PA6, TPU-A 20 untreated and TPU-A 20 treated.

4.3.4 Tensile properties

The tenacity and percentage of elongation of the PA6:TPU-A hybrid fibres untreated and treated are shown in Figure 4.29. It can be seen that TPU-A 20 hybrid fibre has lower strength than PA6 but higher than TPU-A, similar to the PA6:TPU-D hybrid fibres (shown in Figure 4.29). The blending of PA6 and TPU-A is partially immiscible, thus the separation of these two polymers in the fibres weakens the strength. The elimination of the TPU-A in the fibres reduces the strength even further. The morphology of the treated TPU-A 20 shows small pores developed in the centre of the fibres. The pores have created gaps between the PA6, resulting to a weaker fibre.

The percentage of elongation of the TPU-A 20 also shows similarity to the TPU-D hybrid fibres. The elongation decreased for the untreated TPU-A 20 and increased slightly for the treated TPU-A 20. In the untreated TPU-A 20, the TPU-A which was oriented at the centre of the fibre and alternated with PA6, restricted the movement of the polymers (Todros et al., 2014). After DMSO treatment, significant amount of TPU-A was removed thus increases the elongation at break of the fibres. The representative curve of tenacity vs elongation is shown in Figure 4.30.

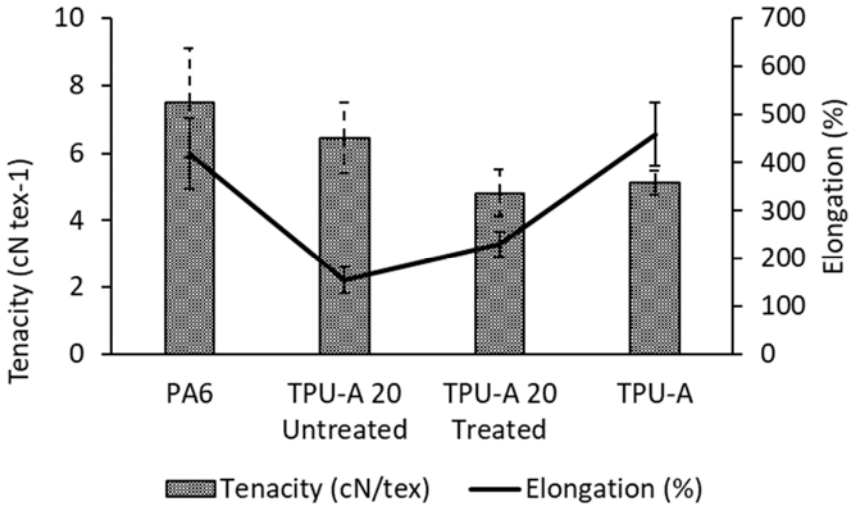

Figure 4.29 Tenacity and elongation of the PA6, TPU-A and TPU-A 20 untreated and treated fibres.

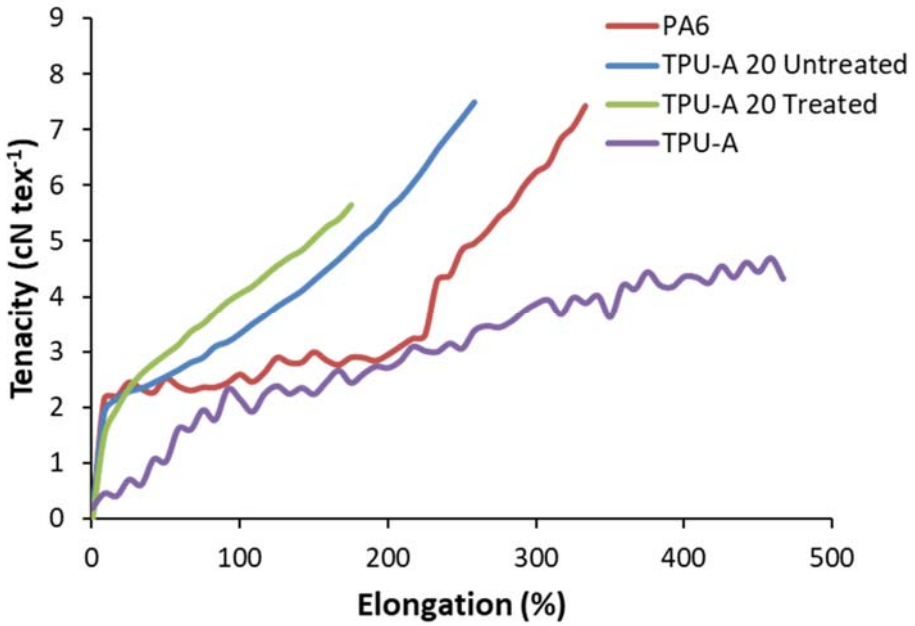

Figure 4.30 Tenacity vs elongation representative curve of PA6, TPU-A and TPU-A 20 untreated and treated fibres.

4.4 Conclusions

The blending of partially miscible polymers between PA6 and TPU into hybrid fibres leads to different fibres morphology as can be seen between the blending of PA6 with TPU-D and TPU-A. The blending of PA6 and TPU-D produced interconnected multi-pores fibres while the blending with TPU-A produced fibres with TPU-A fibrils inside. TPU polymer is a versatile polymer where the soft and hard segment can be varied and costumed to give different characteristic to each type of TPU. TPU-D has harder segment ratio than soft segment, while TPU-A is the opposite. Various types of TPU grade were used in textile applications thus preliminary study is needed to clarify the TPU polymer grade used. Different TPU grade might produce different fibre morphology if blending with PA6.

The thermal analysis shows that PA6 has developed strong interaction with TPU that affects the crystallinity and the strength of the hybrid fibres which corresponded with the chemical and mechanical analysis. The PA6:TPU-D and PA6:TPUD-A hybrid fibres are weaker than PA6 fibres however stronger than TPU fibres that produced at the same processing temperature.

Chapter 5
Manufacturing of hybrid fibre from polyamide 6 and polyethylene terephthalate

5.1 Introduction

The partially interacting polymer blend has been studied in Chapter 4, further investigation was carried out on the non-interacting polymer between PA6 and polyethylene terephthalate (PET). Over two-third of textiles fibres are dominated by synthetic fibres with polyethylene terephthalate (PET) which was ranked first in textile fibre production industry (CIRFS European mand-made fibres association, n.d.). Generally known as polyester in textile industry, PET is excellent in durability at a lower price. Meanwhile PA6 ranked as 3rd in the textile fibre production (Richards, 2005), has superior in strength however, is categorised as one of the expensive textile fibres. Both PET and PA6 are thermoplastic polymer that can be recycled several times without losing much of their properties.

The blending of PA6 and PET was found incompatible to each other. Previous research reported on the blending of PA6 and PET as fibres or film form (Papero et al., 1967; Varma and Dhar, 1987; Fakirov and Evstatiev, 1993). Due to immiscible character of both polymers, recent research focused on blending the polymers with compatibiliser, to enhance the interaction of PA6 and PET, mostly in injection and compressed mould (Iyer and Schiraldi, 2006; Qu et al., 2007). However, the usage of compatibiliser involved extra cost which is not favour for mass production.

The blending of PA6 with 10-50% of PET without compatibiliser shows the 'island-in-the-sea bi-constituent' effect on the fibre blend morphology with PA6 as the 'sea' and PET as the 'island'. The elongation force during fibres production produced the rod-likes/fibrils shape of the dispersed PET. Coarser and irregular PET fibril surface was found by Varma and Dhar (1987) after removing the matrix PA6 from the fibres.

The production of PA6 blend with PET as fibres was studied before, however, little mentioned on the PA6 and PET blend fibres when PET as a major component in the blend. The objective of this work was to investigate the morphology, thermal and mechanical properties of the PA6:PET blend especially when PET is a major

component in the blend. The PA6:PET fibres with several blend compositions were produced in this chapter.

5.2 Viscosity and fibre production

Figure 5.1 shows the apparent viscosity of PA6 and PET measured at 270 °C, corresponded with the processing temperature of the melt extruder (die temperature) during fibre production. The PA6 was found more viscous than PET at 270 °C.

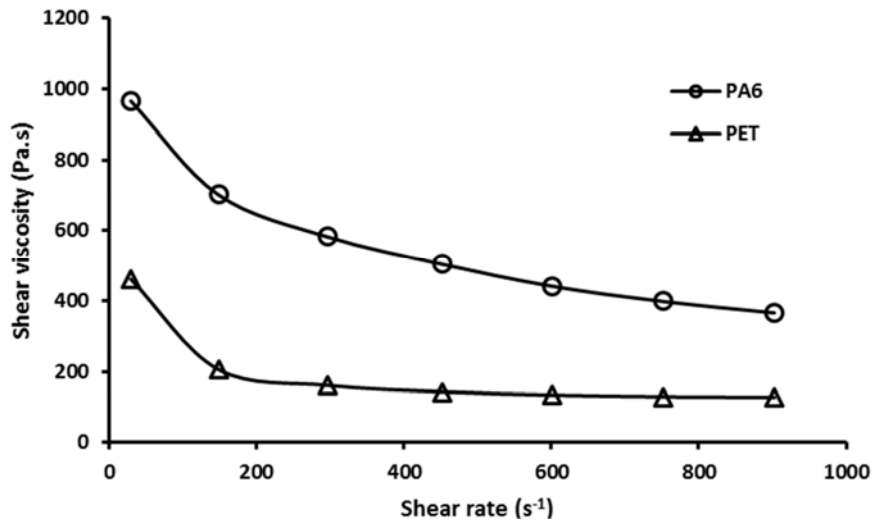

Figure 5.1 Viscosity of PA6 and PET at 270 °C.

To measure the viscosity ratio of the blend, the shear rate during fibre production was calculated using Eq. 2.3 with the screw speed used was 60 rpm, the screw diameter 10 mm and the overflight gap is 0.1 mm. The viscosity ratio calculated using Eq. 2.2 and the estimated shear rate were shown in Table 5.1. Based on the viscosity ratio of the PA6 and PET blend that is bigger than 1, coarser droplets/fibrils might be expected when PA6 dispersed in the PET matrix.

Table 5.1 Shear rate and viscosity of PA6 and PET polymer.

Screw speed (rpm)	Shear rate (s^{-1})	PA6 Viscosity, η_{PA6} (Pa.s)	PET Viscosity, η_{PET} (Pa.s)	Viscosity ratio (η_{PA6}/η_{PET})
60	314	580	160	3.6

The production of PA6:PET hybrid fibres was produced using the method and processing parameter described in section 3.2.2 (Melt extrusion) with the highest temperature processing of 260 °C due to the high melting temperature of PET. PA6:PET hybrid fibres from several blend compositions were successfully produced: 80:20 (PET-20), 70:30 (PET-30), 60:40 (PET-40), 50:50 (PET-50), 40:60 (PET-60), 30:70 (PET-70) and 20:80 (PET-80) of PA6:PET. Single component fibres of PA6 and PET were also produced using the same processing parameter as a reference fibre.

5.3 Polymer extraction

The PA6:PET hybrid fibres were treated in two solvents, formic acid and sodium hydroxide (NaOH), where former was used to remove PA6 while the latter was to remove PET component from the fibres. The treatment was conducted to confirm the location of each constituent polymer and to investigate the shape of the dispersed polymer.

First, the hybrid fibres were immersed in formic acid for 24 h at room temperature and the mass loss was recorded (Table 5.2). PET-20, PET-30 and PET-40 were found disintegrated in the solvent concluded that the PA6 was a matrix and encapsulated the PET in that particular blend composition. For PET-50, PET-60, PET 70 and PET-80, the hybrid fibres remain in the solid fibre form, showed that PET surrounded the hybrid fibres and was not significantly affected by the formic acid. The mass loss recorded shows that total mass of the fibres reduces after the treatment indicated small amount of PA6 was remove during the treatment however not alter the morphology of the fibres.

Next, a treatment to remove the PET from the hybrid fibres was conducted. Several attempts to remove PET using acetone, DMSO and toluene were found unsuccessful. Then, the treatment in boiling NaOH with 5, 50, 70 and 90% concentration was piloted. Only PET-50 hybrid fibres were treated to find suitable NaOH concentration to remove PET. From the preliminary test, the PET-50 hybrid fibres were found not being dissolved in all concentration except for 90% concentration (4 h treatment) which then were used to treat other PA6:PET hybrid fibres. Polyester is a strong polymer with high melting temperature thus encounters difficulty to remove the polymer. Moreover, several solutions such as m-creasol are not suitable to be used as it can dissolve both PA6 and PET polymers.

Based on the result from formic acid treatment, the removal of PET in boiling NaOH (100% concentration) for 4 h was focused only on PET-50, PET-60, PET-70 and PET 80 which has the PET as a matrix phase. In the NaOH treatment, hybrid fibre which has 50% and more of PET content disintegrated, indicated that the PET acted as a matrix while PA6 dispersed in the fibres. In both treatment, the total mass loss is beyond the expectation based on the blend composition ratio set for each hybrid fibres (Table 5.2). After the treatment, the fibres were found disintegrated and destroyed thus significant amount of component might escaped during washing process.

Table 5.2 Fibres mass loss in formic acid and NaOH treatment.

	Formic acid treatment		NaOH treatment	
Fibre	PA6 mass loss (%)	Fibre condition	PET mass loss (%)	Fibre condition
PET-20	97	Disintegrated	-	-
PET-30	81	Disintegrated	-	-
PET-40	68	Disintegrated	-	-
PET-50	42	Solid	89	Disintegrated
PET-60	41	Solid	98	Disintegrated
PET-70	28	Solid	100	Disintegrated
PET-80	23	Solid	98	Disintegrated

5.4 Fibre morphology

The cross-section views of the PA6:PET hybrid fibres before treatment under light microscope were shown in Figure 5.2. The morphology of the hybrid fibres was in a round shape, similar to the single component fibres: PA6 and PET.

The images of the fibre surface of the PET-50 and PET-60 hybrid fibres before treatment, viewed under SEM was found unsmooth as shown in Figure 5.3, unlike single component PA6 fibre (Figure 4.2). Compared to the PA6:TPU-D hybrid fibres, the PA6:PET hybrid fibres produced uneven and coarser fibre surface. The non-interacting of both polymers can cause dispersion of the PA6 component along the fibre axis non-uniform (Kitao et al., 1973).

The morphology of the PA6:PET hybrid fibres was summarised as illustrated in Figure 5.4. Structure I shows fibres with PA6 encapsulated the PET component

while structure II has the PA6 dispersed in the hybrid fibres. Further discussion might only cover structure II as properties on Structure I has been discussed in previous studies (Papero et al., 1967; Savov et al., 1984; Varma and Dhar, 1987; Fakirov and Evstatiev, 1993).

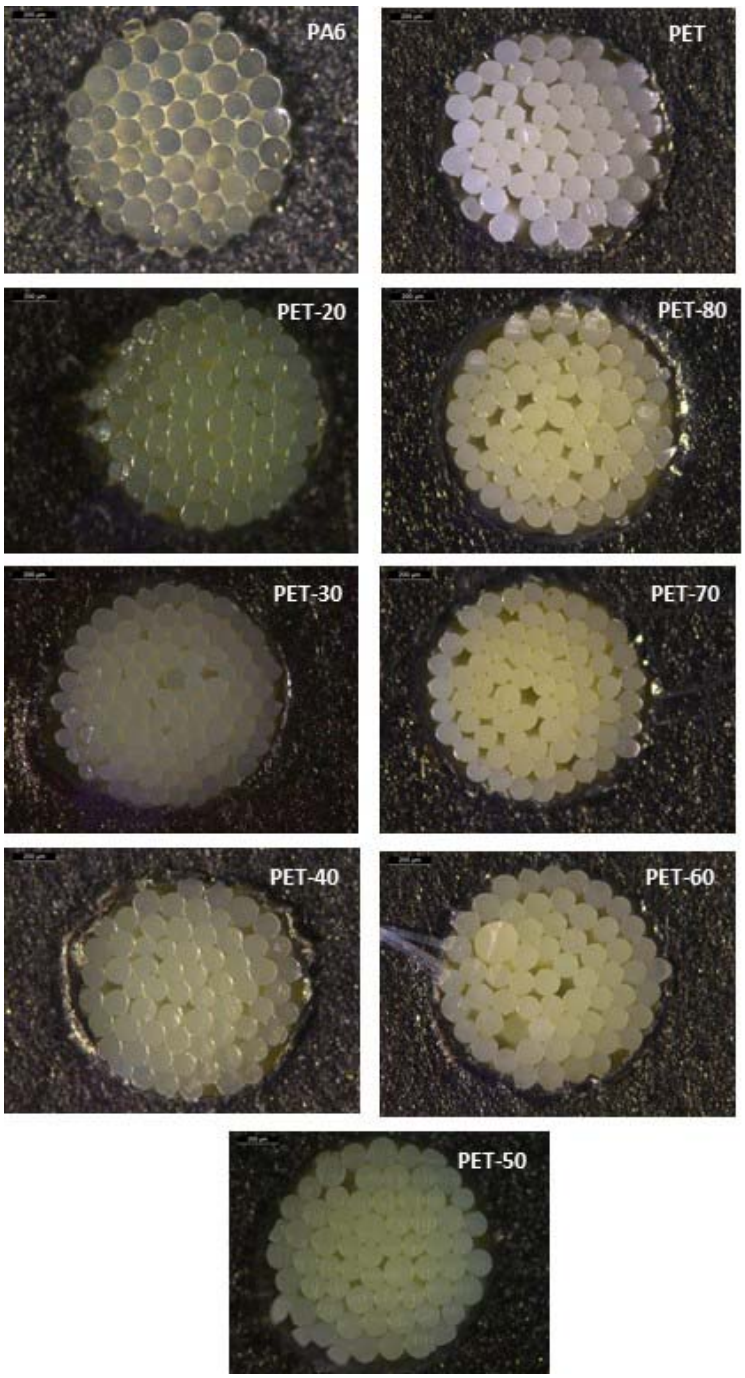

Figure 5.2 Cross section view of the PA6:PET hybrid fibres (taken using Leica Microscope).

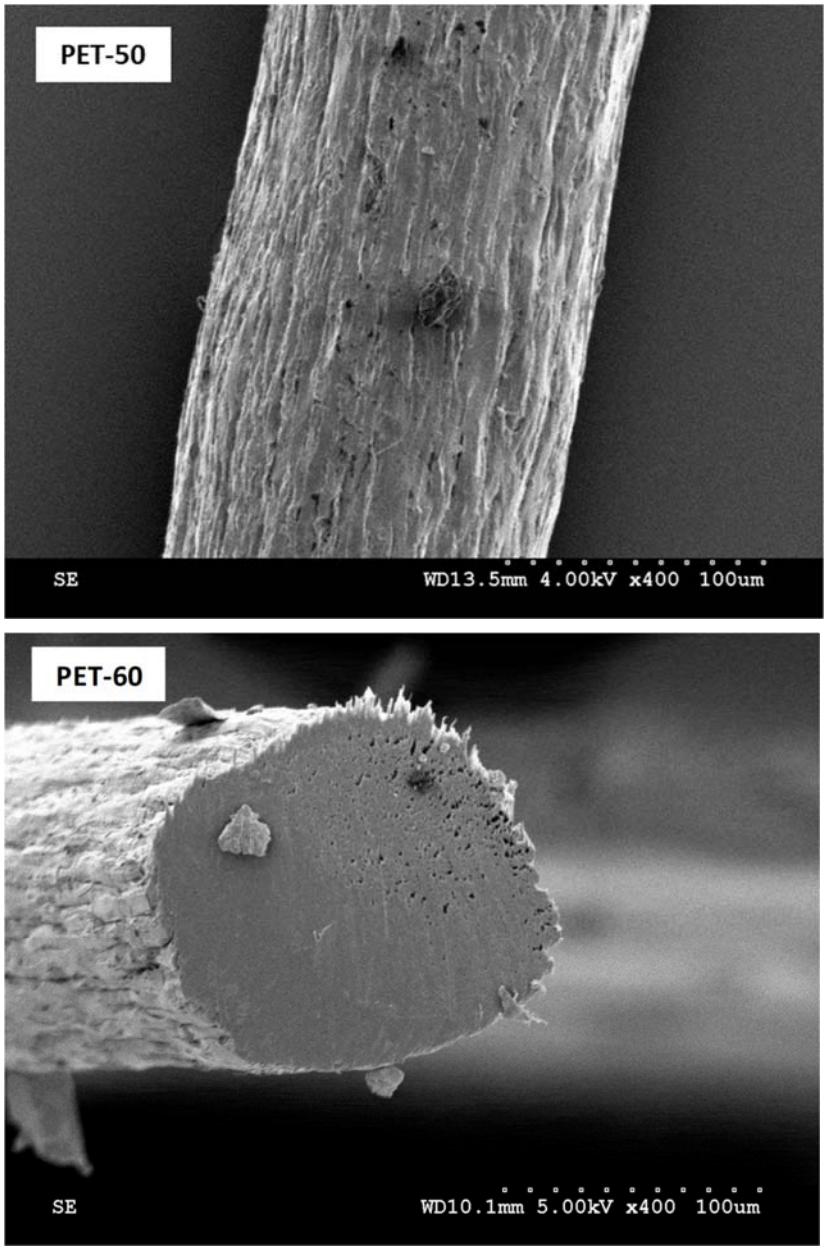

Figure 5.3 SEM images on PET-50 and PET-60 hybrid fibres before treatment.

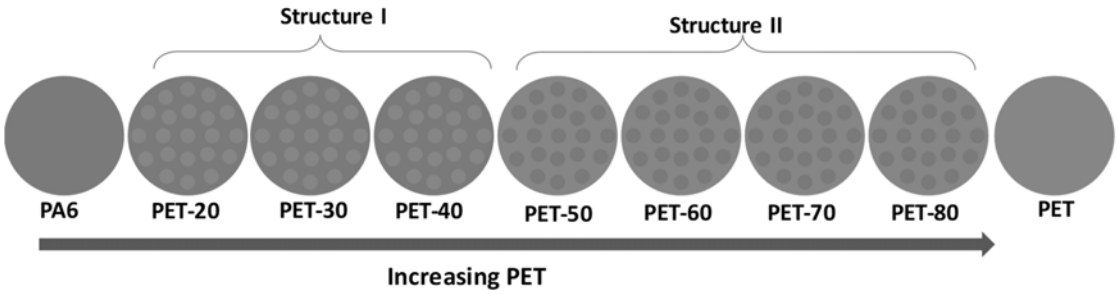

Figure 5.4 Morphology of PA6:PET hybrid fibres.

The morphology of the PA6:PET hybrid fibres in Structure II was found to be a matrix-fibril with PET as a matrix and PA6 as a dispersed phase. The removal of PET in NaOH solution reveals the PA6 component dispersed as fibrils as shown in Figure 5.5. The PA6 was found dispersed as fibrils in PET-50, PET-60 and PET-80. However, the residue from the PET-70 was unable to collect thus the dispersed nature of PA6 in PET-70 was not identified.

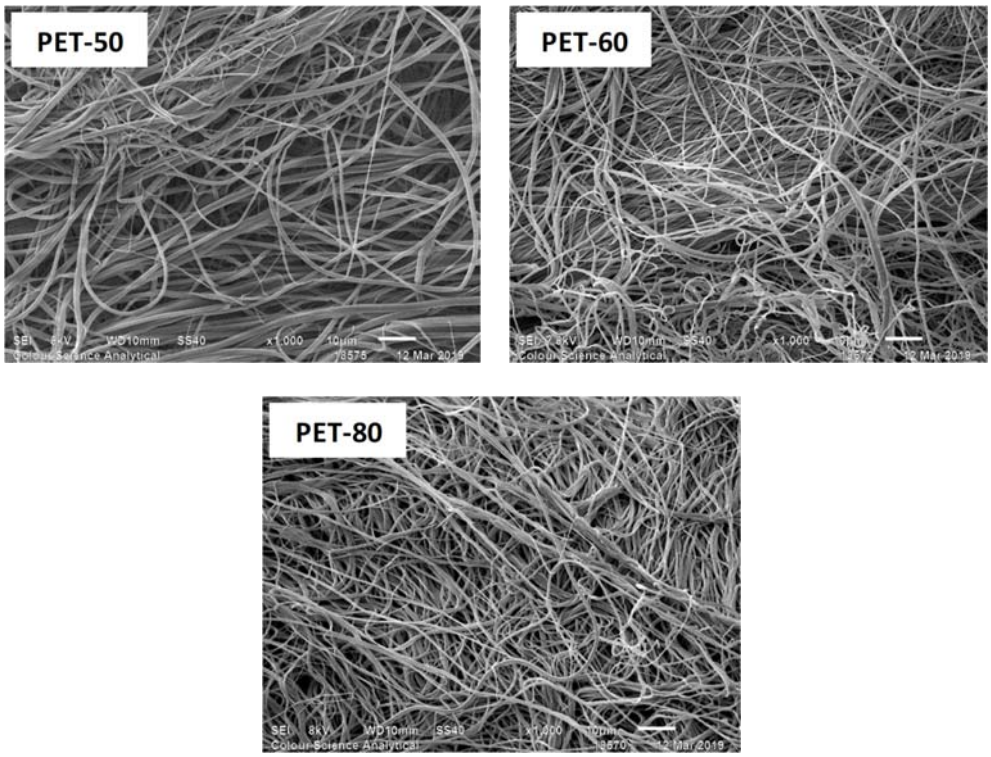

Figure 5.5 SEM images of PA6:PET hybrid fibres after PET etched in NaOH.

The fibre morphology obtained in this study was corresponded with the Jordhamo model, calculated using Eq. 2.1, except for PET-30 and PET-40 (Table 5.3). The

viscosity and weight ratio of both components can be used to predict the final morphology of the hybrid fibres.

Table 5.3 The morphology of fibres based on Jordhamo model.

Fibres	PA6*	PET*	η_{PA6}	η_{PP}	Jordhamo value	Expected morphology	Obtained morphology
PET-20	80	20	580	160	0.9	PA6 as matrix	PA6 as matrix
PET-30	70	30			1.6	PET as matrix	PA6 as matrix
PET-40	60	40			2.4	PET as matrix	PA6 as matrix
PET-50	50	50			3.6	PET as matrix	PET as matrix
PET-60	40	60			5.4	PET as matrix	PET as matrix
PET-70	30	70			8.5	PET as matrix	PET as matrix
PET-80	20	80			14.5	PET as matrix	PET as matrix

Other studies show that at blend composition of 50:50 (PA6:PET), PA6 becomes a matrix and PET becomes a dispersed phase in form of fibrils (Kitao et al., 1973; Fakirov and Evstatiev, 1993) and sphere shape (Varma and Dhar, 1987). When the molecular weight of PET is higher than PA6, it shows that the PET is more viscous than PA6. In the mixing of two different polymers, the less viscosity polymer tends to encapsulate the higher viscous polymer (Ayad et al., 2016). Accordingly, the viscosity of the PA6 is higher than PET in this study (Figure 5.1), resulting to the PET become a matrix in the PA6:PET 50:50 composition. Phase inversion of the PA6 and PET take place in between of PET-40 and PET-50.

5.5 Fibre diameters

Diameter of PA6:PET hybrid fibres (as-spun) was measured using ImageJ software and presented in Figure 5.6. The graph shows no specific trend of the fibre diameter to the content of PA6 or PET in the fibres. Mean diameter of the as-spun fibres was in a range of 103 to 128 μm. The diameter of the PA6 fibrils was also measured in ImageJ software and the results are shown in Figure 5.7. It was found that the size of the PA6 fibrils in the blend decreased in corresponding with the reducing of the PA6 content in the fibres. The diameter of the PA6 fibrils was also found in nano/microfibres size with the mean value in PET-60 and PET-80 showing almost the same, 535 nm (SD=233) and 532 nm (SD=160) respectively.

The PET-50 produced larger fibrils diameter with a mean value of 1026 nm (SD=434).

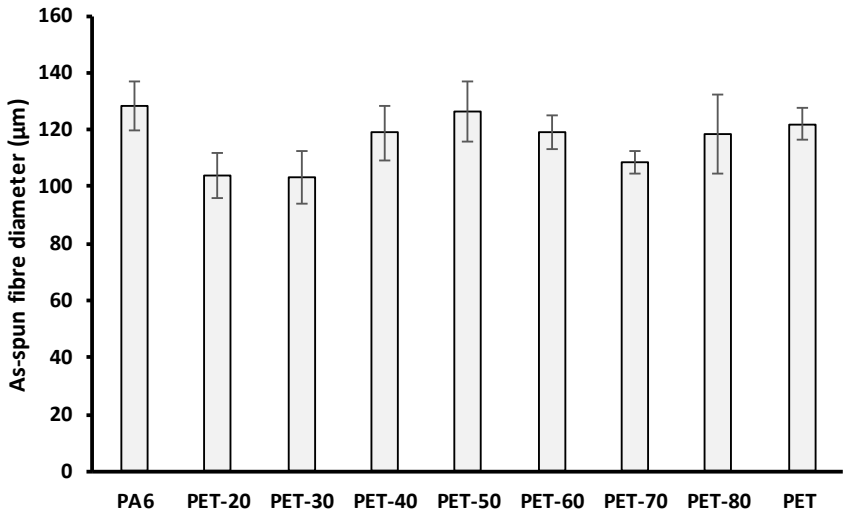

Figure 5.6 PA6:PET hybrid fibres diameter.

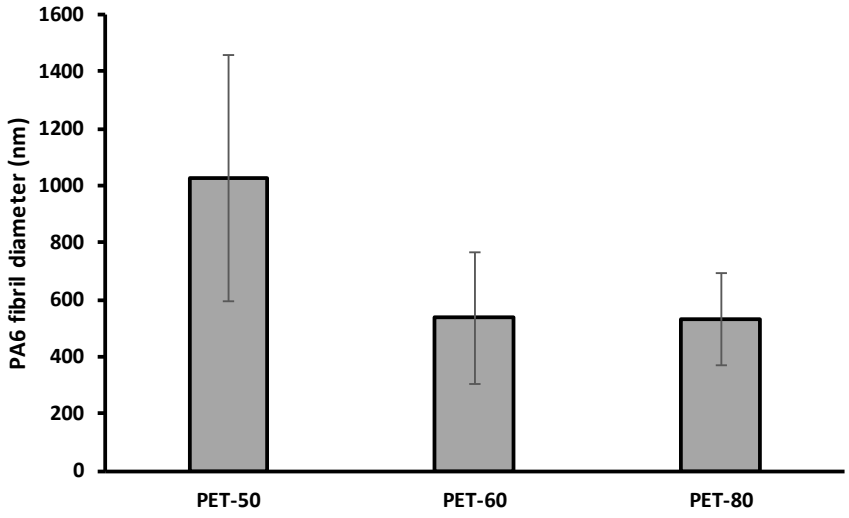

Figure 5.7 Diameter of PA6 fibrils.

Without compatibiliser, the fibril diameter either is coarser or the fibrils were hardly developed (Jayanarayanan et al., 2011). The high content of PA6 in PET-50 compared to PET-60 and PET-80 resulted to the coalescence of disperse phase and formed coarser fibrils. A study on the blend of polypropylene (PP) and polybutylenes terephthalate (PBT) with aided of compatibiliser produced PBT fibrils in between 264-389 nm (Tavanaie et al., 2013).

5.6 Thermal properties

Thermal properties of the single component fibres PA6 and PET and PA6:PET hybrid fibres (untreated and treated) for heating and cooling cycle was presented in Figure 5.8, Figure 5.9 and Figure 5.10, respectively with details in Table 5.4. Since both polymers are immiscible and incompatible to each other, two separated peaks were observed in the DSC curves, as both PA6 and PET are semi-crystalline polymer. In Figure 5.9 and Figure 5.10, the first peak belongs to PA6 which has lower melting temperature than PET that represented by the second peak.

The maximum melting peak for PA6 in hybrid fibres remains the same as PA6 fibres which melted at 220 °C. Different blend composition of PA6 content in the hybrid fibres did not affect the melting properties of the PA6. The endothermic peak of PET increased 1-2 °C than PET fibres, it might be due to the changes in the PET crystal after the first heating cycle. The consistency of melting and crystallisation temperature of both polymers in the hybrid fibres suggests that the polymers crystallise independently and do not significantly interfere with each other. Other studies found that the blending of PA6 and recycled PET shifted the melting temperature to lower temperature and crystallise at higher temperature (Kegel et al., 2003).

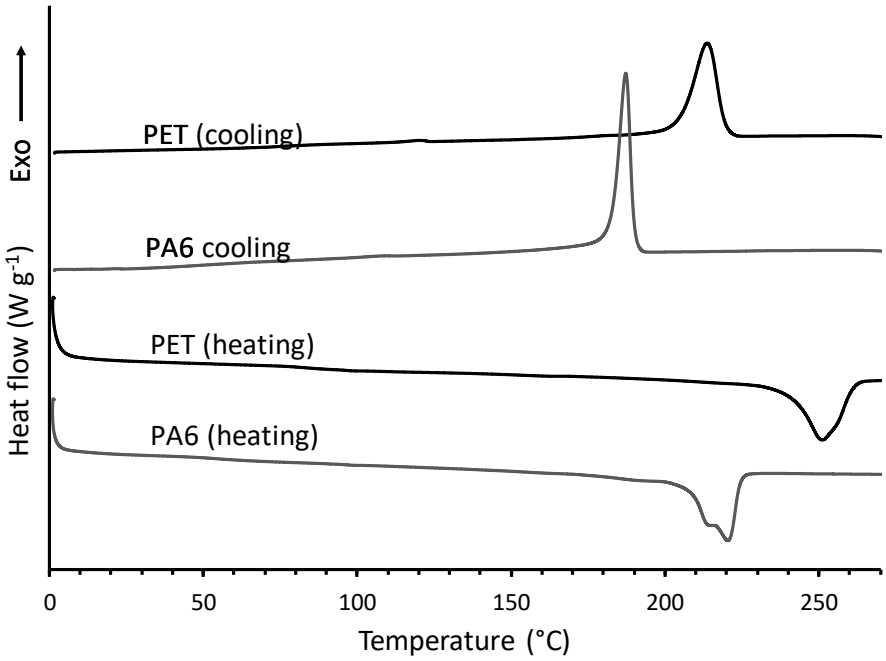

Figure 5.8 DSC curve of PA6 and PET single component fibre (cooling and second heating cycle).

The DSC curves for the treated hybrid fibres show only PA6 peak, indicate the fully removal of PET from the hybrid fibres (Figure 5.9 and Figure 5.10). The non-interacting behaviour of PA6 and PET created phase separation in the internal surface thus aided in removing the PET component from the hybrid fibre. The melting temperature of the residue PA6 was found in the range of 219 to 221 °C.

The melting enthalpy was measured and the crystallinity of both polymers were reported in Table 5.4. PA6 crystal slightly decreased in the PET-50 and PET-60 hybrid fibres compared to PA6 fibres but increased in PET-80. The PET crystal in the hybrid fibres decreased 7-10 % than PET fibres. After the removal of PET, the PA6 residue/fibrils show reduction in percentage of crystallinity except for PET-60.

5.7 Tensile properties

Tenacity, elongation and initial Young's modulus of PA6:PET hybrid fibres are presented in Figure 5.11. The mechanical properties of the PA6:PET after treatment were not conducted since the amount of PA6 residue collected after the treatment was not significant for strength test. From Figure 5.11(tenacity), the optimum strength of the hybrid fibres was obtained in PET-20 fibres, while PET-30 has the strength almost equal to PA6 fibres. The tenacity of the hybrid fibres gradually decreased with the reduction of PA6 content in the fibres while elongation at break and initial Young's modulus increased. The reduction of the hybrid fibres strength relates to the morphology of the blend. Two different fibres morphologies were obtained from PA6:PET hybrid fibres; Structure I and Structure II as mentioned in section 5.4 (Fibre morphology).

PET-20 and PET-30 hybrid fibres which have great fibre strength were categorised in Structure I, where the PA6 is a matrix and encapsulated the PET. Based on DSC curve (Figure 5.10 cooling), the PET crystal solidify in a temperature range of 212-217 °C, earlier than PA6 that crystallite at 188 °C. When the PET solidified, the PA6 matrix will have limited movement during cooling and improve the interfacial adhesion of PA6 and PET inter-surfaces. The increasing of PA6 content in the fibres improved the strength of the fibres. Other studies reported that at 70-80% of PA6 in the blend, the strength of the fibres increased which is higher than pure PA6 and PET fibres (Papero et al., 1967; Varma and Dhar, 1988). In that blend, obviously PA6 becomes a matrix hence created good physical bonding between PA6 and PET interfacial surface and improved the mechanical properties of the blend fibres.

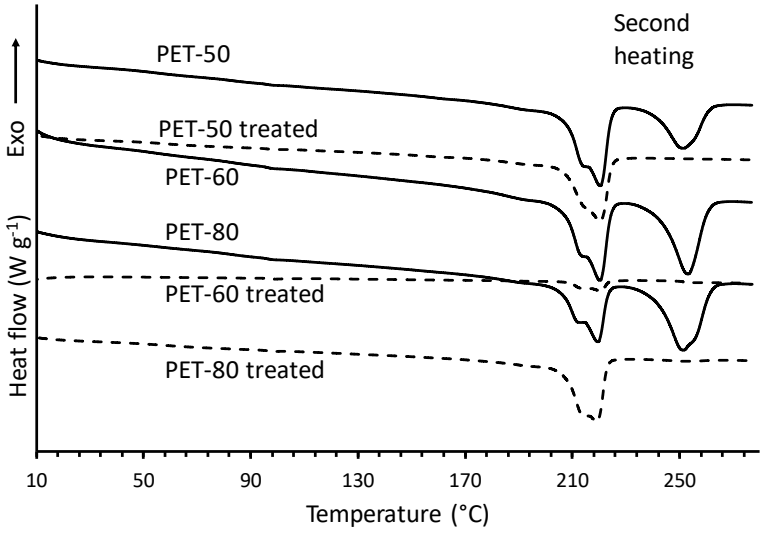

Figure 5.9 DSC second heating curves of PA6:PET hybrid fibres (untreated and treated).

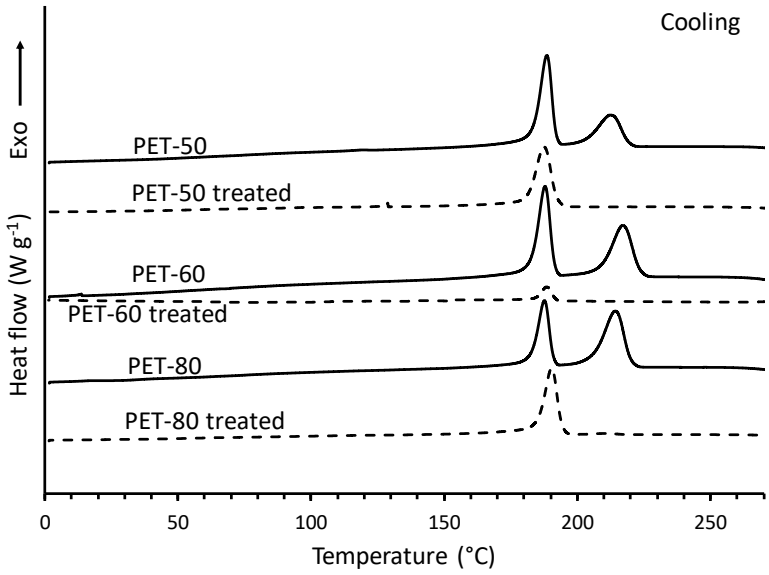

Figure 5.10 DSC cooling curves of PA6:PET hybrid fibres (untreated and treated).

Table 5.4 DSC results on PA6:PET hybrid fibres.

	Second heating		Cooling		Melting enthalpy		Crystallinity	
Fibre	$T_{m\ PA6}$ (°C)	$T_{m\ PET}$ (°C)	$T_{c\ PA6}$ (°C)	$T_{c\ PET}$ (°C)	ΔH_{PA6} (J g^{-1})	ΔH_{PET} (J g^{-1})	X_{PA6} (%)	X_{PET} (%)
PA6	220	-	188	-	63.5	-	27.6	-
PET-50	220	252	189	212	28.9	18.0	25.1	25.7
PET-60	220	253	188	217	23.7	22.9	25.7	27.2
PET-80	220	252	188	214	18.5	27.5	40.1	24.6
PET	-	251	-	214	-	48.4	-	34.6
PET-50 treated	220	-	188	-	65.5	-	28.5	-
PET-60 treated	221	-	189	-	33.8	-	14.7	-
PET-80 treated	219	-	190	-	64.3	-	27.9	-

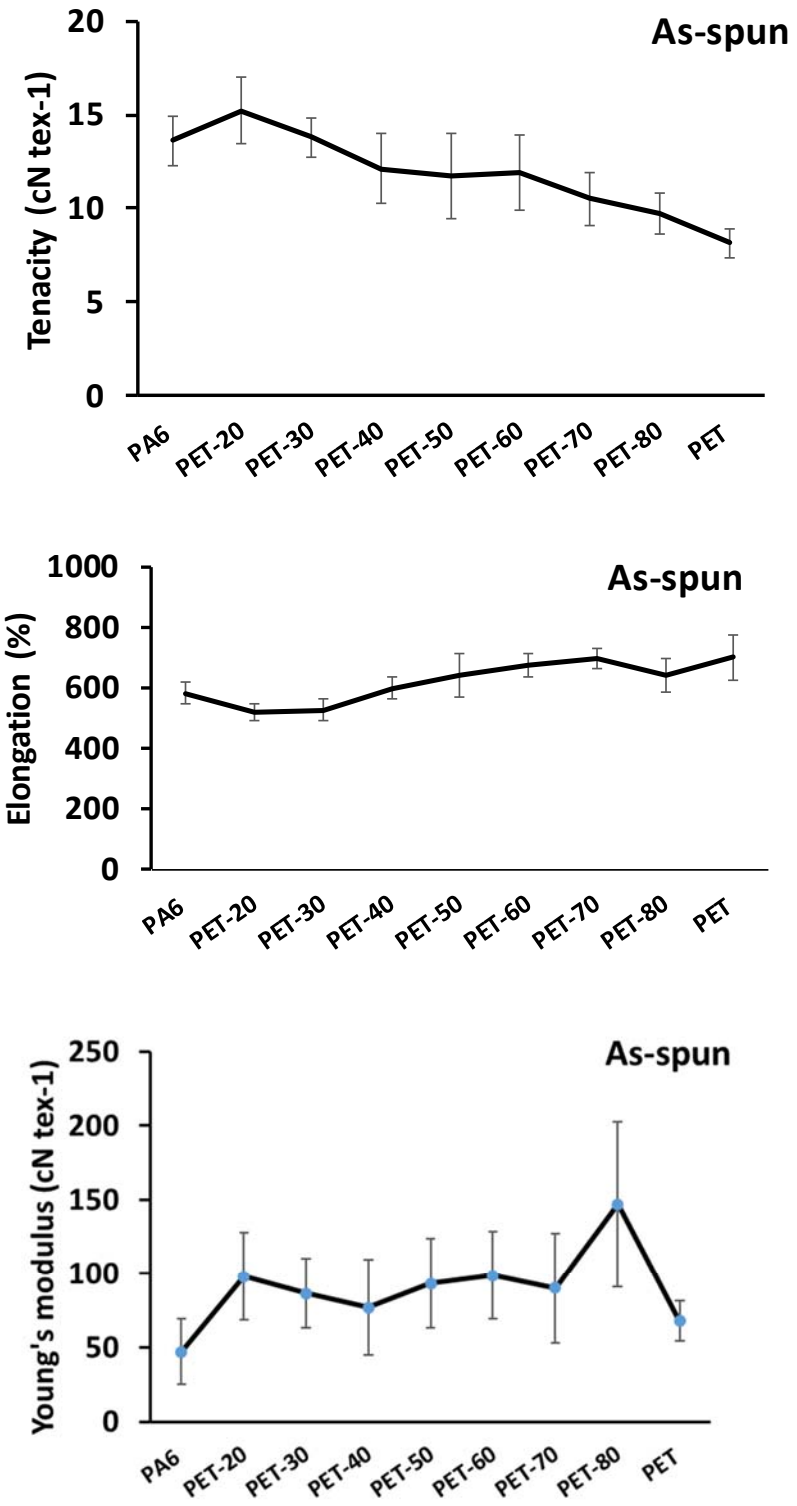

Figure 5.11 Mechanical properties of PA6:PET hybrid fibres; tenacity (top), elongation (middle) and Young modulus (bottom).

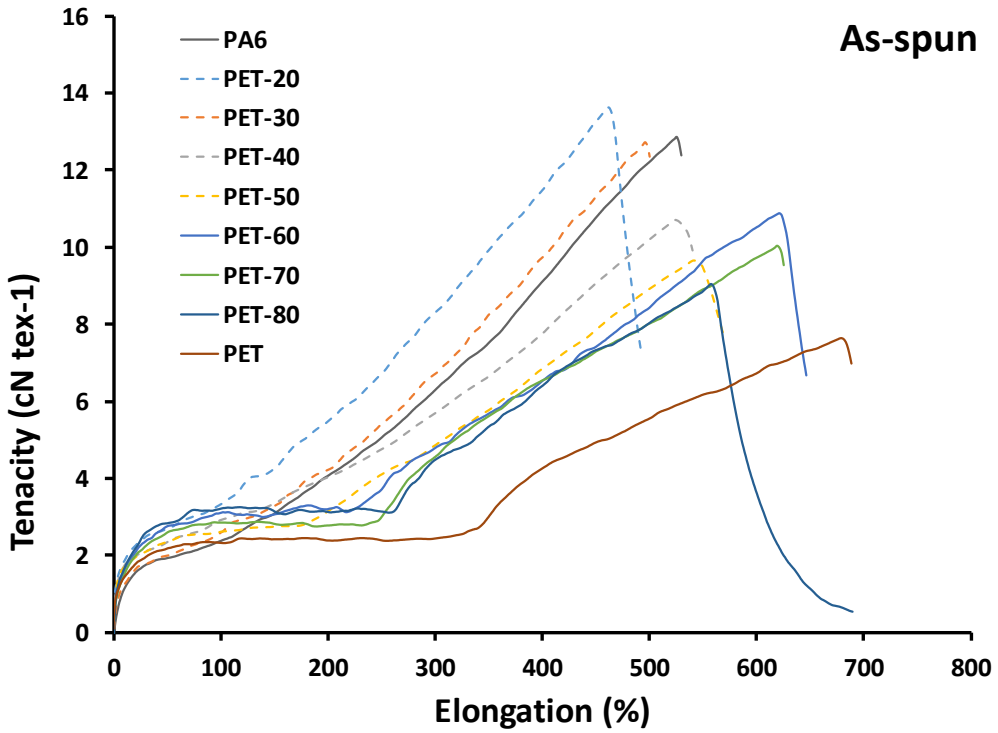

Figure 5.12 Tenacity vs elongation at break of PA6:PET hybrid fibres.

Conversely happen in Structure II where the PET becomes a matrix and encapsulates the PA6 that dispersed as fibrils. When the PET matrix hardened, the PA6 inside which solidify later, has potential to shrink during cooling phase thus created gaps between PA6 and PET surfaces. The gaps that created have lessen the ability of the fibres to encounter the stress applied.

The elongation of the hybrid fibres is also influenced by the position of the polymers in the blend. The hybrid fibres with Structure I elongated less than Structure II due to the interfacial bonding between PA6 and PET surfaces. The bonding restricts the movement of both polymer thus reduce the elongation ability of the fibres. Fibre in Structure II has gap between the surface makes both components move easily and increased the elongation rate of the fibres. The elongation of the hybrid fibres was observed located in between of the single component fibres with PET have better elongation rate than PA6. The mechanical behaviour of the Structure I and Structure II hybrid fibres was almost similar to PA6 and PET, respectively (Figure 5.12), preference to the polymer dominated the outer surface of the fibres.

5.8 Conclusions

This chapter demonstrated the blending of two non-interacting polymers: PA6 and PET into hybrid fibres via single step melt extrusion. The PA6:PET hybrid fibres with different blend composition successfully produced with two fibres morphology structures were obtained; Structure I and Structure II. Structure I has a PA6 as a matrix and PET as a dispersed phase while Structure II has PET matrix and PA6 dispersed in fibril form. The removal of PET from structure II fibres reveals the PA6 nanofibres size in the range of 532 nm to 1026 nm developed in the hybrid fibres. The optimum strength of the hybrid fibres was found in PET-20 and PET-30 and the strength reduced with the reduction of PA6 component in the fibres. The thermal properties of the hybrid fibres have not been significantly changed, due to the non-interacting behaviour of both components. The blending of two incompatible polymers in a conventional melt spinning with PET content higher than PA6 benefits in the production of nano/microfibers after removal of PET matrix.

Chapter 6
The effect of non-interacting blend between polyamide 6 and polypropylene polymer

6.1 Introduction

Blending of two non-interacting or immiscible polymer, polyamide 6 (PA6) and polypropylene (PP) extruded into fibres has been reported by several researchers however, limited to the PA6 as a minority component in the blend. Previous study on PA6 and PP blending also happened with the support of compatibiliser and involved several steps to prepare the blend (Liang et al., 1983; Afshari et al., 2001; Afshari et al., 2005; Hajiraissi et al., 2017). This chapter investigated the effect of blending PA6 and PP extruded into hybrid fibres using a single-step twin-screw melt spinning with PA6 as a majority component in the blend. No compatibiliser was used in this study. Five different PA6:PP blend compositions were produced; 80:20 (PP-20), 70:30 (PP-30), 65:35 (PP-35), 60:40 (PP-40) and 50:50 (PP-50), called as as-spun untreated fibres, along with a single component fibres, 100% PA6 (PA6) and 100% PP (PP) to be as references. However, fibres with 70:30 PA6:PP were not successfully produced in this study due to the unstable viscosity at the polymer blend during extrusion, therefore will not be discussed. The hybrid fibres were then treated with toluene to remove PP component from the fibres which later called as as-spun treated fibres. The effects of drawing process on the fibres were also studied. The as-spun untreated hybrid fibres were stretched at 2.5 draw ratio and treated with toluene to remove PP component which is after this were called as drawn untreated and drawn treated fibres, respectively. The properties of the fibres were investigated via microscopy techniques, DSC, TGA, ATR-FTIR and mechanical strength test.

6.2 Viscosity of the polymers

As mentioned in section 2.5.1, the viscosity of the polymers plays an important role in the blending of immiscible polymers. Figure 6.1 presents the viscosity of PA6 and PP pellets measured at 230 °C, the same temperature used during PA6:PP hybrid fibres extrusion. The graph shows that both polymers exhibit non-newtonian liquid behaviour with shear thinning effect that the viscosity decreased when the shear rate increased. PA6 polymer is more viscous than PP at 230 °C. The viscosity of the polymers contribute to the end morphology of the hybrid fibres to be explained further in section 6.3 (Fibre morphology).

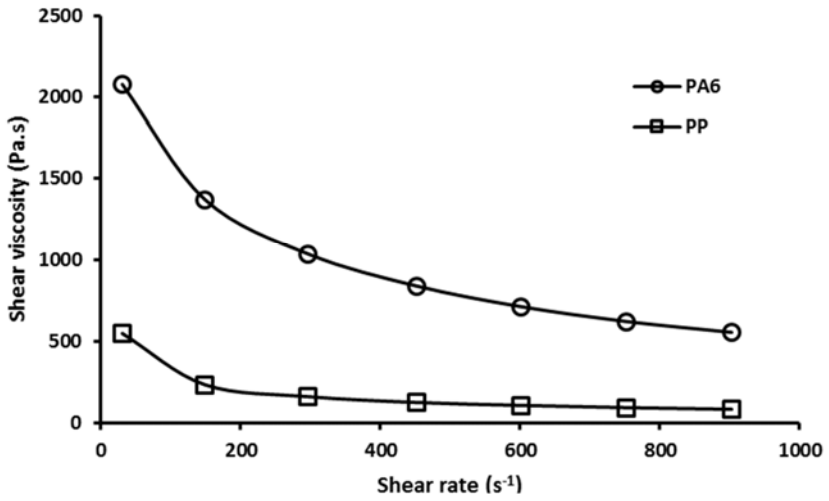

Figure 6.1 Shear viscosity of PA6 and PP pellets at 230 °C.

6.3 Fibre morphology

Figure 6.2 shows the cross-section and longitudinal view of PA6:PP hybrid fibres as-spun untreated and treated fibres. The PP-20 untreated fibres show the development of circular shape cross-section (Figure 6.2 a0). For PP-35 untreated fibres, the hybrid fibres appear slightly oval and crack developed in the middle of the fibres (Figure 6.2 b0). Meanwhile for PP-40 and PP-50, the hybrid fibres developed in round shape with dispersed phase appeared in the fibres (Figure 6.2 c0 & d0).

The removal of PP component from the hybrid fibres reveals the position of both polymers in the fibres as shown in (Figure 6.2 a1- d2). Based on the observation of treated fibres morphology, the structure of PA6:PP hybrid fibres can be divided into three structure groups. Structure I denotes the PP-20, Structure II signifies PP-35 and Structure III represents PP-40 and PP-50 as illustrated in Figure 6.3.

In Structure I, the morphology of the hybrid fibres was found to be a matrix-dispersed phase with PA6 as a matrix and PP as a disperse phase. The structure of treated PP-20, which remained solid and round fibre shape after treatment (Figure 6.2 a1 & a2), confirms that PA6 encapsulated the PP in the fibres. In Structure II, PP-35 treated fibre, the PA6 structure was observed in two forms, solid and fibril form. Significant area of the PP-35 fibres was maintaining the PA6 as a matrix and PP as dispersed phase however the small part of the fibres shows the PA6 become fibril in the PP matrix. This indicated that a phase inversion between PA6 and PP happened in the blend, but not inverted completely (Figure 6.2 b1 & b2).

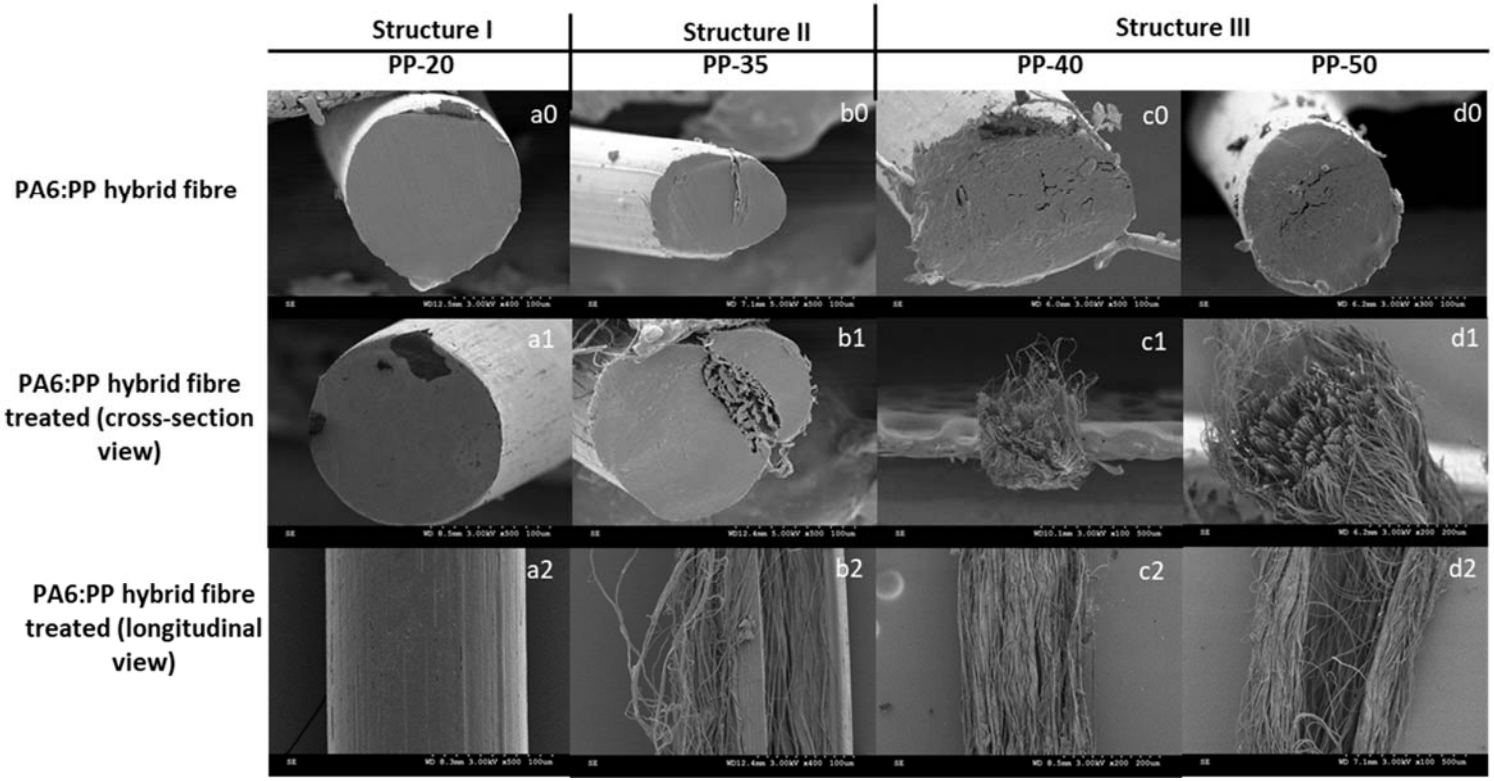

Figure 6.2 SEM images of PA6:PP hybrid fibres before and after treated (cross-section and longitudinal view).

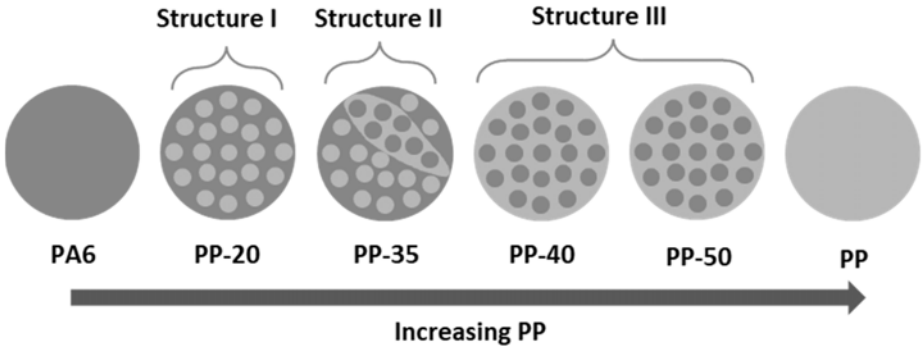

Figure 6.3 Illustration of PA6:PP hybrid fibre structure in different weight compositions.

In contrast, Structure III demonstrates the morphology of matrix-fibril phase with PP as a matrix and PA6 as fibrils. The treated PP-40 (Figure 6.2 c1 & c2) and treated PP-50 fibres (Figure 6.2 d1 & d2) exposed the PA6 in fibrils shape after the removal of PP component.

Mass loss of PP was measured by recording the weight of the fibres before and after treatment, reported in Table 6.1. The mass loss of PP in PP-20 and PP-35 hybrid fibres were 0 and 0.1% respectively, indicating that PP was not removed during the treatment and remained in the hybrid fibres. Meanwhile, the mass loss of PP in PP-40 and PP-50 could be seen equivalent to the weight composition of the PP in the fibres, stipulated complete removal of PP component.

Table 6.1 Mass loss of PP component after treated with toluene.

Fibre	PP mass loss (%)	Fibre morphology
PP-20	0.0	Solid
PP-35	0.1	Solid/fibril
PP-40	40.0	Fibril
PP-50	50.0	Fibril

The morphology of the hybrid fibres is affected by the polymer used, blend composition and viscosity ratio of the blend. The immiscibility and incompatibility between PA6 and PP result to high interfacial tension on both surface area and create phase separation as can be seen in Figure 6.4 shown in the circle.

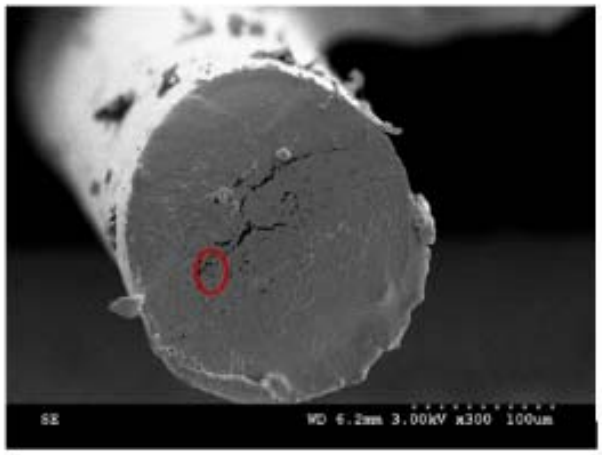

Figure 6.4 SEM image of PP-50 showing phase separation between PA6 fibril and PP matrix.

The composition of the polymers can be used to predict the flow behaviour of the blend polymer. Generally, major component in the blend will become a matrix while the minority will disperse in the blend. In this study, PA6 was set as a major component (50-80%) to fully utilise the PA6 component in the blend. A study by Takahashi produced PA6 as a matrix and encapsulate the minority component of PP (Takahashi et al., 1996a). However, the result obtained in this study shows that even though PA6 is a majority in the blend, it dispersed in PP-40 and PP-50. Other studies reported that PP became a matrix phase and PA6 as a dispersed phase when PA6 is 6-50 % weight composition (Liang et al., 1983; Ďurčová et al., 1992; Liao et al., 2015; Hajiraissi et al., 2017). The PA6 dispersed in the PP-40 and PP-50 in this study can be related to the viscosity of PP and PA6 in the blend.

Table 6.2 reports the predicted morphology of the hybrid fibres using Jordhamo model and viscosity ratio, determined using Eq. 2.1 and Eq. 2.2, respectively. Based on Jordhamo value, it was expected to have PP as a matrix in PP-40 and PP-50. The viscosity of both polymers during melt extrusion is predicted by measuring the shear rate happened during melt processing. The shear rate during melt extrusion is 314 s^{-1} calculated by Eq. 2.3. From the graph shown in Figure 6.1, at 314 s^{-1} shear rate, the viscosity of PA6 and PP is 1000 Pa.s and 150 Pa.s, respectively. The Jordhamo value obtained shows the value for PP-40 and PP-50 is 4.4 and 6.6, respectively. The value is greater than 1, makes PP become a matrix in the blend. Moreover, the PA6 is more viscous than PP makes the PP flow easily than PA6. Esma et al. (2016) shows that less viscous PP tend to encapsulate high viscous PA6 in the side-by-side bicomponent fibres (Ayad et al., 2016).

Table 6.2 Viscosity ratio of PA6 and PP and expected morphology for the hybrid fibres.

Fibres	PA6*	PP*	η_{PA6}	η_{PP}	Jordhamo value	Expected morphology	Obtained morphology
PP-20	80	20	1000	150	1.7	PP as matrix	PA6 as matrix
PP-35	65	35			3.6	PP as matrix	Semi co-continuous
PP-40	60	40			4.4	PP as matrix	PP as matrix
PP-50	50	50			6.6	PP as matrix	PP as matrix

*weight of polymer (%)

The Jordhamo value for PP-35 is 3.6, which is greater than 1 and the PP is predicted to be a matrix in the blend. However, the morphology shows that at PP-35, PA6 became a matrix and in certain area disperses as fibrils. This phenomena is called phase inversion which normally happed when the ratio of the polymers is the same (Afshari et al., 2001; Liao et al., 2015). The phase inversion of PA6 and PP blend in other studies shows the co-continuous morphology of the blend with no trace of matrix or dispersed phase in the blend. There is no research has been done to show the phase inversion happens in the extruded fibres. Afshari et al. (2001) found the co-continuous might happen when PA6 is 50% in the polyblend however could not be spun into hybrid fibres. In this study, the PP-35 shows unstable fibre production with uneven fibre diameters developed along the line. The increased of PA6 content in the blend affects the flow movement of both polymers which determines the position in the blend. This can be seen in PP-20 where the PA6 becomes a matrix even though the Jordhamo value is still more than 1.

6.4 Fibres diameters

Figure 6.5 and Figure 6.6 present diameters for as-spun and drawn fibre for untreated and treated, respectively. The micrographs of the fibres taken using light microscope are shown in Figure 6.7. The PA6 developed in PP-35, PP-40 and PP-50 are called microfibres based on the fibrils size obtained.

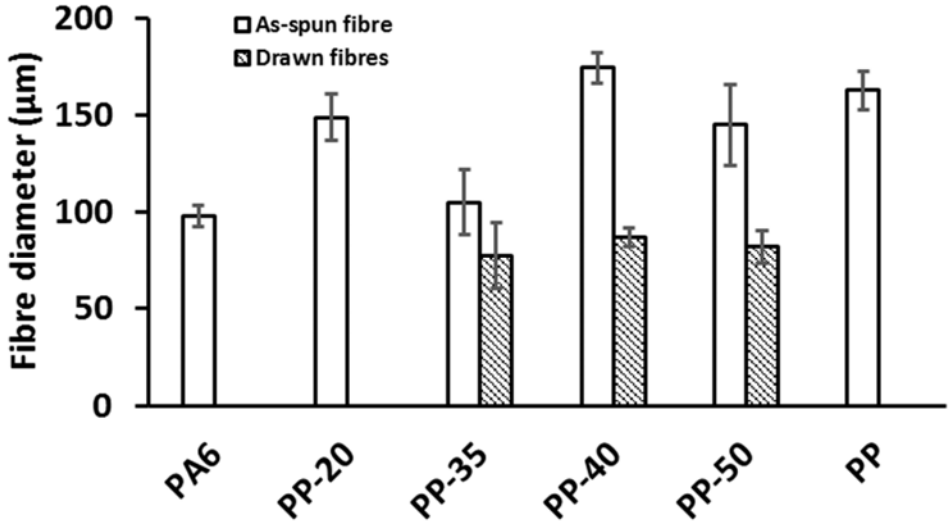

Figure 6.5 Diameter of as-spun and drawn PA6:PP hybrid fibres (untreated).

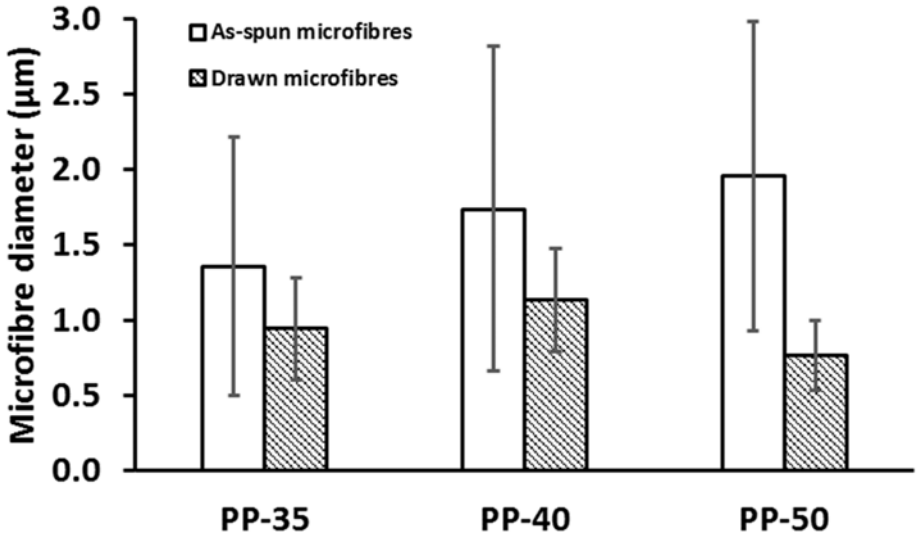

Figure 6.6 Diameter of as-spun and drawn PA6 microfibres (treated).

Diameter of the as-spun hybrid fibres shows no specific trend with the increasing of PA6 content in the fibre. The as-spun PP-40 produced highest fibre diameter than other fibres. Inconsistence fibres diameter were traced for PP-35 and PP-50 showing high variance in the sample. In Figure 6.7, it can be seen that the PP-35 shows uneven fibres diameter with some cracks appear from the cross-section view. The beads also appear on the fibres surface during fibre production. Compared to the diameter of single component fibre, hybrid fibres show almost similar diameter

with PP fibres and larger than PA6. Diameter of the as-spun hybrid fibres decreased 27-43% after drawing.

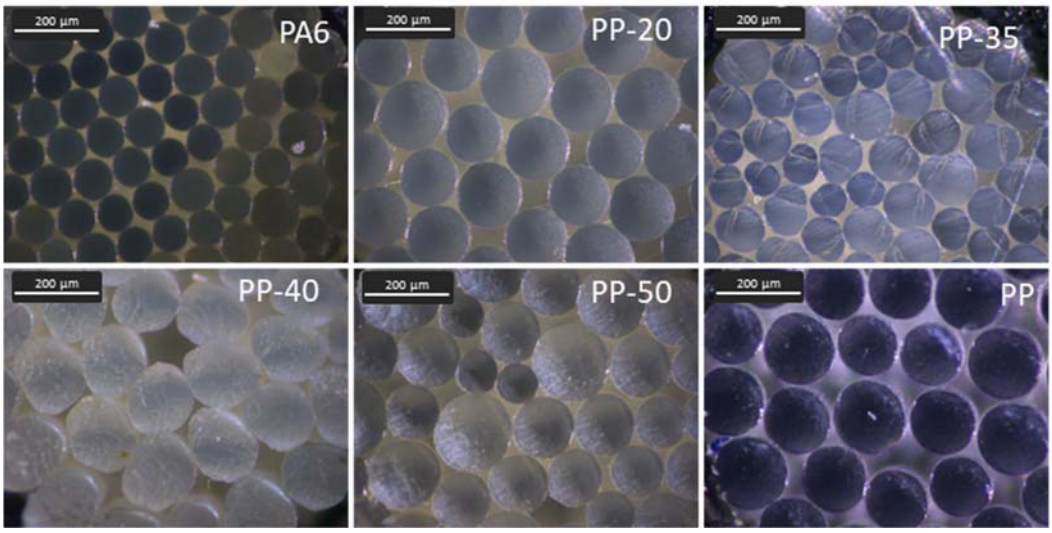

Figure 6.7 Microscopy images of as-spun PA6:PP hybrid fibre.

The mean diameters of as-spun PA6 microfibres obtained from PP-35, PP-40 and PP-50 are in the range of 1.4~2.0 µm as shown in Figure 6.6. The diameter of the microfibres in this study is almost the same with fibrils diameter obtained by Hajiraisi (2017). Interestingly, Hajiraisi obtained the fibrils when the PA6 is 20% in the blend that aided by compatibiliser. The possibility to get PA6 fibrils is high when the PA6 is a minority component in the blend. Additionally, with the help of compatibiliser, finer fibrils can be obtained. In our study, no compatibiliser was used and the PA6 composition is high (50-60%) in the blend, however finer microfibres would be able to produce. The microfibres produced in this study have almost similar diameter with the fibres reported by from electrospinning (H. Zhang et al., 2015) and fibre drawn by carbon dioxide laser supersonic (Hasegawa and Mikuni, 2014).

When the PA6 content was increased, the diameter of the as-spun microfibres was found decreased. However, there was no statistically significant different of the as-spun PA6 microfibres diameter related to the amount of PA6 content in the fibre. PP-50, which has the largest as-spun microfibres diameter, shows the lowest after drawing. In PP-35, the structure of the fibres which having unique fibre morphology, might affect the diameter of the microfibres. In this study, the diameters of the PA6 microfibres were not affected by the content of PA6 in the fibres. Other researchers reported that the morphology of PA6, either in droplet or fibrils will become coarser by the increased of PA6 content (Potente et al., 2000; Afshari et al., 2001; Liao et

al., 2015). Rationally, adding PA6 content in the blend improved the coalescence of small droplet to form bigger droplet. However, the increment of 10% of PA6 (from PP-50 to PP-40) might not show much different in the development of microfibres diameter in the blend. The diameter of the microfibres decreased to 0.8~1.1 μm, with further 30-60% reduction upon drawing. One-way ANOVA shows that after drawing, there was significant difference on the microfibres diameter $F(2,147)=1.69$, $p=0.000$.

The reduction in diameter between fibres and microfibres after drawing was not parallel (Table 6.3). This is due to the high interfacial tension on the surface area of PA6 and PP. The gap between PA6 microfibres and PP matrix, makes the microfibres isolated and did not have parallel movement with PP matrix when the elongation force applied. Therefore, the reduction in microfibres diameter was not the same as hybrid fibres diameter. The microfibres diameter distribution is shown in Figure 6.8. It can be seen that the diameter of the microfibres were well distributed after drawing.

Table 6.3 Percentage of fibres diameter reduction after drawing.

Fibres	Fibres diameter reduction from as-spun to drawn (%)	Microfibres diameter from as-spun to drawn (%)
PP-35	27	31
PP-40	50	35
PP-50	43	61

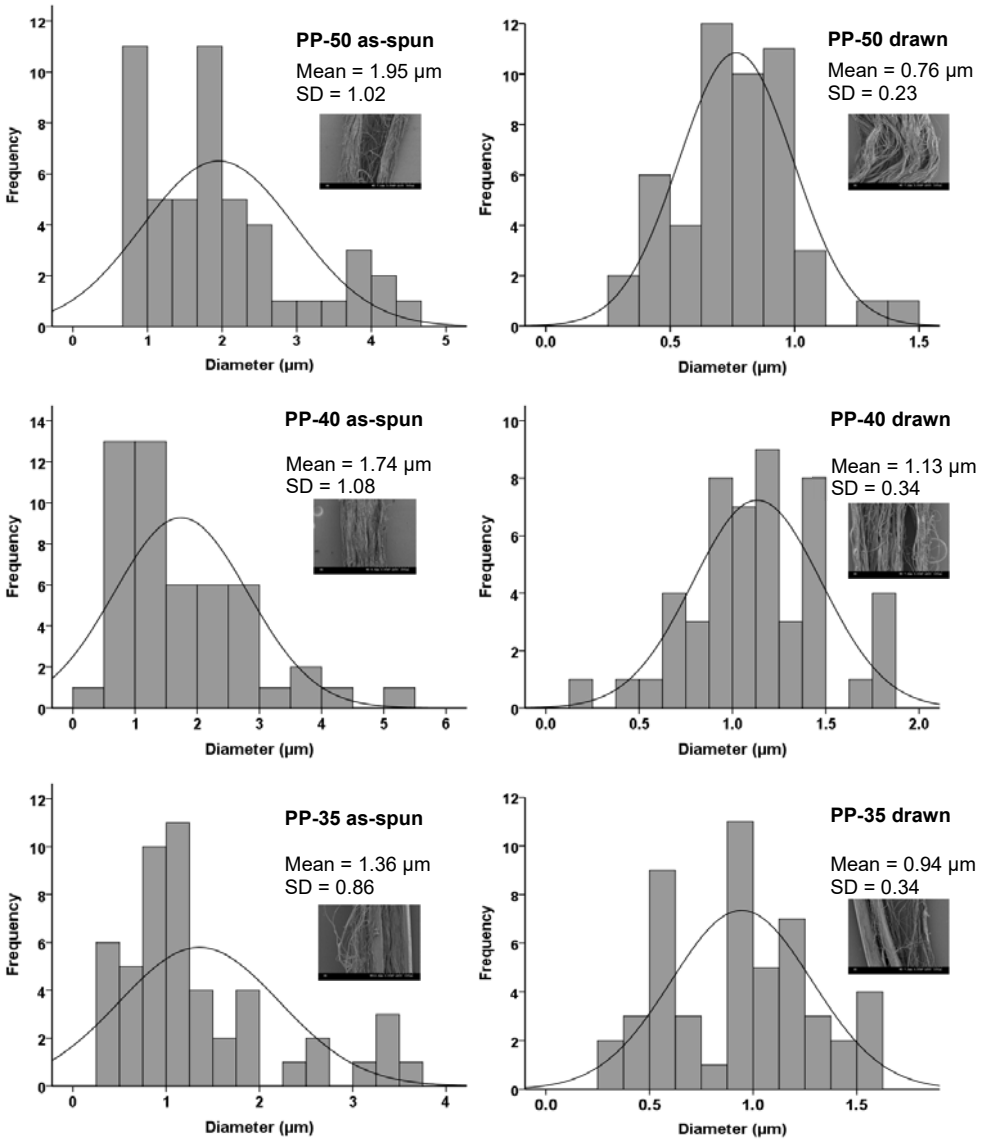

Figure 6.8 Microfibres diameter distribution of PA6 microfibres (as-spun and drawn fibres). (*n*=50)

6.5 Thermal properties

Figure 6.9 and Figure 6.10 show the DSC curves of as-spun hybrid fibres (untreated and treated) at the second heating cycle and cooling cycle, respectively, with the details provided in Table 6.4 and Table 6.5. The maximum melting temperature of PA6 is 221 °C with melting enthalpy of 58.4 J g^{-1} while PP melting peak appears at 160 °C with melting enthalpy of 102.8 J g^{-1}.

The as-spun hybrid fibres before treatment show two endothermic peaks which both represent the peak of PA6 and PP (Figure 6.9 As-spun). The presence of two peaks

indicate the immiscibility of both polymers in the blend. The melting temperature of PA6 in the hybrid fibres was similar with the pure PA6 fibres which completely melted at 221 °C. Near to the PA6 maximum melting temperature, a shoulder peak was appeared at 215 °C. The PA6 crystal morphology was altered after the first heating cycle thus the shoulder indicated energy needed to melt different types of crystal (Schick, 2009; Millot et al., 2015). A melting temperature of PP is shifted from 1 to 3 °C higher than PP fibres. Only PP-20 shows the melting temperature was remain the same as pure PP fibres.

Figure 6.10 (As-spun) shows the DSC curve during cooling cycle with PA6 crystallise at 188 °C and PP crystallise later at 113 °C. The cooling curve of hybrid fibres also showing two exothermic peaks indicate the separation of PA6 and PP. The crystallisation temperature (T_c) of PA6 in the hybrid fibres is almost similar with PA6 fibres. However for PP, the T_c can be seen increased consistence with the addition of the PA6 content in the hybrid fibre. This can be related to the solidification of both PA6 and PP crystal during cooling. The PA6 solidified at 188 °C, earlier than PP, hardened without any disturbance as the PP still remained in the molten state. However, when the PP started to set, the solidified PA6 crystal enhanced the nucleation rate of PP thus changed the PP crystallisation temperature (Jaziri et al., 2008).

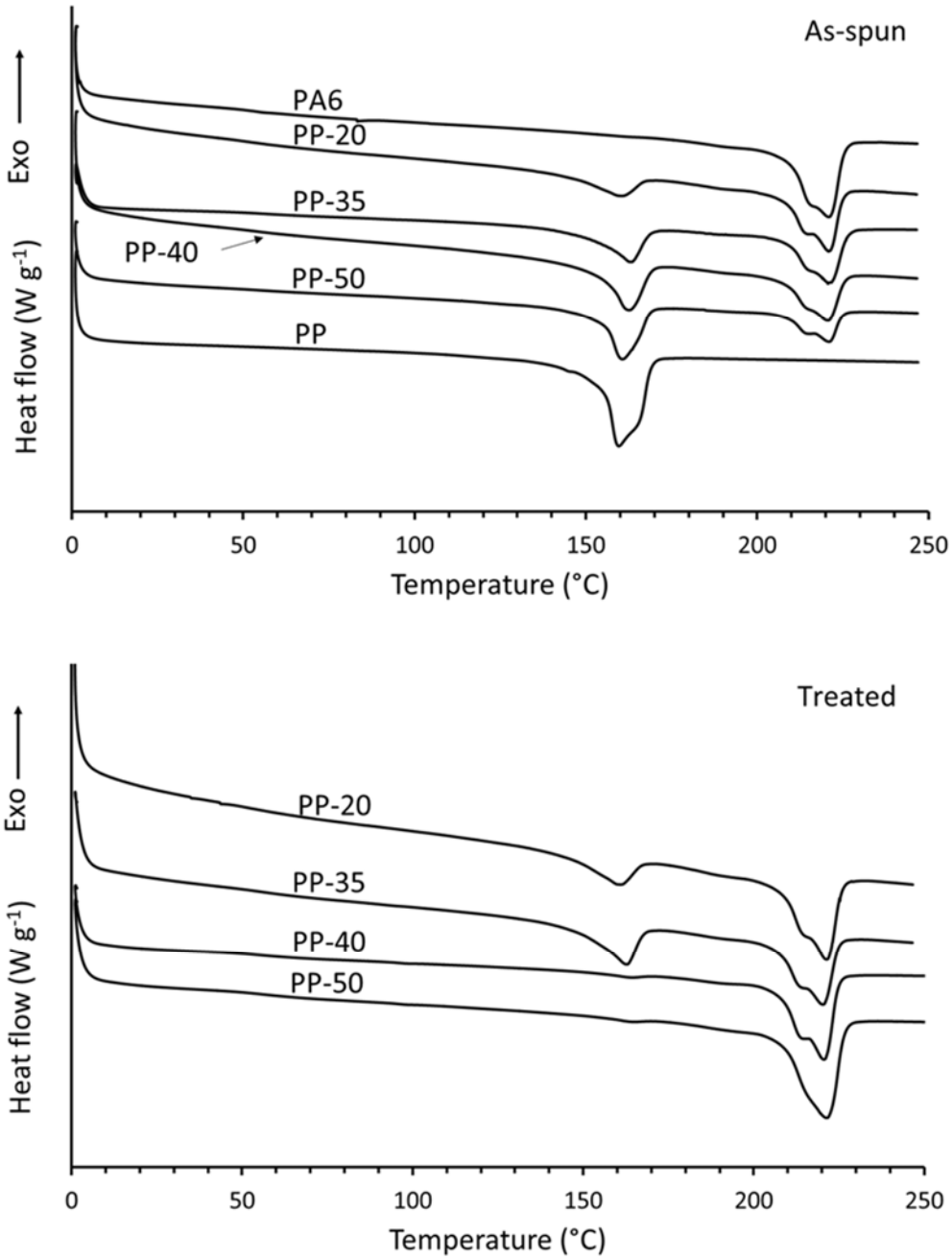

Figure 6.9 DSC curves on second heating cycle of PA6:PP hybrid fibres (as-spun and treated fibre).

Both PA6 and PP are semi-crystalline polymers with pure crystalline enthalpy fusion of 230.1 J g^{-1} and 209.2 J g^{-1}, respectively (Sichina, 2000; Afshari et al., 2005). Melting enthalpy of the polymers can be used to calculate the percentage of crystallinity in the hybrid fibres by using Eq. 3.7. The percentage of crystallinity listed in Table 6.4 shows that PA6 crystal slightly decreased after blended with PP. For PP crystal, the reduction in crystal percentage can be seen correspond to the decreasing of the PP in the blend. Both reduction in the polymer crystal was due to the loss ability of the polymer to form crystal domain, which can be seen clearly in PP (Pedroso et al., 2002).

The hybrid fibres were treated in boiling toluene for 3 h to remove PP component, rinsed and allowed to dry at room temperature. The DSC heating and cooling curves for as-spun treated fibres are shown in Figure 6.9 and Figure 6.10, respectively. By removing the PP from the fibres, the remaining fibres in the hybrid fibres were exposed as shown in Figure 6.2 (treated fibres). From the DSC heating and cooling curves, the peaks of PP was disappeared in the PP-50 and PP-60, indicate the complete removal of PP from the hybrid fibres. In PP-35 and PP-20, the PP peaks still can be observed, indicating the PP component still remained in the fibres after the treatment. Based on the discussion in section 6.3 (Fibre morphology), both PP-20 and PP-35 were found to have PA6 matrix encapsulated the PP component that dispersed in the fibres. The presence of the PP peak in the DSC curve confirms the existence of PP after the treatment. The treatment does not affect much of the thermal properties of the treated fibres (Table 6.5). The melting enthalpy of PP was found decreased but PA6 increased in PP-35 compared to its untreated fibre. During the treatment, small amount of PP component was removed from PP-35 thus influenced the enthalpy of both polymers.

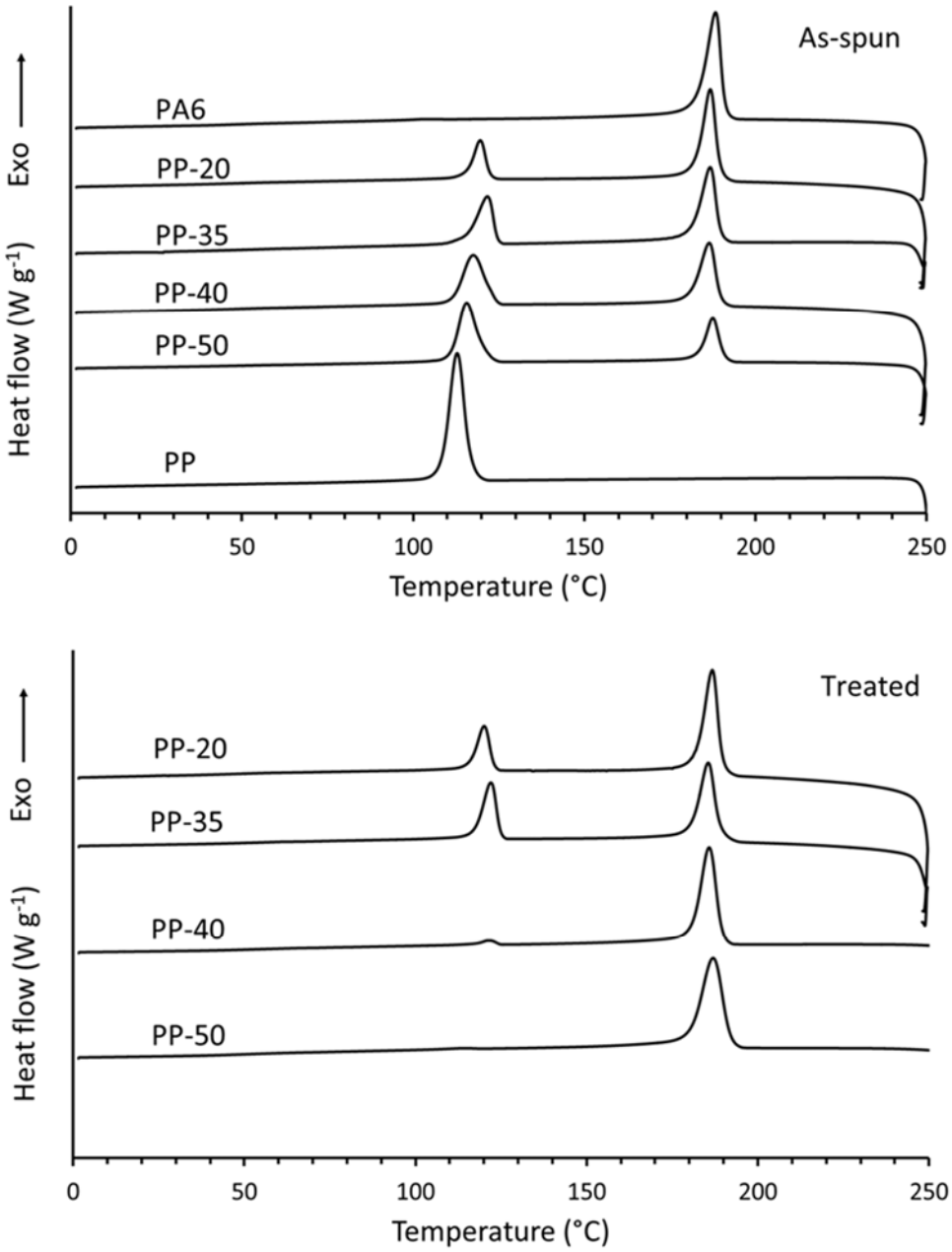

Figure 6.10 DSC curves on cooling cycle of PA6:PP hybrid fibres (as-spun and treated fibre).

Table 6.4: Results of DSC test on as-spun PA6:PP hybrid fibres (untreated).

Fibre (untreated)	*Second heating*		*Cooling*		*Melting enthalpy*		*Crystallinity*	
	$T_{m\,PP}$ (°C)	$T_{m\,PA6}$ (°C)	$T_{c\,PP}$ (°C)	$T_{c\,PA6}$ (°C)	ΔH_{PP} (J g^{-1})	ΔH_{PA6} (J g^{-1})	X_{PP} *(%)*	X_{PA6} *(%)*
PA6	-	221	-	188	-	58.4	-	25.4
PP-20	160	221	120	187	14.6	44.6	34.8	24.2
PP-35	163	221	122	187	24.2	31.4	33.0	21.0
PP-40	163	221	118	187	31.5	33.7	37.7	24.4
PP-50	161	221	116	188	46.5	24.9	44.4	21.6
PP	160	-	113	-	91.7	-	49.1	-

Table 6.5: Results of DSC test on as-spun PA6:PP hybrid fibres (treated).

Fibre (treated)	*Heating*		*Cooling*		*Melting enthalpy*		*Crystallinity*	
	$T_{m\,PP}$ (°C)	$T_{m\,PA6}$ (°C)	$T_{c\,PP}$ (°C)	$T_{c\,PA6}$ (°C)	ΔH_{PP} (J g^{-1})	ΔH_{PA6} (J g^{-1})	X_{PP} *(%)*	X_{PA6} *(%)*
PP-20	160	221	120	187	13.5	41.3	32.3	22.4
PP-35	163	220	122	186	20.8	34.5	28.4	23.1
PP-40	-	221	121	186	-	49.0	-	21.3
PP-50	-	222	-	187	-	55.2	-	24.0

Figure 6.11 and Figure 6.12 illustrate the TGA and DTG curves of the as-spun untreated hybrid fibres, respectively. The results indicate that the degradation of hybrid fibres are in between of its parents fibres which happened in one step degradation excluding PP-35. The T_{onset} of the PA6 is 413 °C and it is completely decomposed at 455 °C as shown in Table 6.6. PP has better thermal stability than PA6 with T_{onset} at 432 °C and its degradation happens at 465 °C. PP-20 and PP-35 hybrid fibres start to decompose at 415 °C which is almost similar with PA6.

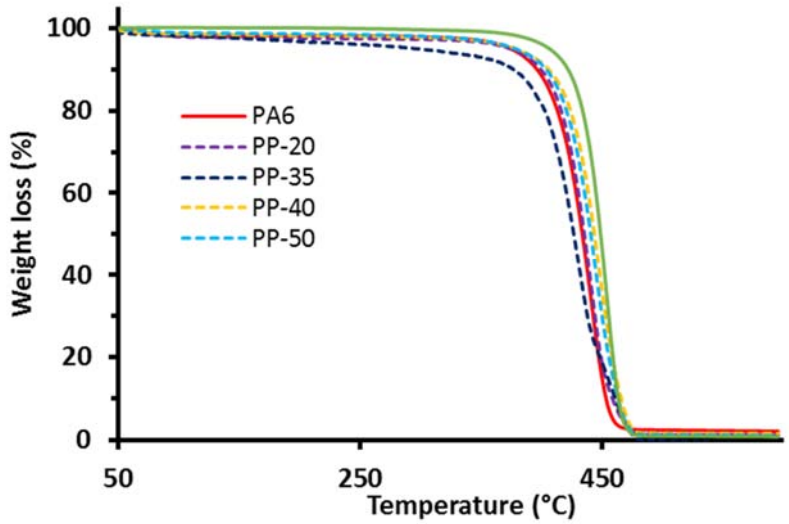

Figure 6.11 Thermal degradation of as-spun PA6:PP hybrid hybrid fibres.

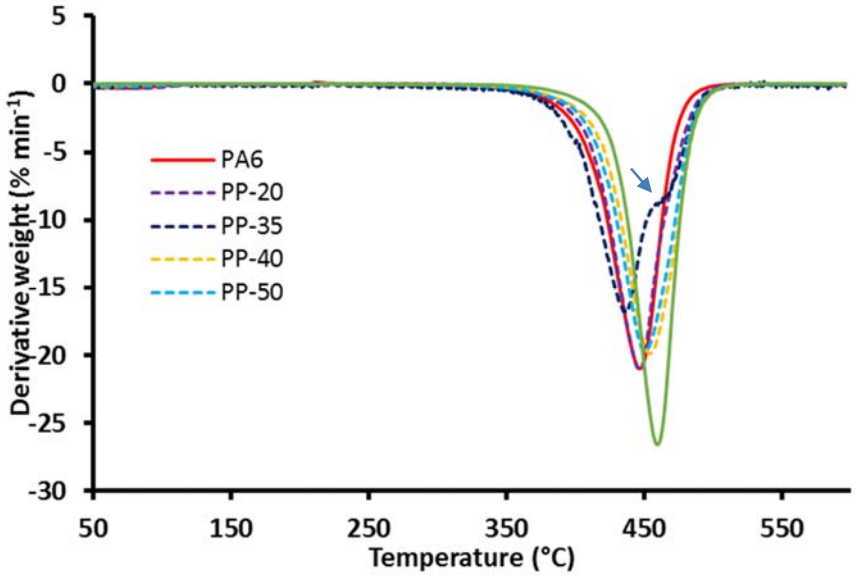

Figure 6.12 Derivative weight curve of as-spun PA6:PP hybrid fibres.

Table 6.6 Thermal degradation of as-spun PA6:PP hybrid fibres (untreated and treated).

Fibre	Untreated				Treated			
	T_{onset} (°C)	T_{50} (°C)	T_{max} (°C)	Residue (%)	T_{onset} (°C)	T_{50} (°C)	T_{max} (°C)	Residue (%)
PA6	413	445	455	2.20	-	-		-
PP-20	415	445	457	1.30	419	448	462	-3.60
PP-35	415	434	467	-1.00	409	446	462	1.60
PP-40	422	451	466	1.70	411	442	455	2.00
PP-50	419	448	463	1.10	407	442	449	5.90
PP	432	458	465	0.83	-	-		-

The outer surface of these hybrid fibres was dominated by PA6 showing the fibres to thermal degradation properties similar to PA6. PP-20 was seen completely degraded at 457 °C, which is slightly higher than PA6 due to the present of 20% PP in the fibres. PP-35 shows different degradation behaviour than other fibres with two steps of degradation. The morphology of the PP-35 with surrounded by PA6 as a matrix makes it start to degrade at 415 °C. Small shoulder peak was found at 445 °C (indicated by arrow in Figure 6.12) after the peak thermal decomposition temperature at 434 °C. The existence of PP as a 'small matrix' in the fibres and PA6 dispersed in the 'small matrix' delayed the degradation to 467 °C, which is slightly higher than PP (Figure 6.13).

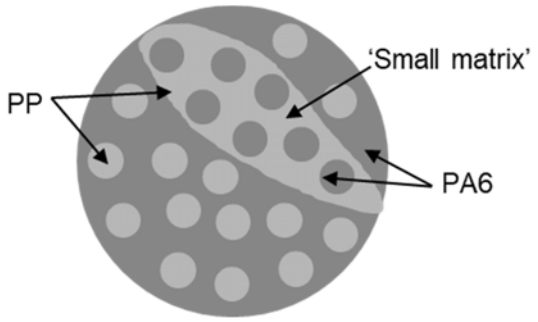

Figure 6.13 Illustration of PP-35 fibre morphology.

The degradation for PP-40 and PP-50 showed higher than PA6 but much lower than PP. Even the outer surface of the fibres was conquered by PP, the PA6 dispersed in the fibres influenced the degradation starting point. On the other hand, the degradation of the fibres improved and degraded almost similar with PP. Such a trend indicated that the morphology of the fibres has major effect on fibres decomposition

rate. Figure 6.14 and Figure 6.15 illustrate the TGA and DTG curve of the as-spun treated hybrid fibres, respectively. The PA6 and PP untreated curves were attached as a comparison to the treated fibres curves.

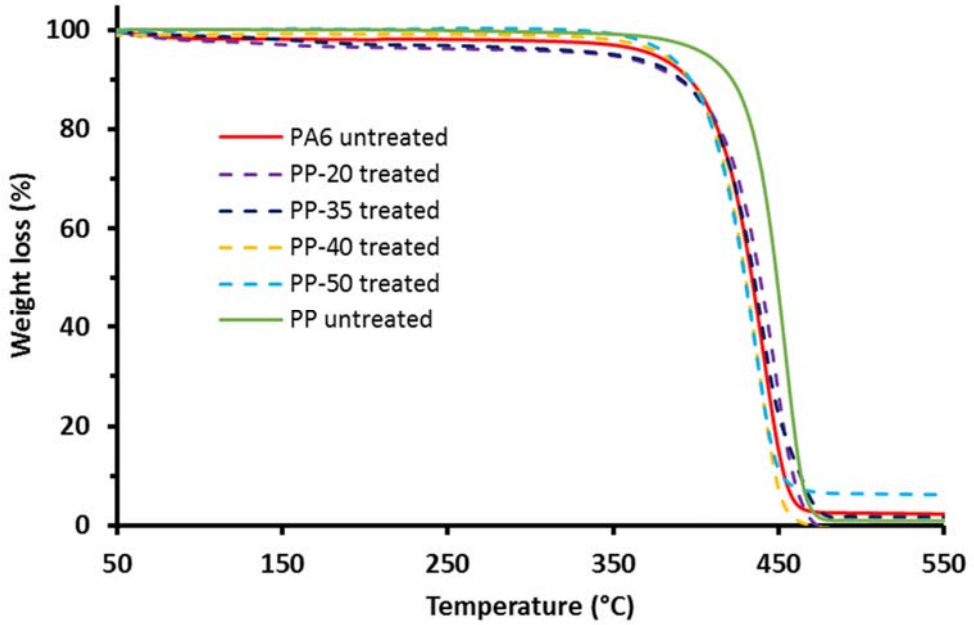

Figure 6.14 Thermal degradation of PA6:PP hybrid fibres (untreated and treated).

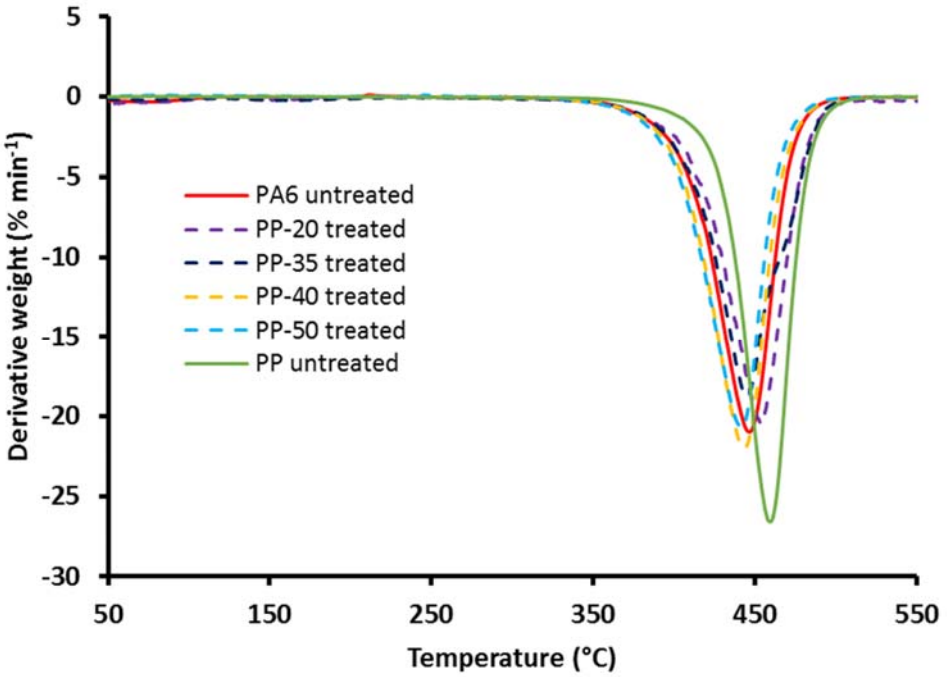

Figure 6.15 Derivative weight curve of PA6:PP hybrid fibres (untreated and treated).

From Figure 6.14 and Figure 6.15, it is obvious that removal of PP from the fibres has altered the thermal decomposition of the hybrid fibres which now shifted more to the PA6 properties. The changes of fibre morphology consequently affect the degradation properties. PP-20 and PP-35 treated fibres show the starting degradation similar to PA6 and completely decompose almost the same with PP. In both hybrid fibres, PP still remained in the fibres after the treatment consequently showing decomposition properties similar to the parent polymers. The PP-40 and PP-50 treated fibres which only have PA6 microfibres left in the fibres after the treatment exhibited the degradation similar to PA6.

6.6 Chemical properties

The morphology study reveals the position of the polymers in the hybrid fibres. ATR-FTIR was then used to investigate the component of the polymers on the fibres surface. Figure 6.16 (as-spun untreated) reveals the existence of PP components on the fibre surface of structure III (PP-40 and PP-50), clearly at the C-H group (2949, 2914 and 2837 cm^{-1}), $C-H_2$ (1453 cm^{-1}) and a sharp peak of $C-H_3$ (1375 cm^{-1}). This confirms that on the structure III hybrid fibres, PP was dominant on the outer surface of the fibres. The weak PA6 peaks were also observed on the structure III hybrid fibres might be due to the location of the PA6 microfibres dispersed near to the wall of the fibres. ATR-FTIR infrared beam can penetrate up to 2 μm from the samples surface.

In structure I, PP-20 hybrid fibres, PA6 component was dominant as a matrix and confirmed by the peaks of PA6 which were obviously seen at 3291 cm^{-1}(N-H), 1633 cm^{-1} (amide I) and 1538 cm^{-1} (amide II). For PP-35, the PA6 peaks were observed except a C-H group (2922 & 2864) which slightly detected on the fibre surfaces. The PP component was also detected on the PP-35 fibres showing the existence of the PP on the fibre surfaces. Morphology of the PP-35 showed the phase inversion between PA6 and PP, thus the existence of PP peaks were expected.

Figure 6.16 (as-spun treated) shows the ATR FTIR peaks of the hybrid fibres after the treatment in toluene to remove the PP component. Obviously seen that PA6 peaks were displayed while PP peaks were diminished on all hybrid fibres. In structure I, PP-20, the peak at 1455 cm-1 ($C-H_2$) shows the same as the untreated indicating the existence of dispersed PP and still remained on the same location even after the treatment. As the PP located inside the fibres and fully covered by PA6, the toluene cannot penetrate the PA6 matrix and left the dispersed PP untouched and

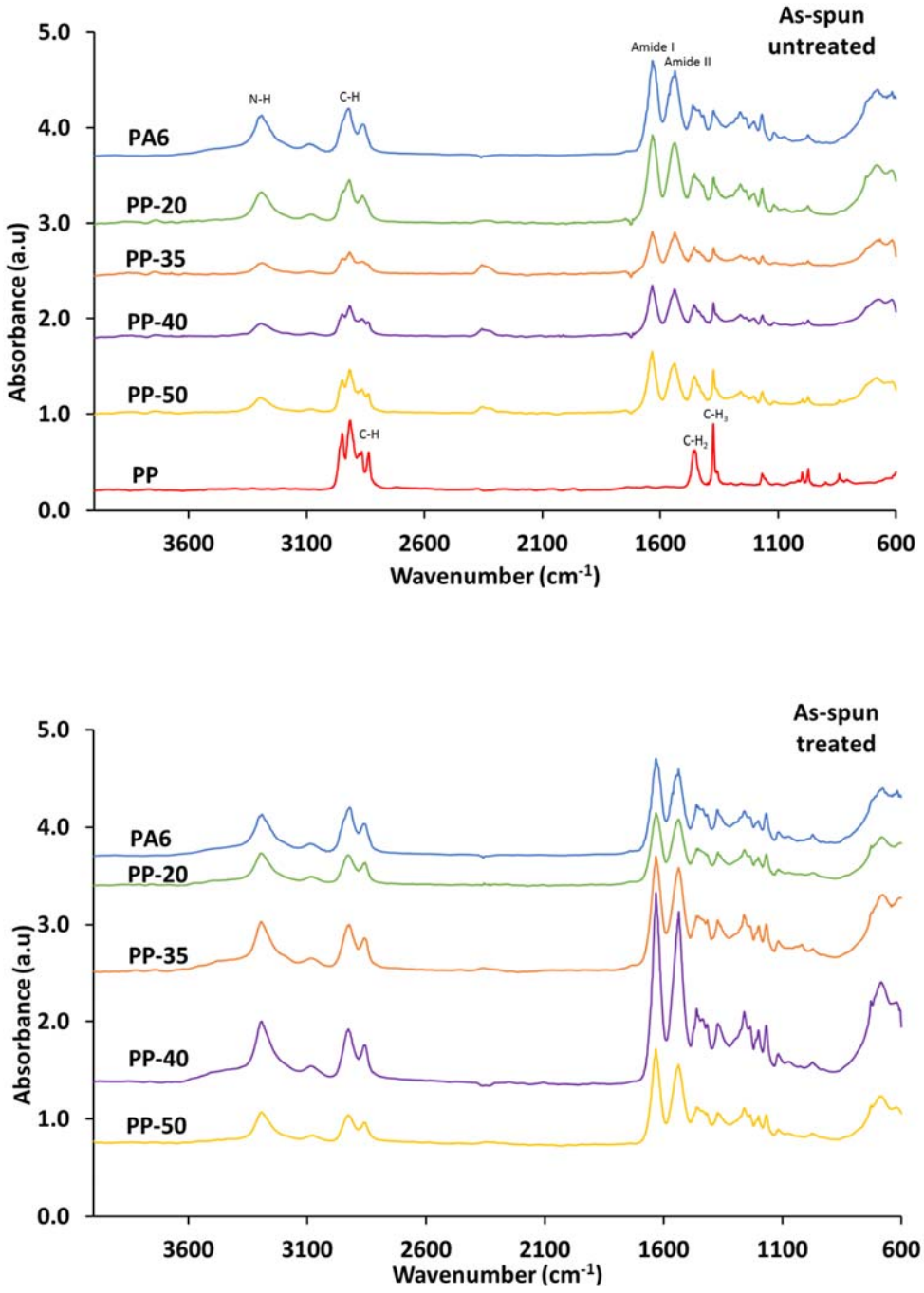

Figure 6.16 FTIR spectra of PA6:PP as-spun hybrid fibres and single component fibres untreated and after treated in toluene. (Normalised at 1634 cm^{-1}).

remained in the fibres. The PP was completely vanished from PP-35, PP-40 and PP-50, as no PP peaks were observed.

6.7 Tensile properties

The tenacity of as-spun fibres (untreated and treated) was shown in Figure 6.17 (as-spun). As-spun untreated hybrid fibres has tenacity between PA6 and PP, with PP-35 exhibits higher strength followed by PP-50, PP-40 and PP-20. The morphology of the fibres and the position of the PP and PA6 in the blend influenced the strength of the fibres. In this study, three different morphologies of the fibres were recognised as mentioned in section 6.3 (Fibre morphology).

PP-20 which has lower strength in as-spun untreated fibres, consisted of PA6 as a matrix and PP as a dispersed phase. The PA6 has crystallisation temperature at 188 °C, solidified earlier than PP that crystallise at ~113 °C (Figure 6.10). The PP inside, which hardened later, shrunk during cooling process and created gaps between PA6 and PP interfacial surface (Ayad et al., 2016). This phenomenon contributes to the decreasing of the hybrid fibres strength. Despite, when PA6 was inside, it will restrict the movement of the PP that located outside and improved the interfacial adhesion between the surfaces. This can be seen in PP-40 and PP-50 hybrid fibres which has better tenacity than PP-20 in as-spun untreated fibres. In PP-35, the tenacity is higher than other hybrid fibres, this might be due to the unique morphology and different structure of PA6 and PP in the fibres (Pötschke and Paul, 2003; Wang et al., 2012).

The removal of PP from the fibres affects the strength of the fibres. The tenacity of PP-40 and PP-50 as-spun treated reduced as there is only PA6 microfibres left after the PP removal. PP-35 also shows reduction in strength, it might be due to the crack developed on the fibres (Figure 6.2 b1 & b2). The removal of ‘small’ PP matrix (Figure 6.13) developed cracks thus affects the ability of the fibres on the force applied. Meanwhile for PP-20, the PA6 was dominant on the outer surface of the fibres which does not affected by the treatment showing better strength than others.

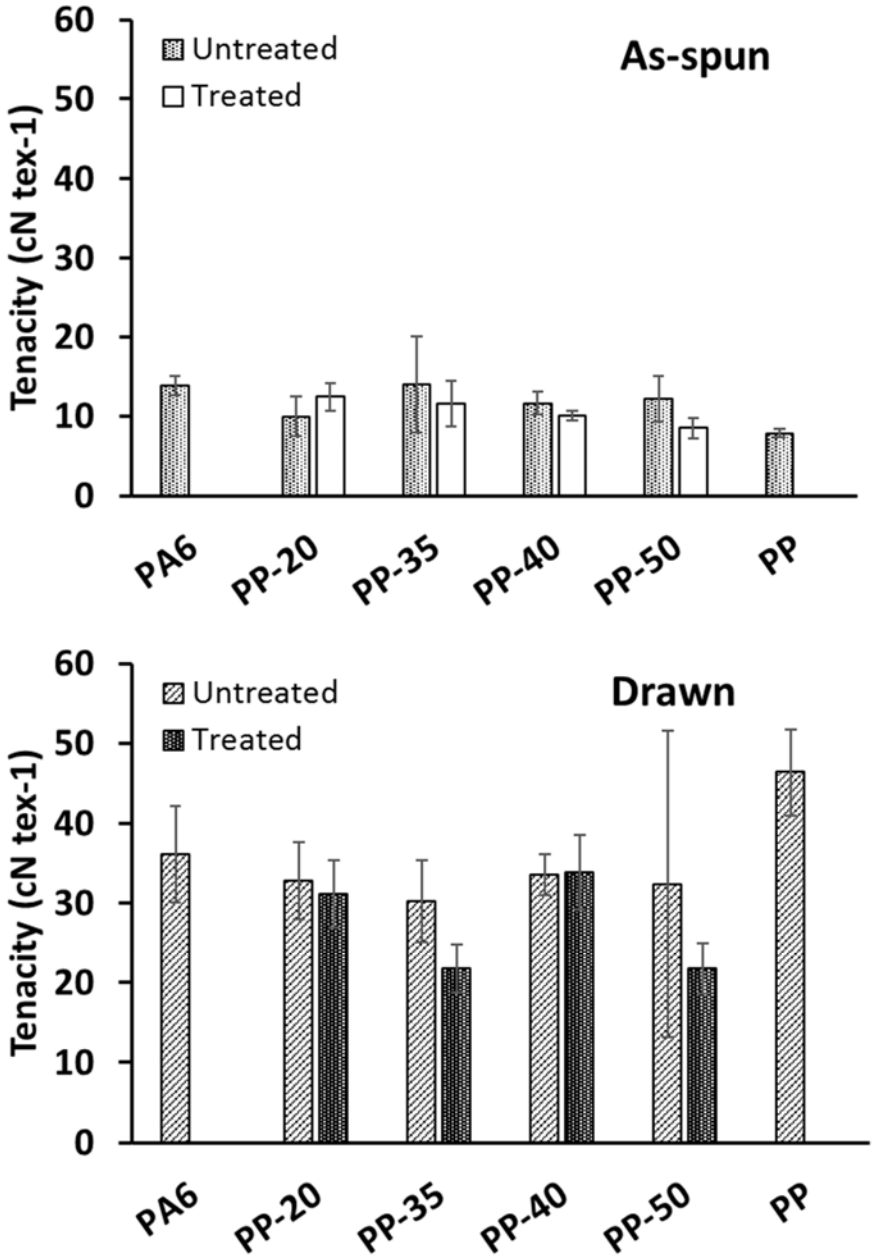

Figure 6.17 Tenacity of as-spun and drawn PA6:PP hybrid fibres (untreated and treated).

The strength of the fibres after drawn was also investigated and shown in Figure 6.17 (drawn). PP-40 has higher strength than others while PP-50 has high variance in strength. As mentioned before, the morphology of hybrid fibres with PP outside and PA6 inside have better interfacial adhesion between surfaces. When the fibres stretched, the PA6 microfibres elongated along with the PP matrix. The increasing of tenacity is also due to the increasing of orientation and crystallisation of the fibres during drawing process (Meyabadi et al., 2010). The tenacity of the drawn untreated fibres increased almost 230% than as-spun untreated fibres. PP-35 drawn untreated fibres display the lowest strength that might be affected by the cracks developed in the fibres. When the fibres elongated, the small PP matrix which has poor interfacial surface with PA6 matrix created bigger gaps and influenced the strength of the fibres.

Drawn fibres were also treated with toluene to remove the PP component. The strength of PP-50 and PP-35 reduced while PP-40 and PP-20 seem unaffected by the treatment as shown by Figure 6.17 (drawn). The strength reduction in PP-35 was caused by the cracks revealed after the treatment. Huge different between PP-40 and PP-50 can be seen after drawn fibres were treated even though both hybrid fibres revealed PA6 microfibres after the removal of PP. The composition of PA6 is higher in PP-40 thus produced larger PA6 microfibres as shown in Figure 6.6, this might influence the strength of the drawn treated fibres.

The tenacity-elongation curve of the as-spun and drawn hybrid fibres are shown in Figure 6.18 and Figure 6.19, respectively. The starting curves of as-spun untreated PP-40 and PP-50 show almost the same as PP. In both fibres, PP became a matrix while PA6 as a microfibres showing the same starting strength behaviour with PP. However, two breaking points were observed in PP-40 as-spun untreated before the fibres snap (shown as pointed arrow). The same trend can be seen in drawn untreated PP-40 and PP-50. This phenomenon relates to the morphology of the fibres. When PP is dominant at the outside of the fibers, the applied force hit the PP first before continued by the PA6 microfibres located inside, thus explained how the two points exist.

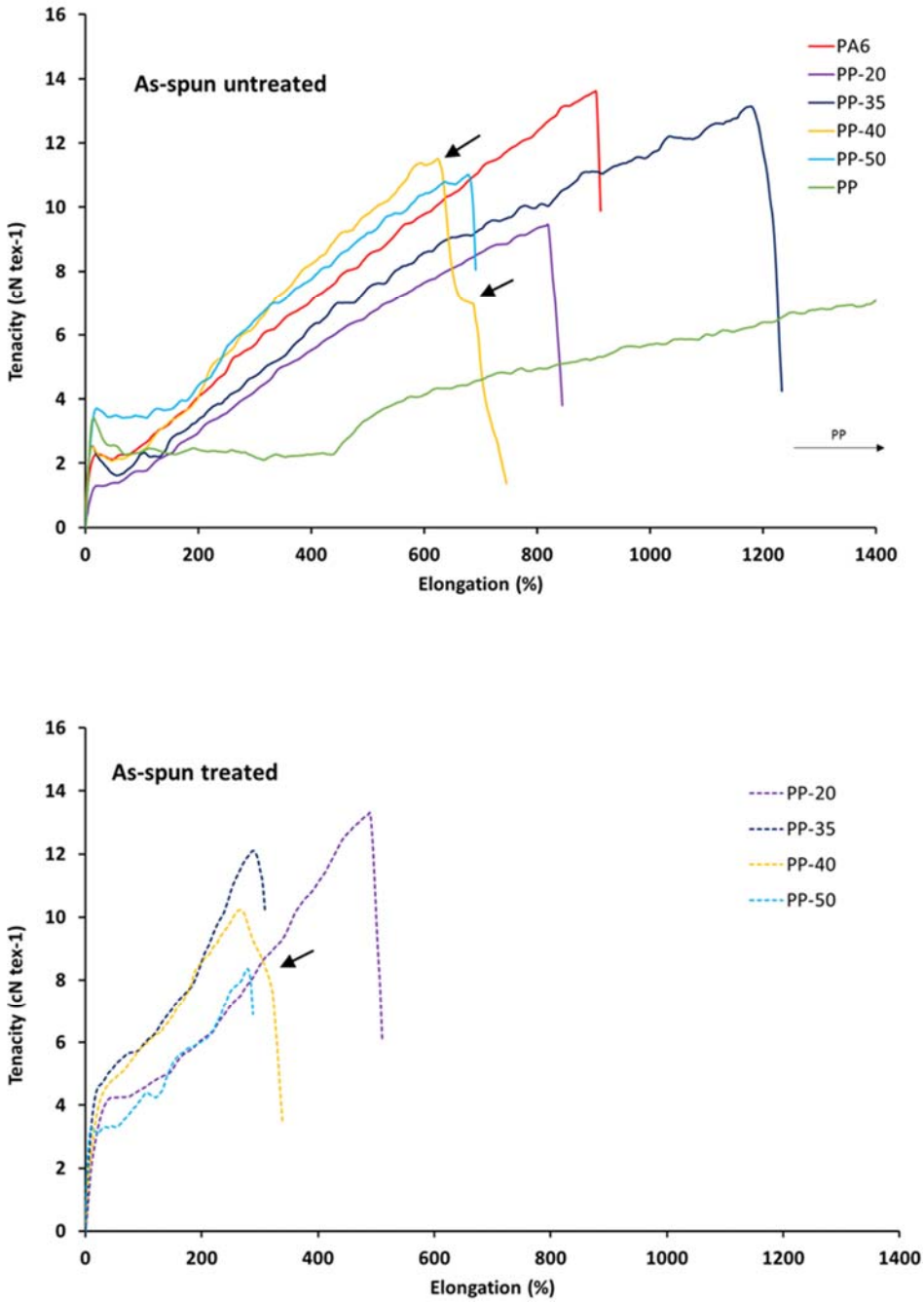

Figure 6.18 Tenacity-elongation curve of as-spun PA6:PP hybrid fibres(untreated and treated).

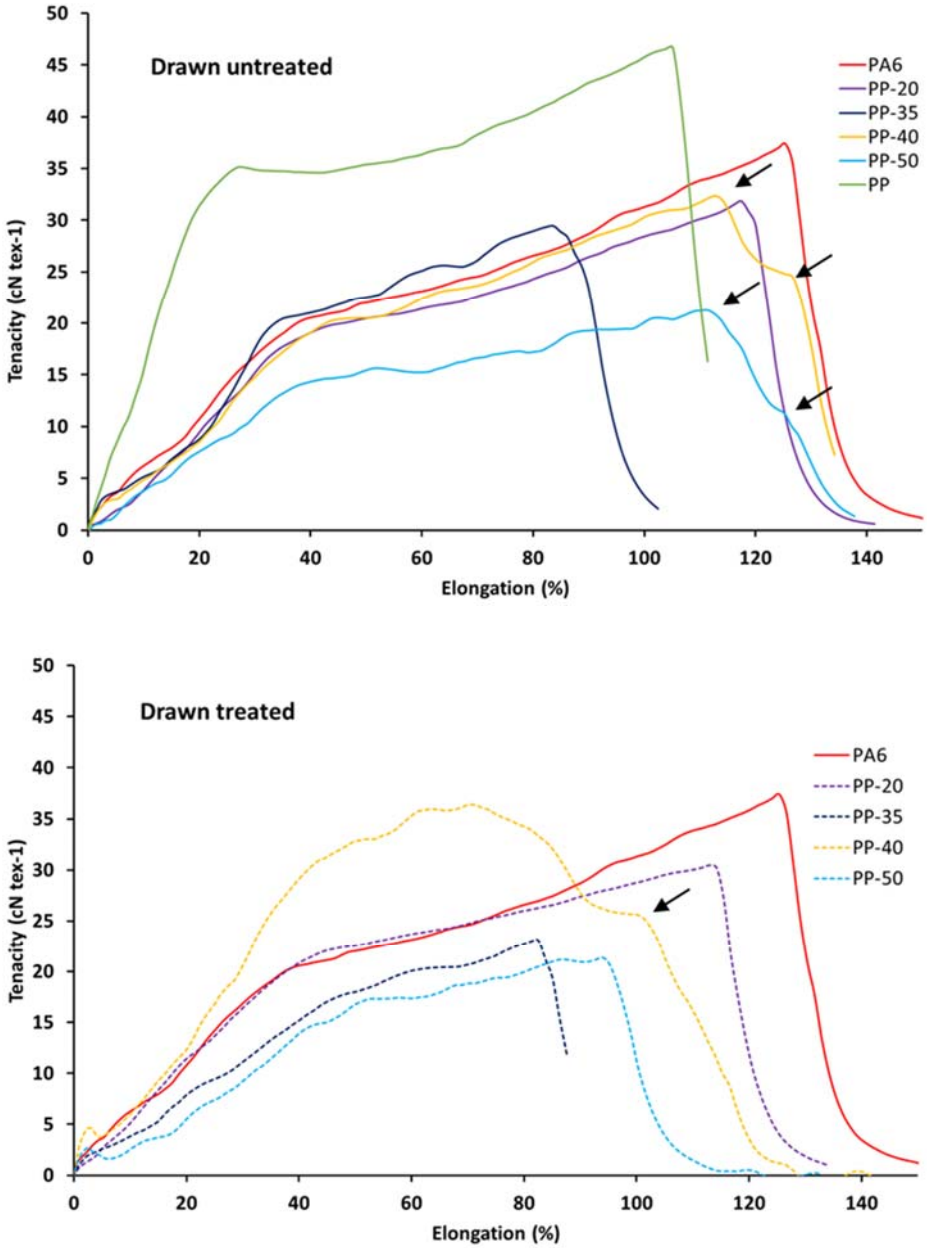

Figure 6.19 Tenacity-elongation curve of drawn PA6:PP hybrid fibres (untreated and treated).

The as-spun and drawn hybrid fibres have breaking elongation in between PA6 and PP fibres as shown in Figure 6.20. Structure III (PP-40 and PP-50) has lower breaking elongation than other structures. As discussed before, structure III has better physical bonding developed between PA6 and PP interfacial surfaces. The bonding created restricted the movement of both polymers during stretching thus broke earlier than other structure. Both PP-20 and PP-35 have poor adhesion between PA6 and PP interfacial surfaces make the PA6, the outer component, elongated easily without distraction from the PP inside.

The breaking elongation after the removal of PP shows PA6 microfibres (PP-40 and PP-50) has weaker elongation than PP-20 which still remained in a solid fibre form. The cracks developed in PP-35 also influence the breaking elongation of the fibres which has significant reduction compared to the untreated. The drawn hybrid fibres display similar breaking behaviour with as-spun fibres.

The initial Young's modulus of the as-spun and drawn fibres shows the hybrid fibres have higher stiffness than PA6 and almost similar with PP fibres excluding PP-20 as-spun hybrid fibres as shown in Figure 6.21. PP-20 which has PA6 as outer component exhibits almost similar modulus with PA6 fibres. Higher stiffness can be seen on the treated drawn PP-40 and PP-50 fibres.

Table 6.7 shows linear density of fibres in tex unit which equivalent to the weight (g) of the fibres in 1000 m length. Higher number indicates coarser fibres and lower number represents finer fibres. The as-spun hybrid fibres have finer fibres than PA6 and PP except for PP-20 which has the highest fibre density. The removal of PP reduces the linear density of the PP-40 and PP-50 hybrid fibres. PP-35 shows no significant density different as most of PP component trapped in the fibres thus did not change the density. For drawn fibres, obviously the fibres become finer after stretching. The linear density of the fibres after PP removal was inconsistence compared to the untreated in term on PA6 content.

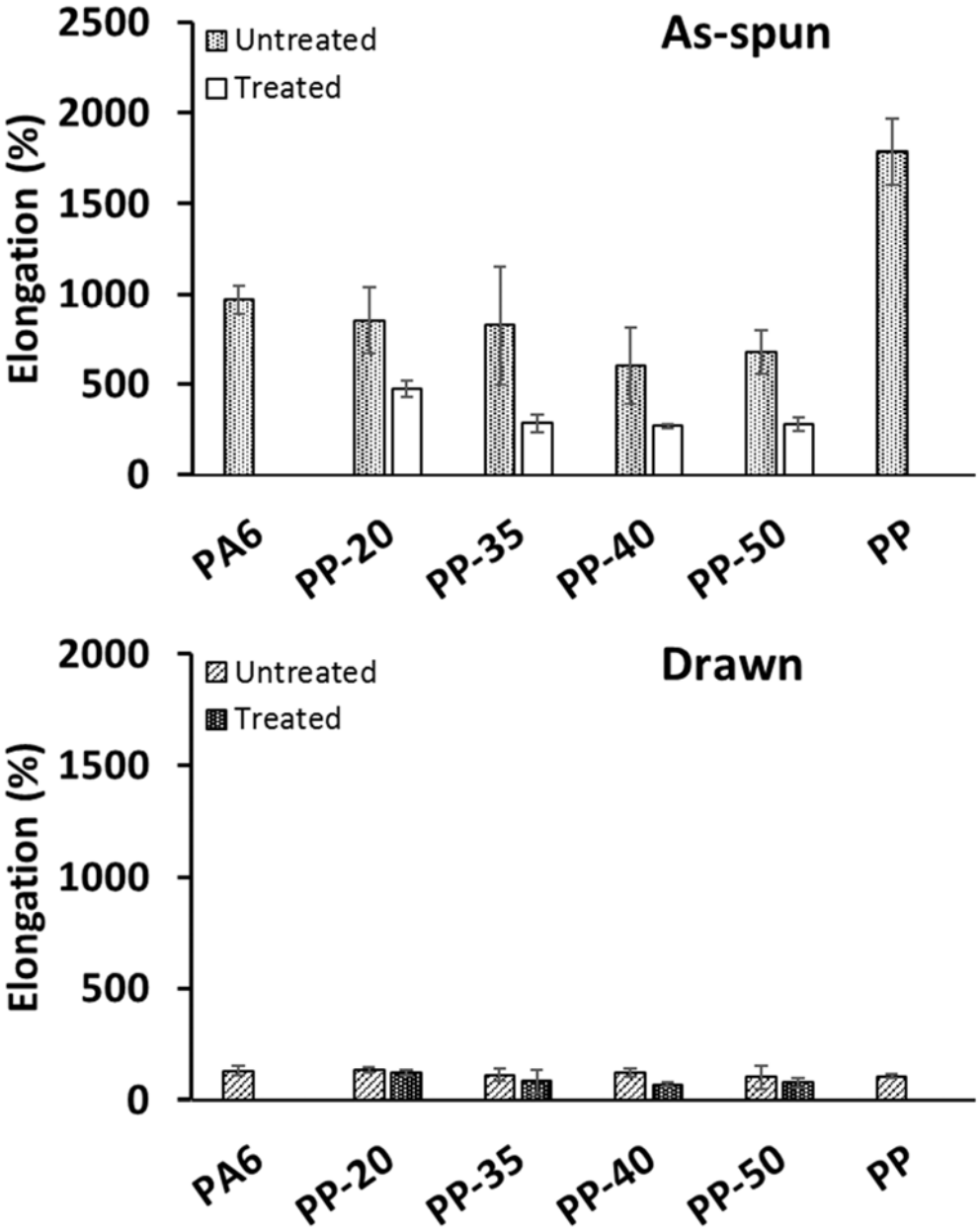

Figure 6.20 Elongation at break for as-spun and drawn PA6:PP hybrid fibres (untreated and treated).

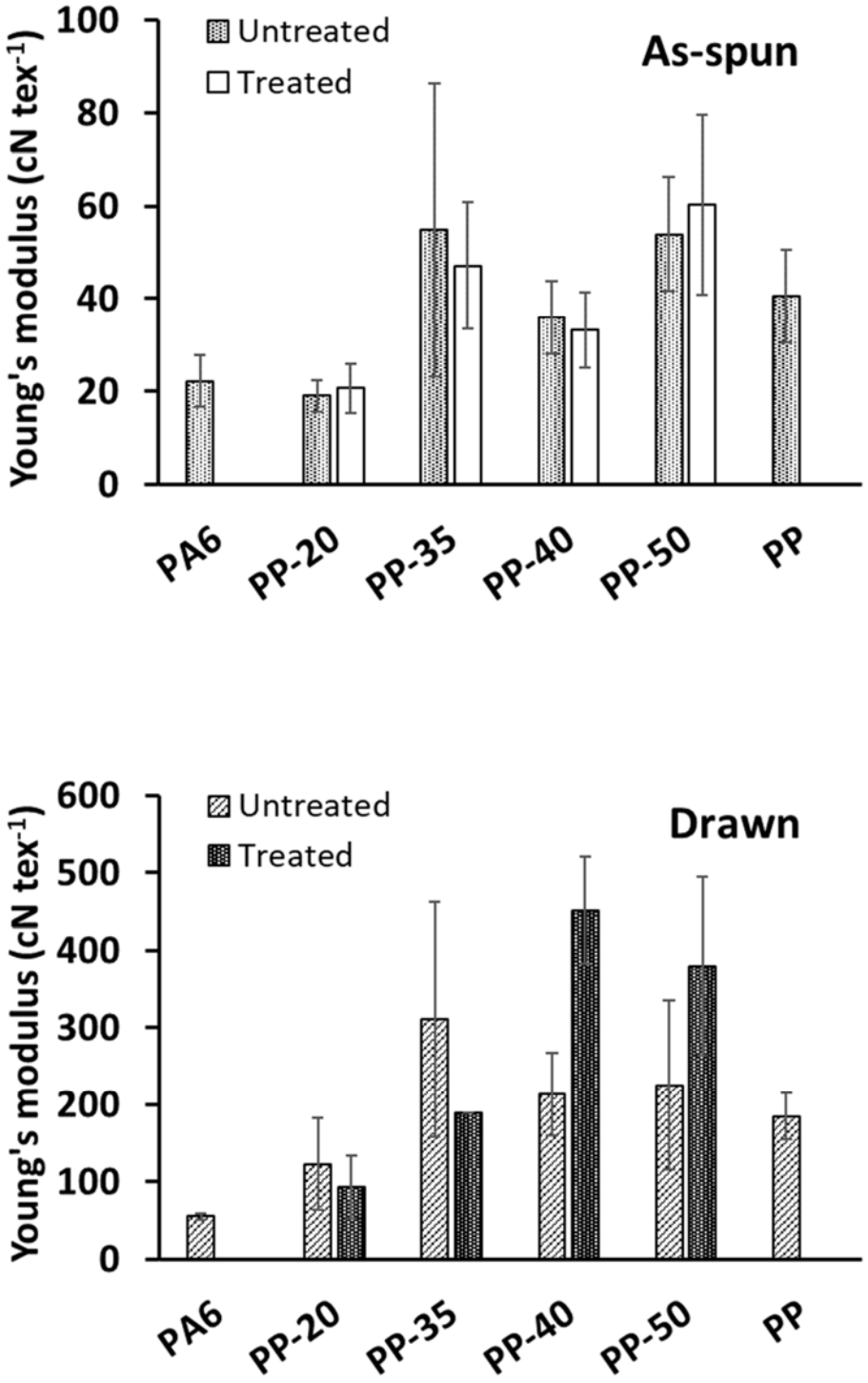

Figure 6.21 Initial Young's modulus of as-spun and drawn PA6:PP hybrid fibres (treated and untreated).

Table 6.7 Tex of the as-spun and drawn PA6:PP fibres.

	Tex			
Fibre	Fibre (as-spun)	Microfibre (as-spun)	Fibre (drawn)	Microfibre (drawn)
PA6	21± 6	-	6 ± 1	
PP-20	28 ± 2	-	8 ± 2	
PP-35	12 ± 5	12 ± 4	4 ± 1	5 ± 1
PP-40	14 ± 2	11 ± 0.2	4 ± 1	2 ± 0.4
PP-50	13 ± 4	7 ± 0.2	3 ± 1	4 ± 2
PP	20 ± 2	-	4 ±1	

6.8 Conclusions

The blending of non-interacting polymer between PA6 and PP shows different fibres morphology regarding the blend composition of the fibres. Higher PA6 composition in the blend is able to produce ‘island-in-the-sea’ bicomponent with PA6 as an island and PP as the “sea”. The removal of PP in toluene solution reveals the development of PA6 microfibres as confirmed in PP-50 and PP-40 hybrid fibres. The average diameters of PA6 microfibres were in the range of 1.74-1.95 µm and it is further reduced to 0.7-1.13 µm upon drawing. PP-35 exhibits partially phase inversion between PA6 and PP with PA6 became a matrix and dispersed at certain area. Meanwhile PP-20 shows PA6 fully encapsulate the dispersed PP. Thermal properties shows the separation of PA6 and PP component with two melting and crystallisation peaks observed in DSC curve. PP peak disappeared in PP-50 and PP-40 confirmed the elimination of PP from the blend. The strength of the hybrid fibres was in between of the single component fibres.

The ability of PP-50 and PP-40 to produce PA6 microfibres was extended into fabric production. However, only PP-40 was selected f fabric production due to the strength shown in the mechanical properties particularly in drawn hybrid fibres after treatment. This is to investigate the potential of producing fabrics by blending two non-interacting polymer into hybrid fibres via single-step melt extrusion, detailed in Chapter 7.

Chapter 7
Properties of upcycled polyamide 6 fabrics

7.1 Introduction

The blending of PA6 with other polymers resulted in various fibre morphologies (see section 4.22, 4.31, 5.4 and 6.3). Among the secondary polymers used, TPU, PET and PP, the blending of PA6 and PP show the ability to produce PA6 microfibres after removal of PP component (Chapter 6). The high surface area of the PA6 microfibres can offer premium mechanical and comfort properties for yarns and subsequently the fabrics made from PA6:PP hybrid fibres. The blend composition of 60% PA6 and 40% PP (PP-40) demonstrated good strength after drawing and was selected for the fabric production process (section 6.7). The monofilament PP-40 was melt-spun (section 3.2.2 for the melt spinning conditions), drawn and winding onto cone before being knitted on a double bed flat knitting machine. The circular plain jersey knitted structure was produced considering a limited amount of the monofilament from lab-scale melt extrusion. The knitted fabric was then treated in toluene, using the same method for PA6:PP hybrid fibre treatment (section 3.3), rinsed and dried for further testing. The process of producing the fabrics and the properties of the fabrics before and after treatment is reported in this chapter.

7.2 Production of PP-40 hybrid fibre

The production of PP-40 hybrid fibres was a pre-requisite for fabric production. The same method was applied to produce PP-40 hybrid fibres as discussed in Chapter 6. The produced hybrid fibres from the melt spinning were wound onto a paper spool as shown in Figure 7.1 (left). The extruded PP-40 hybrid fibres were then drawn (Draw ratio = 2) to improve the strength of the fibres.

PP-40 drawn fibres were processed on the flat-bed knitting machine but withdrawal of the fibres from spool posed challenges in terms of yarn breakages. Therefore, the yarns were rewound on to paper cones for further processing, see Figure 7.1 (right) and section 3.10 for further details. During the winding, a single ply of monofilament PP-40 has been prepared for the next step, knitted fabric production.

Figure 7.1 Paper spool (left) and cone (right).

7.3 Production of PP-40 knitted fabric

The wound PP-40 yarn was brought to a double bed flat knitting machine (hand driven) for fabric production. A circular plain jersey knitted fabric was produced as shown in Figure 7.2. Approximately 32 cm length and 44 cm width of fabric was produced. The fabric was divided into two pieces, one piece of fabric is used for reference (untreated) and the other piece was treated in toluene to remove PP component (treated), with measurement for one piece of fabric is 32 x 22 cm.

The fabric after treatment with toluene is shown in Figure 7.3. The treated fabric's measurement is approximately 25 cm in length and 18 cm wide. Almost 35% of the PP component was removed after the treatment in toluene, considering the mass of fabric before and after treatment.

The untreated and treated fabrics were conditioned prior to testing. Several fabric testing were chosen to investigate the structure of the fabrics (using SEM and light microscope), physical properties (thickness, mass per unit area and stitch density), vertical wicking and tensile properties of the fabrics as described in section 3.12.

Figure 7.2 PP-40 circular plain jersey knitted fabric before treatment.

Figure 7.3 PP-40 circular plain jersey knitted fabric after treated with toluene.

7.4 Fabric

Fabric structure was viewed under light microscope and SEM as shown in Figure 7.4. Significant differences can be seen from the images between the PP-40 untreated and treated fabric. The untreated fabric, which has PP component dominant on the fibre surfaces gave the transparent and glossy look when viewed under light microscope (Figure 7.4 b). After the removal of PP, the treated fabrics was found remained in the original figure without significant distortion of the structure (Figure 7.3 and Figure 7.4 a'). This shows that the PA6 microfibres that dispersed in the hybrid fibres produce long PA6 microfibres enough and remained as multifilament PA6 after the removal of PP. The PA6 microfibres made fabric appears to be white and opaque as shown in Figure 7.4 b'.

The light microscope images has a limitation to view the PA6 microfibres images due to the wavelength of the light thus SEM was used. Figure 7.4 c and c' show the SEM images of the untreated and treated fibres, respectively. From the images, clear distinct between untreated and treated fibres can be seen. PA6 microfibres were clearly shown in Figure 7.4 c' thus approve the development of PA6-40 microfibres in the fabric.

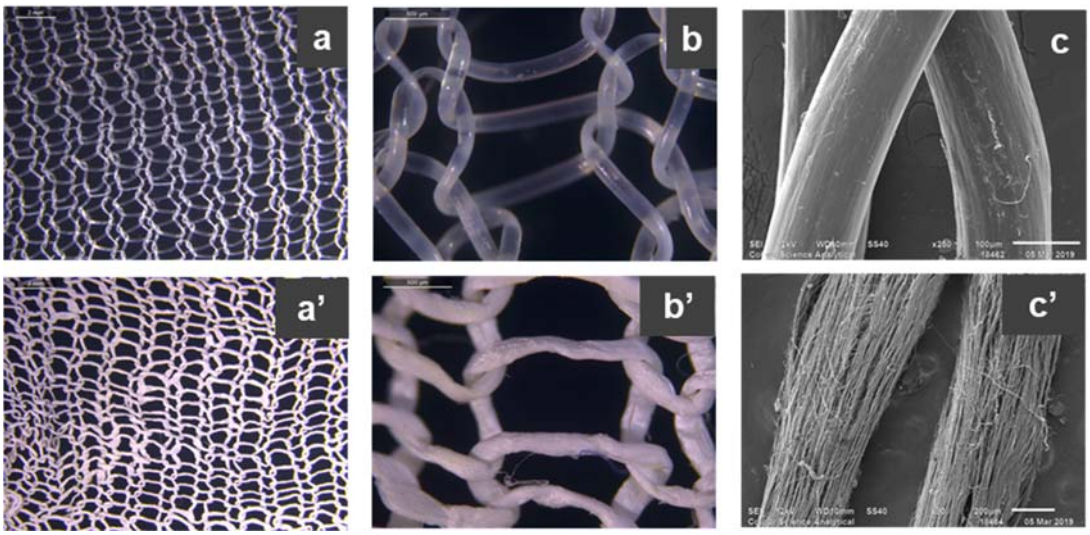

Figure 7.4 The structure of PP-40 knitted fabric untreated (a, b & c) and treated (a', b' & c') viewed under light microscope (a,b, a' & b') and SEM (c & c').

7.5 Physical properties

The results for fabric thickness and fabric mass per unit area of the untreated and treated fabric are illustrated in Figure 7.5. It is clear that the fabric thickness and mass per unit area decreased after the removal of PP component. This could be expected as almost 35% of the PP component was removed from the fibres. The untreated fabrics have both components, PP as an outer structure and PA6 is inside the hybrid fibres produced round and solid fibre structure. After the removal of PP, the structure of the hybrid fibres turns into a significant number of PA6 microfibres, which reduced in term of fibre diameter (as discussed in Chapter 6 section 6.4). Even the number of PA6 microfibres are significant in the yarn, the movable of the microfibres make them flexible thus easily compressed and reduce the thickness of the fabrics. The removal of significant amount of PP during the treatment definitely affects the fabric mass. These factors contribute to the decrement in the thickness and fabric mass of the PP-40 treated fabric.

The independent T-test was conducted to compare the thickness and fabric mass of the untreated and treated fabric. There was a significant difference in the thickness for untreated (M=7, SD=1) and treated (M=3.7, SD=0.57) fabric; t(4)=5.0, p=0.007. However, for the fabric mass, the statistical study shows statistically difference between untreated and treated fabrics with the p-value are slightly above the min number; t(4)=2.7, p=0.054. This can be due to the uneven fabric mass along the fabric.

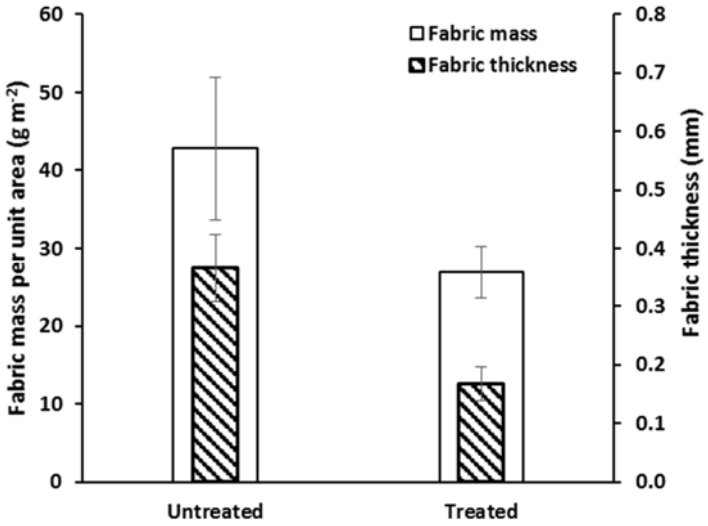

Figure 7.5 Mass and thickness of untreated and treated PP-40 fabric.

The fabrics before and after treatment were also investigated including the courses, wales and stitch density. From the graph shown in Figure 7.6, it can be seen that the fabric was not significantly affected after the PP removal. The wales of the fabric remain the same after treatment with the average of 9 wales/in. The course of the fabric increase by 1 course after the treatment. This shows that the fabric slightly shrunk in course direction. Meanwhile, the stitch density of the fabric slightly increases after the treatment, due to the shrinkage of the fabric in course direction. However, independent T-test shows no significant difference of the fabric structure before and after treatment as p-value is higher than 0.05 (p-value were 0.101, 1.000, and 0.380 for course, wale and stitch density, respectively).

Figure 7.6 Courses, wales and stitch density of untreated and treated PP-40 fabric.

7.6 Fabric Strength

Ball burst strength test was conducted to investigate the strength of the PP-40 fabrics, untreated and treated. Figure 7.7 shows that the treated fabrics have higher burst strength compared to that of untreated fabrics (normalised to the fabric mass per unit area). The results are corresponded well to the results obtained by Gun (2011) and Srinivasanet al. (2007) where the microfibres fabrics show improvement in burst strength compared to the fabric made from conventional fibres. Microfibre fabrics consist of a bundle of microfibres that increase the fabric surface and attain the inter-fibre friction which improve the fabric strength (Kalyanaraman, 1988; Mukhopadhyay and Ramakrishnan, 2008). In the ball burst strength technique, the force was applied from top of the fabrics and applied in all fabric directions, which after testing, left a hole on the fabric (Figure 7.8).

Figure 7.9 shows a representative curves of PP-40 fabrics (untreated and treated) ball burst strength. The untreated fabrics were found elongated more before break. The treated fabric curve shows almost similar with the single fibre result shown in Figure 6.19.

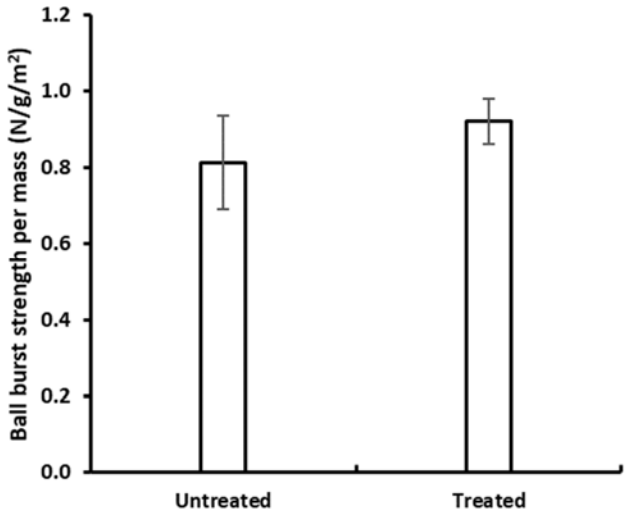

Figure 7.7 Ball burst strength of the PP-40 untreated and treated fabrics.

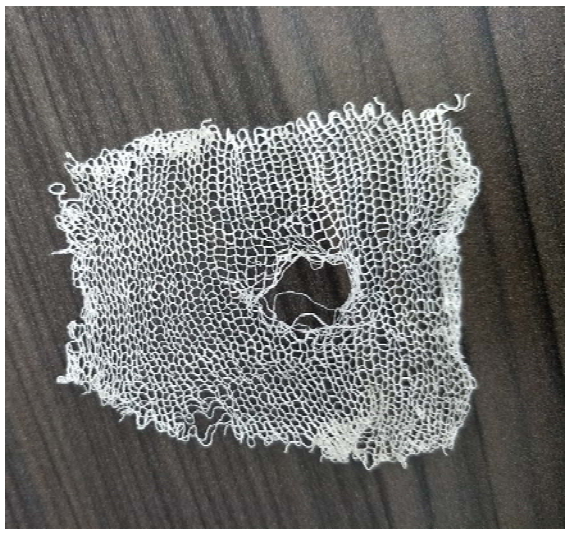

Figure 7.8 Example of PP-40 treated fabrics after ball burst strength test.

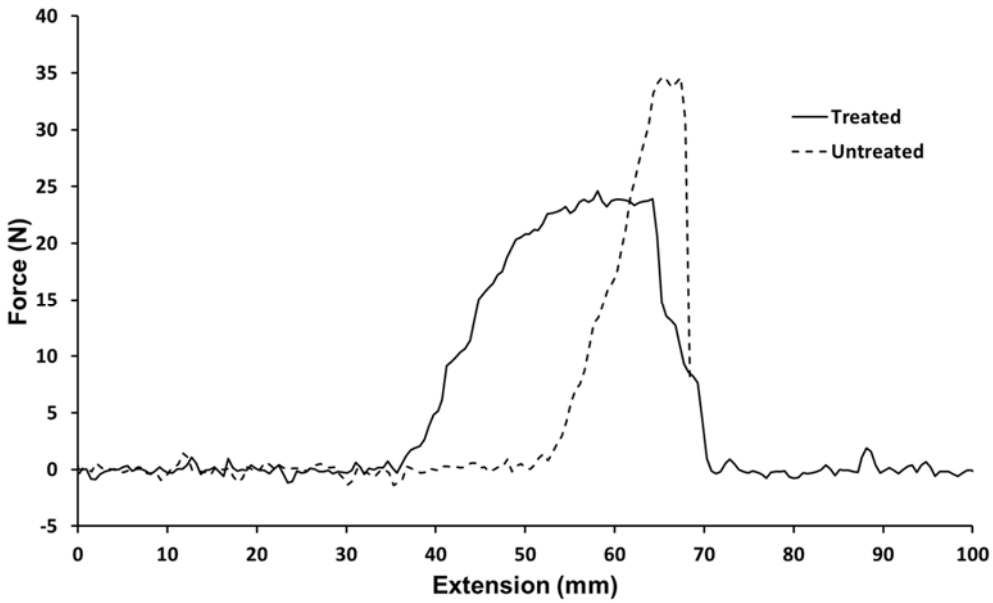

Figure 7.9 The representative curve of force vs extension of PP-40 untreated and treated fabrics.

7.7 Wicking properties

Figure 7.10 displays the vertical wicking properties of the PP-40 treated fabrics, meanwhile no wicking behaviour was observed on the untreated fabrics. The PP-40 untreated fabrics have PP as an outer component on the fabric surfaces. PP is commonly known as hydrophobic polymer which is not water-friendly. Even though there are PA6 inside the fibres, the PP located at the outside of the fibre blocks the water to penetrate through the fabric thus no wicking happened. The structure of the untreated fabric is also an open structure can produce big capillary gap between the fibres, thus having low or weak wicking properties.

Treated fabrics have multiple PA6 microfibres which help in the wicking capabilities of the fabrics. The course direction showing good wicking behaviour with the highest distance recorded at 36 mm after 30 mins in the water. Small capillary gap between microfibres improved the abilities of the water transported between fibres and enhanced the fabric wicking rate (Srinivasan et al., 2007).

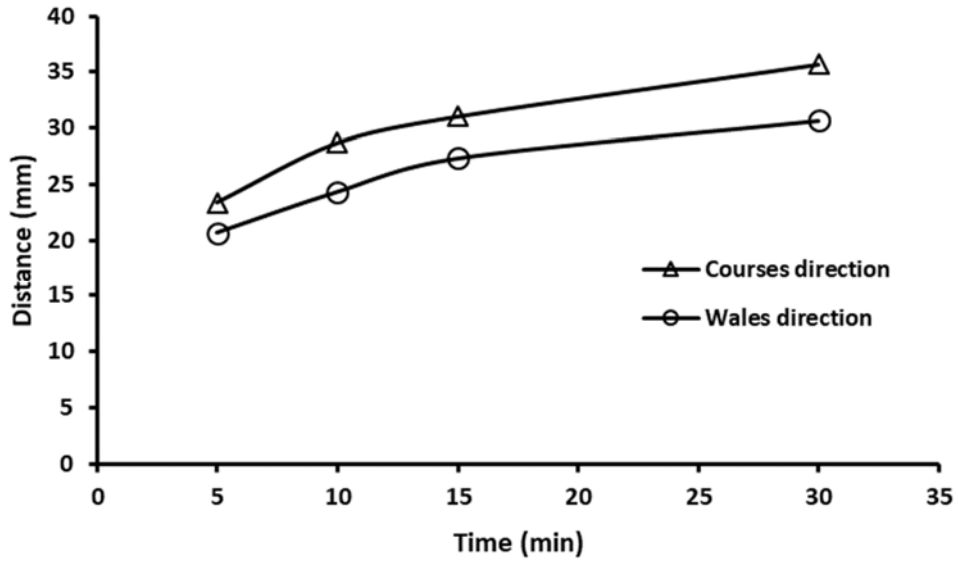

Figure 7.10 Vertical wicking results of PP-40 treated fabrics.

7.8 Bending length

Bending length of the fabrics was investigated using pear loop hanging technique. The bending length will represent the drapeability of the fabric, bigger number shows better drapeability of the fabric. Figure 7.11 shows the result obtained for the untreated and treated fabric bending length. The microfibre fabrics have better drapeability than untreated fabric due to the microfibres diameter. Microfibres have smaller fibre diameter than hybrid fibres result to the lower fineness and stiffness of the fabric (Srinivasan et al., 2007).

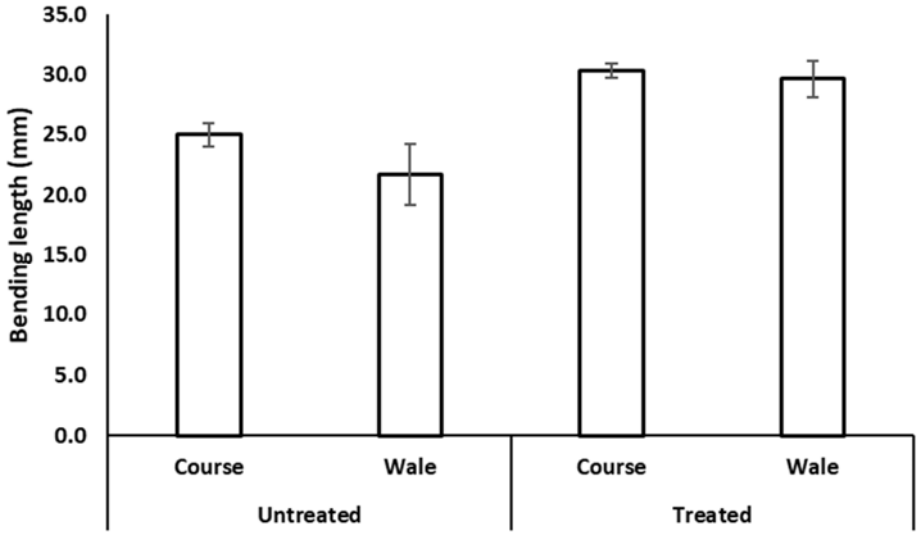

Figure 7.11 Bending length of PP-40 fabrics.

7.9 Conclusions

The PP-40 knitted fabrics were successfully produced from the PP-40 hybrid fibres (monofilament). After the removal of PP component, the treated fabrics remain in fabric forms which only contain PA6 microfibres. This brings to the conclusion that PA6 microfibres fabrics are possible to be produced via direct method single step melt extrusion, without using commercial bicomponent fibre production. The properties of the treated fabric also show excellent properties in the wicking behaviour and has lower stiffness than untreated fabrics. The treated fabric has also shown better strength than the untreated fabric.

Chapter 8
Conclusions and Future work

8.1 Conclusions

This work presents the effect of blending of PA6 polymer with interacting (TPU) and non-interacting polymer (PP and PET) extruded into hybrid fibres via single-step melt spinning method. The blending of two different polymers simulated the scenario of recycling mixed textile waste which has difficulty to be separated into a single component.

The blending of PA6 with TPUD shows development of interconnected multi-pores hybrid fibres (Chapter 4 Part A) in both blend compositions conducted, TPUD-20 and TPUD-50. Fibre diameter of the PA6:TPU hybrid fibres are in the range of 126±1.5 to 136±3.2 μm with pore size range between 7.9±7.8 and 6.7±6.2 μm. The interaction between amide group of PA6 and urethane/urea group in TPU creates partial interaction between the polymers that was proven from the ATR-FTIR result. The interacting behaviour of PA6 and TPU-D affected the melting temperature of the hybrid fibres that melted at 204 °C compare to PA6 which melted at 221 °C. The increasing of the TPU-D content in the blend also decreases the thermal stability of the hybrid fibres. XRD result shows the existence of two peaks of TPU-D 50 hard segment crystallinity that improved the strength of the fibre. The strength of the PA6:TPU-D hybrid fibres was found lower than PA6 but better than TPU-D. The removal of TPUD from the hybrid fibres shows significant porous structure in the PA6:TPU hybrid fibres. Due to the interacting behaviour of PA6:TPU, even after TPU removal, the TPU-D residue can be traced left in the hybrid fibres based on the ATR-FTIR curve and mass loss of the fibres. The PA6:TPUD blend has the potential to produce high functional hybrid fibres which can be applied in various textile applications where porous characteristic fibres needed.

The blending of PA6 with TPUA shows development of TPUA fibrils inside PA6 matrix (Chapter 4 Part B). The removal of TPU-A from the hybrid fibres also shows significant porous morphology in the middle of fibre cross-section. The TPU-A residue can also be traced left in the hybrid fibres based on the ATR-FTIR curve and mass loss of the fibres. The percentage of PA6 crystallinity in the PA6:TPU-A hybrid fibres decrease after the blending with TPU-A. similar with TPU-D, PA6:TPU-A hybrid fibres also show decrement in the tensile strength which can be relate to the separation of these two polymers in the fibres.

The blending of PA6 with non-interacting polymer PET shows development of PA6 fibril developed in PET matrix when PET content is 50% or more (Chapter 5). Mean diameters of the as-spun hybrid fibres were in a range of 103 to 128 µm. After the removal of PET from hybrid fibres, PA6 fibrils were obtained with fibrils diameter in the range of 532 nm to 1026 nm which can be classify as nanofibres size (~ 1000 nm and below). Thermal properties of PA6:PET hybrid fibres suggests that the polymers crystallise independently and do not significantly interfere with each other, thus prove the non-interacting behaviour of both polymers. The optimum strength of the PA6:PET hybrid fibres was obtained in PET-20 fibres, while PET-30 has the strength almost equal to PA6 fibres. The strength reduced with the reduction of PA6 component in the fibres.

The blending of PA6 and non-interacting PP produced PA6 microfibres in PP matrix when PP content is 40% or more (Chapter 6). Mean diameters of the as-spun hybrid fibres were in a range of 103 to 180 µm. The PA6 microfibres diameter range was 1.74-1.95 µm and further reduced to 0.76-1.13 µm upon drawing, obtained when 50-60% of PA6 used in the blend. Thermal properties of PA6:PP hybrid fibres show similar trend with PA6:PET hybrid fibres with the polymers crystallise independently and do not significantly interfere with each other. In TGA result, single step degradation was found on all fibres except PP-35 which shows two steps degradation. Tensile strength of the as-spun hybrid fibres are lower than PA6 but improved than PP. Drawn PP-40 shows improved tenacity after removal of PP component. PP-50 and PP-40 exhibit two breaking points in tenacity-elongation curve relates to the existence of microfibres in the fibres. Another highlight of PA6:PP blend is the PP-35 hybrid fibre where the phase inversion happen between both polymers thus created unique fibre morphology. The removal of PP from the hybrid fibres shows the PA6 microfibres remain in the fibre shape, thus further investigation on the potential to produce microfibres fabrics from the PA6:PP hybrid fibres were performed.

Due to the superior fibre strength after drawing process, the PP-40 hybrid fibres were chosen to produce fabric (Chapter 7). The circular plain jersey PP-40 knitted fabrics were produced in a double bed flat knitting machine. The fabrics were then treated in toluene to remove PP component and PA6 microfibres fabrics were obtained. This concludes that microfibres fabrics were possible to be produced by using single-step melt extrusion of polymer blend which typically produced using commercial bicomponent fibres method that involved high technology facilities.

The sorting and separating of mixed textile waste during recycling process, particularly wastes contain thermoplastic polymers, can be omitted by blending the waste and extruded into hybrid fibres via twin-screw melt extrusion.

8.2 Contributions

The contributions or achievement of this study are as below:

Production of PA6:TPU hybrid fibres

The production of PA6:TPU hybrid fibres via single-step melt extrusion is considered as a novel approach in fibre production. The differences in term of melting temperature and various of the TPU types (ratio of soft and hard segment) produce different fibre morphology as obtained in this study. The development of multi-connected porous hybrid fibres gives benefit in high functional application such as insulation, moisture transport and filtration. Additionally, the non-circular cross-section (NCCS) obtained in the PA6:TPU hybrid fibres produce larger surface areas that have advantages than normal circular round shape cross-section fibres.

Another interesting finding in this chapter is the evolution of PA6:TPU hybrid fibres into unique cross-section fibres after removal of PA6 component (section 4.2.3-Figure 4.8). The fibres with unique cross-section, again can benefit in the larger fibre surface area which has wide potential applications in textile industry.

Production of PA6 microfibres and nanofibres

The blending of PA6 with non-interacting polymers, PET and PP shows the interfacial separation in both blending thus produced PA6 microfibres in the PA6:PP hybrid fibres and nanofibres in the PA6:PET hybrid fibres. The development of microfibres and nanofibres using conventional melt spinning equipment gives a cheaper alternative to produce ‘island in the sea’ bicomponent fibres where currently using high technology equipment to produce microfibres or nanofibres.

Production of microfibres fabric

PA6 microfibre fabrics were successfully produced continuity from the excellent strength behaviour of the PP-40 hybrid fibres. The PP-40 hybrid fibres were constructed into knitted fabric and treated to remove PP component which is then expose the PA6 microfibres knitted fabrics. The favourable microfibre fabrics

production directly from hybrid fibres produced via one-step melt-extrusion is a novel approach which can be commercialised.

8.3 Suggestions for future work

There are several aspects in this study that could be further explored and expanded. Some of the aspects are suggested below:

Expand varieties of polymer blending

This study focussed on the binary blending, the blending of two different polymers that is PA6 as a main polymer and TPU, PET and PP as secondary polymer. The study can be expanded to produce hybrid fibres with TPU, PET, PP or other polymer as main polymer. Different types of TPU which has various soft and hard segment ratio can be explored more in the blending process. Moreover, ternary blending which is a combination of three different polymers are interesting to be explored since possibility to find mixed-waste contain more than two components is high in the recycling centre.

Use recycled polymer as raw material

This study used virgin polymers in order to control the experiment parameters. For further research on using recycled polymers can be explored and the result can be compared with the result obtained in this study.

Study on unique cross-section of PA6:TPU

The PA6:TPUD hybrid fibre, after the treatment in formic acid, produced unique fibre cross-section where the study can be extended to investigate the properties of the treated fibres. The fibres can also turn into fabrics and the fabric characteristic can be explored to find suitable application for the fibres.

Use of environmentally friendly solvent

The solvents used to remove the secondary polymer such as DMSO and toluene are not environmental-friendly and can be harmful to human health. Further study on using appropriate eco-friendly alternatives (e.g. ionic solvent) to remove the sacrificial polymers could be explored.

Properties of microfibres fabrics

Further detailed study can include a range of microfibres fabrics with different structures to investigate the dimensional, physical, thermal and comfort properties of the fabrics.

List of References

Afshari, M., Kotek, R., Gupta, B.S., Kish, M.H. and Dast, H.N. 2005. Mechanical and structural properties of melt spun polypropylene/nylon 6 alloy filaments. *Journal of Applied Polymer Science*. **97**(2), pp.532–544.

Afshari, M., Kotek, R., Kish, M.H., Dast, H.N. and Gupta, B.S. 2001. Effect of blend ratio on bulk properties and matrix-fibril morphology of polypropylene / nylon 6 polyblend fibers. *Polymer*. **43**(2002), pp.1331–1341.

Akovali, G. 2012. Advances in Polymer Coated Textiles. *Advances in Polymer Coated Textiles*., pp.1–24.

Ali, A.M. 2019. The impact of processing conditions on the structural and optical properties of the as-spun polyamides fibers. *Microscopy Research and Technique*. **82**(11), pp.1922–1927.

Alves Fidelis, M.E., Pereira, T.V.C., Gomes, O.D.F.M., De Andrade Silva, F. and Toledo Filho, R.D. 2013. The effect of fiber morphology on the tensile strength of natural fibers. *Journal of Materials Research and Technology*. **2**(2), pp.149–157.

Aparna, S., Purnima, D. and Adusumalli, R.B. 2017. Review on Various Compatibilizers and its Effect on Mechanical Properties of Compatibilized Nylon Blends. *Polymer - Plastics Technology and Engineering*. **56**(6), pp.617–634.

Aranishi, Y. and Nishio, Y. 2017. Cellulosic fiber produced by melt spinning *In*: *Blend and graft copolymers of cellulosics*. Springer, Cham.

Arvidson, S.A., Wong, K.C., Gorga, R.E. and Khan, S.A. 2012. Structure, molecular orientation, and resultant mechanical properties in core/ sheath poly(lactic acid)/polypropylene composites. *Polymer*. **53**(3), pp.791–800.

Asiaban, S. and Moradian, S. 2012. Investigation of tensile properties and dyeing behavior of various polypropylene/amine modifier blends. *Journal of Applied Polymer Science*. **123**, pp.2162–2171.

Aslan, S., Laurienzo, P., Malinconico, M., Martuscelli, E., Pota, F., Bianchi, R., Di Dino, G. and Giannotta, G. 1995. Influence of spinning velocity on mechanical and structural behavior of PET/nylon 6 fibers. *Journal of Applied Polymer Science*. **55**(1), pp.57–67.

Ayad, E., Cayla, A., Rault, F., Gonthier, A., Campagne, C. and Devaux, E. 2016. Effect of Viscosity Ratio of Two Immiscible Polymers on Morphology in Bicomponent Melt Spinning Fibers. *Advances in Polymer Technology*. **0**(0), pp.1–8.

Ayad, E., Cayla, A., Rault, F., Gonthier, A., LeBlan, T., Campagne, C. and Devaux, E. 2016. Influence of rheological and thermal properties of polymers during melt spinning on bicomponent fiber morphology. *Journal of Materials Engineering and Performance*. **25**(8), pp.3296–3302.

Barangi, L., Nazockdast, H. and Taromi, F.A. 2008. Effect of the Melt Viscoelastic Behavior of Components on the Morphology Development of Polymer Blends in a Twin-Screw Extruder. *Journa of Applied Polymer Science*. **108**, pp.2558–2563.

Bosak, D.R. 2005. Bicomponent fibers derived from immiscible polymer blends. *Textile Research Journal*. **75**(1), pp.50–56.

Bukhari, M.A., Carrasco-Gallego, R. and Ponce-Cueto, E. 2018. Developing a national programme for textiles and clothing recovery. *Waste Management and Research*. **36**(4), pp.321–331.

Bunge, C.A., Mohr, B., Vad, T., Beckers, M. and Gries, T. 2018. Fabrication and analysis of side-emitting poly(methyl methacrylate) fibres with non-circular cross-sections. *Polymer International*. **67**(9), pp.1170–1178.

Cai, L.-F., Wang, C.-L., Chen, H.-W., Qian, H., Lin, Z.-Y. and Zhang, X.-C. 2019. Hydrogen bonding-based self-assembly technology for high-performance melt blending TPU/PA6 polymers. *Applied Nanoscience*. **10**, pp.51–59.

Chiu, H.-T. and Chuang, C.-Y. 2009. The mechanical and rheological behavior of the PA/TPU Blend with POE-g-MA Modifier. *Journal of Applied Polymer Science*. **115**, pp.1278–1282.

CIRFS European mand-made fibres association n.d. World man-made fibres production. [Accessed 2 May 2019]. Available from: https://www.cirfs.org/statistics/key-statistics.

Crespo, J.E., Parres, F., Peydro´, M.A. and Navarro, R. 2013. Study of rheological, thermal, and mechanical behavior of reprocessed polyamide 6. *Polymer Engineering & Science*., pp.679–688.

Cui, Y., Gong, H., Wang, Y., Li, D. and Bai, H. 2018. A Thermally Insulating Textile Inspired by Polar Bear Hair. *Advanced Materials*. **30**(14), pp.1–8.

Dasdemir, M., Maze, B., Anantharamaiah, N. and Pourdeyhimi, B. 2012. Influence of polymer type, composition, and interface on the structural and mechanical properties of core/sheath type bicomponent nonwoven fibers. *Journal of Materials Science*. **47**(16), pp.5955–5969.

DEFRA 2013. *Energy from Waste A guide to the debate* [Online]. Available from: https://www.gov.uk/government/publications/energy-from-waste-a-guide-to-the-debate.

Dissanayake, D.G.K., Weerasinghe, D.U., Wijesinghe, K.A.P. and Kalpage, K.M.D.M.P. 2018. Developing a compression moulded thermal insulation panel using postindustrial textile waste. *Waste Management*. **79**, pp.356–361.

Dobrovszky, K. and Ronkay, F. 2017. Effects of Phase Inversion on Molding Shrinkage, Mechanical, and Burning Properties of Injection-molded PET/HDPE and PS/HDPE Polymer Blends. *Polymer - Plastics Technology and Engineering*. **56**(11), pp.1147–1157.

Dotto, G.., Santos, J.M.N., Tanabe, E.H., Bertuol, D.A., Foletto, E.L., Lima, E.C. and

Pavan, F.A. 2017. Chitosan/polyamide nanofibers prepared by Forcespinning®technology: A new adsorbent to remove anionic dyes from aqueous solutions. *Journal of Cleaner Production*. **144**, pp.120–129.

Ďurčová, O., Gróf, I., Jambrich, M. and Mizerák, P. 1992. Fibres from polypropylene/polyamide 6 blends: Application of FT-IR Dichroism for study of fibre molecular orientation. *Polymer Testing*. **11**(3), pp.193–203.

Echeverria, C.A., Handoko, W., Pahlevani, F. and Sahajwalla, V. 2019. Cascading use of textile waste for the advancement of fibre reinforced composites for building applications. *Journal of Cleaner Production*. **208**, pp.1524–1536.

Ellen MacArthur Foundation 2017. A New Textiles Economy: Redesigning Fashion's Future. , p.150. [Accessed 20 August 2018]. Available from: https://www.ellenmacarthurfoundation.org/publications.

Eltahir, Y.A., A.M. Saeed, H., Xia, Y., Yong, H. and Yimin, W. 2016. Mechanical properties, moisture absorption, and dyeability of polyamide 5,6 fibers. *Journal of the Textile Institute*. **107**(2), pp.208–214.

Erez 2018. *2018 Technology Report for Marine Safety Textiles*.

Esfahani, S.M.H. 1983. Extrusion of waste polyamides. *Indian Journal of Textile Research*. **8**(September), pp.89–92.

Explorer, G.O. 2019. Fashion from pre-consumer waste. [Accessed 13 October 2019]. Available from: https://goexplorer.org/fashion-from-pre-consumer-waste/.

Fakirov, S. and Evstatiev, M. 1993. Microfibrillar reinforced composite from drawn poly (ethylene terephthalate) / nylon-6 blend. . **34**(22), pp.4669–4679.

Favis, B.D. 2000. Factors Influencing the Morphology of Immiscibke Polymer Blends in Melt Processing *In*: D. R. Paul and C. . Bucknall, eds. *Polymer Blends Volume I: Formulation*. John Wiley & Sons. Inc., pp.501–538.

Favis, B.D. and Chalifoux, J.P. 1988. Influence of composition on the morphology of polypropylene/polycarbonate blends. *Polymer*. **29**(10), pp.1761–1767.

Fiber Innovation Technology, I. 2015. 4DG Fiber. [Accessed 4 July 2016]. Available from: http://www.fitfibers.com/.

Frick, A. and Rochman, A. 2004. Characterization of TPU-elastomers by thermal analysis (DSC). *Polymer Testing*. **23**(4), pp.413–417.

Genovese, A. and Shanks, R.. 2001. Simulation of the specific interactions between polyamide-6 and a thermoplastic polyurethane. *Computational and Theoretical Polymer Science*. **11**(1), pp.57–62.

Global Fashion Agenda and The Boston Consulting Group, I. 2017. *Pulse of the Fashion Industry* [Online]. Available from: http://globalfashionagenda.com/wp-content/uploads/2017/05/Pulse-of-the-Fashion-Industry_2017.pdf.

Gogolewski, S. and Pennings, A.J. 1985. High-modulus fibres of nylon-6 prepared by a dry-spinning method. *Polymer*. **26**(9), pp.1394–1400.

Grümer, B. and Hopmann, C. 2018. The influence of recycling on the viscosity of polyamide 6 and a general modeling approach. *Progress in Rubber, Plastics and Recycling Technology*. **34**(3), pp.158–167.

Gun, A.D. 2011. Dimensional, physical and thermal comfort properties of plain knitted fabrics made from modal viscose yarns having microfibers and conventional fibers. *Fibers and Polymers*. **12**(2), pp.258–267.

Hajiraissi, R., Jahani, Y. and Hallmann, T. 2017. Investigation of rheology and morphology to follow physical fibrillar network evolution through fiber spinning of PP/PA6 Blend Fiber. *Polymer Engineering and Science*. **58**, pp.1–10.

Haponiuk, J.T. 1995. Dynamic mechanical thermal analysis of polyamide 6/thermoplastic polyurethane blends. *Journal of Thermal Analysis*. **43**, pp.91–101.

Haponiuk, J.T. and Balas, A. 1995. Thermal properties of polyamide 6 / polyurethane blends. *Journal of Thermal Analysis*. **43**, pp.211–214.

Hasan, M.M.B., Nitsche, S., Abdkader, A. and Cherif, C. 2018. Carbon fibre reinforced thermoplastic composites developed from innovative hybrid yarn structures consisting of staple carbon fibres and polyamide 6 fibres. *Composites Science and Technology*. **167**(August), pp.379–387.

Hasegawa, T. and Mikuni, T. 2014. Higher-order structural analysis of nylon-66 nanofibers prepared by carbon dioxide laser supersonic drawing and exhibiting near-equilibrium melting temperature. *Journal of Applied Polymer Science*. **40361**, n/a.

Heidari Golfazani, M.E., Nazockdast, H., Rashidi, A. and Yazdanshenas, E. 2012. The role of nanoclay partitioning on microfibril morphology development in polypropylene/polyamide 6 nanocomposite fibers. *Journal of Macromolecular Science, Part B: Physics*. **51**(5), pp.956–967.

Hilton, M., Daniel, R. and Lahme, V. 2019. *Review of Carpet Waste Management in the UK*.

Hiltz, J.A. 1998. *Characterization of poly(ether)urethane thermoplastic elastomers*. Canada.

Hufenus, R., Affolter, C., Camenzind, M. and Reifler, F.A. 2013. Design and characterization of a bicomponent melt-spun fiber optimized for artificial turf applications. *Macromolecular Materials and Engineering*. **298**(6), pp.653–663.

Huntsman 2010. *A guide to thermoplastic polyurethanes (TPU)* [Online]. Available from: http://www.huntsman.com/portal/page/portal/polyurethanes/Media Library/global/files/guide_tpu.pdf.

Imura, Y., Hogan, R.M.C. and Jaffe, M. 2014. *Dry spinning of synthetic polymer fibers* [Online]. Woodhead Publishing Limited. Available from: http://dx.doi.org/10.1533/9780857099174.2.187.

Iyer, S. and Schiraldi, D.A. 2006. Role of Ionic Interactions in the Compatibility of Polyester Ionomers With Poly(ethylene terephthalate) and Nylon 6. *Journal of Polymer Science: Part B: Polymer Physics*. **44**, pp.2091–2103.

Jafari, S.H. and Gupta, A.K. 1998. Crystallization behavior of polypropylene in polypropylene / nylon 6 blend. *Journal of Applied Polymer Science*. **71**(May), pp.1153–1161.

Jašo, V., Milić, J., Divjaković, V. and Petrović, Z.S. 2013. Novel elastomeric polyurethane fibers modified with polypropylene microfibers. *European Polymer Journal*. **49**(12), pp.3947–3955.

Jašo, V., Rodić, M. V. and Petrović, Z.S. 2015. Biocompatible fibers from thermoplastic polyurethane reinforced with polylactic acid microfibers. *European Polymer Journal*. **63**, pp.20–28.

Jayanarayanan, K., Thomas, S. and Joseph, K. 2011. In situ microfibrillar blends and composites of polypropylene and poly (ethylene terephthalate): Morphology and thermal properties. *Journal of Polymer Research*. **18**(1), pp.1–11.

Jaziri, M., Barhoumi, N., Massardier, V. and Mélis, F. 2008. Blending PP with PA6 industrial wastes: Effect of the composition and the compatibilization. *Journal of Applied Polymer Science*. **107**, pp.3451–3458.

John, B. and Furukawa, M. 2009. Enhanced Mechanical Properties of Polyamide 6 Fibers Coated with a Polyurethane Thin Film. *Polymer Engineering & Science*. **47**, pp.1970–1978.

John, B. and Furukawa, M. 2012. Structure and mechanical behaviors of thermoplastic polyurethane thin film coated polyamide 6 fibers part II. A solution coating method. *Journal of Polymer Research*. **19**(2), pp.1–12.

Jordhamo, G.M., Manson, J.A. and Sperling, L.H. 1986. Phase continuity and inversion in polymer blends and simultaneous interpenetrating networks. *Polymer Engineering and Science*. **26**(8), pp.517–524.

Kalyanaraman, A.R. 1988. Coefficient of friction between yarns and contact surfaces. *Indian Journal of Textile Research*. **13**(1), pp.1–6.

Kanebo 2007. Sideria. [Accessed 4 August 2016]. Available from: https://www.kbseiren.com/english/pro-sid.html.

Kegel, M., Sbarski, I., Iovenitti, P., Masood, S. and Kosior, E. 2003. In-situ reactions between recycled polyethylene terephthalate and Nylon 6 blends. *Progress in Rubber, Plastics and Recycling Technology*. **19**(4), pp.251–259.

Khanna, Y.P. 1990. Evaluation of thermal history of polymeric films and fibers using DSC/TMA/DMA techniques. *Journal of Applied Polymer Science*. **40**, pp.569–579.

Kicińska-Jakubowska, A., Bogacz, E. and Zimniewska, M. 2012. Review of Natural Fibers. Part I-Vegetable Fibers. *Journal of Natural Fibers*. **9**(3), pp.150–167.

Kim, J.M., Song, I.S., Cho, D. and Hong, I. 2011. Effect of carbonization temperature

and chemical pre-treat- ment on the thermal change and fiber morphology of kenaf- based carbon fibers. *Carbon Letters*. **12**(3), pp.131–137.

Kimm, M., Gerstein, N., Schmitz, P., Simons, M. and Gries, T. 2018. On the separation and recycling behaviour of textile reinforced concrete: an experimental study. *Materials and Structures/Materiaux et Constructions*. **51**(5), pp.1–13.

Kitao, T., Kobayashi, H. and Ikegami, S. 1973. Fibers from Polyblends Containing Nylon 6 as Basic Component . I . Melt Spinning and Physical Properties of Blend Fibers. *Journal of Polymer Science*. **11**, pp.2633–2651.

Li, Y. and Shimizu, H. 2004. Novel morphologies of poly(phenylene oxide) (PPO)/polyamide 6 (PA6) blend nanocomposites. *Polymer*. **45**(22), pp.7381–7388.

Liang, B., White, J.L. and Spruiell, J.E. 1983. Polypropylene/nylon 6 blends: Phase distribution morphology, rheological measurements and structure development in melt spinning. *Journal of Applied Polymer Science*. **28**, pp.2011–2032.

Liao, H.Y., Zheng, L.Y., Hu, Y.B., Zha, X.J., Xu, X., Wen, Y.W., Tao, G.L. and Liu, C.L. 2015. Dynamic rheological behavior of reactively compatibilized polypropylene/polyamide 6 blending melts. *Journal of Applied Polymer Science*. **132**(24), pp.1–8.

Lin, X., Qian, Q., Xiao, L., Chen, Q., Huang, Q. and Zhang, H. 2014. Influence of Reactive Compatibilizer on the Morphology, Rheological, and Mechanical Properties of Recycled Poly(Ethylene Terephthalate)/Polyamide 6 Blends. *Journal of Macromolecular Science, Part B: Physics*. **53**(9), pp.1543–1552.

Ling, C., Shi, S., Hou, W. and Yan, Z. 2019. Separation of waste polyester/cotton blended fabrics by phosphotungstic acid and preparation of terephthalic acid. *Polymer Degradation and Stability*. **161**, pp.157–165.

Liu, H., Zhang, T., Cai, Y., Deng, S., Bai, D., Bai, H., Zhang, Q. and Fu, Q. 2018. Towards polylactide/core-shell rubber blends with balanced stiffness and toughness via the formation of rubber particle network with the aid of stereocomplex crystallites. *Polymer*. **159**(September), pp.23–31.

Liu, L., Wu, Y. and Zhu, Z. 2017. Internal structure and crystallinity investigation of segmented thermoplastic polyurethane elastomer degradation in supercritical methanol. *Polymer Degradation and Stability*. **140**, pp.17–24.

Liu, X., Ning, Y. and Wang, F. 2014. Deep-black-coloring effect of fabrics made of noncircular cross-section polyester filaments. *Color Research & Application*. **39**(5), pp.511–518.

Lozano-González, J., Rodriguez-Hernandez, T., Gonzales-De Los Santos, E. and Villalpando-Olmos, J. 2000. Physical–mechanical properties and morphological study on nylon-6 recycling by injection molding. *Journal of Applied Physics*. **76**, pp.851–858.

Lu, X., Zhao, J., Yang, X. and Xiao, P. 2017. Morphology and properties of biodegradable poly (lactic acid)/poly (butylene adipate-co-terephthalate) blends

with different viscosity ratio. *Polymer Testing*. **60**, pp.58–67.

Meng, X., Fan, W., Ma, Y., Wei, T., Dou, H., Yang, X., Tian, H., Yu, Y., Zhang, T. and Gao, L. 2019. Recycling of denim fabric wastes into high-performance composites using the needle-punching nonwoven fabrication route. *Textile Research Journal*. (19).

Meyabadi, T.F., Mohaddes Mojtahedi, M.R. and Mousavi Shoushtari, S. a. 2010. Melt spinning of reused nylon 6: structure and physical properties of as-spun, drawn, and textured filaments. *Journal of the Textile Institute*. **101**(6), pp.527–537.

Millot, C., Fillot, L.., Lame, O., Sotta, P. and Seguela, R. 2015. Assessment of polyamide-6 crystallinity by DSC: Temperature dependence of the melting enthalpy. *Journal of Thermal Analysis and Calorimetry*. **122**(1), pp.307–314.

Mohammadhosseini, H., Tahir, M.M., Mohd Sam, A.R., Abdul Shukor Lim, N.H. and Samadi, M. 2018. Enhanced performance for aggressive environments of green concrete composites reinforced with waste carpet fibers and palm oil fuel ash. *Journal of Cleaner Production*. **185**, pp.252–265.

Moorhouse, D. and Newcombe, H. 2018. Brand interview and case study: Davy J sustainable swimwear. *Clothing Cultures*. **5**(1), pp.163–166.

Morishita, T., Katagiri, Y., Matsunaga, T., Muraoka, Y. and Fukumori, K. 2017. Design and fabrication of morphologically controlled carbon nanotube/polyamide-6-based composites as electrically insulating materials having enhanced thermal conductivity and elastic modulus. *Composites Science and Technology*. **142**, pp.41–49.

Mukhopadhyay, S. and Ramakrishnan, G. 2008. Microfibres. *Textile Progress*. **40**(1), pp.1–86.

NPTEL 2013. Smart/functional specialty fibres. *National Programme on Technology Enhanced Learning*. [Online]. [Accessed 27 July 2016]. Available from: http://nptel.ac.in/courses/116102006/19.

Oertel, R.W. and Brentin, R.P. 1992. Thermoplastic polyurethane for coated fabrics. *Journal of Coated Fabrics*. **22**(22, October), pp.150–160.

Orasutthikul, S., Unno, D. and Yokota, H. 2017. Effectiveness of recycled nylon fiber from waste fishing net with respect to fiber reinforced mortar. *Construction and Building Materials*. **146**, pp.594–602.

Östlund, Å., Wedin, H., Bolin, L., Berlin, J., Jönsson, C., Posner, S., Smuk, L., Eriksson, M. and Sandin, G. 2015. Textilåtervinning Tekniska möjligheter och utmaningar [Tetxile recycling-technical opportunities and challanges]. *Naturvårdsverket*. [Online]. (Rapport 6685). [Accessed 20 August 2018]. Available from: https://www.naturvardsverket.se/Documents/publikationer6400/978-91-620-6685-7.pdf?pid=15536.

Palme, A., Peterson, A., de la Motte, H., Theliander, H. and Brelid, H. 2017. Development of an efficient route for combined recycling of PET and cotton from mixed fabrics. *Textiles and Clothing Sustainability*. **3**(1), p.4.

Pan, G., Zhao, Y., Xu, H., Hou, X. and Yang, Y. 2016. Compression molded composites from discarded nylon 6/nylon 6,6 carpets for sustainable industries. *Journal of Cleaner Production*. **117**, pp.212–220.

Papero, P. V., Kubu, E. and Roldan, L. 1967. Fundamental Property Considerations in Tailoring a New Fiber. *Textile Research Journal*. **37**(10), pp.823–833.

Pedroso, A.G., Mei, L.H.I., Agnelli, J.A.M. and Rosa, D.S. 2002. The influence of the drying process time on the final properties of recycled glass fiber reinforced polyamide 6. *Polymer Testing*. **21**(2), pp.229–232.

Peirce, F.T., Inst.P, F. and F.T.I 1930. The handle of cloth as a measurable quantity. *Journal of the Textile Institute Transactions*. **21**(9), pp.T377–T416.

Potente, H., Bastian, M., Gehring, A., Stephan, M. and Pötschke, P. 2000. Experimental investigation of the morphology development of polyblends in corotating twin-screw extruders. *Journal of Applied Polymer Science*. **76**(5), pp.708–721.

Pötschke, P. and Paul, D.R. 2003. Formation of Co-continuous Structures in Melt-Mixed Immiscible Polymer Blends. *Journal of Macromolecular Science, Part C: Polymer Reviews*. **43**(1), pp.87–141.

Pourdeyhimi, B. and Chappas, W. 2012. United State Patent: 8129019B2 - High surface area fiber and textiles made from the same. Issued 06 Mar 2012.

Pure Waste Textiles n.d. Pure Waste Textiles. [Accessed 13 October 2019]. Available from: http://www.purewastetextiles.com/#top.

Pustak, A., Švab, I., Govorčin Bajsić, E., Denac, M., Musil, V. and Šmit, I. 2018. Polypropylene Blends with m-EPR Copolymers: Structure, Morphology and Thermal Properties. *Polymer - Plastics Technology and Engineering*. **57**(3), pp.229–241.

Qu, C., Yang, H., Liang, D., Cao, W. and Fu, Q. 2007. Morphology and properties of PET/PA-6/SiO2 Ternary Composite. *Journal of Applied Polymer Science*. **104**, pp.2288–2296.

Radici Group n.d. Polyester and Polyamide Bicomponent Yarn: Radyarn BiCo. , pp.0–1.

Rahbar, R.S. and Mrm, M. 2011. Influence of hot multistage drawing on structure and mechanical properties of nylon 6 multifilament yarn. *Journal of Engineered Fibers and Fabrics*. **6**(2), pp.7–16.

Rashmi, B.J., Loux, C. and Prashantha, K. 2017. Bio-based thermoplastic polyurethane and polyamide 11 bioalloys with excellent shape memory behavior. *Journal of Applied Polymer Science*. **134**(20), pp.1–10.

Rashmi, B.J., Rusu, D., Prashantha, K., Lacrampe, M.F. and Krawczak, P. 2013. Development of bio-based thermoplastic polyurethanes formulations using corn-derived chain extender for reactive rotational molding. *Express Polymer Letters*. **7**(10), pp.852–862.

Reimschuessel, H.K. 1998. Polyamide fibers *In*: M. Lewin and E. M. Pearce, eds. *Handbook of Fiber Chemistry*. Marcel Dekker, Inc., pp.71–152.

Richards, A.F. 2005. Nylon fibres *In*: J. E. McIntyre, ed. *Synthetic fibres: nylon, polyester, acrylic, polyolefin*. Woodhead Publishing Limited, pp.20–88.

Robert, B. 2016. To Reuse or to Incinerate? A case study of the environmental impacts of two alternative waste management strategies for household textile waste in nine municipalities in northern Stockholm, Sweden. , p.70.

S. Murase, M. Kashima, K. Kudo and M. Hirami 1997. Structure and properties of high-speed spun fibers of nylon 6. *Macromolecular Chemistry and Physics*. **198**(2), pp.561–572.

Sandin, G. and Peters, G.M. 2018. Environmental impact of textile reuse and recycling – A review. *Journal of Cleaner Production*. **184**, pp.353–365.

Santhanam, S., Bharani, M., Temesgen, S., Atalie, D. and Ashagre, G. 2019. Recycling of cotton and polyester fibers to produce nonwoven fabric for functional sound absorption material. *Journal of Natural Fibers*. **16**(2), pp.300–306.

Saunders, J.H., Burroughs, J.A., Williams, L.P., Martin, D.H., Southern, J.H., Ballman, R.L. and Lea, K.R. 1975. Biconstituent fibers from segmented polyurethanes and nylon 6. *Journal of Applied Polymer Science*. **19**, pp.1387–1401.

Savov, M., Bechev, C., Georgiev, Y. and Dimov, K. 1984. DSC studies on polyester-polyamide biconstituent fibers. *Die Angewandte Makromolekulare Chemie*. **127**(1), pp.7–26.

Schick, C. 2009. Differential scanning calorimetry (DSC) of semicrystalline polymers. *Analytical and Bioanalytical Chemistry*. **395**(6), pp.1589–1611.

Serra, A., Tarrés, Q., Llop, M., Reixach, R., Mutjé, P. and Espinach, F.X. 2019. Recycling dyed cotton textile byproduct fibers as polypropylene reinforcement. *Textile Research Journal*. **89**(11), pp.2113–2125.

Sharma, R. and Goel, A. 2017. Development of Nonwoven Fabric from Recycled Fibers. *Journal of Textile Science & Engineering*. **07**(02), pp.6–8.

Sichina, W.J. 2000. *DSC as problem solving tool: measurement of percent crystallinity of thermoplastics* [Online]. Available from: http://scholar.google.com/scholar?hl=en&btnG=Search&q=intitle:DSC+as+Problem+Solving+Tool+:+Measurement+of+Percent+Crystallinity+of+Thermoplastics#0.

SMART Secondary Materials and Recycled Textiles n.d. Update on East African Community Ban on Importation of Used Clothing. [Accessed 15 October 2019]. Available from: https://www.smartasn.org/advocacy/update-on-east-african-community-ban-on-importation-of-used-clothing/.

Sotayo, A., Green, S. and Turvey, G. 2015. Carpet recycling: A review of recycled carpets for structural composites. *Environmental Technology and Innovation*. **3**,

pp.97–107.

Srinivasan, J., Ramakrishnan, G., Mukhopadhyay, S. and Manoharan, S. 2007. A study of knitted fabrics from polyester microdenier fibres. *Journal of the Textile Institute*. **98**(1), pp.31–35.

Stankowski, M., Kropidłowska, A., Gazda, M. and Haponiuk, J.T. 2008. Properties of polyamide 6 and thermoplastic polyurethane blends containing modified montmorillonites. *Journal of Thermal Analysis and Calorimetry*. **94**(3), pp.817–823.

Su, K.-H., Lin, J.-H. and Lin, C.-C. 2007. Influence of reprocessing on the mechanical properties and structure of polyamide 6. *Journal of Materials Processing Technology*.

Suvari, F., Ulcay, Y. and Pourdeyhimi, B. 2019. Influence of sea polymer removal on sound absorption behavior of islands-in-the-sea spunbonded nonwovens. *Textile Research Journal*. **89**(12), pp.2444–2455.

Takahashi, T., Konda, A. and Shimizu, Y. 1996a. Effect of viscosity ratio on structure of polypropylene / polyamide 6 blend fiber. . **52**(10), pp.507–515.

Takahashi, T., Konda, A. and Shimizu, Y. 1996b. The changes of structure and tensile strength and elongation characteristics for the polypropylene/polyamide 6 blend fibers upon drawing. *Sen'i Gakkaishi*. **52**(8), pp.38–46.

Tavanaie, M.A., Shoushtari, A.M., Goharpey, F. and Mojtahedi, M.R. 2013. Matrix-fibril morphology development of polypropylene / poly (butylenes terephthalate) blend fibers at different zones of melt spinning process and its relation to mechanical properties. *Fibers and Polymers*. **14**(3), pp.396–404.

Textile Exchange 2018. Preferred Fiber and Materials Market Report 2018. , pp.1–96.

Todros, S., Venturato, C., Natali, A.N., Pace, G. and Noto, V. Di 2014. Effect of steam on structure and mechanical properties of biomedical block copolymers. *Journal of Polymer Science, Part B: Polymer Physics*. **52**(20), pp.1337–1346.

Toray 2007. Fiber and textile recycling. [Accessed 20 July 2016]. Available from: http://www.toray.com/csr/value/val_005.html.

Tran, N.H.A., Brünig, H., Auf der Landwehr, M., Vogel, R., Pionteck, J. and Heinrich, G. 2016. Controlling micro- and nanofibrillar morphology of polymer blends in low-speed melt spinning process. Part II: Influences of extrusion rate on morphological changes of a PLA/PVA blend through a capillary die. *Journal of Applied Polymer Science*. **133**(47), pp.1–10.

Tuna, B. and Benkreira, H. 2017. Chain Extension of Recycled PA6. *Polymer Engineering and Science*. **58**(7), pp.1037–1042.

UNEP 2002. Gas emission from waste disposal. *United Nations Environment Programme*. [Online]. [Accessed 6 March 2016]. Available from: http://www.grid.unep.ch/waste/html_file/42-43_climate_change.html.

UNIFI 2008. Unifi's 100% recycled REPREVE® nylon 6,6 now available in China. [Accessed 20 July 2016]. Available from: http://unifi.com/un_news_pr.aspx?id=12.

Varma, D.. and Dhar, V.. 1988. Nylon 6/PET Polymer Blends: Mechanical Properties of Fibers. *Textile Research Journal*., pp.274–279.

Varma, D.S. and Dhar, V.K. 1987. Studies of Nylon 6 / PET Polymer Blends : Structure and Some Physical Properties. *Journal of Applied Polymer Science*. **33**, pp.1103–1124.

Vinckier, I., Moldenaers, P. and Mewis, J. 1996. Relationship between rheology and morphology of model blends in steady shear flow. *Journal of Rheology*. **40**(4), pp.613–631.

Wang, L., Guo, Z.-X. and Yu, J. 2012. Cocontinuous phase morphology for an asymmetric composition of polypropylene/polyamide 6 blend by melt mixing of polypropylene with premelted polyamide 6/organoclay masterbatch. *Journal of Applied Polymer Science*. **123**, pp.1218–1226.

Wang, M., Yu, B., Han, J., Song, W. and Zhu, F. 2017a. The influence of drawing pressure on the properties of PET/PA6 bicomponent spunbonded fibers. *Journal of Industrial Textiles*. **46**(5), pp.1281–1293.

Wang, M., Yu, B., Han, J., Song, W. and Zhu, F. 2017b. The influence of drawing pressure on the properties of PET/PA6 bicomponent spunbonded fibers. *Journal of Industrial Textiles*. **46**(5), pp.1281–1293.

Wesołowski, J. and Płachta, K. 2016. The polyamide market. *Fibres & Textiles in Eastern Europe*. **24**(6), pp.12–18.

Worn Again 2016. FIBERSORT project. [Accessed 4 July 2016]. Available from: http://wornagain.info/wp-content/uploads/TextilesPressRelease.pdf.

WRAP 2019. *Textiles Market Situation Report 2019*.

Xu, D., Zhou, Y., Guo, J., He, W., Wu, H., Qin, S. and Yu, J. 2019. Different component ratio of polyamide 1212/thermoplastic polyurethane blends: Effect on phase morphology, mechanical properties, wear resistance, and crystallization behavior. *Journal of Thermoplastic Composite Materials*.

YNFX 2020. *YnFx Monthly Pricewatch Report*.

Yoon, B.S., Joang, J.Y., Suh, M.H., Lee, Y.M. and Lee, S.H. 1997. Mechanical properties of polypropylene/polyamide 6 blends: Effect of manufacturing processes and compatibilization. *Polymer Composites*. **18**(6), pp.757–764.

Yousefi, A.M., Smucker, B., Naber, A., Wyrick, C., Shaw, C., Bennett, K., Szekely, S., Focke, C. and Wood, K.A. 2018. Controlling the extrudate swell in melt extrusion additive manufacturing of 3D scaffolds: a designed experiment. *Journal of Biomaterials Science, Polymer Edition*. **29**(3), pp.195–216.

Zainab, Z.I. and Ali, R.T. 2016. Recycled medical cotton industry waste as a source of biogas recovery. *Journal of Cleaner Production*. **112**, pp.4413–4418.

Zhang, H., Zhang, L., Jia, Q., Shi, C. and Yang, J. 2015. Preparation of porous Nylon 6 fiber via electrospinning. *Polymer Engineering & Science*. **47**, pp.1133–1141.

Zhang, P., Xu, D. and Xiao, R. 2015. Morphology development and size control of PA6 nanofibers from PA6/CAB polymer blends. *Journal of Applied Polymer Science*. **132**(27), pp.1–8.

Zhou, S., Huang, J. and Zhang, Q. 2012. Mechanical and tribological properties of polyamide-based composites modified by thermoplastic polyurethane. *Journal of Thermoplastic Composite Materials*. **27**(1), pp.18–34.

Zo, H.J., Joo, S.H., Kim, T., Seo, P.S., Kim, J.H. and Park, J.S. 2014. Enhanced mechanical and thermal properties of carbon fiber composites with polyamide and thermoplastic polyurethane blends. *Fibers and Polymers*. **15**(5), pp.1071–1077.

Appendix A

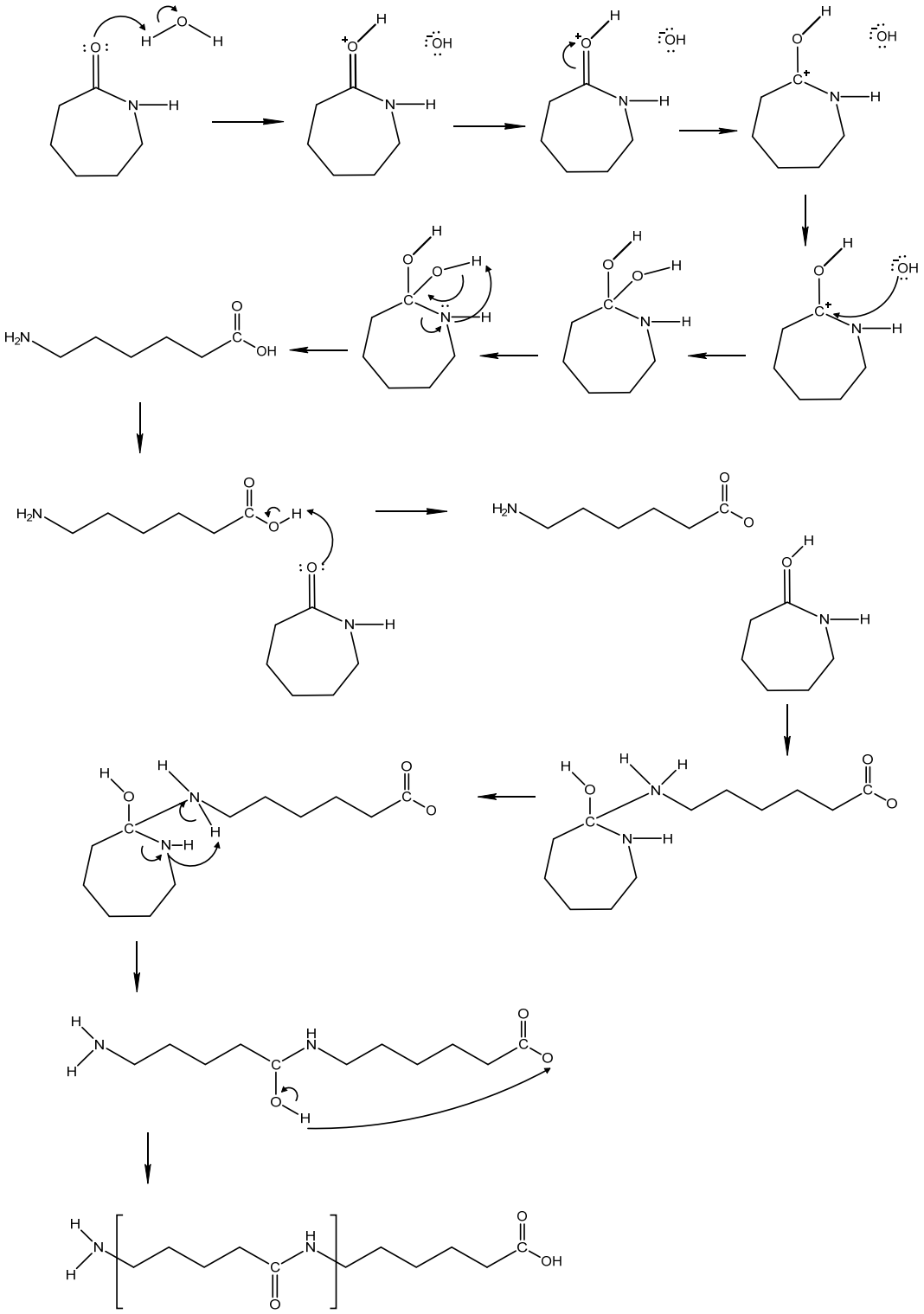

Polyamide 6

Appendix B

Thermal properties of PA6 pellets and filaments for different drying times and temperatures
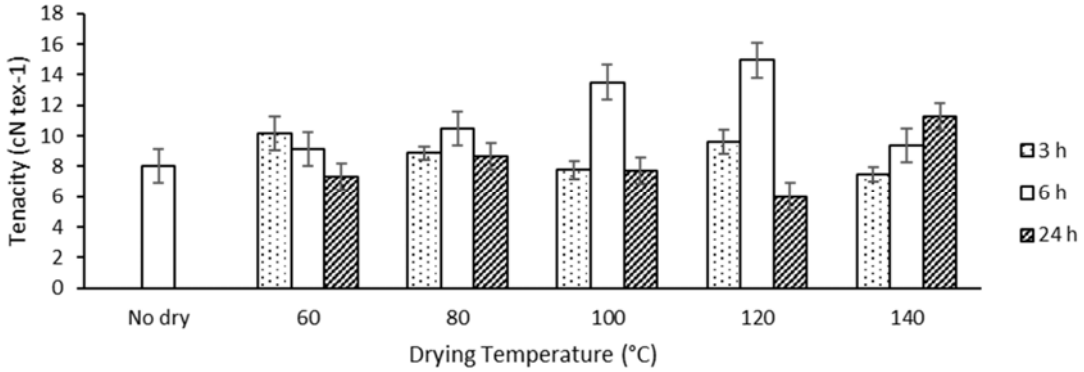
		PA6 Pellets			PA6 Filaments		
Drying time	**Drying temperature (°C)**	**Melting temperature (°C)**	**Melting enthalpy (J g^{-1})**	**Crystallinity (%)**	**Melting temperature (°C)**	**Melting enthalpy (J g^{-1})**	**Crystallinity (%)**
Undried	0	225	63.5	27.6	221	50.8	22.1
3 hours	60	221	64.5	28.0	221	63.5	27.6
	80	225	58.4	25.4	222	58.4	25.4
	100	225	50.4	21.9	221	39.2	17.0
	120	223	63.5	27.6	220	65.6	28.5
	140	221	72.3	31.4	222	61.8	26.9
6 hours	60	221	58.5	25.4	220	39.9	17.3
	80	223	50.2	21.8	220	57.7	25.1
	100	225	67	29.1	220	54.4	23.6
	120	224	63.5	27.6	220	50.9	22.1
	140	223	50.2	21.8	220	58.7	25.5
24 hours	60	224	62.3	27.1	220	44.7	19.4
	80	224	66.3	28.8	220	59.8	26.0
	100	221	43.3	18.8	220	51.3	22.3
	120	222	63.7	27.7	220	58.5	25.4
	140	221	45.7	19.9	220	46.2	20.1